Habilitation thesis

Advancing Electron Microscopy for the Development of Durable Low-Cement Cementitious Composites

Zdeněk Prošek

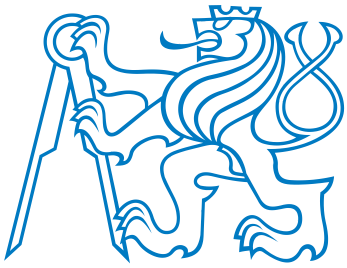

Czech Technical University in Prague
Faculty of Civil Engineering
Department of Mechanics

Prague, June 2025

Acknowledgements

I would like to express my sincere gratitude to Prof. Ing. Pavel Tesárek, Ph.D. for his invaluable support, insightful advice, and constructive feedback throughout the preparation of this work and during my professional development.

This work was supported by the RECONMATIC project funded by the European Union under the Horizon Europe programme (Grant Agreement No. 101058580), and by the Czech Science Foundation (GA ČR) under project 23-05500S, Effect of surface treatments on the performance of silicon-based secondary materials in cementitious composites.

I would also like to express my sincere thanks to my partner, Ing. Tereza Nedvědová, for her patience, continuous support, and understanding throughout the demanding process of this work. Her encouragement has been an important source of motivation during its completion.

Abstract

This work focuses on the use of electron microscopy as a key tool for the development and optimization of cementitious composites with reduced Portland cement content. Scanning electron microscopy (SEM-BSE) and energy-dispersive spectroscopy (EDS) were employed to analyze microstructural changes resulting from the incorporation of micronized additives such as marble sludge, recycled concrete powder, and plasma-treated glass particles. Special attention was given to the characterization of hydration products, interfacial transition zones (ITZ), and pore distribution. Advanced image analysis methods enabled accurate quantification of phase distribution and detection of subtle morphological features that would otherwise remain unnoticed. The effectiveness of bacteria-induced calcite precipitation (BICP) as a self-healing mechanism was also evaluated, and its microstructural effects were confirmed via SEM and μCT analysis. This study demonstrates that appropriately applied microscopy provides critical insights necessary for optimizing composite design and predicting long-term material performance.

Abstrakt

Předkládaná práce se zaměřuje na využití elektronové mikroskopie jako klíčového nástroje pro vývoj a optimalizaci cementových kompozitů s nízkým obsahem portlandského cementu. Pomocí skenovací elektronové mikroskopie (SEM-BSE) a energiově disperzní spektroskopie (EDS) byly analyzovány změny v mikrostruktuře způsobené použitím mikromletých příměsí, jako jsou mramorový kal, recyklovaný betonový prášek nebo plazmaticky ošetřené skleněné částice. Důraz byl kladen na charakterizaci hydratačních produktů, přechodové zóny (ITZ) a distribuce pórů. Využití pokročilé obrazové analýzy umožnilo kvantifikovat rozložení fází a detekovat jemné morfologické změny, které by běžnou vizuální analýzou zůstaly nerozpoznány. Dále byla sledována účinnost bakteriálně indukované kalcitové precipitace (BICP) jako mechanismu pro samohojení trhlin a její mikrostrukturální dopady byly potvrzeny pomocí kombinace SEM a μCT analýz. Práce dokládá, že správně aplikovaná mikroskopie poskytuje zásadní informace pro optimalizaci složení cementových kompozitů a pro predikci jejich dlouhodobých vlastností.

Contents

Chapter 1

Introduction

Electron microscopy (SEM) is a powerful imaging and analytical technique based on the interaction of a focused electron beam with the material's surface. Unlike optical microscopy, which is limited by the wavelength of visible light, electron microscopy enables imaging at nanometer to sub-nanometer resolution, making it ideal for studying the microstructure of cementitious composites. It is particularly useful for identifying hydration products, observing crack propagation, evaluating pore structure, and analyzing interfacial transition zones (ITZ) between the binder and aggregate.

By combining imaging with various spectroscopic techniques, electron microscopy provides not only morphological information but also quantitative data on chemical composition, crystallography, and phase distribution. The versatility and precision of this method make it essential in both fundamental research and applied material development.

Several key detectors are used for microstructural analysis of cementitious composites:

- **SE (Secondary Electrons)** – provides high-resolution surface topography information, enabling detailed surface phase analysis.
- **BSE (Backscattered Electrons)** – allows identification of individual phases based on atomic number, enabling quantification of phase proportions.
- **EDS (Energy Dispersive Spectroscopy)** – used for elemental analysis of the sample, allowing determination of the chemical composition of hydration products and phases.
- **WDS (Wavelength Dispersive Spectroscopy)** – offers higher elemental analysis accuracy than EDS and is used for detecting trace elements in complex material systems.
- **EBSD (Electron Backscatter Diffraction)** – allows analysis of the crystal structure of hydration products and identification of phase transformations in cementitious composites.

The results obtained through electron microscopy are significantly influenced by multiple operational parameters. Among the most critical are the accelerating voltage and the beam current settings.:

- **Accelerating voltage** (commonly between 5–20 kV) affects the interaction volume within the material and thus influences both the resolution and depth of information. Lower voltages enhance surface sensitivity and reduce charging, whereas higher voltages increase penetration depth and are preferred for deeper phase identification or BSE contrast.
- **Beam current** influences the signal-to-noise ratio and the strength of the detected signal. Higher current improves the quality of EDS/WDS spectra but may cause local heating or beam damage, especially in porous or poorly conductive materials like cement pastes.

Careful calibration of imaging parameters – particularly accelerating voltage, working distance, BSE detector gain, and pixel resolution – is therefore essential to ensure that the acquired microstructural data in cement-based composites accurately reflect the morphology and contrast differences within the ITZ. Improper calibration may lead to artificial contrast shifts, blurred phase boundaries, or misinterpretation of porosity gradients, which are critical for evaluating the mechanical integrity and durability of the composite. Specifically in BSE mode, where image contrast depends heavily on atomic number, the precise setting of acquisition conditions directly affects the ability to differentiate hydration products from unreacted particles and to characterize microstructural gradients across the ITZ. As such, rigorous optimization is a prerequisite for any meaningful SEM-based analysis of the interfacial microstructure.

This work is focused on new possibilities for using electron microscopy as a tool for effective design and optimization of advanced materials with respect to their composition and resulting performance. Within the scope of both fundamental and applied research – where I have been actively involved – electron microscopy was employed to address a wide range of research tasks. These include Czech grant projects (GA ČR, TA ČR, MPO, and CTU in Prague), the international HORIZON project No. 101058580 RECONMATIC, and also contracted research for industrial partners in the Czech Republic and international corporations e.g. KNAUF Praha, spol. s r.o. and KNAUF Insulation, spol. s r.o. [1, 2].

Electron microscopy has become an integral part of the methods used for characterizing input materials, analyzing samples from existing structures, and designing and optimizing new materials and products. It also offers further opportunities, which are described in this work [3–5]. In my professional and scientific practice involving electron microscopy, I have tested materials based on wood, gypsum and gypsum board waste, polymer fibers, glass, metal 3D-printed structures, and more [6–9]. However, the main and most frequent focus of my research is on cement-based composite materials utilizing recycled concrete, secondary raw materials, or waste.

In general, the research addresses the characterization of the input material – recycled concrete. In the first step, electron microscopy enables the determination of a range of properties and parameters (e.g., chemical and mineralogical composition, particle size, degree of hydration, amount of unhydrated clinker minerals, etc. [10]), which help define the waste material. These findings are used to predict effective recycling strategies, including appropriate technology and subsequent utilization in new materials or composites [11].

In the second step, the processed recycled concrete and other raw materials – already subjected to technological processes such as crushing, grinding, or surface treatments (e.g., plasma, thermal, chemical) – are characterized again. Based on this characterization, further treatment can be proposed, including the addition of admixtures or additives to improve the final product's

performance. In this way, a dry mixture can be designed and prepared, to be later combined with cement (or a reduced cement content), fillers (natural or recycled), and other components to produce a different type of cementitious composite. Depending on the stage of experimental development, such mixtures are used to prepare cement paste, mortar, or concrete – allowing a gradual understanding of how individual ingredients affect the final material [12].

In the third step, the designed dry mix is used to prepare a hardened cementitious composite, which is then tested in terms of its intended performance. The primary objective is to verify the hypotheses formulated in the previous steps. Depending on the application and durability requirements, samples are taken from the hardened material (from the lab or structures), thin sections are prepared, and analyzed via electron microscopy in the same way as in the previous steps.

The core aim of the research is to design a new type of cementitious composite that:

- Uses a **reduced amount of cement**, primarily by substituting with processed recycled aggregate (e.g., 0/4 mm or 0/1 mm) depending on the intended application.
- Efficiently incorporates modified recycled aggregate to **reduce or replace** the amount of natural aggregate.
- Is **100% recyclable** at the end of its service life.
- Has **extended durability/lifespan** depending on the environment and specific application – making the composite effectively "tailored" for its purpose.

The investigation centered primarily on sustainable materials and circular approaches. A significant part of the research involved the utilization of marble dust (Annex A), marble sludge (Annex B), and waste concrete (Annex C). These materials were subjected to high-speed mechanical activation (grinding) to enhance their reactivity and subsequently incorporated into cementitious systems. Their use contributed not only to reducing clinker content but also to fostering the formation of hydration products – especially in systems where fine recycled concrete was combined with fly ash, blast furnace slag, and lime (Annex D). The intended outcome was to develop functional applications for materials with reduced carbon and environmental footprints – such as masonry blocks optimized for low-impact construction (Annex E). The research further explored strategies to improve the durability and extended service life of these sustainable composites. One innovative approach included the incorporation of specific bacterial strains capable of self-healing cracks. These bacteria can utilize calcium ions released from the marble- and concrete-based waste materials, thereby promoting autonomous crack repair and enhancing long-term material performance (Annex F). In many cases, the incorporation of recycled or waste materials led to a slight decrease in mechanical performance, due to their limited bonding ability within the cementitious matrix. To address this issue, plasma surface treatments were applied to modify the wettability and interfacial properties of material. These treatments demonstrated a positive effect on the microstructural integration of the waste materials – particularly by improving the ITZ in the vicinity of reinforcing fibers, where better particle dispersion and enhanced bonding with the matrix were observed (Annex G).

Examples of fundamental and experimental research and development conducted over the past seven years are briefly described in Chapter 2, including typical issues addressed using

electron microscopy and other methods. These focus on determining material properties in relation to raw materials used, their ratios, water-to-binder ratios, applied admixtures, time dependency, and more.

Newly tested materials and currently ongoing research are briefly described in Chapter 3. Based on the insights from Chapter 2 and other activities, new approaches and options for using electron microscopy are presented, along with a more detailed description of studied phenomena, including less conventional methods in construction research – such as plasma treatments – in collaboration with the Institute of Physics of the Czech Academy of Science [13].

Chapter 2

Modification of Cementitious Composites with Micronized and Activated Additives

Fine and micronized materials play a key role in the development of modern cementitious composites, as they enable optimization of mechanical properties, increase durability, and reduce the environmental impact of concrete mixtures [14, 15]. Their addition improves the reactivity of the cement binder, which positively affects the microstructure and mechanical behavior of the final material [16].

Traditionally used micronized additives typically include silica fume, fly ash, slag, and pozzolans. Silica fume is valued for its high reactivity and ability to reduce porosity, while fly ash and slag contribute to the long-term strength and durability of the mix [17, 18]. However, the availability of these materials is limited, and current research is therefore focusing on the use of secondary raw materials and recycled materials as replacements for conventional additives [19].

In accordance with the standard ČSN EN 206–1 [20], the studied additives can be considered inert, and their influence on the final microstructure of the composite was examined. Parameters such as the size of the ITZ, the distribution and interaction of particles with the cement matrix, the formation and development of hydration phases, mineralogical composition, and changes in pore structure were analyzed. The effect of micronized particles is significantly dependent on their composition and grain shape, which can influence their effectiveness in cementitious composites [10].

In the ongoing basic and applied research, it was necessary to combine various methods to determine the relationship between the quality of the recycled material, the type of its processing, and other used components on the final performance of the composite mixtures and samples produced from them. Samples were prepared in sizes of 20 × 20 × 100 mm and 40 × 40 × 160 mm for paste and mortar testing, and 150 × 150 × 150 mm for concrete mixture testing.

Within the experimental research, a wide variety of recycled and secondary raw materials were tested, including:

- Various types of concretes or concrete products, aged from 1 to 100 years.

- Marble powder from the West Bank of Jordan.
- Stone dust.
- Fly ash.
- Air-cooled blast furnace slag.
- Limestone.
- Waste glass.

From several research directions, four main themes were selected for the purpose of this work:

- Micronized marble sludge.
- Micronized recycled concrete.
- Synergy of lime, slag, fly ash, and recycled concrete.
- Self-healing concrete.

Testing of cementitious composites with micronized materials includes a range of experimental methods focused on evaluating mechanical, physical, and chemical properties [21]. Standard testing methods include compressive and flexural strength testing, porosity determination, and microstructural analysis, including electron microscopy.

Electron microscopy plays a key role in assessing the distribution and interaction of micronized particles with the cement binder [22]. It also enables detailed characterization of the interfacial transition zone between the cement matrix and filler, which is essential for understanding the mechanical behavior of the resulting composite. The resulting microstructural description allows for a detailed analysis of particle size, mix homogeneity, and presence of potential defects [23].

Another important analytical method is mercury intrusion porosimetry, which enables determination of pore size and distribution in the material – critical for predicting its durability and resistance to aggressive environments [18]. By combining these analytical methods, the relationship between material composition, microstructure, and macroscopic properties such as compressive and flexural strength or overall durability of the composite can be established.

2.1 Use of Micronized Marble Sludge

Micronized marble sludge has been investigated as an additive in cementitious composites to optimize mechanical properties and reduce the porosity of the resulting material. Although marble is often considered an inert component, its fine-grained fraction can significantly affect cement hydration and the development of the cement matrix microstructure [24]. The presence of carbonate particles has the potential to promote the growth of hydration products and contribute to structural homogenization, thereby reducing porosity and improving the mechanical characteristics of the cement composite [25].

The microstructure of cement composites containing marble sludge was analyzed using scanning electron microscopy in backscattered electron mode (SEM-BSE) and energy-dispersive spectroscopy (EDS) [26]. Differentiating marble from portlandite ($Ca(OH)_2$) was challenging due to their similar chemical composition and contrast properties in BSE images. Two main methods were used for their identification:

- **EDS analysis:** Allowed phase differentiation due to the presence of carbon in the carbonate ions of marble, whereas portlandite contains no carbon [25].
- **SEM-BSE image entropy-based analysis:** Enabled phase identification based on texture and contrast [27].

The latter method significantly reduced the analysis time – whereas generating a full elemental map using EDS takes several hours, entropy-based analysis provided results within seconds [27]. Phase composition analysis showed that during cement hydration, several key products form, particularly C-S-H gel, portlandite, and carbonate hydrates, resulting from the interaction between marble sludge and clinker minerals [28]. Marble sludge acts as a nucleation center for portlandite growth, increasing microstructural homogeneity and reducing porosity [25]. The presence of ground marble powder also accelerated the hydration of tricalcium aluminate (C_3A) and promoted the formation of stable carbonate phases, such as monocarbonate ($3CaO{\cdot}Al_2O_3{\cdot}3CaCO_3{\cdot}32H_2O$) [29, 30].

The ITZ around marble particles played a key role in determining the mechanical properties. It was found that the ITZ is generally a weaker region with lower C-S-H gel density and higher portlandite concentration, leading to microcracks that reduce compressive strength and durability [26] (see Fig. 2.1(a) and 2.1(b)). Nanoindentation confirmed that the mechanical parameters (modulus of elasticity) of the ITZ are lower than those of the cement matrix, consistent with higher porosity and lower density of hydration products in this region [25] (see Fig. 2.1(c)).

Compressive strength tests indicated that replacing up to 10 wt.% of Portland cement with micronized marble did not reduce strength; on the contrary, it can increase it due to improved microstructure and reduced porosity [25]. This effect is attributed not only to the microfiller function, but also to interactions with hydration products, as marble promotes nucleation [26]. The experimental results confirm that micronized marble sludge can be effectively used as an additive in cementitious composites, significantly influencing cement hydration, improving the distribution of hydration products, and reducing porosity. Minimizing the weak ITZ is a key factor in achieving optimal mechanical properties (see Fig. 2.1(d)).

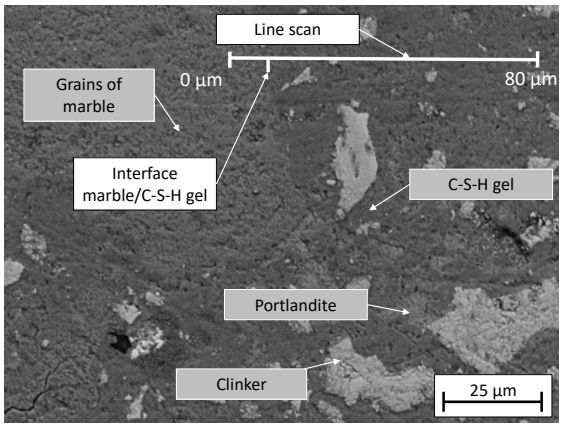

(a) Line scan position for SEM-EDS analysis; cementitious materials with 10 % marble sludge at 500× magnification [25].

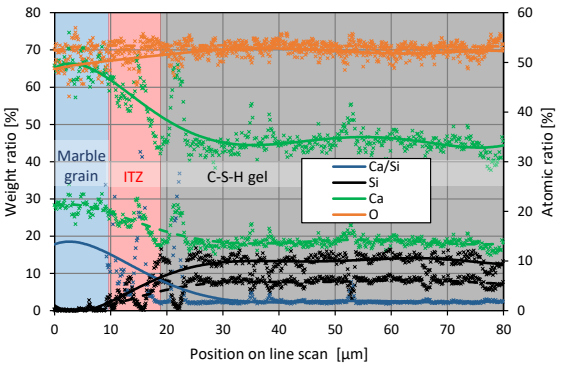

(b) Results from the line scan in Figure 2.1(a) placed across an ITZ, with weight (solid line) and atomic (dashed line) concentrations [25].

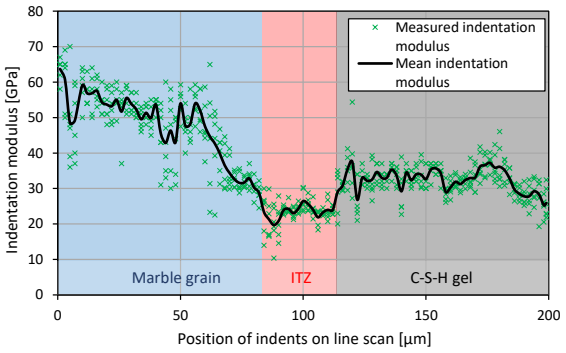

(c) Indentation results along a line scan across an ITZ between a marble grain and a cementitious matrix [25].

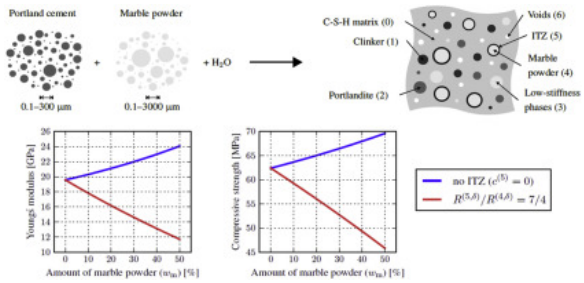

(d) Scheme of the micromechanical model representing cement–marble powder interaction and the impact of the ITZ on stiffness (left) and compressive strength (right) of cement pastes with varying marble powder content [26].

Figure 2.1: SEM-EDS and micromechanical analysis of the ITZ in cementitious composites containing marble powder.

2.2 Use of Micronized Recycled Concrete Aggregate

This research focused on recycled concrete of 0/4 mm fraction, which is not commonly used in concrete due to concerns about its potentially negative impact on the mechanical properties of cementitious composites [31]. This fraction contains a high amount of old cement paste, distinguishing it from typical recycled aggregates. Composition analysis revealed that the fraction contains a significant amount of unhydrated clinker particles, which can be reactivated through micronization and used as secondary cementitious components [14, 15]. Micronized recycled concrete powder (RCP) represents a valuable source of both active and inert components that can replace a portion of Portland cement in cementitious composites, while also mitigating landfill disposal.

The aim of this study was to verify the reactivation potential of these unhydrated clinker particles and the use of RCP as a binder component in cementitious composites. Advanced techniques such as SEM, X-ray diffraction (XRD), and thermogravimetric analysis (TGA) were used to study the microstructure and reactivity of these materials in detail [32].

The phase composition of the recycled material varied depending on the type and origin of the old concrete. Recycled aggregate from high-strength concrete contained a higher amount of unhydrated clinker particles, whereas recycled materials from older reinforced concrete structures had a lower content due to long-term exposure to moisture and rehydration [10]. It was found that a higher content of unhydrated particles enables further hydration when remixed with water, as confirmed by isothermal calorimetry which recorded additional heat release during hydration [33]. Micronization of recycled concrete was shown to increase the reactivity of unhydrated clinker by exposing particle surfaces and facilitating hydration. Detailed SEM-BSE analysis enabled quantification of unhydrated particles and examination of their distribution and relationship to the ITZ [31]. ITZ in recycled concrete was found to be generally weaker than in new cementitious composites, influencing the mechanical properties of the final material.

Comparison of different analytical techniques showed that XRD and TGA provide valuable information about phase composition but are insufficient for accurate quantification of unhydrated particles. In contrast, SEM-BSE allows for fast and accurate identification of these particles based on image contrast between bright (unhydrated clinker) and darker areas (C-S-H gel/portlandite) [34]. Additionally, it enables assessment of the exposure of unhydrated clinker through micronization, see Fig. 2.2(a).

Mechanical testing revealed that replacing Portland cement with micronized recycled concrete in weight amounts up to 20% increased flexural strength while maintaining sufficient compressive strength [31]. These findings confirm that fine recycled concrete fractions can function not only as filler but also as secondary binder due to the presence of unhydrated clinker and other components [10]. The results of this study confirm that 0/4 mm recycled concrete contains a significant amount of unhydrated clinker that can be activated through micronization and subsequently used in cementitious composites. This approach reduces the consumption of primary raw materials and improves the mechanical performance of cement-based materials. The development of hydration heat, as shown in Fig. 2.2(b) [10], clearly indicates that reactive phases are present in the recycled fraction and contribute to the ongoing hydration process.

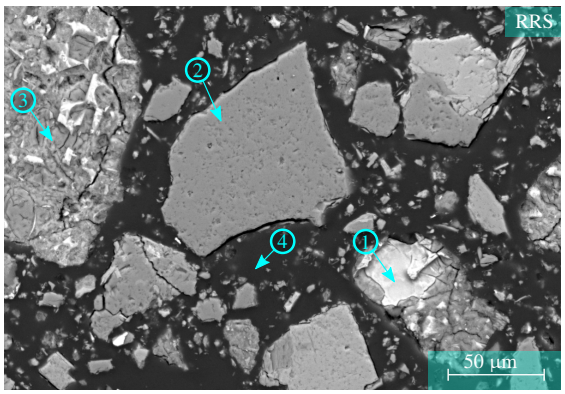

(a) Microscopy image at 1000× magnification of RCO embedded in epoxy resin. Phases: (1) white residual anhydrous clinker, (2) light gray aggregate fragments, (3) textured hydrated matrix, (4) dark gray epoxy [25].

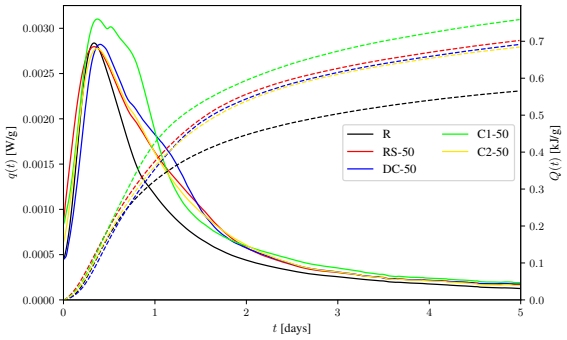

(b) Specific heat flow $q(t)$ (solid lines) and cumulative hydration heat $Q(t)$ (dashed lines) over the first 5 days of hydration, normalized per 1 g of Portland cement (PC). R – reference sample with CEM I 42.5 R; RS-50 – 1:1 mix of PC and recycled material from a railway sleeper; DC-50 – 1:1 mix of PC and recycled material from a drainage channel; C1-50 – 1:1 mix of PC and recycled fines from a monolithic column; C2-50 – 1:1 mix of PC and recycled coarse fraction from a monolithic column [25].

Figure 2.2: Comparison of microstructure and hydration behavior in cementitious composites containing recycled materials.

2.3 Use of Lime, Slag, and Fly Ash in Combination with Recycled Concrete

The use of micronized recycled concrete as a partial replacement for Portland cement presents challenges related to its lower reactivity and changes in microstructure, which can affect the mechanical properties of the final material [35, 36]. This study examined the potential for chemical activation of recycled concrete using lime, slag, and fly ash, with the aim of improving the cohesion and reactivity of these materials within the cement matrix.

Lime ($Ca(OH)_2$) was used to adjust the alkaline environment, leading to more effective hydration of the cement phase and stabilization of the microstructure [37]. Slag and fly ash acted as latent hydraulic and pozzolanic additives that reacted with $Ca(OH)_2$ to form stable hydration phases such as C-S-H and C-A-S-H, thereby ensuring greater strength and better resistance to degradation [38, 39]. SEM revealed that the presence of recycled concrete led to microstructural changes, including different phase compositions of hydration products. It was confirmed that finely ground recycled components serve as nucleation sites for new hydration products, promoting a more homogeneous distribution and stabilization of the microstructure [3], see Fig. 2.3.

Mechanical tests demonstrated that the addition of fly ash and slag contributed to increased flexural strength and reduced shrinkage, thereby improving the long-term durability of cementitious composites [40]. The hydration of fly ash and slag led to the formation of stable C-S-H phases, which mitigated the negative impact of recycled concrete on the mechanical properties of the cement binder. The addition of lime optimized the pH environment and accelerated reactions between components, improving the cohesion of the microstructure and the ITZ between the cement matrix and recycled particles [3].

The study also addressed the degradation of mechanical properties depending on the amount of added recycled concrete. Results showed that using recycled concrete without chemical activation led to a decrease in compressive strength by 5–20%, depending on the recycled content [41]. The simultaneous use of lime, slag, and fly ash compensated for this loss, achieving compressive and flexural strengths comparable to those of standard cement composites. It was found that the optimal replacement level of Portland cement is up to 50 wt.% without significant deterioration of mechanical performance [3].

Another key aspect was the improvement of the ITZ between the cement matrix and recycled particles. The modification of ITZ using additives led to better cohesion between the cement matrix and recycled components, manifested by lower porosity and a more uniform distribution of hydration products [3]. The presence of lime and pozzolanic additives reduced structural heterogeneity and eliminated weak points in the material's microstructure.

Another significant finding was the change in hydration mechanisms with the use of recycled concrete. It was confirmed that fine particles of recycled concrete can act as nucleation sites, but without activators such as lime, their contribution remains limited [3]. Conversely, with proper activation, more effective reactions occur with pozzolanic components, resulting in better mechanical stability and higher density of hydration products (Fig. 2.3) [3].

The experimental results of this study confirm that chemical activation of micronized recycled concrete using lime, slag, and fly ash represents a sustainable approach to reducing depen-

dence on primary cement materials. This combination enables more efficient use of recycled components, thereby not only improving the mechanical properties of the resulting material but also reducing the environmental impact of the construction industry.

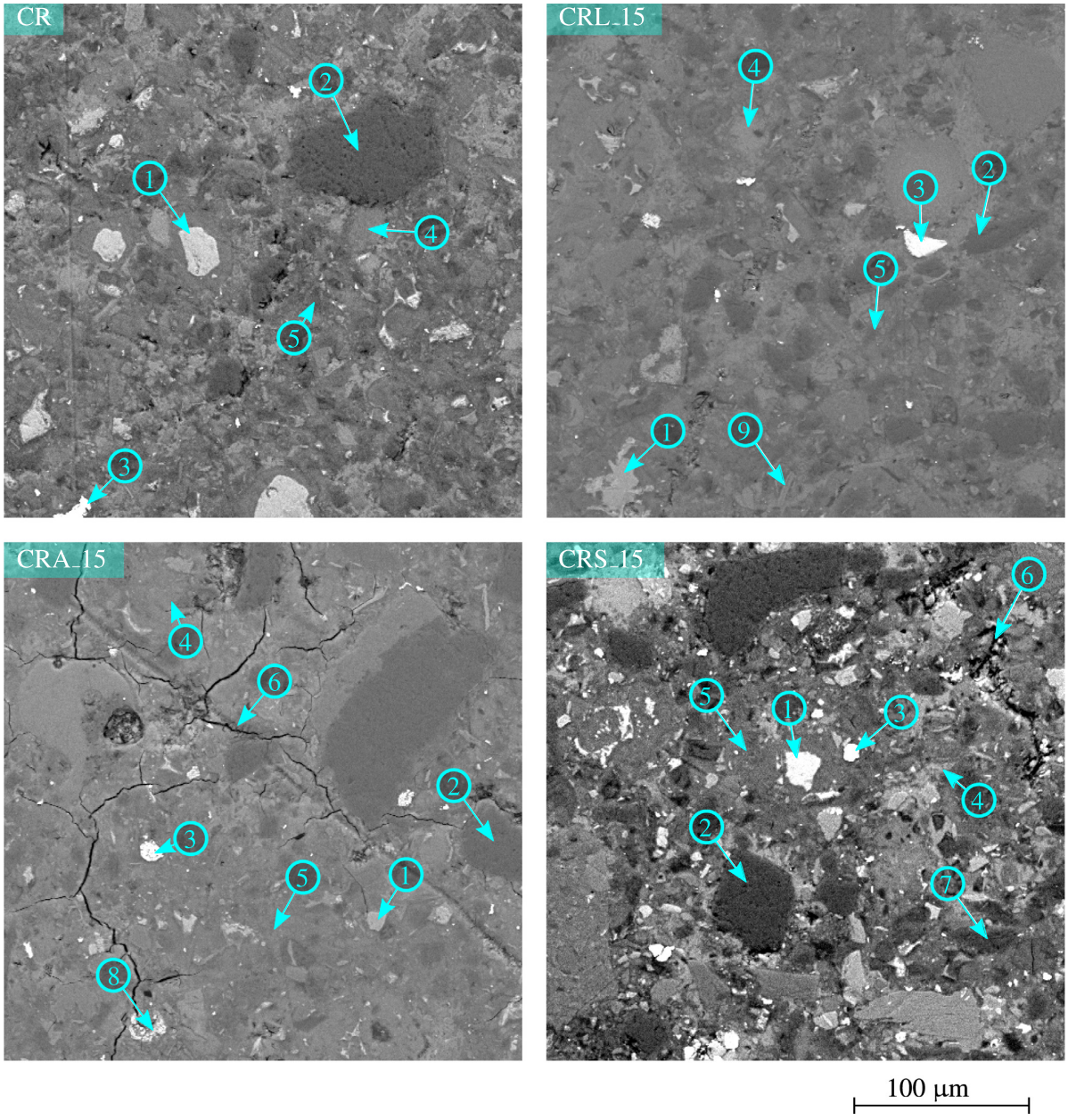

Figure 2.3: Microscopy images at 500× magnification of selected pastes (CR – sample containing recycled concrete with no activators; CRL – sample containing recycled concrete with lime; CRA – sample containing recycled concrete with fly ash; CRS – sample containing recycled concrete with slag) with markers denoting phases of interest: 1. unhydrated clinker, 2. SiO_2, 3. metal alloy, 4. $Ca(OH)_2$, 5. C-S-H/C-A-S-H gel, 6. microcracks, 7. $CaCO_3$, 8. glassy components of fly ash, and 9. healed cracks [3].

2.4 Bacterial Calcite Precipitation for Enhanced Durability of Cement-Based Composites

The durability of concrete structures is one of the key factors influencing their service life and overall maintenance costs. One of the main causes of degradation is the ingress of water and harmful substances through microcracks, which accelerates reinforcement corrosion and reduces material strength. Due to increasing pressure on sustainability in constructions, there is growing interest in improving concrete durability through not only new material solutions but also the use of recycled components. However, incorporating recycled materials in concrete can adversely affect its microstructure, leading to increased porosity and reduced compressive strength. Therefore, this study focuses on the use of bacterially induced calcite precipitation (BICP) as a method for enhancing concrete durability.

Concrete exhibits a natural ability for autogenous crack healing, driven by unhydrated cement particles and spontaneous calcite precipitation in an alkaline environment [42]. However, this process is often slow and insufficient for complete crack sealing, limiting its practical effectiveness over the long term [4]. In recent years, the use of microorganisms – particularly bacterial strains such as *Bacillus pseudofirmus* and *Bacillus cohnii* – has proven more effective in promoting BICP [42]. In the alkaline environment of concrete, these microorganisms act as nucleation centers that initiate and accelerate the precipitation of calcium carbonate ($CaCO_3$), thereby sealing cracks and improving mechanical properties [43].

Scanning electron microscopy confirmed that in the presence of bacteria, fine-grained calcite crystals (less than 1 μm) formed, filling pores and improving the material's microstructural properties [42]. Compared to spontaneous healing in concrete without bacteria, which leads to larger and more porous crystals (up to 30 μm), BICP was shown to be a more effective method for enhancing material density and durability [44]. Experimental results confirmed that samples containing microorganisms had lower water absorption, significantly reducing the risk of freeze–thaw and chemical degradation [4].

The main challenge in SEM analysis was sample preparation, as grinding and polishing disrupted the calcite layer formed by bacterial activity. To address this, two series of samples were prepared. The first series was analyzed using the SE detector, allowing the surface structure and calcite crystal morphology to be described. The second series was repeatedly embedded in epoxy resin after each cut to reinforce the structure and allow polishing without microstructural damage. These samples were then analyzed with a BSE detector in combination with EDS to determine the chemical composition of the calcite layers and other mineral phases. Without this preparation, no continuous calcite layer was observed in the cracks, indicating that mechanical sample preparation can completely remove the delicate calcite structure. Even with optimized preparation, some damage to the calcite microstructure occurred during polishing. To verify whether calcite layers actually filled the entire crack volume and not just surface fragments, the microstructure was also analyzed using micro-computed tomography (μ-CT). This method confirmed that the deeper layers of the composite retained an intact calcite microstructure, and the fragments observed at the surface were only the result of mechanical destruction during sample preparation [4], see Fig. 2.4.

One key factor for successful bacterial healing is ensuring an adequate supply of calcium

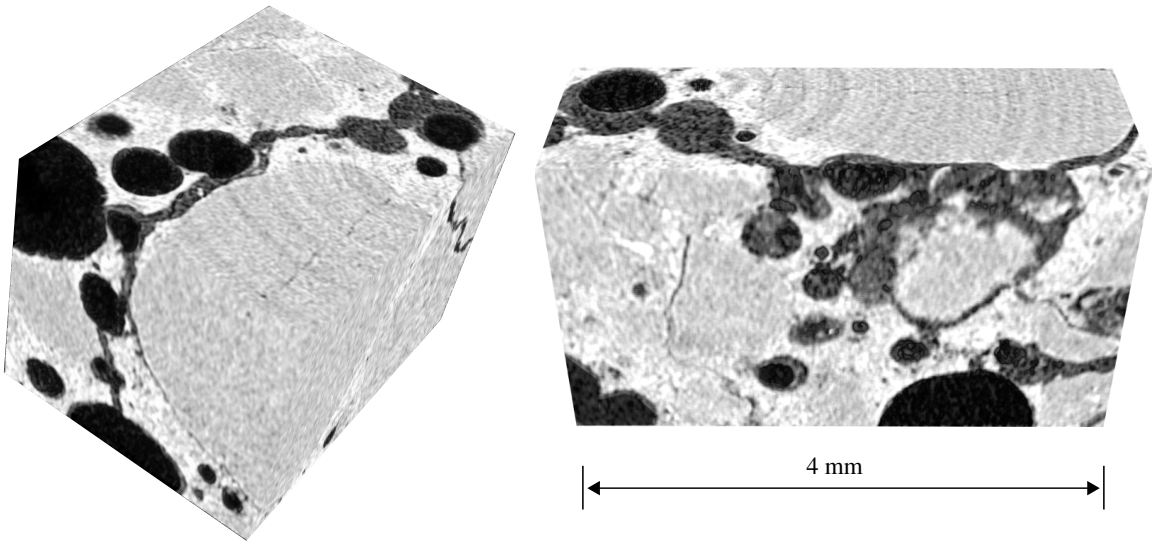

Figure 2.4: Sections of the μ-CT scan showing cemented cracks and pores partially filled with $CaCO_3$ [4].

ions necessary for calcite formation [45]. In this context, micronized marble waste was tested as an alternative calcium source to enhance the remediation properties of concrete [46]. Results showed that the presence of micronized marble positively influenced the stability of the BICP layer, leading to increased compressive strength and improved cohesion [46].

Another significant innovation in BICP is the use of hydrogels with immobilized bacteria. It has been shown that hydrogels enable more efficient crack sealing than the direct application of bacterial spores, as they provide a more stable environment and ensure better nutrient distribution [47]. Furthermore, the combination of bacterial healing with polyvinyl alcohol (PVA) enhances the effectiveness of the process through improved bacterial stabilization and controlled nutrient release [4]. The presence of PVA also positively affects the mechanical properties of cementitious composites by reducing the number of disconnected pores and increasing flexural strength [48].

BICP represents a promising approach for extending the service life of concrete structures and reducing maintenance costs. Process optimization using micronized marble as a calcium source, along with bacterial immobilization in hydrogels or PVA, significantly enhances the efficiency of the method and improves the material's resistance to degradation, see Fig. 2.5(a) and 2.5(b).

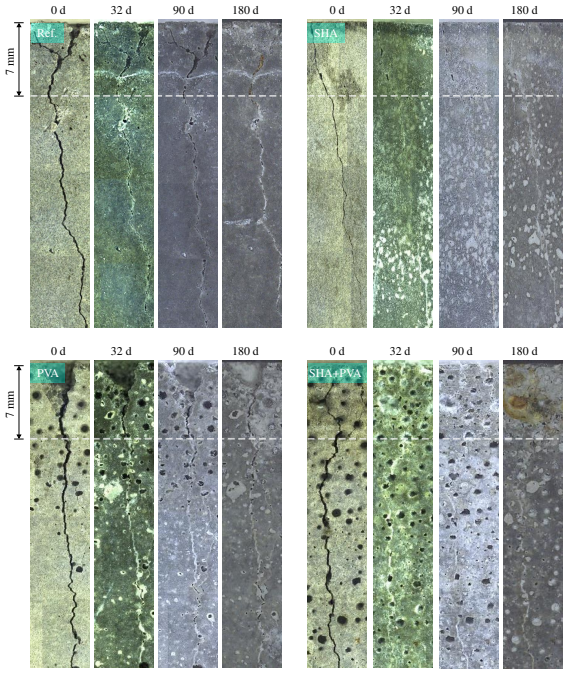

(a) : Optical microscopy images of the cracks in the studied specimens after 0, 32, 90, and 180 days, Ref. – reference sample of cement pastes, SHA – sample with self healing agents, PVA – sample with PVA, SHA + PVA – sample with self healing agent in PVA [4].

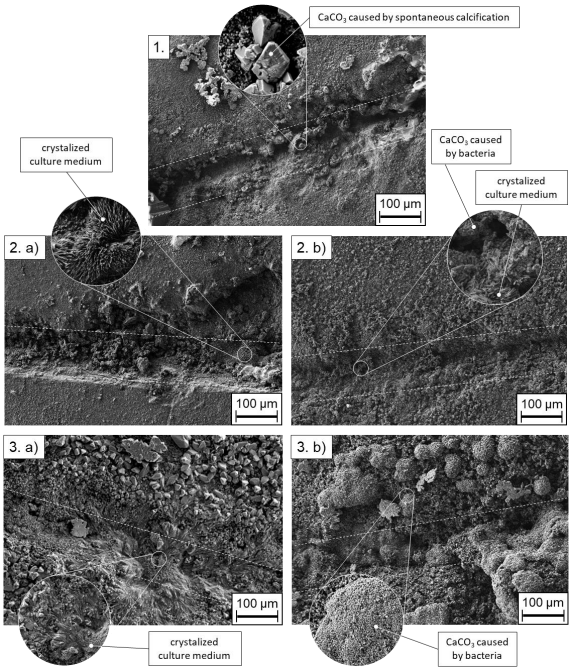

(b) SEM images of cement paste surfaces with highlighted groove (dashed line). 1 – Sample No. 1 with water, 2.a) – Sample No. 2 with medium 253, 2.b) – Sample No. 2 with medium 253 and bacteria, 3.a) – Sample No. 3 with medium 253 and 2% $CaCl_2$, 3.b) – Sample No. 3 with medium 253, 2% $CaCl_2$ and bacteria. Magnification: 400×; for cutouts: 3000× [49].

Figure 2.5: Crack development and microstructural changes in cementitious composites with self-healing functionality and bacterial treatments.

Chapter 3

Ongoing research

Currently, several basic and applied research projects related to the recycling of construction materials are underway, driven by the needs of our industrial partners. From the broad scope of topics being addressed, two key themes were selected for the purposes of this study:

- The use of AI for phase identification and image analysis.
- Reduction of ITZ in composites using nanotechnology and plasma-treated particles.

3.1 Use of AI – Gray Level Differentiation

Artificial Intelligence (AI) and machine learning are playing an increasingly important role in the analysis of the microstructure of cementitious composites. Advanced machine learning methods enable automated analysis of SEM-BSE images, leading to faster and more accurate results in phase identification and quantification of microstructural features. This approach eliminates subjective errors in human evaluation and allows analysis of large data volumes in a short time.

In current research, AI is mainly used for:

- **Automated phase detection** – AI models are trained on large image datasets annotated with known phases (e.g., C-S-H gel, portlandite, unhydrated clinker). Neural networks can accurately distinguish individual phases based on texture, contrast, and other BSE image parameters.
- **Quantification of the distribution and amount of individual phases** – Image analysis can precisely determine the proportion of different hydration products, enabling detailed evaluation of the effect of additives on material microstructure.

New AI-based image analysis methods focus on advanced approaches such as convolutional neural networks (CNNs) and deep learning, which allow extraction of relevant features from SEM images and their use in image reconstruction, resolution enhancement, or artifact removal. Deep learning also helps analyze defocused images by automatically refocusing blurry areas to improve accuracy in microstructural characterization [50].

For the most precise microstructure characterization, it is beneficial to combine different image analysis approaches:

- **Gray level and entropy analysis** – Gray levels help distinguish phases based on material density, while entropy provides information on the degree of disorder in the microstructure and helps identify highly variable areas, such as ITZ.
- **Haralick texture features (GLCM – Gray Level Co-occurrence Matrix)** – This method analyzes pixel relationships and identifies hydration products based on material texture.
- **Fractal analysis** – Quantifies porosity and complexity of the microstructure, offering insight into pore distribution and phase influence on mechanical properties.
- **Deep learning-based image segmentation (U-Net, Mask R-CNN)** – Modern neural networks allow detailed segmentation of phases and more accurate recognition of microstructural characteristics.
- **Multimodal approach** – Combining SEM-BSE images with EDS, XRD, and Raman spectroscopy enables comprehensive material composition characterization.

The development of advanced AI algorithms for image analysis represents a significant step forward in the accuracy and efficiency of microstructural analysis of cementitious materials. New approaches are also being tested that integrate AI with analytical methods such as X-ray diffraction (XRD) or thermogravimetric analysis (TGA) for even more comprehensive compositional characterization of cement composites [51].

3.2 ITZ Optimization in Composites Using Plasma-Treated Particles

As part of basic research conducted in collaboration with the Institute of Physics of the Czech Academy of Sciences, the use of surface-treated fine particles based on waste container glass (WGP) and other silica-based materials is being investigated. The initial focus was placed on glass particles due to their well-defined chemical composition and surface properties, which made them a suitable model material for evaluating treatment effects. Several types of surface modifications have been designed and tested, with current attention primarily on hydrogen and oxygen plasma treatments aiming to improve the ITZ [13]. Building on the findings obtained with glass, future experiments will extend these surface treatment methods to other recycled materials, such as waste concrete or marble processing residues.

Plasma surface treatment has emerged in recent years as an effective method to enhance interaction between the binder and filler in cementitious composites or fibers [52]. One of the key factors influencing the mechanical properties of cementitious materials is the quality of the ITZ between the cement matrix and the additives. Plasma-treated particles exhibit higher reactivity, which improves hydration reactions and reduces porosity in the ITZ.

Plasma modification can be carried out using various gases, such as oxygen or hydrogen, which influence the final properties of the material. The intensity and duration of exposure also

play significant roles. Studies have shown that oxygen plasma treatment creates a hydrophilic surface on the particles, which promotes the formation of C-S-H gel and reduces the volume of fine pores in the cement matrix. The result is a denser and more homogeneous microstructure with improved adhesion between the cement paste and the modified particles.

Experimental studies have shown that cementitious composites with 10 wt.% and 20 wt.% replacement of cement by plasma-treated waste glass exhibit an increase in compressive strength of 10–15% after 90 days of curing. This phenomenon suggests that plasma treatment contributes to better bonding between the binder and additives, supporting more efficient use of secondary raw materials in construction [13].

Microstructural analyses using SEM-BSE reveal that the ITZ becomes significantly denser due to plasma treatment, with a notable reduction in capillary porosity. This effect can be attributed to enhanced interaction between the modified filler and hydration products, leading to stronger bonding and a more uniform distribution of hydration phases.

Plasma treatment also improves the pozzolanic activity of certain secondary materials such as waste glass particles, recycled concrete powder, and fly ash. Increased reactivity of these additives allows for partial or complete replacement of cement, thereby reducing the environmental footprint of cement composite production [53].

In terms of mechanical performance, it has been shown that ITZ optimization via plasma treatment can lead to improved strength characteristics (compressive and flexural strength), reduced shrinkage cracking, and enhanced resistance to aggressive environments. Importantly, this process can be scaled and applied to various secondary raw materials, opening new opportunities for sustainable construction and the incorporation of recycled materials in cementitious composites. For more see Fig. 3.1 and Fig. 3.2 [13].

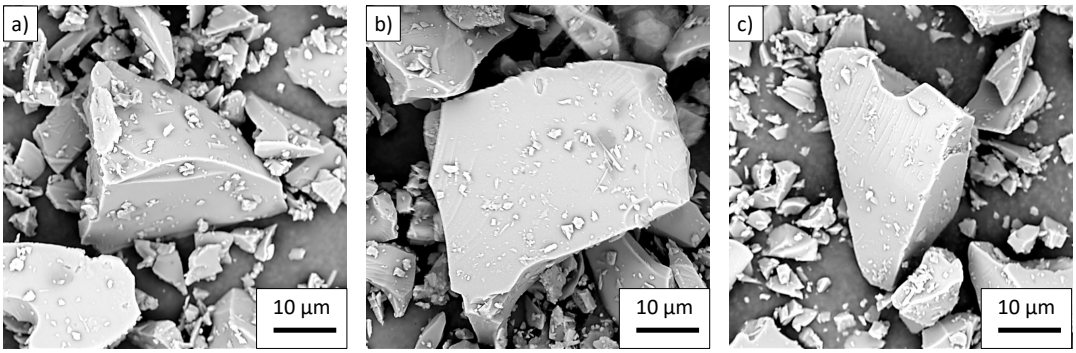

Figure 3.1: Images from the SEM microscope, magnified 4.5k×, BSE detector: a) untreated WGP, b) WGP treated with oxygen plasma O_2, c) WGP treated with hydrogen plasma H_2 [13].

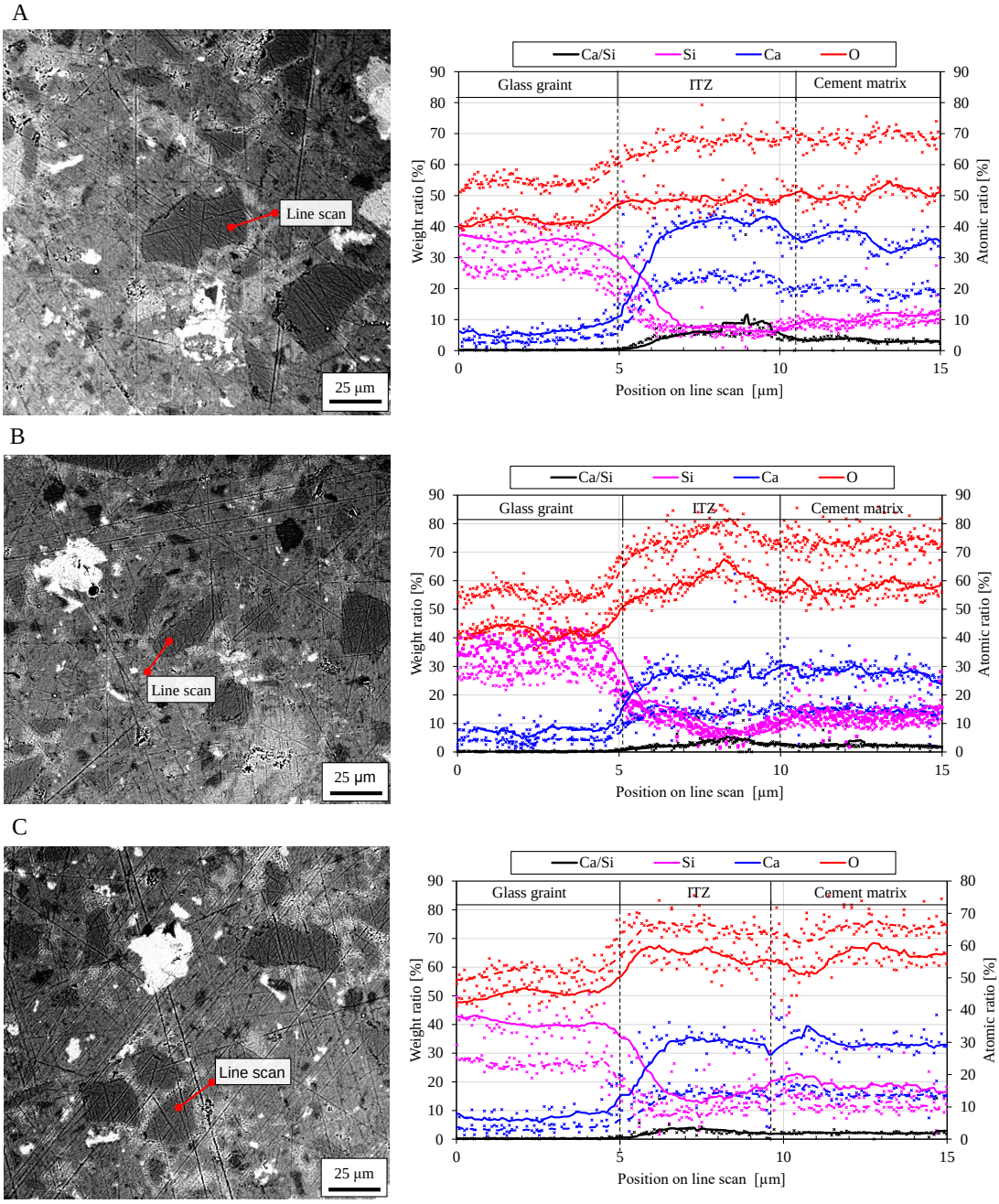

Figure 3.2: EDS line scan analysis over a 15 μm distance by SEM, showing the ITZ between glass grains and the cement matrix in samples with WGP treted: (a) Untreated, (b) oxygen-treated, and (c) hydrogen-treated. The graphs display the weight and atomic ratios of silicon (Si), calcium (Ca), and oxygen (O), along with the Ca/Si ratio [13].

Chapter 4

Conclusion

In addition to publications in peer-reviewed journals and contributions to conference proceedings, the data obtained from the research enabled further developments within applied research. These were carried out in cooperation with industrial partners, either as part of national projects, one European project, or via contract research under institutional economic activities.

The following outputs, directly linked to the research field of this work, have been registered:

Utility Models:

- Tesárek, P.; **Prošek, Z.**; Podolský, J.; Neckář, I.; Karra'a, G.; Žyrek, M.; Nyč, M.; Sekavová, H. *Dry gypsum mixture*. Czechia. Utility Model CZ 37560. 2023-12-12.
- **Prošek, Z.**; Trejbal, J.; Zobal, O.; Karra'a, G.; Pokrivčák, M. *Dry mortar mix*. Czechia. Utility Model CZ 36153. 2022-06-14.
- Tesárek, P.; **Prošek, Z.**; Ryparová, P.; Sekavová, H.; Nyč, M. *Gypsum-based composite mixture*. Czechia. Utility Model CZ 34414. 2020-09-22.
- Valentin, J.; **Prošek, Z.**; Vacková, P. *Road blended hydraulic binder with activated blast furnace slag and mineral dust*. Czechia. Utility Model CZ 33780. 2020-02-25.
- Valentin, J.; **Prošek, Z.**; Vacková, P. *Alternative hydraulic binder with activated blast furnace slag*. Czechia. Utility Model CZ 33781. 2020-02-25.
- Tesárek, P.; **Prošek, Z.**; Sekavová, H.; Karra'a, G.; Nyč, M. *Dry gypsum mixture*. Czechia. Utility Model CZ 33058. 2019-07-30.
- Tesárek, P.; **Prošek, Z.**; Karra'a, G. *Lightweight composite construction element*. Czechia. Utility Model CZ 32790. 2019-04-16.

Verified Technologies:

- Karra'a, G.; Tesárek, P.; **Prošek, Z.**; Podolský, J.; Sekavová, H.; Nyč, M. *Simplified separation and recycling line for gypsum board waste*. 2023.

- Tesárek, P.; Pavlů, T.; Podolský, J.; Foltýn, J.; **Prošek, Z.** *Pilot project for building deconstruction*. 2023.
- Sekavová, H.; Nyč, M.; Zobal, O.; Karra'a, G.; Tesárek, P.; **Prošek, Z.** *Recycling of gypsum boards from production to production*. 2020.
- Karra'a, G.; Cibulka, M.; **Prošek, Z.**; Tesárek, P. *Production of lightweight blocks with treated recycled concrete aggregate*. 2019.

European Patent:

- Demo, P.; **Prošek, Z.** *Use of a layer for surface protection and/or preservation of a tangible cultural heritage*. 2020.

Through collaboration with industrial partners, these outputs have contributed to achieving the project's primary goal – the implementation of micronized recycled materials into practice through applied research. Ongoing experimental research and development activities are building on the published results and are expected to yield further practically applicable outcomes.

References

[1] Hana Sekavová, **Zdeněk Prošek**, and Pavel Tesárek. Optimizing properties of gypsum mixtures through modifications of construction gypsum board waste. *Waste Forum*, (1): 29–38, 2024. ISSN 1804–0195.

[2] Pavel Tesárek, Jan Trejbal, Jan Richter, and **Zdeněk Prošek**. Use of mineral wool in building envelopes with regards to their future recycling. *Waste Forum*, (2):97–107, 2021. ISSN 1804–0195.

[3] **Zdeněk Prošek**, Václav Nežerka, Radim Hlůžek, Jan Trejbal, Pavel Tesárek, and George Karra'a. Role of lime, fly ash, and slag in cement pastes containing recycled concrete fines. *Construction and Building Materials*, 201:702–714, 2019. DOI: 10.1016/j.conbuildmat.2018.12.227.

[4] **Zdeněk Prošek**, Václav Nežerka, Tomáš Plachý, Martin Bartoš, and Pavel Tesárek. PVA increases efficiency of bacterially-induced self-healing in cement mortars. *Cement and Concrete Composites*, 131:104593, 2022. DOI: 10.1016/j.cemconcomp.2022.104593.

[5] Petr Svora, Sylwia Svorová Pawełkowicz, Petra Ecorchard, Jiří Plocek, Alena Schieberová, **Zdeněk Prošek**, Petr Ptáček, Jan Pošta, Piotr Targowski, and Petr Kuklík. Study of interactions between titanium dioxide coating and wood cell wall ultrastructure. *Nanomaterials*, 12(15):2678, 2022. DOI: 10.3390/nano12152678.

[6] Petr Kuklík, **Zdeněk Prošek**, and Anna Gregorová. Comprehensive approach to ensure durabilty of external wooden structures. *WOOD RESEARCH*, 66(6):900–911, 2021. DOI: 10.37763/WR.1336-4561/66.6.900911.

[7] Sylwia Svorová Pawełkowicz, Petr Svora, **Zdeněk Prošek**, Martin Keppert, Eva Vejmelková, Natalija Murafa, Tomasz Sawoszczuk, Justyna Syguła-Cholewińska, and Hana Bíbová. Laboratory assessment of a photoactive gypsum-based repair plaster. *Construction and Building Materials*, 346:128426, 2022. DOI: 10.1016/j.conbuildmat.2022.128426.

[8] Jan Trejbal, Tereza Horová, and **Zdeněk Prošek**. Pullout behavior of oxygen plasma treated polymer fibers from cement matrix. *Acta Polytechnica CTU Proceedings*, 13: 130–134, 2017.

[9] Oleg Babčenko, Zdeněk Remeš, Klára Beranová, Kateřina Kolářová, Jan Čermák, Alexander Kromka, **Zdeněk Prošek**, and Pavel Tesárek. Characterization of different

types of silica-based materials. In *Journal of Physics: Conference Series*, volume 2712, page 012010. IoP Publishing, 2024.

[10] **Zdeněk Prošek**, Jan Trejbal, Václav Nežerka, Viktor Goliáš, Miloš Faltus, and Pavel Tesárek. Recovery of residual anhydrous clinker in finely ground recycled concrete. *Resources, Conservation and Recycling*, 155:104640, 2020. DOI: 10.1016/j.resconrec.2019.104640.

[11] Jan Pešta and **Zdeněk Prošek**. Environmental perspectives of fine grounded concrete powder: LCA case study of light-weight concrete block. *Acta Polytechnica CTU Proceedings*, 34:69–74, 2022.

[12] Václav Nežerka, **Zdeněk Prošek**, Jan Trejbal, Jan Pešta, Juan Antonio Ferriz-Papi, and Pavel Tesárek. Recycling of fines from waste concrete: Development of lightweight masonry blocks and assessment of their environmental benefits. *Journal of Cleaner Production*, 385:135711, 2023. DOI: 10.1016/j.jclepro.2022.135711.

[13] **Zdeněk Prošek**, Jiří Němeček, Martina Záleská, Oleg Babcenko, Klára Beranová, Pavel Machek, Alexander Kromka, and Pavel Tesárek. Surface modification of waste glass powder by plasma treatment: Impact on cement paste microstructure and strength development. *Construction and Building Materials*, 485:141693, 2025. DOI: 10.1016/j.conbuildmat.2025.141693.

[14] D. Gastaldi, F. Canonico, L. Capelli, L. Buzzi, E. Boccaleri, and S. Irico. An investigation on the recycling of hydrated cement from concrete demolition waste. *Cement and Concrete Composites*, 61:29–35, 2015. DOI: 10.1016/j.cemconcomp.2015.04.010.

[15] M.V.A. Florea, Z. Ning, and H.J.H. Brouwers. Activation of liberated concrete fines and their application in mortars. *Construction and Building Materials*, 50:1–12, 2014. DOI: 10.1016/j.conbuildmat.2013.09.012.

[16] N Ganesan, Ruby Abraham, and S Deepa Raj. Durability characteristics of steel fibre reinforced geopolymer concrete. *Construction and Building Materials*, 93:471–476, 2015.

[17] D.P Bentz, O.M Jensen, A.M Coats, and F.P Glasser. Influence of silica fume on diffusivity in cement-based materials. *Cement and Concrete Research*, 30:953–962, 2000. DOI: 10.1016/s0008-8846(00)00264-7.

[18] Aliakbar Gholampour and Togay Ozbakkaloglu. Performance of sustainable concretes containing very high volume class-f fly ash and ground granulated blast furnace slag. *Journal of Cleaner Production*, 162:1407–1417, 2017. DOI: 10.1016/j.jclepro.2017.06.087.

[19] L. Evangelista and J. de Brito. Concrete with fine recycled aggregates: a review. *European Journal of Environmental and Civil Engineering*, 18:129–172, 2013. DOI: 10.1080/19648189.2013.851038.

[20] *BS EN 206-1:2013: Concrete. Specification, performance, production and conformity*. British Standards Institution, London, 2013. DOI: 10.3403/30257890u.

[21] Shengli Zhang, Changsuo Zhang, Lin Liao, and Chenlong Wang. Numerical study of the effect of ITZ on the failure behaviour of concrete by using particle element modelling. *Construction and Building Materials*, 170:776–789, 2018. DOI: 10.1016/j.conbuildmat.2018.03.040.

[22] Dale P. Bentz and Paul E. Stutzman. Evolution of porosity and calcium hydroxide in laboratory concretes containing silica fume. *Cement and Concrete Research*, 24: 1044–1050, 1994. DOI: 10.1016/0008-8846(94)90027-2.

[23] F. Cartuxo, J. de Brito, L. Evangelista, J.R. Jiménez, and E.F. Ledesma. Rheological behaviour of concrete made with fine recycled concrete aggregates – influence of the superplasticizer. *Construction and Building Materials*, 89:36–47, 2015. DOI: 10.1016/j.conbuildmat.2015.03.119.

[24] Ali A. Aliabdo, Abd M. Elmoaty, and Esraa M. Auda. Re-use of waste marble dust in the production of cement and concrete. *Construction and Building Materials*, 50:28–41, jan 2014. ISSN 09500618. DOI: 10.1016/j.conbuildmat.2013.09.005. URL http://www.sciencedirect.com/science/article/pii/S0950061813008453.

[25] **Zdeněk Prošek**, Václav Nežerka, and Pavel Tesárek. Enhancing cementitious pastes with waste marble sludge. *Construction and Building Materials*, 255:119372, 2020. DOI: 10.1016/j.conbuildmat.2020.119372.

[26] Václav Nežerka, Vladimír Hrbek, **Zdeněk Prošek**, Michal Somr, Pavel Tesárek, and Josef Fládr. Micromechanical characterization and modeling of cement pastes containing waste marble powder. *Journal of Cleaner Production*, 195:1081–1090, 2018. DOI: 10.1016/j.jclepro.2018.05.284.

[27] Václav Nežerka and Jan Trejbal. Assessment of aggregate-bitumen coverage using entropy-based image segmentation. *Road Materials and Pavement Design*, pages 1–12, 2019. DOI: 10.1080/14680629.2019.1605304.

[28] Deepankar Kumar Ashish. Concrete made with waste marble powder and supplementary cementitious material for sustainable development. *Journal of cleaner production*, 211: 716–729, 2019.

[29] Alyamaç,, Ehsan Ghafari, and Ragip Ince. Development of eco-efficient self-compacting concrete with waste marble powder using the response surface method. *Journal of Cleaner Production*, 144:192–202, 2017. DOI: 10.1016/j.jclepro.2016.12.156.

[30] Omrane Benjeddou, Rayed Alyousef, Hossein Mohammadhosseini, Chokri Soussi, Mohamed Amine Khadimallah, Hisham Alabduljabbar, and Mahmood Md Tahir. Utilisation of waste marble powder as low-cost cementing materials in the production of mortar. *Journal of Building Engineering*, 32:101642, 2020.

[31] Jaroslav Topič and **Zdeněk Prošek**. Properties and microstructure of cement paste including recycled concrete powder. *Acta Polytechnica*, 57(1):49–57, 2017.

[32] Joris Schoon, Klaartje De Buysser, Isabel Van Driessche, and Nele De Belie. Fines extracted from recycled concrete as alternative raw material for portland cement clinker production. *Cement and Concrete Composites*, 58:70–80, 2015.

[33] Zhonghe Shui, Dongxing Xuan, Huiwen Wan, and Beibei Cao. Rehydration reactivity of recycled mortar from concrete waste experienced to thermal treatment. *Construction and Building Materials*, 22:1723–1729, 2008. DOI: 10.1016/j.conbuildmat.2007.05.012.

[34] Jaroslav Topič and **Zdeněk Prošek**. Micronized concrete powder as mircofiller in cement paste: Influence on hydration and structure. *Acta Polytechnica CTU Proceedings*, 30:109–113, 2021.

[35] Ravindra K Dhir OBE, Jorge de Brito, Rui V Silva, and Chao Qun Lye. *Sustainable construction materials: recycled aggregates*. Woodhead Publishing, 2019.

[36] Carlos Thomas García, J de Brito, Ana Isabel Cimentada Hernández, José Adolfo Sainz-Aja Guerra, et al. Macro-and micro-properties of multi-recycled aggregate concrete. 2020.

[37] Paul O Awoyera, Olusola E Babalola, and Oluwatobi G Aluko. The use of slags in recycled aggregate concrete. In *The Structural Integrity of Recycled Aggregate Concrete Produced with Fillers and Pozzolans*, pages 145–170. Elsevier, 2022.

[38] Georgiy Kovalchuk, A Fernández-Jiménez, and A Palomo. Alkali-activated fly ash. relationship between mechanical strength gains and initial ash chemistry. *Materiales de construccion*, 58(291):35–52, 2008.

[39] MCG Juenger, Frank Winnefeld, J Lt Provis, and JH Ideker. Advances in alternative cementitious binders. *Cement and concrete research*, 41(12):1232–1243, 2011.

[40] Christian Meyer. The greening of the concrete industry. *Cement and concrete composites*, 31(8):601–605, 2009.

[41] Vivian WY Tam, XF Gao, and Chi M Tam. Microstructural analysis of recycled aggregate concrete produced from two-stage mixing approach. *Cement and concrete research*, 35(6):1195–1203, 2005.

[42] Pavla Ryparová, **Zdeněk Prošek**, Hana Schreiberova, Petr Bílý, and Pavel Tesárek. The role of bacterially induced calcite precipitation in self-healing of cement paste. *Journal of Building Engineering*, 39:102299, 2021.

[43] Virginie Wiktor and Henk M Jonkers. Quantification of crack-healing in novel bacteria-based self-healing concrete. *Cement and concrete composites*, 33(7):763–770, 2011.

[44] Yusuf Çağatay Erşan, Emma Hernandez-Sanabria, Nico Boon, and Nele De Belie. Enhanced crack closure performance of microbial mortar through nitrate reduction. *Cement and concrete composites*, 70:159–170, 2016.

[45] Henk M Jonkers, Arjan Thijssen, Gerard Muyzer, Oguzhan Copuroglu, and Erik Schlangen. Application of bacteria as self-healing agent for the development of sustainable concrete. *Ecological engineering*, 36(2):230–235, 2010.

[46] **Zdeněk Prošek**, Pavla Ryparová, and Pavel Tesárek. Využití odpadního mramorového kalu jako zdroje vápníku pro samohojivé betony s využitím bioremediace. *Waste Forum*, 3:177–184, 2020.

[47] J.Y. Wang, D. Snoeck, S. Van Vlierberghe, W. Verstraete, and N. De Belie. Application of hydrogel encapsulated carbonate precipitating bacteria for approaching a realistic self-healing in concrete. *Construction and Building Materials*, 68:110–119, 2014. ISSN 0950-0618. DOI: https://doi.org/10.1016/j.conbuildmat.2014.06.018.

[48] Jaroslav Topič, **Zdeněk Prošek**, Kateřina Indrová, Tomáš Plachý, Václav Nežerka, Lubomír Kopecký, and Pavel Tesárek. Effect of PVA modification on properties of cement composites. *Acta Polytechnica*, 55(1):64–75, 2015.

[49] **Zdeněk Prošek**, Pavla Ryparová, and Pavel Tesárek. Application of bacteria as self-healing agent for the concrete and microscopic analysis of the microbial calcium precipitation process. *Key Engineering Materials*, 846 KEM:237 – 242, 2020. DOI: 10.4028/www.scientific.net/KEM.846.237. Cited by: 5.

[50] Chunxiao Li, Dongmei Wang, and Lingyun Kong. Application of machine learning techniques in mineral classification for scanning electron microscopy - energy dispersive x-ray spectroscopy (sem-eds) images. *Journal of Petroleum Science and Engineering*, 200:108178, 2021. ISSN 0920-4105. DOI: https://doi.org/10.1016/j.petrol.2020.108178.

[51] Juwon Na, Gyuwon Kim, Seong-Hoon Kang, Se-Jong Kim, and Seungchul Lee. Deep learning-based discriminative refocusing of scanning electron microscopy images for materials science. *Acta Materialia*, 214:116987, 2021. ISSN 1359-6454. DOI: https://doi.org/10.1016/j.actamat.2021.116987.

[52] Radim Hlůžek, Jan Trejbal, Václav Nežerka, Petr Demo, **Zdeněk Prošek**, and Pavel Tesárek. Improvement of bonding between synthetic fibers and a cementitious matrix using recycled concrete powder and plasma treatment: from a single fiber to frc. *European Journal of Environmental and Civil Engineering*, 24(16):1910–1927, 2020. DOI: 10.1080/19648189.2020.1824821.

[53] K. Shafiei and B. Hillemeier. Feasibility of plasma technology utilization in concrete industry. *International Journal of Research in Engineering and Technology*, 3(25): 63–70, 2014. DOI: 10.15623/ijret.2014.0325011.

Appendix A

Nežerka, V.; Hrbek, V.; **Prošek, Z.**; Somr, M.; Tesárek, P.; Fládr, J.: Micromechanical characterization and modeling of cement pastes containing waste marble powder, *Journal of Cleaner Production*. 2018, 195. 1081–1090. ISSN 0959-6526. doi: 10.1016/j.jclepro.2018.05.284

Author's contribution: main idea, SEM microscopy, data analysis, design of experiments, preparation of specimens.

Journal of Cleaner Production 195 (2018) 1081–1090

Contents lists available at ScienceDirect

Journal of Cleaner Production

journal homepage: www.elsevier.com/locate/jclepro

Micromechanical characterization and modeling of cement pastes containing waste marble powder

V. Nežerka*, V. Hrbek, Z. Prošek, M. Somr, P. Tesárek, J. Fládr

Faculty of Civil Engineering, Czech Technical University in Prague, Thákurova 7, 166 29, Praha 6, Czech Republic

ARTICLE INFO

Article history:
Received 1 March 2018
Received in revised form
28 May 2018
Accepted 31 May 2018
Available online 4 June 2018

Keywords:
Waste marble powder
Cement paste
Characterization
Micromechanics
Nanoindentation

ABSTRACT

A comprehensive study consisting of a microstructure investigation, nanoindentation, and micromechanical modeling was performed to identify phases and assess their impact on macroscopic properties of cement pastes containing waste marble powder. The proposed model, built on the Mori-Tanaka scheme, was used to estimate the effective Young's modulus and compressive strength at a low computational cost. After model validation, the effects of an interfacial transition zone (ITZ) and increased porosity of marble powder rich-pastes were quantified. The study revealed a fundamental role of the ITZ formed around stiff marble powder inclusions, responsible for performance deterioration. These findings indicate that elimination of the ITZ and reduction of porosity would considerably enhance the strength of cement-based materials containing waste marble powder. As a consequence, larger amounts of waste marble could be incorporated as a cement replacement without sacrificing structural performance.

1. Introduction

The energetically demanding production of Portland cement (Siddique, 2004) significantly contributes to CO_2 emissions and environmental pollution (Aruntaş et al., 2010) as concrete has become the most widely used construction material (Gautam et al., 2014). Therefore, even partial substitution of cement with powdered waste can provide significant economic and environmental benefits on the global scale (Nagarajan et al., 2014). Mining by-products appear to be a promising substance for their abundance (Levy and Helene, 2004; Sudarshan and Vyas, 2016) and costs connected to their disposal.

Huge demands for marble products in recent years resulted in utilization of blast mining techniques yielding a massive amount of waste material (Mashaly et al., 2016; Singh et al., 2017). There are basically two types of waste: (1) disintegrated rocks and (2) more challenging fine-grained powder produced by sawing, shaping, and polishing of final products (Akbulut and Gürer, 2007; Sata et al., 2007). The former can be easily sorted and utilized as coarse aggregate in construction industry (Rai et al., 2011). However, the latter constitutes an enormous environmental burden (Corinaldesi et al., 2010; da Silva et al., 2014), and the waste accumulation prevents expansion of the mining sites. Because of the composition rich in $CaCO_3$ (Mashaly et al., 2016), marble or limestone powder can be efficiently utilized in a production of self-compacting concrete (Corinaldesi et al., 2010; Lee et al., 2008; Ho et al., 2002; Alyamaç et al., 2017), light-weight concrete (Turgut and Murat Algin, 2007), prefabricated building units (Dhanapandian and Gnanavel, 2010; Kaosol, 2010), or bricks (Marras et al., 2017; Alzboon and Mahasneh, 2009; Bilgin et al., 2012).

The majority of authors concluded that 5–10% addition of marble powder contributes to strength enhancement, while incorporation of higher amounts results in an opposite effect (Corinaldesi et al., 2010; Topçu and Canbaz, 2007; Aliabdo et al., 2014). Alyamaç and Aydin (2015) carried out a feasibility study to find that up to 40% sand replacement in concrete is acceptable from structural and economical point of view. However, most of the studies are purely experimental, and little attention is paid to the micromechanical behavior of cementitious composites containing the marble powder. The knowledge of microstructure and micromechanical behavior combined with the formulation of a suitable micromechanical model can significantly increase utilization of the powder in cementitious composites without sacrificing their structural performance.

Despite the complexity of concrete microstructure, the mechanical behavior can be successfully predicted using models based

* Corresponding author.
E-mail address: vaclav.nezerka@fsv.cvut.cz (V. Nežerka).

https://doi.org/10.1016/j.jclepro.2018.05.284
0959-6526/

Table 1
Chemical composition of Portland cement and marble powder; most important components identified by the XRF.

Component	Portland cement	Marble powder
	wt% (±0.5%)	
CaO	66.1	57.5
SiO_2	20.4	1.02
Al_2O_3	3.90	0.14
Fe_2O_3	2.86	1.22
SO_3	2.87	0.06
MgO	1.92	0.39
Na_2O	0.00	0.73
LOI	1.95	37.4

on continuum micromechanics (Šmilauer et al., 2011; Vorel et al., 2012; Pichler et al., 2007; Pichler and Hellmich, 2011). In order to formulate the micromechanical model properly, it is essential to have deep knowledge about properties and distribution of individual phases that can be recognized at the modeled scale. Such detailed information about elastic properties of the phases can be provided by nanoindentation. This technique was exploited, e.g., for assessment of micromechanical properties of cement pastes (Hughes and Trtik, 2004; Constantinides and Ulm, 2004; Němeček et al., 2013), identification of phases in gypsum (Tesárek and Němeček, 2011) or interfacial transition zone (ITZ) around crushed brick fragments in ancient mortars (Nežerka et al., 2015). Neubauer et al. (1996) determined elastic properties of the ITZ around aggregates in concrete by fitting a micromechanical model to experimental data.

In the presented study, microscopy investigation combined with grid nanoindentation were employed to investigate the individual phases in cement pastes containing marble powder, including the ITZ between the marble powder inclusion and the surrounding cementitious matrix. The analytical Mori-Tanaka homogenization scheme was employed to compute effective elasticity parameters and the deviatoric stress invariant (J_2) in the matrix was calculated in order to estimate the effective compressive strength based on the von Mises failure criterion. The micromechanical model was validated against experimental measurements on macroscopic specimens containing a variable amount of marble powder.

2. Material and methods

Many authors have addressed a purely experimental approach to find an optimum mix design, and their studies provide valuable information about the impact of marble powder additions on the behavior of cementitious composites. The presented holistic strategy consisting of the micromechanical characterization and analytical homogenization allowed to explain the phenomena leading to the changes in their effective stiffness/strength. All the presented calculations can be reproduced using Python scripts available at the author's website.[1]

2.1. Investigated materials and samples

The pastes were prepared from Portland cement CEM I 42.5R and marble powder from marble waste produced during mining in the West Bank of Jordan River, finely ground using a high-speed 2×30 kW mill SKD 600, produced by Lavaris company.

The chemical composition of both components (Table 1) was determined by the X-ray fluorescence (XRF) spectrometry using a SPECTRO XEPOS spectrometer equipped with 50 W/60 kV X-ray tube. The results indicate that the marble powder consisted mostly of calcium carbonate ($CaCO_3$), derived from the detected concentration of CaO, while the minor phases represent impurities in the form of clay size fraction rich in silica (Si) (Mashaly et al., 2012). The particle size distribution curves, determined using a Malvern Mastersizer 3000 laser diffraction particle size analyzer, are provided in Fig. 1. The curves indicate that, in terms of micromechanical modeling, cement grains and marble inclusions can be distinguished at the same scale. The inclination of the curves indicates similar packing of both materials.

When preparing the samples, Portland cement was blended with the marble powder using an electric blender for 5 min at 235 rotations per minute, and for 10 min at the same speed after adding water into the dry homogenized mixture. The ratio between the weight of water and mixture of cement and marble powder (w/cm) was kept constant and relatively low, $w/cm = 0.35$, to avoid excessive shrinkage cracking (Idiart et al., 2012; Nežerka et al., 2014a). The pastes were cast into prismatic molds with dimensions $40 \times 40 \times 160$ mm and removed after 24 h. During casting, the pastes were compacted using the shaking table in order to eliminate bubbles. The standard flow table test was carried out according to European Standard EN 12350-5 (2009); the records measured in two perpendicular directions after 15 table drops are summarized in Table 2. Curing was executed in atmospheric air at 22 ± 1 °C and relative humidity of 50 ± 2% for 28 days. Six prismatic specimens represented each batch with a distinct cement-to-marble powder ratio.

Besides the prismatic specimens, each batch was represented by three cylindrical specimens of 25 mm in diameter. These were cut into 15 mm thick slices and polished to be investigated by microscopy and nanoindentation. In addition, samples of pure marble powder embedded in epoxy resin (marble-resin mass ratio 1:3), having the same cylindrical geometry, were also prepared to assess the elastic stiffness of pure marble inclusions not influenced by the cementitious matrix. The specimens were polished on MD-Piano

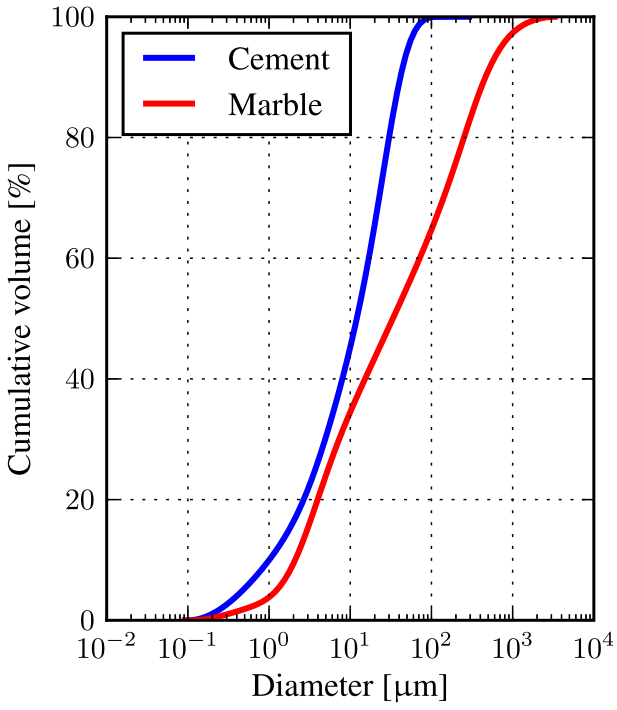

Fig. 1. Particle size distribution curves for Portland cement and marble powder.

[1] http://mech.fsv.cvut.cz/~nezerka/software.htm.

Table 2
Summary of prepared mixes; percentages represent mass ratio of individual constituents.

Mix	Portland cement	Marble powder	w/cm	Flow test result [mm]
C100	100%	0%	0.35	25.2×25.6
C95	95%	5%	0.35	26.0×26.0
C90	90%	10%	0.35	26.4×26.2
C85	85%	15%	0.35	26.3×26.3
C80	80%	20%	0.35	26.3×26.4
C75	75%	25%	0.35	26.3×26.8
C50	50%	50%	0.35	26.9×26.9

grinding plate using 1200, 2000, and 4000 grain/cm^2 grit under 0.25 N compression without using any lubricants. Moreover, the specimens were cleaned with ethanol after each step using an ultrasound cleaner. Such a sequential approach ensured non-invasive polishing (Hrbek et al., 2017).

2.2. Microstructure investigation

The knowledge of a microstructure is essential for micromechanical modeling and understanding the behavior of a composite at the microscale. Many authors investigated the micromechanical properties of cement paste, e.g., Hughes and Trtik (2004); Constantinides and Ulm (2004); Němeček et al. (2013), and the properties of powdered marble can be derived from the behavior of macroscopic marble specimens. The most scientifically challenging and attractive part is the interface between these components when blended. The presence of stiff inert aggregates in a cementitious matrix results in the formation of the ITZ, which is usually weaker than the matrix (Neubauer et al., 1996; Dela and Stang, 2000; Nežerka et al., 2014b). On the other hand, several authors suggested that the addition of fine-grained marble/limestone can have a positive effect on hydration (Adu-Amankwah et al., 2017; Moon et al., 2017).

2.2.1. Porosimetry

The pore size distribution was determined using mercury intrusion porosimetry. It has been proven by Quellet et al. (2007) that, despite several simplifying assumptions, this method can determine the size of pores in cement-based materials with sufficient accuracy. The analysis was carried out using Poremaster PM 60-13 Quantachrome instrument working within the pressure range of 0.005–413 MPa. The surface tension of the mercury was equal to 480 erg/cm^2 and the contact angle to 140°.

2.2.2. Morphological and chemical analyses

The polished samples, coated with a 30 nm carbon layer to increase electric conductivity, were investigated by scanning electron microscope (SEM) using a FEG-SEM Merlin ZEISS microscope. The SEM analysis in backscattered electron microscopy (BSE) mode enabled highlighting individual phases of interest, i.e., cementitious matrix and marble powder inclusions (Scrivener et al., 1986).

2.2.3. Nanoindentation

The stiffness assessment of the individual phases was accomplished using a nanohardness tester TI 750 Hysitron Triboindentor (Hysitron Inc., Minnesota, USA) equipped with Berkovich diamond tip. The indentation was displacement-controlled, and Young's modulus was determined from the unloading part of the load-displacement diagram using Oliver and Pharr method (Oliver and Pharr, 1992). The stiffness of marble powder inclusions was determined from several measurements. Selective indentation with a constant load function was applied to the samples of marble powder embedded in epoxy resin in order to obtain mechanical parameters of the raw material.

2.3. Testing of macroscopic stiffness and strength

The Young's modulus of the $40 \times 40 \times 160$ mm specimens was assessed using the resonance method, which is based on the equation for a longitudinal vibration of prismatic specimens with homogeneous mass distribution. The uniaxial compression test was carried out on the $40 \times 40 \times 40$ mm specimens using the LabTest 4.100SP1 loading frame. The loading of specimens was displacement-controlled with a rate of 0.5 mm/min. Compressive strength was calculated by dividing the maximum loading force by the loaded area.

3. Micromechanical model

Micromechanical modeling was employed to confirm the assumptions about the impact of the weak ITZ formed around marble powder inclusions and to make the design of cementitious composites easier, compared to purely experimental trial-and-error procedures. The model formulation has been inspired to a great extent by the previous work dealing with modeling of lime-based mortars (Nežerka et al., 2017) and the work by Pichler and Hellmich (2011). They utilized Mori-Tanaka homogenization scheme (Mori and Tanaka, 1973; Benveniste, 1987) combined with von Mises failure criterion to upscale the compressive strength of cement pastes. The von Mises, J_2 invariant based, the criterion was also used in phenomenological models of cementitious composites, e.g., by Feenstra and de Borst (1995).

3.1. Model description

The proposed micromechanical model of cement pastes containing marble powder operates at a single scale. A representative volume element (RVE) composed of m phases indexed by r is considered. The matrix is represented by $r = 0$ and indices $r = 1, \ldots, m$ refer to heterogeneities of a spherical shape or, in the case of the ITZ, a spherical shell (Fig. 2). Such a simplification of morphology (Table 3) brings computational benefits, while the introduced error (Stránský et al., 2011; Pichler et al., 2009) is minor with respect to the large scatter of input data (Section 4.4). The volume fraction of the individual phases was calculated as a ratio of the volume occupied by the rth phase and the total RVE volume, $c^{(r)} = \Omega^{(r)}/\Omega$.

3.1.1. Elasticity homogenization

The assumed geometrical and material isotropy allows to decompose the stiffness matrix $\mathbf{L}^{(r)}$ using the orthogonal volumetric and deviatoric projections $\mathbf{I}_\mathrm{V}$ and $\mathbf{I}_\mathrm{D}$, e.g., (Milton, 2002, p. 23), as

$$\mathbf{L}^{(r)} = 3K^{(r)}\mathbf{I}_\mathrm{V} + 2G^{(r)}\mathbf{I}_\mathrm{D}, \tag{1}$$

where $K^{(r)}$ and $G^{(r)}$ denote the bulk and shear moduli, respectively.

In the Mori-Tanaka scheme, the strain in individual phases is related to the macroscopic strain, $\boldsymbol{\varepsilon}$, using dilute concentration factors $\mathbf{A}_\mathrm{dil}^{(r)}$ as $\boldsymbol{\varepsilon}^{(r)} = \mathbf{A}_\mathrm{dil}^{(r)}\boldsymbol{\varepsilon}^{(0)}$, where $\boldsymbol{\varepsilon}^{(0)}$ is the strain within the matrix found as

$$\boldsymbol{\varepsilon}^{(0)} = \mathbf{A}_\mathrm{MT}\boldsymbol{\varepsilon}, \tag{2}$$

in which the Mori-Tanaka strain concentration factor $\mathbf{A}_\mathrm{MT}$ is provided as

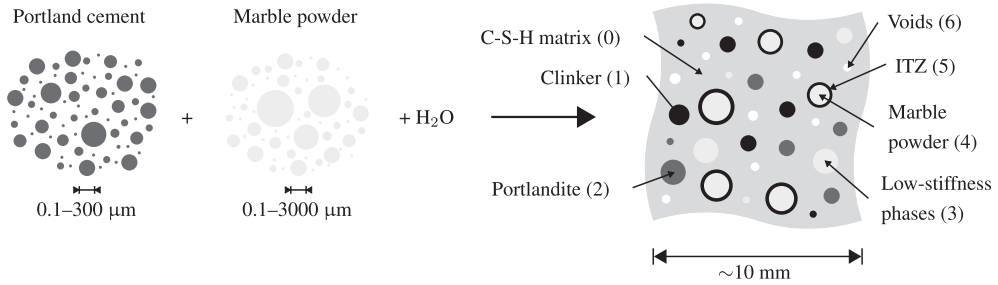

Fig. 2. Scheme of the micromechanical model representing cement-marble powder pastes; the numbers in parentheses refer to the indexes of individual phases. The term "Clinker" refers to the mixture of clinker compounds, mostly alite and belite.

Table 3
Assumptions in a development of the micromechanical model.

Phase	Assumption
C-S-H matrix	Homogeneous and isotropic, von Mises failure criterion in compression
Clinker and Portlandite	Isotropic spherical inclusions, perfect bond with the matrix, elastic
Low-stiffness phases	Isotropic compliant spherical inclusions, perfect bond with the matrix, elastic
Marble powder	Isotropic spherical stiff inclusions, surrounded by the compliant ITZ, elastic
ITZ	Isotropic spherical shells, formed around the marble powder inclusions, elastic
Voids	Isotropic spherical inclusions with zero stiffness

$$\mathbf{A}_{\mathrm{MT}} = \left(c^{(0)}\mathbf{I} + \sum_{r=1}^{m} c^{(r)}\mathbf{A}_{\mathrm{dil}}^{(r)} \right)^{-1}. \tag{3}$$

Because of the assumed isotropy, the effective stiffness can be expressed in terms of the effective bulk and shear moduli as

$$\begin{aligned} K_{\mathrm{eff}} &= \frac{c^{(0)}K^{(0)} + \sum_{r=1}^{m} c^{(r)}K^{(r)}A_{\mathrm{dil,V}}^{(r)}}{c^{(0)} + \sum_{r=1}^{m} c^{(r)}A_{\mathrm{dil,V}}^{(r)}}, \\ G_{\mathrm{eff}} &= \frac{c^{(0)}G^{(0)} + \sum_{r=1}^{m} c^{(r)}G^{(r)}A_{\mathrm{dil,D}}^{(r)}}{c^{(0)} + \sum_{r=1}^{m} c^{(r)}A_{\mathrm{dil,D}}^{(r)}}. \end{aligned} \tag{4}$$

The volumetric and deviatoric components of the dilute concentration factors, $A_{\mathrm{dil,V}}^{(r)}$ and $A_{\mathrm{dil,D}}^{(r)}$, can be expressed as

$$\mathbf{A}_{\mathrm{dil}}^{(r)} = A_{\mathrm{dil,V}}^{(r)}\mathbf{I}_{\mathrm{V}} + A_{\mathrm{dil,D}}^{(r)}\mathbf{I}_{\mathrm{D}}, r = 1, \ldots, m. \tag{5}$$

Analogically to Eq. (4), the volumetric and deviatoric components of the dilute concentration factors for spherical inclusions, following the work of Eshelby (1957), can be decomposed to

$$\begin{aligned} A_{\mathrm{dil,V}}^{(r)} &= \frac{K^{(0)}}{K^{(0)} + \alpha^{(0)}\left(K^{(r)} - K^{(0)}\right)}, \\ A_{\mathrm{dil,D}}^{(r)} &= \frac{G^{(0)}}{G^{(0)} + \beta^{(0)}\left(G^{(r)} - G^{(0)}\right)}, \end{aligned} \tag{6}$$

where $\alpha^{(0)}$ and $\beta^{(0)}$ depend purely on the Poisson's ratio of the C-S-H matrix, $\nu^{(0)}$, as

$$\alpha^{(0)} = \frac{1+\nu^{(0)}}{3\left(1+\nu^{(0)}\right)}, \quad \beta^{(0)} = \frac{2\left(4-5\nu^{(0)}\right)}{15\left(1-\nu^{(0)}\right)}. \tag{7}$$

The expressions for the dilute concentrations factors of particles coated by spherical shells were derived by Herve and Zaoui (1993). To respect the sensitivity of the model to the particle size distribution, the marble powder inclusions and the ITZ must be grouped into m^{δ} sub-phases corresponding to individual particle size intervals denoted by indices (4,δ) and (5,δ), respectively. Then the dilute concentration factors depend on their outer radii, $R^{(4,\delta)}$ and $R^{(5,\delta)}$, and Poisson's ratios, $\nu^{(4)}$ and $\nu^{(5)}$, as follows

$$A_{\mathrm{dil,V}}^{(4,\delta)} = \frac{1}{Q_{11}^2}, \quad A_{\mathrm{dil,V}}^{(5,\delta)} = \frac{Q_{11}^1}{Q_{11}^2} \tag{8}$$

and

$$\begin{aligned} A_{\mathrm{dil,D}}^{(2,\delta)} &= A_1 - \frac{21}{5}\,\frac{R^{(2,\delta)2}}{1-2\nu^{(2)}}B_1, \\ A_{\mathrm{dil,D}}^{(3,\delta)} &= A_2 - \frac{21}{5}\,\frac{R^{(3,\delta)5} - R^{(2,\delta)5}}{\left(1-2\nu^{(3)}\right)\left(R^{(3,\delta)3} - R^{(2,\delta)3}\right)}B_2, \end{aligned} \tag{9}$$

where the auxiliary factors Q_{11}^1, Q_{11}^2, A_1, A_2, B_1, and B_2 are provided in (Nežerka and Zeman, 2012, Appendix A).

The volume fractions of the ITZ, $c^{(5,\delta)}$, are determined from volume fractions of the marble powder sub-phases, $c^{(4,\delta)}$, as

$$c^{(5,\delta)} = \left(\left(\frac{R^{(5,\delta)}}{R^{(4,\delta)}} \right)^3 - 1 \right) c^{(4,\delta)}, \tag{10}$$

and the total ITZ volume fraction $\sum_{\delta=1}^{m^{\delta}} c^{(5,\delta)}$ is subtracted from the volume fraction of matrix, $c^{(0)}$.

3.1.2. Strength upscaling

To estimate the response of cement-marble powder pastes to uniaxial compression, the von Mises failure criterion defined as

$$\sqrt{J_2^{(0)}} - \frac{f_{\mathrm{c}}^{(0)}}{\sqrt{3}} = 0, \tag{11}$$

is considered. The matrix compressive strength is represented by $f_{\mathrm{c}}^{(0)}$, while the second deviatoric stress invariant for the matrix, $J_2^{(0)}$, is determined from the average matrix stress, $\boldsymbol{\sigma}^{(0)}$, as

$$J_2^{(0)} = \frac{1}{2}\boldsymbol{\sigma}^{(0)\mathrm{T}}\mathbf{I}_\mathrm{D}\boldsymbol{\sigma}^{(0)}. \tag{12}$$

The average stress in the matrix $\boldsymbol{\sigma}^{(0)}$ is related to the macroscopic stress $\boldsymbol{\sigma}$ via

$$\boldsymbol{\sigma}^{(0)} = \mathbf{L}^{(0)}\mathbf{A}_\mathrm{MT}\left(\mathbf{L}_\mathrm{eff}\right)^{-1}\boldsymbol{\sigma}. \tag{13}$$

The effective compressive strength of the cement-marble powder pastes, f_c, can be found by subjecting the sample to $\boldsymbol{\sigma} = [-f_c, 0, 0, 0, 0, 0]^\mathrm{T}$, so that the von Mises condition (Eq. (11)) is satisfied.

4. Results and discussion

4.1. Porosity

The presence of marble powder in cement pastes increased the total porosity and size of pores, see Table 4 and Fig. 3 where selected pore size distribution curves are presented. The increased porosity in pastes rich in marble powder is attributed to excessive kneading water bound to the fine inert marble particles. The w/c ratio increased with the higher amount of incorporated marble powder and the excessive water was evaporated from the matrix to form voids. In the pure cement pastes, the diameter of pores ranging between 0.01 μm and 0.1 μm fell between 5th and 95th percentile. After addition of marble powder, the range was extended to 0.01–1.0 μm. Such an increase of pore size is in agreement with findings of Moon et al. (2017).

It was found that there is almost a linear relationship between the portion of cement replaced by marble powder (w_m [%]) and the total porosity of pastes (p_tot [%]), see Fig. 4. By a linear fit to the measured data using least squares, the following relationship was found:

$$p_\mathrm{tot} = 25.535 - 0.113(100 - w_\mathrm{m}). \tag{14}$$

4.2. Distribution of elements

The energy dispersive X-ray detector (EDX) attached to the microscope allowed to study the chemical composition of individual phases in a high resolution. The high concentration of calcium (Ca), revealed by the EDX, represents the marble powder inclusions (Fig. 5).

The distributions of Ca and Si were plotted along a representative line scan, see Fig. 6. The fluctuations in the concentrations result from the chemical heterogeneity of the cementitious materials, consisting of minerals with a various Ca/Si ratio (silicates, aluminates, gypsum, ettringite, portlandite, etc.). The increased Ca content at the inclusion positions reflects that the marble powder was rich in $CaCO_3$. The presence of Si within the inclusion, although very limited, resulted from the contamination by clay size fraction. The Si concentration was about 15 wt% lower in the vicinity (0–40 μm) of the inclusion, followed by a gradual increase in the distance of about 40–80 μm. The high Ca/Si ratio in the close vicinity of the marble powder inclusion (0–40 μm) indicates an increase in the concentration of low-density calcium-silica-hydrate gel (LD C-S-H) (Pellenq et al., 2009; Lothenbach and Nonat, 2015). On the other hand, the low Si concentration and high Ca/Si ratio around 140 μm from the line scan beginning suggests the presence of portlandite ($CaOH_2$).

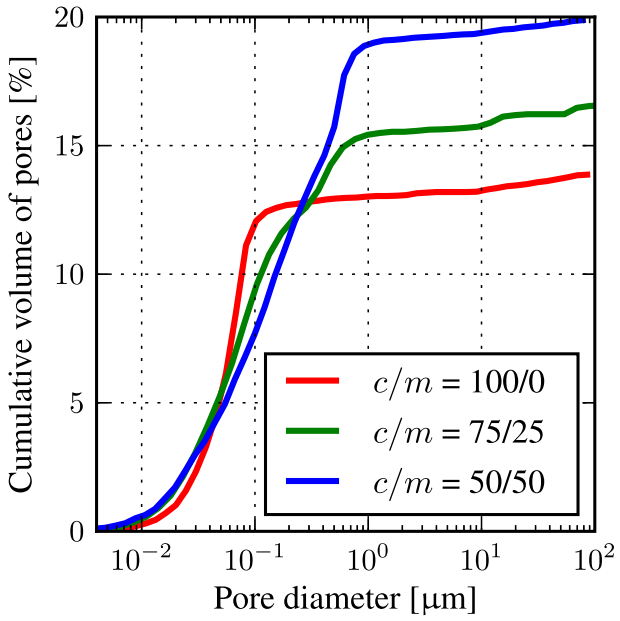

Fig. 3. Pore size distribution for pastes with selected cement/marble ratios.

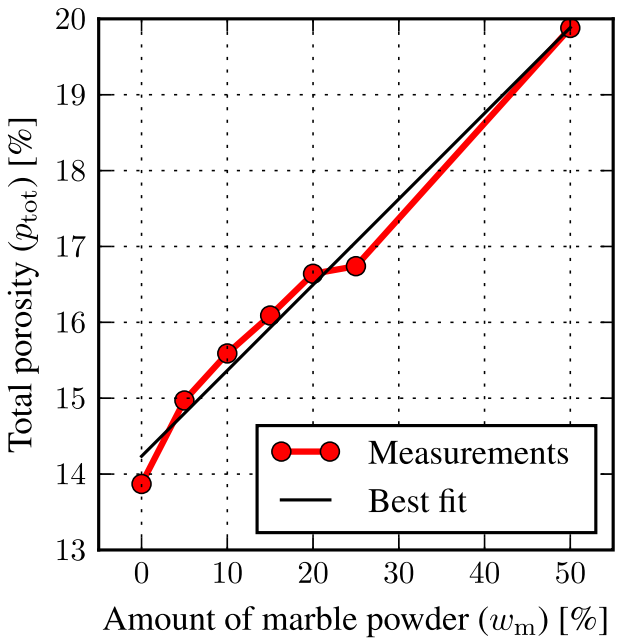

Fig. 4. Dependence of total porosity on the amount of cement replaced by marble powder.

Table 4
Total porosity of pastes with various cement-to-marble powder ratio (c/m).

c/m	100/0	95/5	90/10	85/15	80/20	75/25	50/50
Total porosity (p_tot) [%]	13.87	14.97	15.59	16.09	16.64	16.74	19.88

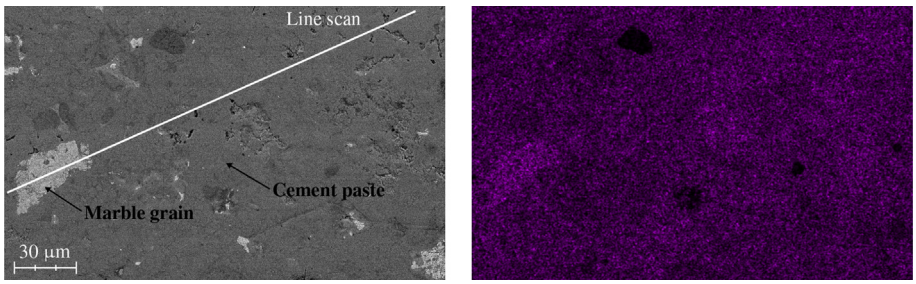

Fig. 5. The BSE image of a marble powder inclusion embedded in a cementitious matrix of the C50 mix sample (left) and the map of Ca distribution over the same area provided by the EDX (right); the black spot in the BSE image represents an area with zero concentration of Ca and rich in SiO_2.

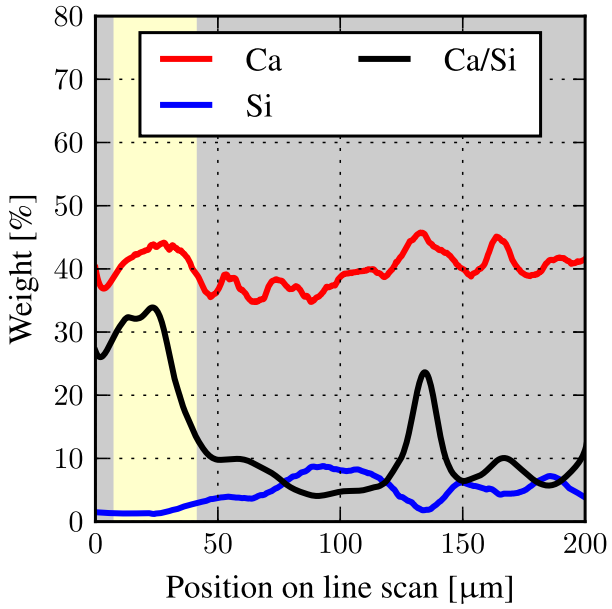

Fig. 6. Concentration of calcium (Ca) and silica (Si), and Ca/Si ratio within a cementitious matrix (grey patch) and a marble powder inclusion (light yellow patch) along a line scan indicated in Fig. 5. (For interpretation of the references to colour in this figure legend, the reader is referred to the Web version of this article.)

4.3. Stiffness distribution

Nanoindentation allowed to study the stiffness distribution and in a sufficient distribution with respect to the scale of micromechanical model. The Young's modulus of marble powder was established as 62.0 ± 1.2 GPa. When embedded in a cementitious matrix, the indentation of marble inclusions was biased by the matrix compliance, yielding about 5 GPa lower values. Moreover, investigating the marble powder separately from the cementitious matrix helped to distinguish between the indentation moduli of the C-S-H phases and the marble powder inclusions, because their similar moduli collide within the statistical deconvolution of the indentation data.

The interface between a marble powder inclusion and the C-S-H matrix interface was indented in six parallel rows to form a regular rectangular grid with the raster size equal to 1.0 μm to assess Young's modulus of the ITZ. The maximum indentation depth, set to 150 nm, and the spacing of individual indents were chosen to minimize their mutual influence. The nanoindentation results, presented in Fig. 7, are in agreement with the SEM-EDX observations. The weak ITZ with Young's modulus equal to 15.3 ± 1.9 GPa was detected in the vicinity (up to 24 μm) of the marble powder inclusion. The value of Young's modulus for the homogenized C-S-H matrix, equal to 23.363 GPa as indicated in Fig. 7, was established by Němeček (2012).

4.4. Model inputs

A comprehensive micromechanical study of cement pastes, prepared from CEM I 42.5R with water-to-cement ratio $(w/c) = 0.5$, was accomplished by Němeček (2009), who assessed the volumetric ratio and elasticity parameters of four major phases. These are C-S-H matrix (low- and high-density C-S-H gel (Constantinides and Ulm, 2004; Constantinides et al., 2006)), clinker, Portlandite, and low-stiffness phases in the volumetric ratio of 0.8951, 0.0483, 0.0461, and 0.0105, respectively. The elasticity parameters of these phases determined by nanoindentation (Table 5) are in agreement with other studies, e.g., Constantinides and Ulm (2004, 2007). The zero-porosity compressive strength of the C-S-H matrix was adopted from the research by Hlobil et al. (2016).

Based on own measurements, it was found that the mass ratio between the cement paste and raw Portland cement is equal to 1.40. The volume of the cementitious matrix and marble powder was calculated from the mass of the paste constituents and the measured mass density, determined using the pycnometer method. It was found that the density of cement paste is equal to 2805 ± 9.4 kg/m^3, while the density of marble was established as 2710 ± 14.1 kg/m^3. The elasticity parameters of marble powder and the ITZ (Table 5) were determined by nanoindentation, see Section 2.2.3.

4.5. Macroscopic stiffness

The Young's modulus of the $40 \times 40 \times 160$ mm specimens was assessed using the resonance method, which is based on the equation for a longitudinal vibration of prismatic specimens with homogeneous mass distribution.

The Young's modulus of cement pastes decreases with the increasing amount of incorporated marble powder as demonstrated in Fig. 8. By fitting the model predictions to the macroscopic measurements of Young's moduli, the ITZ thickness was established as 3/4 of the marble powder inclusion radius, therefore, $R^{(5,\delta)}/R^{(4,\delta)} = 7/4$. Such a definition of the ITZ thickness, dependent on the size of coated inclusions, renders the model insensitive to the size distribution of marble powder inclusions.

The stiffness reduction connected with the addition of stiff marble powder grains is attributed, besides the presence of the relatively compliant ITZ, to the increased porosity of pastes rich in marble powder, recall Section 4.3. The correlation between the porosity and Young's modulus of cementitious materials is well-known (Neville, 1996) and the relationship was recently confirmed also for mortars containing marble powder by Kabeer and Vyas (2018).

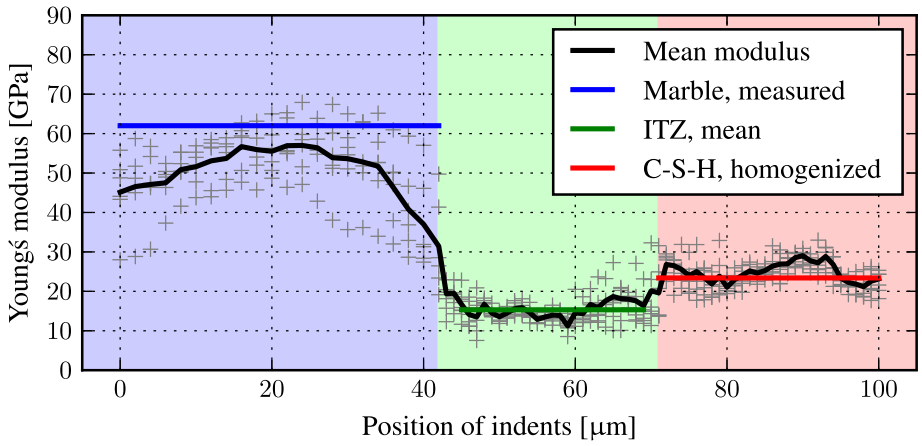

Fig. 7. The elastic stiffness profile across the interface between the marble powder inclusion and cementitious matrix; the blue, green, and red patches represent the marble inclusion, ITZ, and C-S-H matrix, respectively. (For interpretation of the references to colour in this figure legend, the reader is referred to the Web version of this article.)

Table 5
Model input parameters for individual phases; E, ν, and f_c denote the Young's modulus, Poisson's ratio, and compressive strength, respectively.

Phase	E [GPa]	ν [-]	f_c [MPa]
C-S-H matrix	23.4	0.2	68.7
Clinker	113.0	0.3	×
Portlandite	43.9	0.3	×
Low-stiffness phases	7.5	0.2	×
Marble powder	62.0	0.2	×
ITZ	15.3	0.2	×
Voids	0.0	0.2	×

4.6. Compressive strength

The uniaxial compression test was carried out on the $40 \times 40 \times 40$ mm specimens using the LabTest 4.100SP1 loading frame. The loading of specimens was displacement-controlled with a rate of 0.5 mm/min. Compressive strength was calculated by dividing the maximum loading force by the loaded area.

A similar linear trend as for the macroscopic Young's modulus was also observed for compressive strength, see Fig. 9. This trend was correctly predicted by the micromechanical model, confirming the suitability of the chosen homogenization scheme and failure criterion.

Based on outcomes of his comprehensive study, Arel (2016) derived a formula for a compressive strength estimation in cement-based composites containing marble powder:

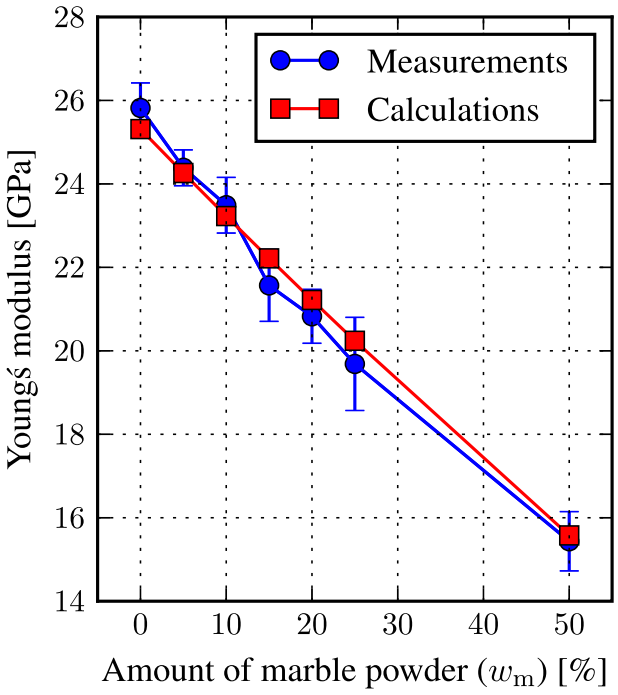

Fig. 8. Young's modulus of cement pastes containing a variable amount of marble powder.

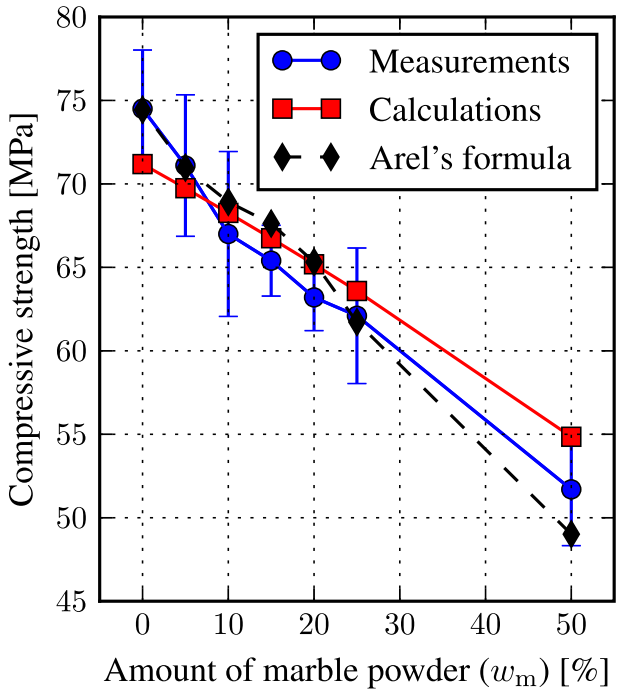

Fig. 9. Compressive strength of cement pastes containing a variable amount of marble powder.

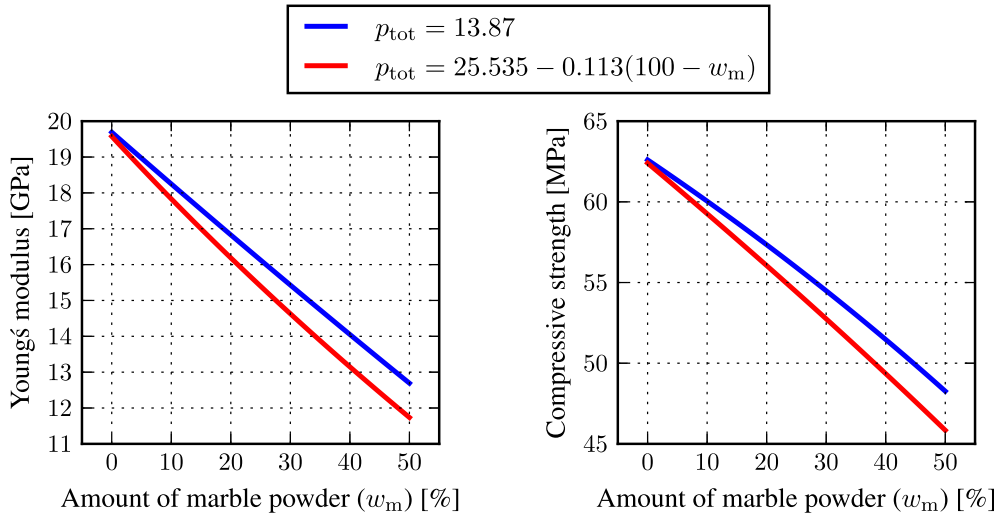

Fig. 10. Impact of porosity on the stiffness (left) and compressive strength (right) of cement pastes containing a variable amount of marble powder.

$$f_{\mathrm{c}} = 68.3 + \tan(0.74c) - \sin(be) - 0.5b - 34.06\cos(-5.73d), \tag{15}$$

where b is the weight percentage of cement replaced by marble powder, while c, d, and e are the percentages of SiO_2, CaO, and Al_2O_3 in the marble, respectively. The constant term equal to 68.3, which is suitable for concrete, was adjusted to 55.3 in order to fit the compressive strength of the pure cement paste. This empirical formula proved to be efficient and accurate estimator (see plot in Fig. 9, dashed line), especially when considering the limited amount of required input data.

The presented findings are in agreement with Topçu and Canbaz (2007), who investigated the impact of marble powder additions on the strength of self-compacting concrete. They found that the more of the cement replaced with marble powder, the lower compressive strength. Some authors admit a slight increase in compressive strength of concretes with small replacements of cement by marble powder (Ergun, 2011; Uysal and Sumer, 2011; Uysal and Yilmaz, 2011), but it is generally accepted that 10% or higher replacements adversely affect the mechanical properties (Gesoğlu et al., 2012; Arel, 2016).

4.7. Influence of porosity and ITZ

The negative effect of marble powder on the strength of cement pastes is twofold: (1) increased porosity and (2) formation of the weak ITZ in the vicinity of the marble powder inclusions. The micromechanical model allowed defining relationships between the amount of marble powder and Young's modulus/compressive strength of cement pastes with: (1) a constant porosity of 13.87% (corresponding to pure cement paste) and (2) porosities calculated based on Eq. (14), see Fig. 10. The results indicate that measures reducing porosity, such as the use of plasticizers to keep the w/c ratio as low as possible, would lead to cementitious composites of higher stiffness and strength.

However, the effect of porosity reduction is rather small in comparison with the effect of the ITZ elimination which would significantly increase stiffness/strength of the pastes, see the model outcomes in Fig. 11. Unfortunately, unlike porosity reduction, the elimination of ITZ formation represents a much more complex problem, involving alteration of the morphology of the cementitious matrix at the microscale. For future research aiming at the efficient utilization of waste marble powder for concrete

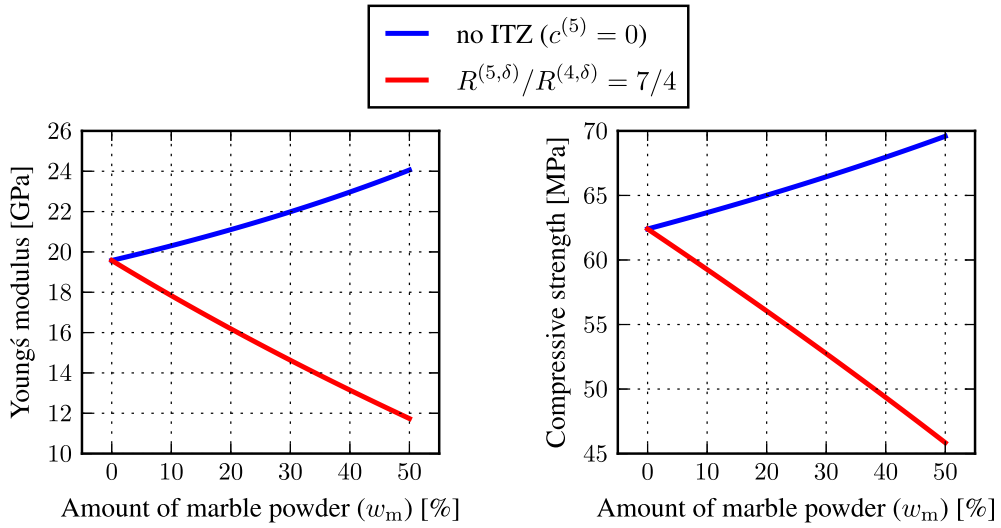

Fig. 11. Impact of the ITZ on stiffness (left) and compressive strength (right) of cement pastes containing a variable amount of marble powder.

production, the papers by, e.g., Akçaoğlu et al. (2004); Zimbelmann (1985); Scrivener et al. (2004), or Prokopski and Halbiniak (2000), dealing with the ITZ elimination through chemical reactions could be a great inspiration. Nevertheless, minimizing ITZ influence by keeping w/c ratio as low as possible appears to be the most simple measure to be adopted in the first place.

5. Conclusions

A comprehensive microscopic experimental study, complemented by micromechanical modeling, provided an unprecedented insight into micromechanics of cement pastes containing waste marble powder. The micromechanical model, based on the Mori-Tanaka homogenization scheme coupled with J_2-based failure criterion, successfully reproduced the macroscopic measurements of elastic stiffness and compressive strength.

The most important findings can be summarized as follows:

1. The presence of marble powder in cement pastes negatively affects the macroscopic performance.
2. The ITZ formed around stiff marble inclusions plays a crucial role, and its thickness dictates the macroscopic performance.
3. The increased porosity of the marble powder-rich pastes has a minor effect on their stiffness/strength compared to the effect of ITZ.

Understanding the role of the individual phases allows establishing measures for improving the cement-based materials containing waste marble powder. It is conjectured that reduction of porosity and altering the chemical processes responsible for the ITZ formation would lead to the production of relatively cheap and eco-friendly concrete without compromising its structural performance. In particular, such developments would enable utilization of waste marble powder, being a worldwide environmental problem, and contribute to the reduction of CO_2 emissions by lowering the demands for Portland cement in the construction industry.

Funding

This work was supported by the Czech Science Foundation [grant number GA ČR 17-06771S] and the internal grant of the Faculty of Civil Engineering at CTU in Prague [grant number SGS18/037/OHK1/1T/11].

Acknowledgment

The authors wish to thank the Lavaris company for providing the finely ground marble used in the presented study.

References

Adu-Amankwah, S., Zajac, M., Stabler, C., Lothenbach, B., Black, L., 2017. Influence of limestone on the hydration of ternary slag cements. Cement Concr. Res. 100, 96–109. https://doi.org/10.1016/j.cemconres.2017.05.013.

Akbulut, H., Gürer, C., 2007. Use of aggregates produced from marble quarry waste in asphalt pavements. Build. Environ. 42, 1921–1930. https://doi.org/10.1016/j.buildenv.2006.03.012.

Akçaoğlu, T., Tokyay, M., Çelik, T., 2004. Effect of coarse aggregate size and matrix quality on ITZ and failure behavior of concrete under uniaxial compression. Cement Concr. Compos. 26, 633–638. https://doi.org/10.1016/s0958-9465(03)00092-1.

Aliabdo, A., Abd Elmoaty, A., Auda, E., 2014. Re-use of waste marble dust in the production of cement and concrete. Construct. Build. Mater. 60, 28–41. https://doi.org/10.1016/j.conbuildmat.2013.09.005.

Alyamaç, K.E., Aydin, A.B., 2015. Concrete properties containing fine aggregate marble powder. KSCE J. Civ. Eng. 19, 2208–2216. https://doi.org/10.1007/s12205-015-0327-y.

Alyamaç, K.E., Ghafari, E., Ince, R., 2017. Development of eco-efficient self-compacting concrete with waste marble powder using the response surface method. J. Clean. Prod. 144, 192–202. https://doi.org/10.1016/j.jclepro.2016.12.156.

Alzboon, K., Mahasneh, K., 2009. Effect of using stone cutting waste on the compression strength and slump characteristics of concrete. Int. J. Environ. Ecol. Eng. 3, 491–496.

Arel, H., 2016. Recyclability of waste marble in concrete production. J. Clean. Prod. 131, 179–188. https://doi.org/10.1016/j.jclepro.2016.05.052.

Aruntaş, H.Y., Gr, M., Dayı, M., Tekin, İ., 2010. Utilization of waste marble dust as an additive in cement production. Mater. Des. 31, 4039–4042. https://doi.org/10.1016/j.matdes.2010.03.036.

Benveniste, Y., 1987. A new approach to the application of Mori-Tanaka theory in composite materials. Mech. Mater. 6, 147–157. https://doi.org/10.1016/0167-6636(87)90005-6.

Bilgin, N., Yeprem, H., Arslan, S., Bilgin, A., Gnay, E., Marşoglu, M., 2012. Use of waste marble powder in brick industry. Construct. Build. Mater. 29, 449–457. https://doi.org/10.1016/j.conbuildmat.2011.10.011.

Constantinides, G., Ulm, F.J., 2004. The effect of two types of C-S-H on the elasticity of cement-based materials: results from nanoindentation and micromechanical modeling. Cement Concr. Res. 34, 67–80. https://doi.org/10.1016/s0008-8846(03)00230-8.

Constantinides, G., Ulm, F.-J., 2007. The nanogranular nature of c-s-h. J. Mech. Phys. Solid. 55, 64–90. https://doi.org/10.1016/j.conbuildmat.2016.12.189.

Constantinides, G., Chandran, K.R., Ulm, F.J., Vliet, K.V., 2006. Grid indentation analysis of composite microstructure and mechanics: principles and validation. Mater. Sci. Eng., A 430, 189–202.

Corinaldesi, V., Moriconi, G., Naik, T., 2010. Characterization of marble powder for its use in mortar and concrete. Construct. Build. Mater. 24, 113–117. https://doi.org/10.1016/j.conbuildmat.2009.08.013.

da Silva, W.R.L., Němeček, J., Štemberk, P., 2014. Methodology for nanoindentation-assisted prediction of macroscale elastic properties of high performance cementitious composites. Cement Concr. Compos. 45, 57–68.

Dela, B.F., Stang, H., 2000. Two-dimensional analysis of crack formation around aggregates in high-shrinkage cement paste. Eng. Fract. Mech. 65, 149–164. https://doi.org/10.1016/s0013-7944(99)00113-7.

Dhanapandian, S., Gnanavel, B., 2010. Using granite and marble sawing power wastes in the production of bricks: spectroscopic and mechanical analysis. Res. J. Appl. Sci. 2, 73–86.

Ergun, A., 2011. Effects of the usage of diatomite and waste marble dust as partial replacement of cement on the mechanical properties of concrete. Construct. Build. Mater. 25, 806–812. https://doi.org/10.1016/j.conbuildmat.2010.07.002.

Eshelby, J.D., 1957. The determination of the elastic field of an ellipsoidal inclusion, and related problems. Proc. Roy. Soc. Lond. 241, 376–396. https://doi.org/10.1098/rspa.1957.0133.

European Standard EN 12350-5, 2009. Testing Fresh Concrete; Flow Table Test.

Feenstra, P.H., de Borst, R., 1995. Constitutive model for reinforced concrete. J. Eng. Mech., ASCE 121, 587–595. https://doi.org/10.1061/(asce)0733-9399(1995)121:5(587).

Gautam, N., Krishna, V., Srivastava, A., 2014. Sustainability in the concrete construction. Int. J. Environ. Res. Dev. 4, 81–90.

Gesoğlu, M., Gneyisi, E., Kocabağ, M.E., Bayram, V., Mermerdaş, K., 2012. Fresh and hardened characteristics of self compacting concretes made with combined use of marble powder, limestone filler, and fly ash. Construct. Build. Mater. 37, 160–170. https://doi.org/10.1016/j.conbuildmat.2012.07.092.

Herve, E., Zaoui, A., 1993. n-layered inclusion-based micromechanical modelling. Int. J. Eng. Sci. 31, 1–10. https://doi.org/10.1016/0020-7225(93)90059-4.

Hlobil, M., Šmilauer, V., Chanvillard, G., 2016. Micromechanical multiscale fracture model for compressive strength of blended cement pastes. Cement Concr. Res. 83, 188–202. https://doi.org/10.1016/j.cemconres.2015.12.003.

Ho, D., Sheinn, A., Ng, C., Tam, C., 2002. The use of quarry dust for SCC applications. Cement Concr. Res. 32, 505–511. https://doi.org/10.1016/s0008-8846(01)00726-8.

Hrbek, V., Koudelková, V., Prošek, Z., Tesárek, P., 2017. Micro-mechanical performance of concrete used as recycled raw material in cementitious composite. Acta Polytech. CTU Proceed. 13, 55. https://doi.org/10.14311/app.2017.13.0055.

Hughes, J.J., Trtik, P., 2004. Micro-mechanical properties of cement paste measured by depth-sensing nanoindentation: a preliminary correlation of physical properties with phase type. Mater. Char. 53, 223–231. https://doi.org/10.1016/j.matchar.2004.08.014.

Idiart, A., Bisschop, J., Caballero, A., Lura, P., 2012. A numerical and experimental study of aggregate-induced shrinkage cracking in cementitious composites. Cement Concr. Res. 42, 272–281. https://doi.org/10.1016/j.cemconres.2011.09.013.

Kabeer, K.S.A., Vyas, A.K., 2018. Utilization of marble powder as fine aggregate in mortar mixes. Construct. Build. Mater. 165, 321–332. https://doi.org/10.1016/j.conbuildmat.2018.01.061.

Kaosol, T., 2010. Reuse water treatment sludge for hollow concrete block manufacture. Energy Res. J. 1, 131–134. https://doi.org/10.3844/erjsp.2010.131.134.

Lee, M., Ko, C., Chang, F., Lo, S., Lin, J., Shan, M., Lee, J., 2008. Artificial stone slab production using waste glass, stone fragments and vacuum vibratory compaction. Cement Concr. Compos. 30, 583–587. https://doi.org/10.1016/j.cemconcomp.2008.03.004.

Levy, S., Helene, P., 2004. Durability of recycled aggregates concrete: a safe way to sustainable development. Cement Concr. Res. 34, 1975–1980. https://doi.org/10.1016/j.cemconres.2004.02.009.

Lothenbach, B., Nonat, A., 2015. Calcium silicate hydrates: solid and liquid phase

composition. Cement Concr. Res. 78, 57–70. https://doi.org/10.1016/j.cemconres.2015.03.019.
Marras, G., Careddu, N., Internicola, C., Siotto, G., 2017. Characterization methodology for re-using marble slurry in industrial applications. Energy Procedia 125, 656–665. https://doi.org/10.1016/j.egypro.2017.08.277.
Mashaly, A.O., Shalaby, B.N., El-Hefnawi, M.A., 2012. Characterization of the marble sludge of the Shaq El Thoaban industrial zone, Egypt and its compatibility for various recycling applications. Aust. J. Basic Appl. Sci. 6, 153–161.
Mashaly, A., El-Kaliouby, B., Shalaby, B., El-Gohary, A., Rashwan, M., 2016. Effects of marble sludge incorporation on the properties of cement composites and concrete paving blocks. J. Clean. Prod. 112, 731–741. https://doi.org/10.1016/j.jclepro.2015.07.023.
Milton, G.W., 2002. The Theory of Composites. Cambridge Monographs on Applied and Computational Mathematics. Cambridge University Press. https://doi.org/10.1115/1.1553445.
Moon, G.D., Oh, S., Jung, S.H., Choi, Y.C., 2017. Effects of the fineness of limestone powder and cement on the hydration and strength development of PLC concrete. Construct. Build. Mater. 135, 129–136. https://doi.org/10.1016/j.conbuildmat.2016.12.189.
Mori, T., Tanaka, K., 1973. Average stress in matrix and average elastic energy of materials with mixfitting inclusions. Acta Metall. 21, 571–574. https://doi.org/10.1016/0001-6160(73)90064-3.
Nagarajan, V., Devi, S., Manohari, S., Santha, M., 2014. Experimental study on partial replacement of cement with coconut shell ash in concrete. Int. J. Sci. Res. 3, 651–661.
Neubauer, C.M., Jennings, H.M., Garboczi, E.J., 1996. A three-phase model of the elastic and shrinkage properties of mortar. Adv. Cement Base Mater. 4, 6–20. https://doi.org/10.1016/s1065-7355(96)90058-9.
Neville, A.M., 1996. Properties of Concrete: Fourth Edition. Longman.
Nežerka, V., Zeman, J., 2012. A micromechanics-based model for stiffness and strength estimation of cocciopesto mortars. Acta Polytech. 52, 29–37.
Nežerka, V., Slížková, Z., Tesárek, P., Plachý, T., Frankeová, D., Petráňová, V., 2014a. Comprehensive study on microstructure and mechanical properties of lime-pozzolan pastes. Cement Concr. Res. 64, 17–29. https://doi.org/10.1016/j.cemconres.2014.06.006.
Nežerka, V., Tesárek, P., Zeman, J., 2014b. Fracture-micromechanics based model of mortars susceptible to shrinkage. Key Eng. Mater. 592–593, 189–192. 10.4028/www.scientific.net/kem.592-593.189.
Nežerka, V., Němeček, J., Slížková, Z., Tesárek, P., 2015. Investigation of crushed brick-matrix interface in lime-based ancient mortar by microscopy and nano-indentation. Cement Concr. Compos. 55, 122–128. https://doi.org/10.1016/j.cemconcomp.2014.07.023.
Nežerka, V., Zeman, J., Němeček, J., 2017. Micromechanics-based simulations of compressive and tensile testing on lime-based mortars. Mech. Mater. 105, 49–60. https://doi.org/10.1016/j.mechmat.2016.11.011.
Němeček, J., 2009. Creep effects in nanoindentation of hydrated phases of cement pastes. Mater. Char. 60, 1028–1034. https://doi.org/10.1016/j.matchar.2009.04.008.
Němeček, J., 2012. Nanoindentation based analysis of heterogeneous structural materials. In: Nanoindentation in Materials Science. InTech. https://doi.org/10.5772/50968.
Němeček, J., Králík, V., Vondřejc, J., 2013. Micromechanical analysis of heterogeneous structural materials. Cement Concr. Compos. 36, 85–92. https://doi.org/10.1016/j.cemconcomp.2012.06.015.
Oliver, W.C., Pharr, G.M., 1992. An improved technique for determining hardness and elastic modulus using load and displacement sensing indentation experiments. J. Mater. Res. 7, 1564–1583. https://doi.org/10.1557/jmr.1992.1564.
Pellenq, R.J.-M., Kushima, A., Shahsavari, R., Vliet, K.J.V., Buehler, M.J., Yip, S., Ulm, F.-J., 2009. A realistic molecular model of cement hydrates. Proc. Natl. Acad. Sci. Unit. States Am. 106, 16102–16107. https://doi.org/10.1073/pnas.0902180106.
Pichler, B., Hellmich, C., 2011. Upscaling quasi-brittle strength of cement paste and mortar: a multi-scale engineering mechanics model. Cement Concr. Res. 41, 467–476. https://doi.org/10.1016/j.cemconres.2011.01.010.
Pichler, B., Hellmich, C., Mang, H., 2007. A combined fracture-micromechanics model for tensile strain-softening in brittle materials, based on propagation of interacting microcracks. Int. J. Numer. Anal. Meth. GeoMech. 31 (2), 111–132.
Pichler, B., Hellmich, C., Eberhardsteiner, J., 2009. Spherical and acicular representation of hydrates in a micromechanical model for cement paste: prediction of early-age elasticity and strength. Acta Mech. 203 (3), 137–162. https://doi.org/10.1007/s00707-008-0007-9.
Prokopski, G., Halbiniak, J., 2000. Interfacial transition zone in cementitious materials. Cement Concr. Res. 30, 579–583. https://doi.org/10.1016/s0008-8846(00)00210-6.
Quellet, S., Bussiere, B., Aubertin, M., Bnzaazoua, M., 2007. Microstructural evolution of cemented paste backfill: mercury intrusion porosimetry test results. Cement Concr. Res. 37, 1654–1665. https://doi.org/10.1016/j.cemconres.2007.08.016.
Rai, B., Khan, N., Abhishek, K., Tabin, R., Duggal, S., 2011. Influence of marble powder/granules in concrete mix. Int. J. Civ. Struct. Eng. 1, 827–834.
Sata, V., Jaturapitakkul, C., Kiattikomol, K., 2007. Influence of pozzolan from various by-product materials on mechanical properties of high-strength concrete. Construct. Build. Mater. 21, 1589–1598. https://doi.org/10.1016/j.conbuildmat.2005.09.011.
Scrivener, K.L., Patel, H.H., Pratt, P.L., Parrott, L.J., 1986. Analysis of phases in cement paste using backscattered electron images, methanol adsorption and thermogravimetric analysis. MRS Proceed. 85, 321–332. https://doi.org/10.1557/proc-85-67.
Scrivener, K.L., Crumbie, A.K., Laugesen, P., 2004. The interfacial transition zone (ITZ) between cement paste and aggregate in concrete. Interface Sci. 12, 411–421. https://doi.org/10.1023/b:ints.0000042339.92990.4c.
Siddique, R., 2004. Performance characteristics of high-volume Class F fly ash concrete. Cement Concr. Res. 34, 487–493. https://doi.org/10.1016/j.cemconres.2003.09.002.
Singh, M., Choudhary, K., Srivastava, A., Sangwan, K., Bhunia, D., 2017. A study on environmental and economic impacts of using waste marble powder in concrete. J. Build. Eng. 13, 87–95. https://doi.org/10.1016/j.jobe.2017.07.009.
Šmilauer, V., Hlaváček, P., Škvára, F., Šulc, R., Kopecký, L., Němeček, J., 2011. Micromechanical multiscale model for alkali activation of fly ash and metakaolin. J. Mater. Sci. 1–11. https://doi.org/10.1007/s10853-011-5601-x.
Stránský, J., Vorel, J., Zeman, J., Šejnoha, M., 2011. Mori-Tanaka based estimates of effective thermal conductivity of various engineering materials. Micromachines 2, 129–149.
Sudarshan, D., Vyas, A., 2016. Impact of marble waste as coarse aggregate on properties of lean cement concrete. Case Stud. Constr. Mater. 4, 85–92. https://doi.org/10.1016/j.cscm.2016.01.002.
Tesárek, P., Němeček, J., 2011. Microstructural and micromechanical study of gypsum. Chem. Listy 105, 852–853.
Topçu, I., Canbaz, M., 2007. Effect of different fibers on the mechanical properties of concrete containing fly ash. Construct. Build. Mater. 21, 1486–1491. https://doi.org/10.1016/j.conbuildmat.2006.06.026.
Turgut, P., Murat Algin, H., 2007. Limestone dust and wood sawdust as brick material. Build. Environ. 42, 3399–3403. https://doi.org/10.1016/j.buildenv.2006.08.012.
Uysal, M., Sumer, M., 2011. Performance of self-compacting concrete containing different mineral admixtures. Construct. Build. Mater. 25, 4112–4120. https://doi.org/10.1016/j.conbuildmat.2011.04.032.
Uysal, M., Yilmaz, K., 2011. Effect of mineral admixtures on properties of self-compacting concrete. Cement Concr. Compos. 33, 771–776. https://doi.org/10.1016/j.cemconcomp.2011.04.005.
Vorel, J., Šmilauer, V., Bittnar, Z., 2012. Multiscale simulations of concrete mechanical tests. J. Comput. Appl. Math. 236, 4882–4892. https://doi.org/10.1016/j.cam.2012.01.009.
Zimbelmann, R., 1985. A contribution to the problem of cement-aggregate bond. Cement Concr. Res. 15, 801–808. https://doi.org/10.1016/0008-8846(85)90146-2.

Appendix B

Prošek, Z.; Nežerka, V.; Tesárek, P.: Enhancing cementitious pastes with waste marble sludge, *Construction and Building Materials* 255 (2020), 119372,
doi: 10.1016/j.conbuildmat.2020.119372

Author's contribution: main idea, SEM microscopy, data analysis, design of experiments, preparation of specimens.

Construction and Building Materials 255 (2020) 119372

Contents lists available at ScienceDirect

Construction and Building Materials

journal homepage: www.elsevier.com/locate/conbuildmat

Enhancing cementitious pastes with waste marble sludge

Z. Prošek [a,*], V. Nežerka [a], P. Tesárek [a]

[a] Faculty of Civil Engineering, Czech Technical University, in Prague, Thákurova 7, 166 29 Praha 6, Czech Republic

HIGHLIGHTS

- Waste marble sludge (WMS) was studied as an admixture to cementitious composites.
- Replacement of Portland cement (PC) with WMS by up to 15 wt% enhances strength.
- Effect of weak transition zones around WMS inclusions was negligible.
- Inert WMS inclusions reinforce brittle PC matrix and act as a microfiller.

ARTICLE INFO

Article history:
Received 28 January 2020
Received in revised form 24 April 2020
Accepted 26 April 2020
Available online 7 May 2020

Keywords:
Waste marble sludge
Portland cement
Hydration
Microstructure
Strength

ABSTRACT

Several researchers have considered waste marble sludge (WMS) as an admixture to cementitious composites. However, the scientific community is divided into two groups—one advocating WMS as a suitable microfiller, while the other claiming that WMS inhibits hydration of clinker minerals. Here, the role played by WMS during Portland cement (PC) hydration was placed under scrutiny. SEM-BSE microscopy, EDX analysis, porosimetry, and nanoindentation were employed for investigating the microstructure of cement pastes, and calorimetry for studying the rate of hydration. The impacts of hydration and microstructure development in the presence of WMS on mechanical properties of blended pastes were assessed using the resonance method and destructive tests. It was found that replacing PC with WMS by up to 15 wt% can lead to an increase of compressive and flexural strength because WMS lowers the porosity of pastes, contributing to a more homogeneous distribution of phases, and reinforces the brittle cementitious matrix. A weak transition zone around marble grains was observed, but this was not significant for WMS replacement at 15 wt% or less. Given the amount of WMS produced annually, its utilization for the production of building materials, even in relatively low concentrations, could potentially have a considerable impact on the sustainable reuse of WMS.

1. Introduction

The efficient utilization of construction and demolition (C&D) waste has become a major topic of research in civil engineering over the last decade [1–4]. C&D waste is associated with the construction industry, but also sawing, shaping, and polishing of marble products has resulted in creation and accumulation of massive amounts of fine-grained waste marble sludge (WMS) [5–8]. The amount of landfilled WMS comprises up to 66% of quarried material in developing countries [9], with Egypt being the largest producer with 6.4 million tons of marble waste annually [10,11]. Heaps of deposited marble slurry currently hinder the expansion of quarries and pose a significant environmental risk [12,13].

Despite smaller amounts of quarried marble, countries in the European Union and other developed nations also face the same environmental burdens [14,15], which have fueled efforts to use the waste in the form of aggregates and as dust/sludge in experimental research as well as industrial applications. The incorporation of fine marble fractions into cementitous composites can enhance mechanical strength [16–18], but the percentage of incorporated WMS in a production of new materials is currently negligible [19–22]. Concentrations from 5 to 10 wt% have been reported to improve workability of fresh mortars [23,24,20,25,23,26], to increase both compressive and flexural strengths of hardened composites [27,26,10], and reduce their porosity [19]. For particles large enough to be classified as aggregates, even higher replacements (up to 50 wt %) can be considered without sacrificing the performance of cementitous composites [28–32].

The limited body of research available to date illustrates two completely different views on the issue of WMS in cementitious

* Corresponding author.
E-mail address: zdenek.prosek@fsv.cvut.cz (Z. Prošek).

https://doi.org/10.1016/j.conbuildmat.2020.119372
0950-0618/

composites and its interaction with clinker minerals. Several studies reported that WMS affects the formation of portlandite crystals (CH), making them small and evenly dispersed across the entire matrix [33] due to presence of nucleation centers provided by marble inclusions. The presence of these nucleation centers can lead to accelerated hydration of silicate and aluminate phases, especially tricalcium-aluminate (C_3A) in clinker to form calcium-carbonate-aluminate-hydrate ($3\ CaO \cdot Al_2O_3 \cdot 3\ CaCO_3 \cdot 32\ H_2O$). This phenomenon is evident in types of cement with a high C_3A concentration, because C_3A can transform into more stable monocarbonate in later stages of hydration. The other group researchers rejects the theory that WMS has a positive effect on the morphology of a cementitious matrix [34] based on microscopy investigation and thermogravimetry [8,10]. Seghir et al. [35] concluded, for example, WMS prevents water from accessing clinker grains and can stop their involvement in the hydration process.

In our previous research, we revealed a positive effect of WMS on mechanical properties, assuming that WMS or finely ground recycled concrete can act as suitable microfillers [36–38]. Here, we investigate the influence of WMS on the hydration of Portland cement (PC) pastes in terms of phase composition and its mechanical properties. A clear answer to whether WMS can enhance the performance of cementitious pastes could promote its utilization. This study focuses on pure cement pastes without aggregates, chemical additives, or admixtures to eliminate additional biases caused by their presence.

2. Materials and samples

Three sets of cement pastes were prepared for experimental testing. The first set was used to investigate the raw materials in a powder form using granulometry and X-ray fluorescence (XRF) analysis; the samples contained WMS from the west bank of the Jordan River, produced during processing of marble, and Portland cement (PC) CEM I 42.5R [39]. WMS activity was enhanced using Lavaris SBD 600 2 × 30 kW high-speed mills; the milling of larger grains also improved the workability of the fresh pastes and ensured a well-defined grain-size distribution. The second set of samples consisted of hardened pastes with different percentages of WMS replacing PC prepared for macroscopic testing. Pure cement paste was used as a reference material. A third set was extracted after destructive testing from broken pieces in the form of slices for microscopy investigation.

Percentages of WMS as a replacement for PC in the tested pastes ranged from 5 to 50% (Table 1) and each set consisted of twelve 40 × 40 × 160 mm specimens. The PC-to-WMS ratios were selected based on previous studies indicating that optimum lies below 15% and that high ratios around 50% lead to significant deterioration of the performance of hardened pastes [36]. The water-to-binder ratio (w/b), where binder represents the mixture of PC and WMS, was adjusted for each mixture to reach constant workability determined based on results of a flow test defined in EN 12350-2 [40]. Flow test spill was measured after 10 and 20 impacts to reach target diameters of 160 ± 5 mm and 190 ± 5 mm, respectively. The specimens were demolded after 1 day of hardening and stored in a laboratory at 22 ± 1 °C and relative humidity of 50 ± 2%.

Before preparing thin sections for microscopy investigation and nanoindentation, the macroscopic specimens were vacuum-impregnated with an epoxy resin (Araldit 2020 A/B) to avoid loosening of grains and alteration of the structure of pores. Abrasive papers (220–4000 grain/cm^2 grit) were successively used to eliminate irregularities and to polish the specimens. Polishing was carried out in dry conditions and each step lasted 2 min. In the final step, samples were polished using a 0.25 μm nanodiamond emulsion for 1 min and subsequently sputtered with a 30 nm carbon layer to improve surface conductivity.

3. Experimental methods

3.1. Characterization of raw materials

Granulometry was conducted using a Fritsch Anlysette 22 MicroTec Plus laser granulometer to determine particle size distributions of raw and ground WMS and PC. The device was equipped with a source of red and green laser radiation (532 and 940 nm wavelengths) and was capable of detecting particles with sizes ranging from 0.08 to 1800 μm in diameter. The particles were dispersed in an ultrasonic bath. The Fraunhofer diffraction model was employed to evaluate the diffraction patterns. The fineness and specific surface were determined using the Blaine method with a Matest E009 device. XRF analysis was performed using a Spectro Xepos device equipped with 50 W/60 kV X-ray emitters according to the EN-196-2 standard [41].

3.2. Calorimetry

Hydration heat flow was measured using a TAM Air isothermal calorimeter equipped with eight chambers; each mixture occupied two chambers and hydration heat flux was measured for 7 days at a constant temperature of 20 °C. After compaction, each container to be inserted into a chamber contained a sample having weighing between 25 and 38 g. By integrating the heat flow over the measurement time, the cumulative hydration heat was calculated.

3.3. Testing of strength and stiffness

The dynamic Young's modulus was determined from natural frequencies of the 40 × 40 × 160 mm specimens [42], using the Brüel & Kjaer device type 3560-B-120. The same specimens were subjected to destructive testing after 28 and 90 days of hardening [43]. First, flexural strength was determined in displacement-controlled three-point bending at a constant rate of 0.1 mm/s. The span between supports was 100 mm and six specimens represented each mixture. Next, broken halves of specimens following the three-point bending test were loaded over an effective area of 40 × 40 mm in uniaxial compression at a cross-head displacement rate of 0.3 mm/s to determine compressive strength.

Table 1
Composition of tested pastes; w/c represents a water-to-cement ratio.

Mix	WMS content [wt.%]	Amount [kg]				Bulk density [kg/m^3]	Porosity [%]
		PC	WMS	w/b	w/c		
M0	0	3.00	0.00	0.35	0.35	1942 ± 4	26.6 ± 0.5
M5	5	2.85	0.15	0.32	0.34	1950 ± 10	25.8 ± 0.4
M10	10	2.70	0.30	0.32	0.35	1960 ± 9	25.1 ± 0.7
M15	15	2.55	0.45	0.32	0.38	1920 ± 10	26.0 ± 1.0
M50	50	1.50	1.50	0.32	0.64	1760 ± 8	30.4 ± 0.4

3.4. Porosimetry

Mercury-intrusion porosimetry was employed to determine the porosity of hardened pastes. Fragments of up to 1 g were extracted from cores of samples dried at 105 ± 5°. These dried samples were placed in a glass dilatometer and the whole assembly was inserted into a Pascal 140 instrument capable of detecting pores 10–500 μm in diameter. After decompression, the dilatometer was filled with mercury (approximately 500 mm^3) and gradually compressed to 100 kPa. In the second step, the assembly was weighed and placed in the steel chamber of a Pascal 440 hydraulic apparatus capable of detecting pores 0.003–10 μm by applying pressure up to 400 MPa.

3.5. Microscopy

The heart of this study lies in microscopic identification of phases. This was accomplished using an FEG Merlin Zeiss scanning electron microscope (SEM) equipped with a Schottky cathode. The morphology was mapped using a backscattered electrons (BSE) detector with 50–200 nm resolution. Microanalysis of chemical composition was performed with an X-ray energy-dispersive spectrometer (EDS) from Oxford instruments. The SEM setting was as follows: accelerating voltage 10 kV, current 1 nA, working table distance 8.5 mm, single point measurement time 50 μs, and resolution 1024 px.

BSE results indicated spatial distributions of individual phases resulting in different density and grayscale images of these phases, acquired at 300× and 500× magnifications, and further analyzed using PyPAIS software [44]. Next, a composition of each phase was studied using EDS, both point-wise to determine the weight and atomic percentages of individual elements and using line scans to reveal the composition of transition zones around marble grains. These transition zones were studied on five carefully selected marble grains, 10–30 μm in diameter; there were three line scans placed over each grain. The phases were identified from the elemental compositions using stoichiometry.

3.6. X-ray diffraction

Semiquantitative X-ray diffraction (XRD) was meassured by using a Malvern PANalytical X'Pert Pro X-ray diffraction system operating at 30 mA, 40 kV and radiation of λ = 1.54060 Å. XRD provided unique diffraction patterns. All scans were measured over an angular range of 5–90°2θ with a 0.039°2θ step size and accumulated time per step of 115 s, resulting in a total measurement time of 18 min per scan. The analysis of XRD data was accomplished using HighScorePlus software.

3.7. Nanoindentation

Static nanoindentation using a T750 Hysitron TriboIndenter device was employed as a complementary method to microscopy for revealing the formation of phases and assessment of elastic stiffness, with a focus on the transition zones around marble grains. Indentation was carried out in lines across the boundaries of marble grain inclusions.

The indentation modulus was obtained from the unloading phase of the diamond tip to eliminate the impact of plastic deformations for the indented materials. The reduced moduli, E_r, were evaluated based on values of maximum indentation forces, P_{max}, corresponding deformation, h_{max}, and slopes of the unloading curves dP/dh at P_{max} [45]:

$$E_r = \frac{\sqrt{\pi}\,dP}{2\beta\sqrt{A}\,dh}, \tag{1}$$

where A is the diamond tip contact surface at P_{max} and β is the correction factor to include the effect of asymmetric tip shapes for the Berkovich tip β = 1.034 used in this study [46]. The indentation modulus can be calculated from E_r according to the following relationship [45]:

$$\frac{1}{E_r} = \frac{1-\nu^2}{E} + \frac{1-\nu_r^2}{E_i}, \tag{2}$$

where ν is the Poisson's ratio of the indented material, E_i and ν_i are the elastic modulus and the Poisson's ratio of the tip (for a diamond tip equal to 1140 GPa and 0.07, respectively).

Here, the maximum applied force was 13 μN, the indentation depth was 150 nm, and the distance between indents was 5 μm. Both loading and unloading parts of the indentation curve lasted 5 s, and the hold time was 60 s.

4. Results and discussion

4.1. Characterization of raw materials

4.1.1. Granulometry and structural analysis

The impact of grinding is obvious from the particle size distribution in Fig. 1. Particle sizes of both ground and raw WMS were shifted towards smaller effective diameters when compared to pure PC, having mean grain sizes equal to 5.24 and 12.8 μm, respectively (Table 2). The shape of WMS particles was angular, see Fig. 2.

4.1.2. Chemical and mineralogical composition

XRF results (Table 3) showed that approximately 95% of WMS is $CaCO_3$ and the remaining 5% consists of $MgCO_3$ and minor clay minerals containing silica. The conversion from chemical to mineralogical composition (Table 4) was performed according to Bogue, defined in ASTMC150 standard [47]. The allitic PC with its high C_3S content was supposed to exhibit an early strength gain.

The semiquantitative results of XRD allowed to validate the XRF results, however, the accuracy is relatively low. The 32.65° peak was used to calculate the amount of clinker minerals in PC (Fig. 3). It indicates that there is about 90 ± 5 wt% C_3S and C_2S. For WMS, the 29.42° peak yields about 98 ± 1 wt% $CaCO_3$. Other clay minerals were represented mainly by quartz (peak 26.66°, 2 ± 0.5 wt%).

4.2. Mechanical properties of pastes

4.2.1. Young's modulus

The results of a long-term non-destructive stiffness measurement (Fig. 4) showed that the addition of WMS contributed to a reduction of the Young's modulus and this observation was consistent for all measurements at any stage of hardening. The most rapid increase in stiffness gain was detected during the first 5 days of hardening and its deterioration was observed between the 7th and 28th days of hardening, attributed to drying and formation of pores [48,49]. This deterioration was delayed by 14 days in pure cement pastes (M0), which reached their peak stiffness 7 days later than pastes containing WMS. The relatively high stiffness of M10 specimens opens a new research gap to be investigated. We conjecture that, given the pore distribution presented in Fig. 6, 10% could be closest to an optimum amount of WMS for formation of nucleation centers and formation of a dense matrix, as discussed below.

These findings are in agreement with other studies [50,22,23], whose authors recommended replacing PC with WMS by 5–20 wt% to retain sufficient stiffness. However, it must be noted that these findings were reached for concretes containing aggregates

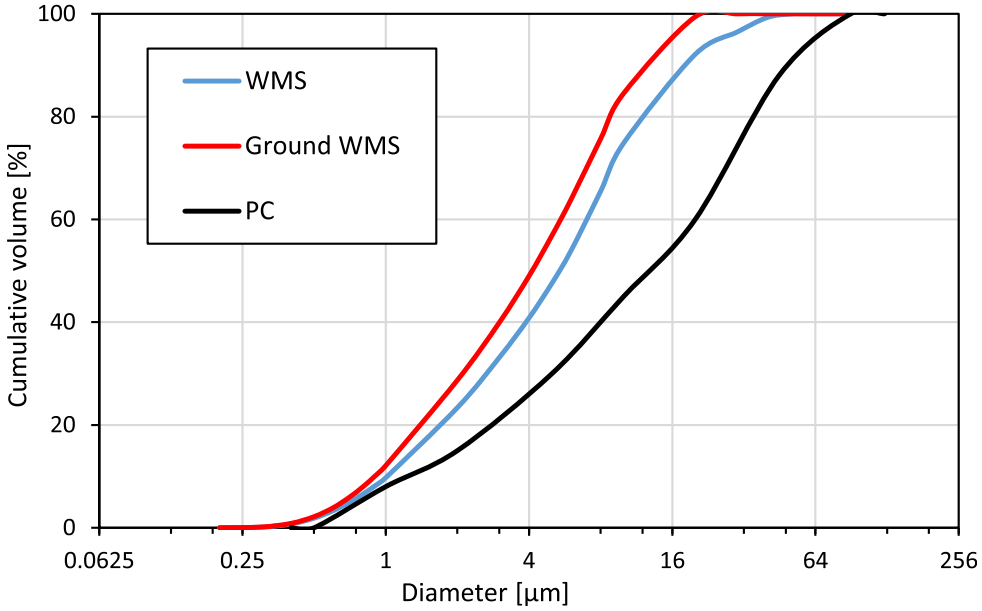

Fig. 1. Particle-size distribution for raw WMS, ground WMS, and PC.

Table 2
Granulometry characteristics.

	PC	WMS	Ground WMS
Blaine surface (m^2/kg)	380	436	455
Density of matrix (kg/m^3)	3105	2818	2776
Medium grain size (µm)	12.8	7.73	5.24

with size fractions up to 16 mm and the authors used the ultrasonic method for evaluating the Young's moduli.

4.2.2. Strength

Destructive testing demonstrated positive impacts on the mechanical properties of cementitious pastes containing WMS. The relationships between the amount of incorporated WMS and flexural/compressive strength (Fig. 5) indicate that moderate additions of WMS, up to 15 wt%, do not result in strength deterioration. The differences between such mixtures were within standard deviations for flexural strength measurements reaching up to 12% for compressive strength. However, the mixture containing 50 wt% of WMS exhibited a completely different behavior—by mixing PC and WMS at a 1:1 weight ratio, considerably higher values of both 28-day and 90-day flexural strength were achieved, but compressive strength was reduced by an even higher factor.

The high flexural strength can be attributed to enhanced fracture energy due to the presence of inert marble grains that impede opening and propagation of microcracks due to tensile stresses [51–54]. On the other hand, the reduction of compressive strength reflects an increased porosity of M50 (see Section 4.2.3), considered to be the main factor influencing compressive strength of cementitious materials [55,12,56]. These results are consistent with other studies dealing with concrete, concluding that 5–10 wt% PC-by-WMS replacement appears to be optimum for strength enhancement [34,50,20].

4.2.3. Porosity

Quasi-brittle cementitious materials are designed mainly to sustain compression; thus, high compressive strength is desirable. For this reason, lowering porosity by adding WMS is vital for cementitious composites. Total porosities of pastes, calculated by integrating pore size distributions in Fig. 6, demonstrate that this effect can achieved via a microfilling effect with WMS added in moderate amounts (5–15 wt%), see Table 1. For the 50 wt% addition, total porosity increased by 5% due to higher peaks of pore vol-

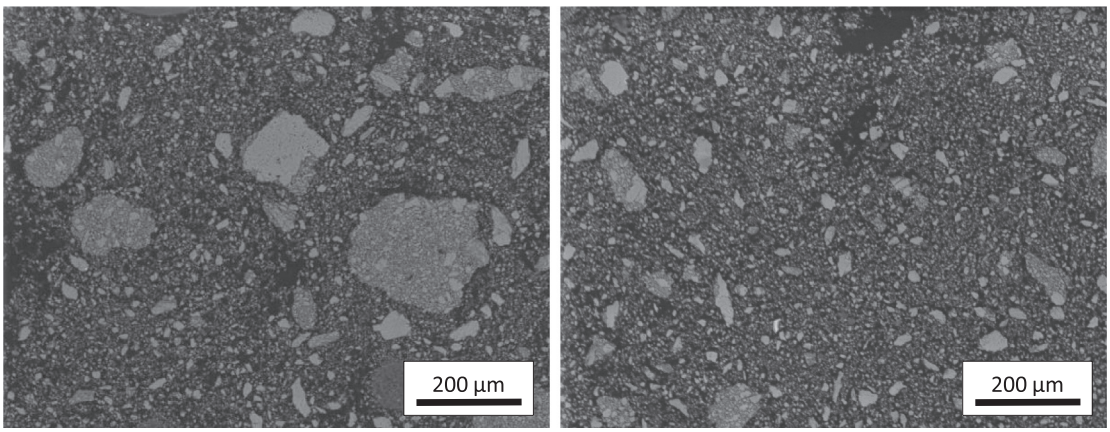

Fig. 2. SEM images of raw (left) and ground (right) WMS at 100× magnification.

Table 3
Chemical composition of PC and WMS (XRF results).

Chemical composition [%]	PC	WMS
CaO	64.8	57.5
SiO_2	20.1	5.02
Fe_2O_3	2.51	1.22
Na_2O	0.13	0.73
MgO	1.92	0.39
Al_2O_3	4.02	0.14
SO_3	3.01	0.06
Other elements	0.45	0.14
LOI	3.05	34.8

Table 4
Mineralogical composition of PC and WMS calculated from XRF results using the Bogue method.

Mineralogical composition [%]	PC	WMS
C_3	74.6	–
C_2S	7.2	–
C_3A	8.1	–
C_4AF	8.5	–
MgO	1.6	–
$CaCO_3$	–	95
Other clay minerals	–	5

ume, around 10 and 500 μm. These findings are in agreement with other studies [57,58,10]. Several authors have studied the impact of coarser fractions and concluded that they are not capable of reducing the porosity of cementitious matrices regardless of the amount incorporated [19,35,21], which supports the assumption of microfilling effects.

4.3. Hydration and development of microstructure

4.3.1. Hydration heat

Calorimetry revealed the positive effects WMS has on hydration, because the more WMS in a mixture, the more cumulative heat was released during the first 7 days of hardening if recalculated to 1 g of PC in the mixtures (Table 5). Similar results were reached by Péra [59], who investigated impacts of $CaCO_3$ on C_3S hydration. Here, we used PC having a high C_3S content (74.6 wt %) and marble powder composed mostly of $CaCO_3$ (95 wt%).

Not only cumulative heat but also heat flow development was affected by the presence of WMS. The values plotted in Fig. 7 that represent absolute heat/heat flux (recalculated to 1 g of the mixture, not PC only), indicate that presence of WMS inhibits rapid hydration of C_3S. On the other hand, heat flux was slightly accelerated by the presence of WMS for the 20–40 h period.

4.3.2. Setting and hardening

The initial and final setting times were determined according to the ČSN EN 196-3 [60] standard using a Vicamatic 2 automatic Vicat apparatus and the results are summarized in Table 5. The initial setting time was reduced with small WMS-for-PC substitutions (the minimum of 191 min was reached for M10), but mixing PC with WMS in a 1:1 weight ratio (M50) led to a similar initial setting time as for pure cement paste (96 min). However, the shorter the initial setting time, the longer the overall duration of setting. In this study, M50 exhibited the shortest setting duration (67 min) and M10 (119 min), the longest. According to Demirel et al. [33], such effects can be attributed to the introduction of $CaCO_3$ to the mixtures, forming nucleation centers for portlandite formation which accelerates the onset of setting. In the mixtures with high concentrations of $CaCO_3$, the portlandite nucleation consists only of the secondary phase, while the primary nucleation of the first crystals from the solution saturated by Ca can be omitted [61]. see Table 6.

4.3.3. Microstructure

SEM images of hardened pastes in Fig. 8 show the impact of WMS on the development of microstructure in pastes. These images were analyzed, and fractions of individual phases were calculated using intensity and entropy thresholding [44]. The images demonstrate that there are no substantial changes in the microstructure except for M50, which contained almost no unhydrated clinker grains and was more porous than other pastes. This is consistent with other analyses performed.

Most importantly, the amount of residual unhydrated clinker decreased non-proportionally according to the percentage of WMS replacement. 15% WMS-for-PC replacement resulted in a

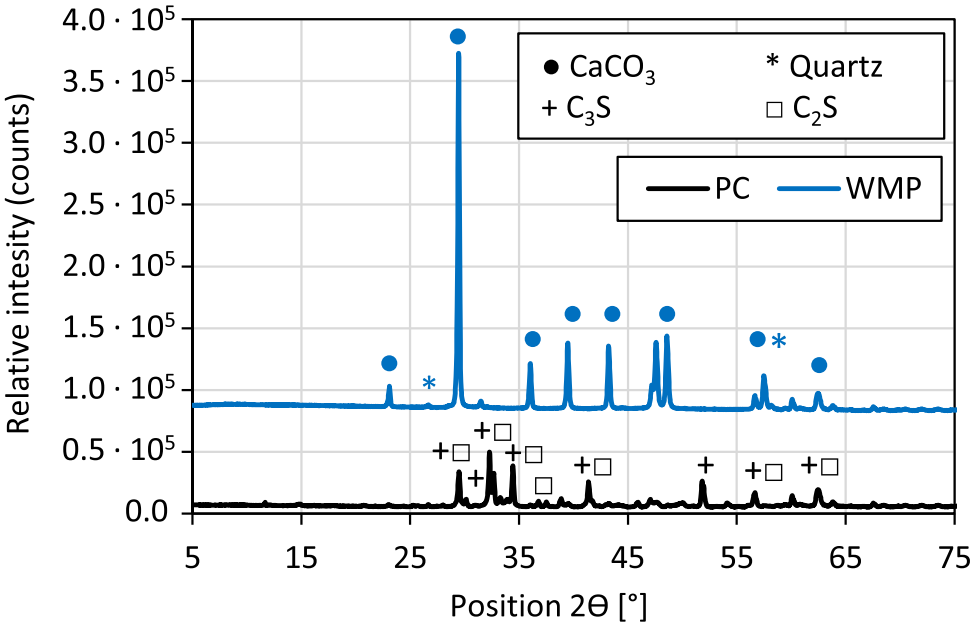

Fig. 3. XRD patterns for PC and WMP.

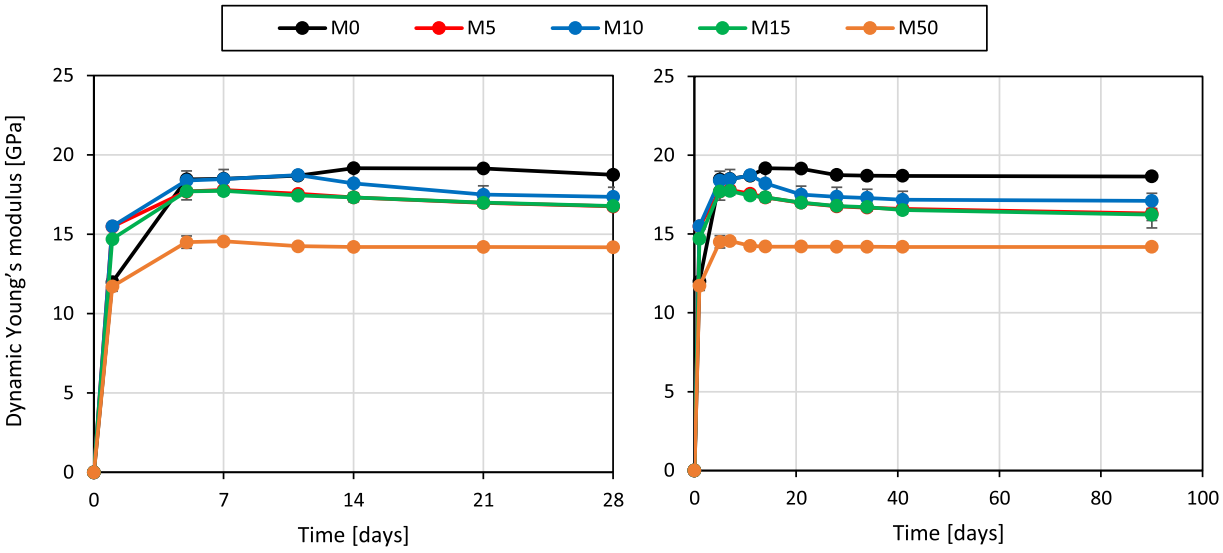

Fig. 4. Development of the dynamic Young's during the first 28 days (left) and first 90 days (right) of hardening.

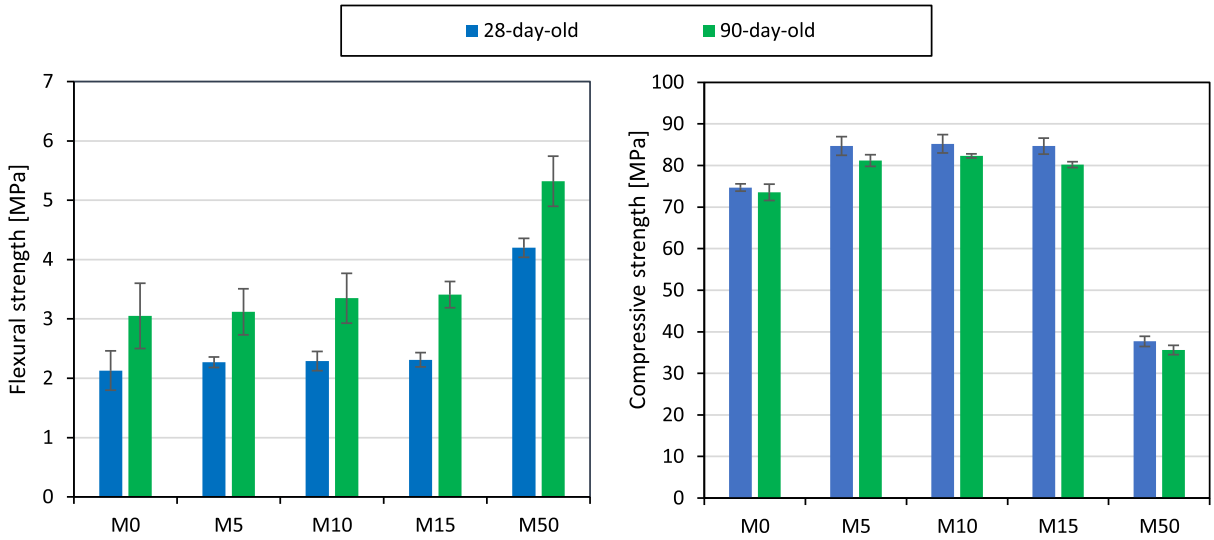

Fig. 5. Flexural (left) and compressive (right) strength of the studied pastes after 28 and 90 days of hardening.

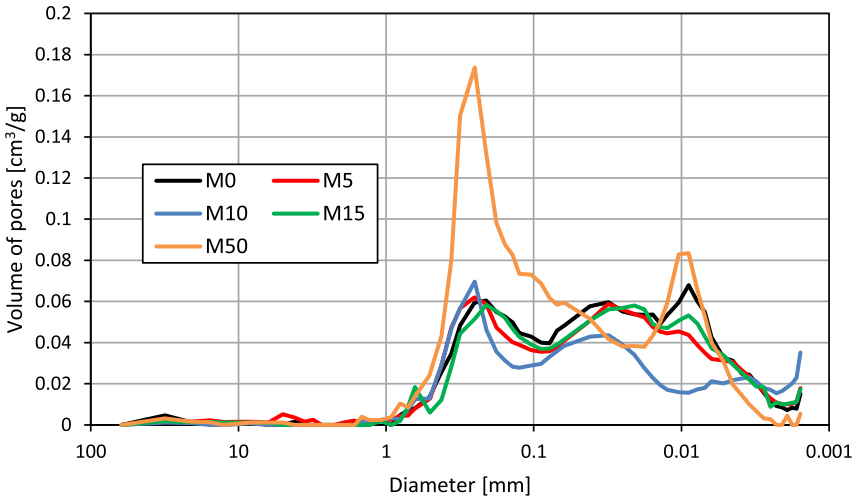

Fig. 6. Pore size distribution curves for pastes with various amount of WMS.

Table 5
Setting and hydration of mixtures.

Mixture	Heat released during first 7 days		Initial setting	Setting duration
	[J/g of mixture]	[J/g of PC]	[min]	[min]
M0	332.5 ± 3.1	332.5 ± 3.1	207 ± 3	96 ± 2
M5	319.7 ± 4.5	336.5 ± 4.7	197 ± 2	95 ± 2
M10	313.8 ± 4.8	348.6 ± 5.3	191 ± 3	119 ± 4
M15	297.5 ± 3.2	350.0 ± 3.8	193 ± 2	79 ± 3
M50	184.6 ± 4.4	369.2 ± 8.8	204 ± 1	67 ± 1

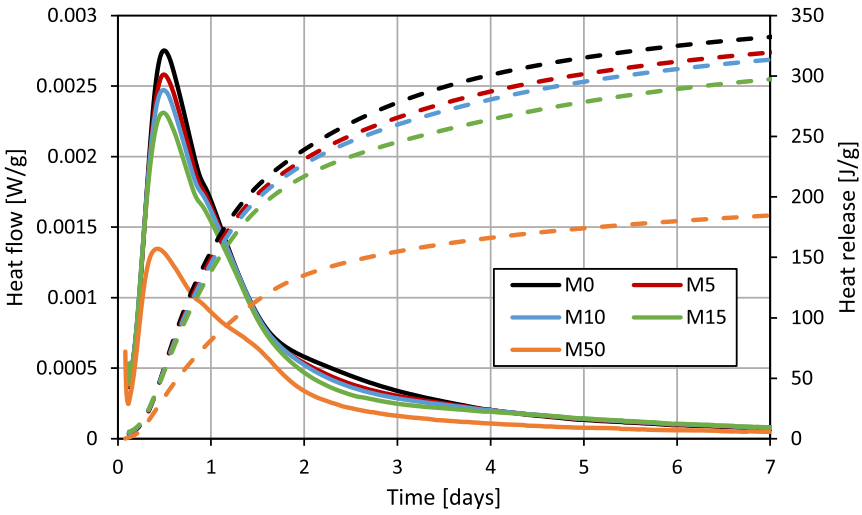

Fig. 7. Hydration heat flow (solid lines) and cumulative heat (dashed line).

Table 6
Fraction of phases [%] identified from SEM-BSE maps.

Mix	Clinker	Marble grains	Portlandite	C-S-H gel	Voids
M0	17.26 ± 2.31	–	18.49 ± 1.84	61.61 ± 4.22	2.63 ± 0.11
M5	15.14 ± 2.01	4.99 ± 1.11	12.98 ± 1.51	64.25 ± 3.25	2.65 ± 0.25
M10	14.27 ± 1.91	10.21 ± 1.45	12.86 ± 1.48	60.12 ± 3.68	2.53 ± 0.32
M15	10.68 ± 1.18	14.22 ± 1.48	13.38 ± 1.61	59.11 ± 2.96	2.62 ± 0.28
M50	6.58 ± 0.59	51.21 ± 3.69	9.40 ± 1.55	29.42 ± 2.99	3.39 ± 0.48

38% reduction in the residual clinker concentration in the hardened pastes. This effect can be attributed to deposition of free water and the water supply of clinker grains during hydration. Moreover, clinker grains can become separated by fine marble particles if blended properly [35]. The maps of calcium distribution in Fig. 8 support this idea, because they indicate that portlandite crystals ($CaOH_2$) are more uniformly distributed within a sample containing WMS (M10). On the other hand, visible clusters of such crystals can be identified in the map of pure cement paste (M0). Similar conclusions were reported by Demirel et al. [33], who suggested that WMS rich in calcium provided nucleation centers for portlandite growth. However, opposite findings were reported by Aliabdo et al. [10], who claimed that marble powder cannot provide nucleation centers and behaves only as a microfiller.

The distribution of Ca/Si along line scans passing across interfaces between marble grains and a cementitious matrix (Fig. 9) revealed the significance and thickness of transition zones. The weight and atomic representations of oxygen, calcium, silicon, and also the Ca/Si ratios are provided in Fig. 10; the presence of aluminum was neglected because the PC used here contained low amounts of aluminates (C_3A and C_4AF). The Ca/Si ratio indicated the presence and density of C-S-H gels, since they can be chemically described as [62]:

$$x\mathrm{CaO} \cdot y\mathrm{SiO_2} \cdot z\mathrm{H_2O}, \quad (3)$$

where $x = 0.5 - 1.5, y = 1, z = 0.5 - 2.5$ represent high density C-S-H gel and $x = 1.5 - 2, y = 1, z = 1 - 4$ represent low density C-S-H gel.

Based on line scan data, it is evident that there is a higher concentration of calcium at location of grains, but also up to 10 μm from the boundary of grains. The Ca/Si ratio stabilizes at a distance of 20 μm. Therefore, it can be conjectured that low-density C-S-H gel forms in the vicinity of grains as suggested by an experimental-computational approach proposed by Nežerka et al. [36].

4.3.4. XRD results

The XRD diffractograms (Fig. 11) show distinct peaks for the hardened pastes, allowing to identify the following phases: alite, Brownmillerite, calcite (and its various forms aragonite and vaterite), and Portlandite; quartz, gypsum, and ettringite were traced in amounts lower than 5 wt%. The diffraction spectra show that the amount of clinker in M0 sample was approximately 40 wt%, for M5 35 wt%, for M10 29 wt%, for M15 23 wt%, and for M50 5 wt %. After recalculating the percentages of crystalline phases (without C-S-H and voids) detected using SEM-BSE, the amounts of clin-

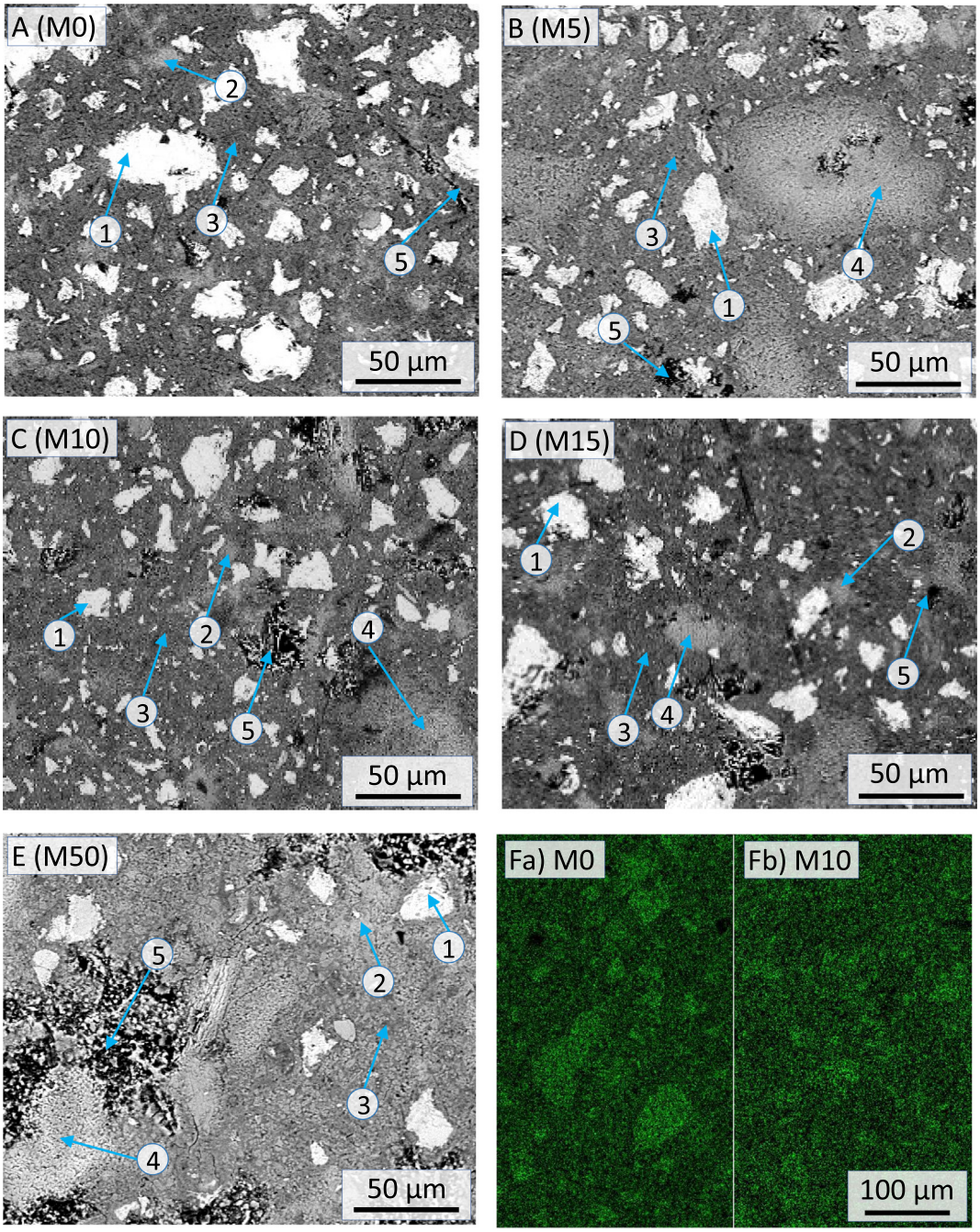

Fig. 8. A–E: Representative SEM-BSE images of microstructure in samples M0–M50 at a 500× magnification with indication of the following phases: clinker (1), portlandite (2), C-S-H gel (3), marble grain (4), and voids (5); F: SEM-EDS maps of a) M0 and b) M10 at a 400× magnification showing a distribution of calcium.

ker, marble inclusions, and Portlandite correspond to XRD within 5 wt%.

4.3.5. Nanoindentation results

The assumption of the formation of weak (and relatively compliant) low-density C-S-H gel was tested using nanoindentation. Here, line scans were placed across interfaces of marble grains in the same fashion as for the SEM-EDS analysis. Fig. 12 shows a distribution of the indentation modulus along a line scan and the identified transition zone of lower stiffness in the 30-µm-thick region next to a marble grain. The indentation modulus at the marble grain location was on average 55 GPa, while moduli for the transition zone ranged from 5 to 10 GPa. Such a distribution of indentation moduli confirms the assumptions based on SEM-EDS analysis and conclusions from Nežerka et al. [36].

5. Conclusion

This experimental study tested the potential suitability of using waste marble sludge, an industrial by-product, as a replacement for Portand cement in cementious pastes. Prior researchers found conflicting results for the incorporation of fine marble particles into such composites. Here, we focused on the development of the microstructure in cement pastes containing marble sludge and resultant mechanical properties. The sludge used in this study was finely ground in order to attain microfilling properties, to

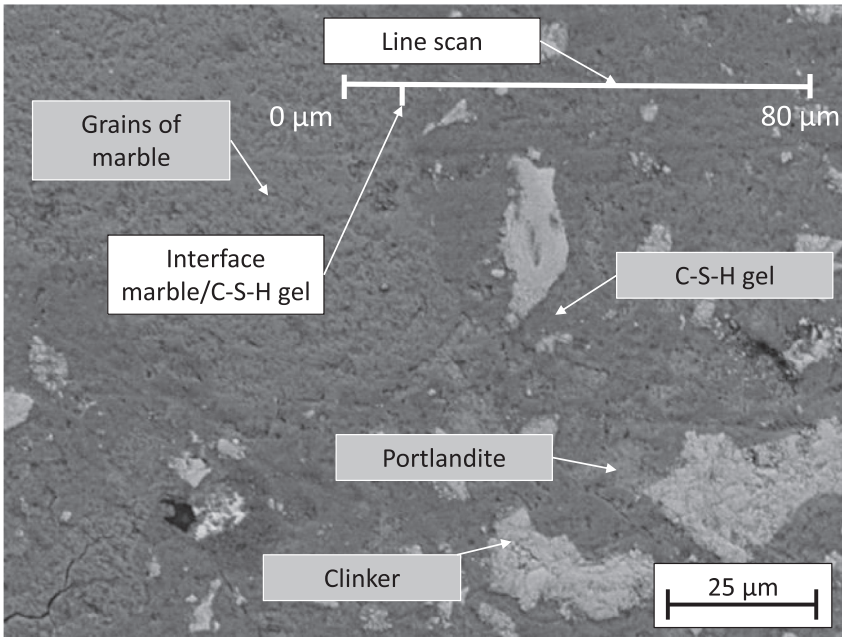

Fig. 9. Line scan position for SEM-EDS analysis; M10 sample at a 500× magnification.

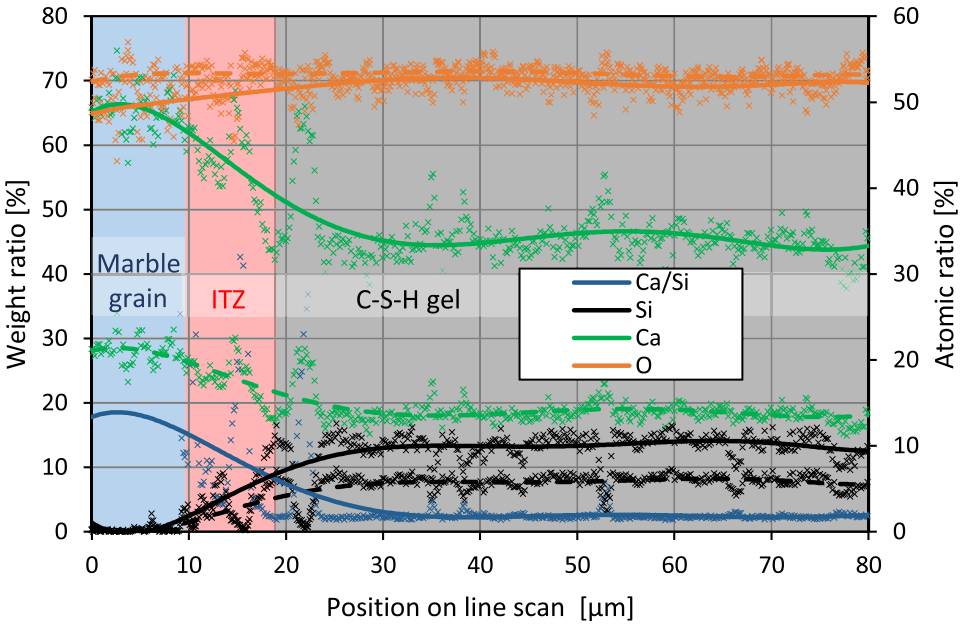

Fig. 10. Results from the line scan in Fig. 9 placed across an interfacial transition zone (ITZ), with weight (solid line) and atomic (dashed line) concentrations.

potentially increase reactivity, and to improve workability of the mixtures. Based on results of the analyses at both micro- and macro-scale, it can be concluded that:

- Moderate replacements of PC about 5–10 wt% with marble sludge led to plasticizing effects, reducing the amount of kneading water necessary for reaching sufficient workability,
- The microfilling effect of marble sludge particles was responsible for reduced porosity of pastes when added in amounts up to 15 wt%,
- The presence of marble sludge particles contributed to smaller clusters of portlandite crystals and more homogeneous distribution of phases,
- High replacement of Portland cement with marble sludge, 50 wt %, resulted in a significant increase of flexural strength, but compressive strength was greatly reduced, by about a factor of 2.0,
- Chemical composition detected using SEM-BSE and the stiffness assessed using nanoindentation indicated a presence of low-density C-S-H gel in the vicinity of marble grains, making the transition zone a weak link within the microstructure for all samples.

The formation of a weak transition zone around marble particles limits the ability of marble sludge to be used in cementitious composites—even though the inert particles reinforce the brittle cementious matrix to sustain tensile stresses, the transition zone

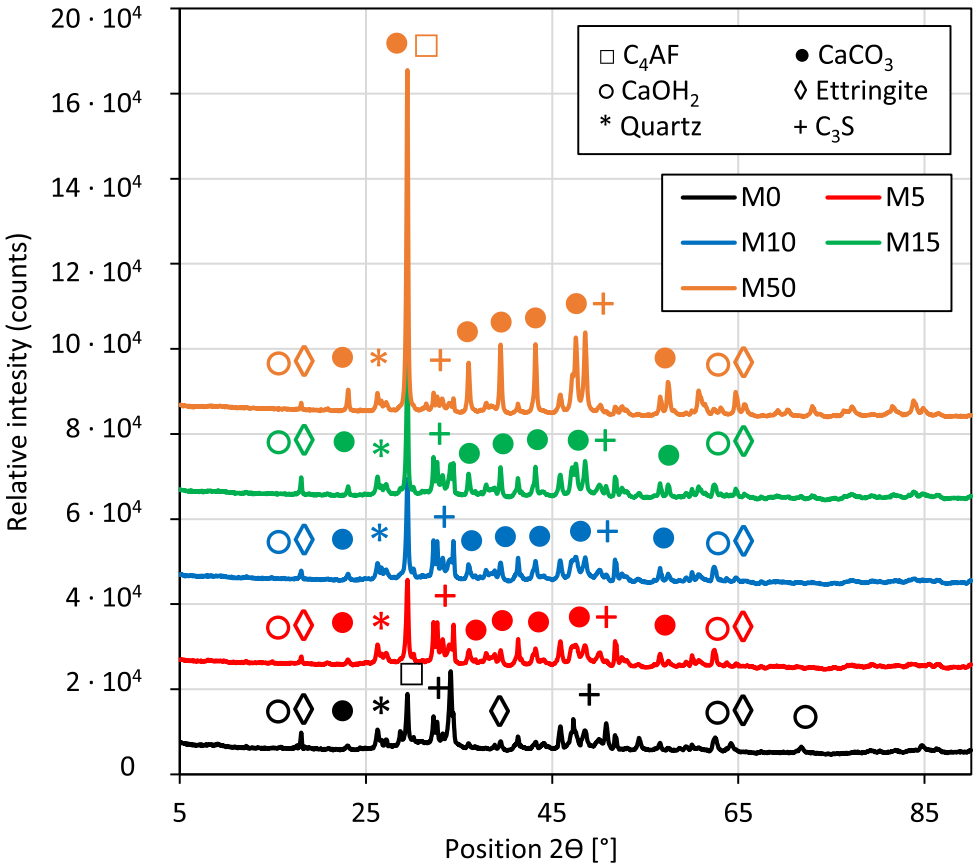

Fig. 11. XRD patterns of hardening pastes.

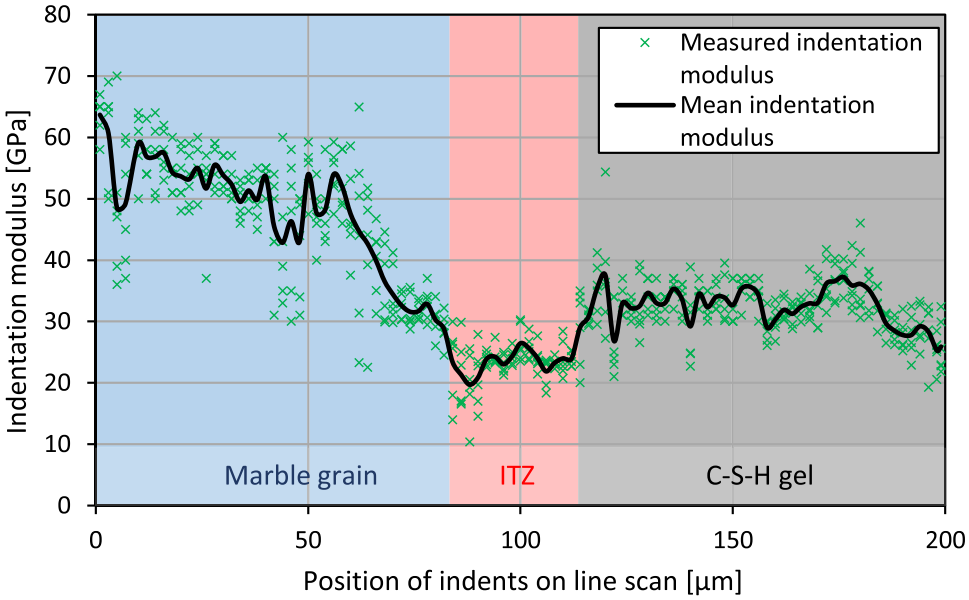

Fig. 12. Indentation results along a line scan across an ITZ between a marble grain and a cementitious matrix in an M10 sample.

makes composites containing high amounts of marble inclusions weaker in compression. Despite this limitation, blending WMS with Portland cement in amounts lower than 15 wt%, which appears reasonable in terms of mechanical performance, holds promise. Given the large amount of concrete and marble sludge produced worldwide, such incorporation could potentially have a considerable impact on the sustainable reuse of WMS, reducing landfilling requirements.

Funding

This work was supported by the Czech Science Foundation [Grant No. GA ČR 17-06771S].

Declaration of Competing Interest

The authors declare that they have no known competing financial interests or personal relationships that could have appeared to influence the work reported in this paper.

Acknowledgment

The help of Dr. Stephanie Krueger, who provided editorial assistance, is gratefully acknowledged. The authors also wish to thank Dr. George Karra'a from the Lavaris company for providing the ground marble used in this study.

References

[1] T.U.J. Ganiron, Recycling concrete debris from construction and demolition waste, Int. J. Adv. Sci. Technol. 77 (2015) 7–24, https://doi.org/10.14257/ijast.2015.77.02.
[2] R. Jin, B. Li, T. Zhou, D. Wanatowski, P. Piroozfar, An empirical study of perceptions towards construction and demolition waste recycling and reuse in China, Resour. Conserv. Recycl. 126 (2017) 86–98, https://doi.org/10.1016/j.resconrec.2017.07.034.
[3] J.-L. Gálvez-Martos, D. Styles, H. Schoenberger, B. Zeschmar-Lahl, Construction and demolition waste best management practice in Europe, Resour. Conserv. Recycl. 136 (2018) 166–178, https://doi.org/10.1016/j.resconrec.2018.04.016.
[4] R. Islam, T.H. Nazifa, A. Yuniarto, A.S. Uddin, S. Salmiati, S. Shahid, An empirical study of construction and demolition waste generation and implication of recycling, Waste Manage. 95 (2019) 10–21, https://doi.org/10.1016/j.wasman.2019.05.049.
[5] H. Akbulut, C. Gürer, Use of aggregates produced from marble quarry waste in asphalt pavements, Build. Environ. 42 (2007) 1921–1930, https://doi.org/10.1016/j.buildenv.2006.03.012.
[6] V. Sata, C. Jaturapitakkul, K. Kiattikomol, Influence of pozzolan from various by-product materials on mechanical properties of high-strength concrete, Constr. Build. Mater. 21 (2007) 1589–1598, https://doi.org/10.1016/j.conbuildmat.2005.09.011.
[7] A. Mashaly, B. El-Kaliouby, B. Shalaby, A. El-Gohary, M. Rashwan, Effects of marble sludge incorporation on the properties of cement composites and concrete paving blocks, J. Cleaner Prod. 112 (2016) 731–741, https://doi.org/10.1016/j.jclepro.2015.07.023.
[8] M. Singh, K. Choudhary, A. Srivastava, K. Sangwan, D. Bhunia, A study on environmental and economic impacts of using waste marble powder in concrete, J. Build. Eng. 13 (2017) 87–95, https://doi.org/10.1016/j.jobe.2017.07.009.
[9] A.O. Mashaly, B.N. Shalaby, M.A. El-Hefnawi, Characterization of the marble sludge of The Shaq El Thoaban industrial zone, Egypt and its compatibility for various recycling applications, Aust. J. Basic Appl. Sci. 6 (2012) 153–161.
[10] A. Aliabdo, A. Abd Elmoaty, E. Auda, Re-use of waste marble dust in the production of cement and concrete, Construction and Building, Materials 60 (2014) 28–41, https://doi.org/10.1016/j.conbuildmat.2013.09.005.
[11] M.S. Ibrahim, E.-S.A. Badr, S.A. Asker, N.M. El-galad, Health risk assessment of marble dust at marble workshops, Nat. Sci. 9 (11) (2011) 144–154.
[12] H. Arel, Recyclability of waste marble in concrete production, J. Cleaner Prod. 131 (2016) 179–188, https://doi.org/10.1016/j.jclepro.2016.05.052.
[13] F.J. Aukour, Incorporation of marble sludge in industrial building, Marble and Beige Marble Industry Report 3 (1) (2009) 58–65.
[14] O. Vavruška, Současnost a perspektiva těžby a úpravy nerudních surovin II, VŠB – Technická univerzita, Ostrava, 2002.
[15] J. Lederová, P. Leber, Využití prumyslových odpadních materiálu při výrobě stavebních hmot, Stavebnictví 8 (04) (2008).
[16] K. Alzboon, K. Mahasneh, Effect of using stone cutting waste on the compression strength and slump characteristics of concrete, Int. J. Environ. Ecol. Eng. 3 (2009) 491–496.
[17] I. Topçu, M. Canbaz, Effect of different fibers on the mechanical properties of concrete containing fly ash, Constr. Build. Mater. 21 (2007) 1486–1491, https://doi.org/10.1016/j.conbuildmat.2006.06.026.
[18] N. Almeida, F. Branco, J.R. Santos, Recycling of stone slurry in industrial activities: application to concrete mixtures, Build. Environ. 42 (2007) 810–819, https://doi.org/10.1016/j.buildenv.2005.09.018.
[19] A. Rana, P. Kalla, L.J. Csetenyi, Sustainable use of marble slurry in concrete, J. Cleaner Production.https://doi.org/10.1016/j.jclepro.2015.01.053.
[20] A. Khodabakhshian, J. de Brito, M. Ghalehnovi, E.A. Shamsabadi, Mechanical, environmental and economic performance of structural concrete containing silica fume and marble industry waste powder, Constr. Build. Mater. 169 (2018) 237–251, https://doi.org/10.1016/j.conbuildmat.2018.02.192.
[21] A. Talah, F. Kharchi, R. Chaid, Influence of marble powder on high performance concrete behavior, Proc. Eng. 114 (2015) 685–690, https://doi.org/10.1016/j.proeng.2015.08.010.
[22] E. Bacarji, R.D. Toledo Filho, E.A. Koenders, E.P. Figueiredo, J.L. Lopes, Sustainability perspective of marble and granite residues as concrete fillers, Constr. Build. Materi. 45 (2013) 1–10. https://doi.org/10.1016/j.conbuildmat.2013.03.032.
[23] N.M. Soliman, Effect of using marble powder in concrete mixes on the behavior and strength of RC slabs, Int. J. Current Eng. Technol. 3 (5) (2013) 1863–1870.
[24] H.Y. Aruntaş, M. Gürü, M. Dayi, I. Tekin, Utilization of waste marble dust as an additive in cement production, Mater. Des.https://doi.org/10.1016/j.matdes.2010.03.036.
[25] A. Ergun, Effects of the usage of diatomite and waste marble dust as partial replacement of cement on the mechanical properties of concrete, Constr. Build. Mater. 25 (2011) 806–812, https://doi.org/10.1016/j.conbuildmat.2010.07.002.
[26] B. Rai, N. Khan, K. Abhishek, R. Tabin, S. Duggal, Influence of marble powder/granules in concrete mix, Int. J. Civil Struct. Eng. 1 (2011) 827–834.
[27] S. Agarwal, D. Gulati, Utilization of industrial wastes and unprocessed microfillers for making cost effective mortars, Constr. Build. Mater. 20 (2006) 999–1004, https://doi.org/10.1016/j.conbuildmat.2005.06.009.
[28] O.M. Omar, G.D.A. Elhameed, M.A. Sherif, H.A. Mohamadien, Influence of limestone waste as partial replacement material for sand and marble powder in concrete properties, HBRC J. 8 (2012) 193–203, https://doi.org/10.1016/j.hbrcj.2012.10.005.
[29] V. Corinaldesi, G. Moriconi, T. Naik, Characterization of marble powder for its use in mortar and concrete, Constr. Build. Mater. 24 (2010) 113–117, https://doi.org/10.1016/j.conbuildmat.2009.08.013.
[30] N. Ural, C. Karakurt, A.T. Cömert, Influence of marble wastes on soil improvement and concrete production, J. Mater. Cycles Waste Manage. 16 (2013) 500–508, https://doi.org/10.1007/s10163-013-0200-3.
[31] O. Keleştemur, S. Yildiz, Estimation of compressive strength of waste marble dust and glass fibre included concretes by artificial neural network, Eng. Sci. 6 (2011) 1292–1303, https://doi.org/10.12739/nwsaes.v6i4.5000066941.
[32] H. Binici, T. Shah, O. Aksogan, H. Kaplan, Durability of concrete made with granite and marble as recycle aggregates, J. Mater. Process. Technol. 208 (2008) 299–308, https://doi.org/10.1016/j.jmatprotec.2007.12.120.
[33] B. Demirel, The effect of the using waste marble dust as fine sand on the mechanical properties of the concrete, Int. J. Phys. Sci. 5 (9) (2010) 1372–1380.
[34] M.J. Munir, S.M.S. Kazmi, Y.-F. Wu, Efficiency of waste marble powder in controlling alkali-silica reaction of concrete: a sustainable approach, Constr. Build. Mater. 154 (2017) 590–599, https://doi.org/10.1016/j.conbuildmat.2017.08.002.
[35] N.T. Seghir, M. Mellas, Ł. strok;. Sadowski, A. Krolicka, A. Zak, K. Ostrowski, The utilization of waste marble dust as a cement replacement in air-cured mortar, Sustainability (Switzerland) 11 (8).https://doi.org/10.3390/su11082215.
[36] V. Nežerka, V. Hrbek, Z. Prošek, M. Somr, P. Tesárek, J. Fládr, Micromechanical characterization and modeling of cement pastes containing waste marble powder, J. Cleaner Prod. 195 (2018) 1081–1090, https://doi.org/10.1016/j.jclepro.2018.05.284.
[37] Z. Prošek, V. Nežerka, R. Hlužek, J. Trejbal, P. Tesárek, G. Karra'a, Role of lime, fly ash, and slag in cement pastes containing recycled concrete fines, Constr. Build. Mater. 201 (2019) 702–714, https://doi.org/10.1016/j.conbuildmat.2018.12.227.
[38] V. Nežerka, P. Bílý, V. Hrbek, J. Fládr, Impact of silica fume, fly ash, and metakaolin on the thickness and strength of the ITZ in concrete, Cem. Concr. Compos. 103 (2019) 252–262, https://doi.org/10.1016/j.cemconcomp.2019.05.012.
[39] European Committee for Standardization, EN 197-1:2011: Cement. Composition, specifications and conformity criteria for common cements., BSI, 2011.
[40] European Standard EN 12350-5, Testing fresh concrete; flow table test.
[41] European Committee for Standardization, EN 196-2:2013: Method of testing cement. Chemical analysis of cement, BSI, 2013.
[42] V. Nežerka, Z. Slížková, P. Tesárek, T. Plachý, D. Frankeová, V. Petráňová, Comprehensive study on microstructure and mechanical properties of lime-pozzolan pastes, Cem. Concr. Res. 64 (2014) 17–29, https://doi.org/10.1016/j.cemconres.2014.06.006.
[43] European Committee for Standardization, EN 196-1:2016: Methods of testing cement. Determination of strength, BSI, 2016.
[44] V. Nežerka, J. Trejbal, Assessment of aggregate-bitumen coverage using entropy-based image segmentation, Road Mater. Pavement Des. (2019) 1–12, https://doi.org/10.1080/14680629.2019.1605304.
[45] W. Oliver, G. Pharr, An improved technique for determining hardness and elastic modulus using load and displacement sensing indentation experiments, J. Mater. Res. 7 (06) (2011) 1564–1583, https://doi.org/10.1557/JMR.1992.1564.
[46] M. Shah, Nanotechnology Applications for Improvements in Energy Efficiency and Environmental Management, Advances in Environmental Engineering and Green Technologies (2326–9162), IGI Global, 2014.
[47] ASTM C1356-07, Standard Test Method for Quantitative Determination of Phases in Portland Cement Clinker by Microscopical Point-Count Procedure, Annual Book of ASTM Standards, ASTM International, West Conshohocken, PA.
[48] J. Topič, J. Trejbal, T. Plachý, Z. Prošek, Relationship between compressive strength and young's modulus of cement paste with recycled concrete powder, in: Key Engineering Materials, vol. 722, Trans Tech Publ, 2017, pp. 254–259.

[49] R. Jones, 1 a review of the non-destructive testing of concrete, in: Non-destructive testing of concrete and timber, Thomas Telford Publishing, 1970, pp. 1–7.
[50] R. Rodrigues, J. De Brito, M. Sardinha, Mechanical properties of structural concrete containing very fine aggregates from marble cutting sludge, 2015. https://doi.org/10.1016/j.conbuildmat.2014.12.104.
[51] P.C. Strange, A.H. Bryant, The role of aggregate in the fracture of concrete, J. Mater. Sci. 14 (1979) 1863–1868, https://doi.org/10.1007/bf00551025.
[52] B. Karihaloo, A. Carpinteri, M. Elices, Fracture mechanics of cement mortar and plain concrete, Adv. Cem. Based Mater. 1 (1993) 92–105, https://doi.org/10.1016/1065-7355(93)90014-f.
[53] I. Rhee, J.S. Lee, Y.-S. Roh, Fracture parameters of cement mortar with different structural dimensions under the direct tension test, Materials 12 (2019) 1850, https://doi.org/10.3390/ma12111850.
[54] Z. Prošek, J. Trejbal, V. Nežerka, V. Goliáš, M. Faltus, P. Tesárek, Recovery of residual anhydrous clinker in finely ground recycled concrete, Resour. Conserv. Recycl. 155 (2020), https://doi.org/10.1016/j.resconrec.2019.104640 104640.
[55] A.M. Neville, Properties of Concrete, fourth ed., Longman, 1996.
[56] V. Nežerka, J. Zeman, J. Němeček, Micromechanics-based simulations of compressive and tensile testing on lime-based mortars, Mech. Mater. 105 (2017) 49–60, https://doi.org/10.1016/j.mechmat.2016.11.011.
[57] H. Hebhoub, H. Aoun, M. Belachia, H. Houari, E. Ghorbel, Use of waste marble aggregates in concrete, Constr. Build. Mater. 25 (2011) 1167–1171, https://doi.org/10.1016/j.conbuildmat.2010.09.037.
[58] T. Uygunoğlu, I.B. Topcu, O. Gencel, W. Brostow, The effect of fly ash content and types of aggregates on the properties of pre-fabricated concrete interlocking blocks (PCIBs), Constr. Build. Mater. 30 (2012) 180–187, https://doi.org/10.1016/j.conbuildmat.2011.12.020.
[59] J. Péra, S. Husson, B. Guilhot, Influence of finely ground limestone on cement hydration, Cem. Concr Compos. 21 (1999) 99–105, https://doi.org/10.1016/s0958-9465(98)00020-1.
[60] European Committee for Standardization, EN 196-3:2016: Methods of testing cement. Determination of setting times and soundness, BSI, 2016.
[61] G.D. Botsaris, Secondary Nucleation – A Review, Industrial Crystallization (1976), https://doi.org/10.1007/978-1-4615-7258-9_1.
[62] H. Taylor, Cement chemistry, Thomas Telford Publishing, 1997, https://doi.org/10.1680/cc.25929.

Appendix C

Prošek, Z.; Trejbal, J.; Nežerka, V.; Goliáš, V.; Faltus, M.; Tesárek, P.: Recovery of residual anhydrous clinker in finely ground recycled concrete, *Resources, Conservation and Recycling* 155 (2020) 104640, doi: 10.1016/j.resconrec.2019.104640

Author's contribution: main idea, SEM microscopy, data analysis, design of experiments, preparation of specimens.

Resources, Conservation & Recycling 155 (2020) 104640

Contents lists available at ScienceDirect

Resources, Conservation & Recycling

journal homepage: www.elsevier.com/locate/resconrec

Recovery of residual anhydrous clinker in finely ground recycled concrete

Z. Prošek[a], J. Trejbal[a], V. Nežerka[a,*], V. Goliáš[b], M. Faltus[b], P. Tesárek[a]

[a] Faculty of Civil Engineering, Czech Technical University in Prague, Thákurova 7, 166 29 Praha 6, Czech Republic
[b] Institute of Geochemistry, Mineralogy and Mineral Resources, Faculty of Science, Charles University in Prague, Albertov 6, 128 43 Praha 2, Czech Republic

ARTICLE INFO

Keywords:
Construction and demolition waste
Recycling
Concrete
Cement paste
Residual anhydrous clinker

ABSTRACT

The costs of construction waste handling, a scarcity of landfill sites, and requirements for sustainable construction have placed recycling of concrete—the most abundant construction material in the world—under scrutiny. Unlike recycling of aggregates, utilization of sub-sieve fractions from recycled concrete has not yet been adopted in the construction industry. In this study, we investigate the possibility of recovering residual anhydrous clinker embedded in grains of stripped mortar within these fines. Different samples of waste concrete were finely ground and studied using microscopy and chemical analyses to assess the amount of residual clinker. Its contribution to hydration processes was measured by calorimetry, and the impact of recycled concrete fines on mechanical properties of cement pastes was tested. The results indicate that residual anhydrous clinker is present in waste concrete and can be recovered by grinding. Replacing Portland cement with the recycled material in pastes led to a significant increase of tensile strength, while deterioration of compressive strength was negligible when the concrete fines contained higher amounts of residual clinker and when the amount of fines did not exceed 30% of Portland cement weight.

1. Introduction

A directive adopted in 2008 by the European Parliament set an ambitious target to reuse or recycle a minimum of 70% weight of construction and demolition waste by 2020 (The European Parliament and of the Council, 2008; Oksri-Nelfia et al., 2015). Incorporation of ground waste in concrete mixes represents a cheap solution to meet the objectives set by the European Parliament, and to tackle the environmental burden of landfilling (Gastaldi et al., 2015) and CO_2 emissions related to the production of Portland cement (US Geological Survey, 2009; Paris et al., 2016; da Silva and de Oliveira Andrade, 2017; Lee et al., 2018; Nežerka et al., 2018). Moreover, the use of mobile grinders at demolition sites and exploiting the potential of waste can also have economic benefits, especially in densely populated areas where construction waste disposal is complicated and expensive. The development of technologies enabling the utilization of demolition waste in the production of new concrete could have a beneficial effect on the reconstruction of cities affected by armed conflicts, e.g., in the Middle East (Srour et al., 2013; Madi and Srour, 2019).

A partial replacement of quarried aggregates with recycled ones has become common practice in the construction industry (Tabsh and Abdelfatah, 2009; Silva et al., 2014; Kapoor et al., 2016; Colangelo et al., 2018; Khoury et al., 2018; Tam et al., 2018a, 2018b). The inconveniences connected to the use of recycled aggregates such as altered workability (Belin et al., 2013), lower strength (Katz, 2003; Etxeberria et al., 2007; Kwan et al., 2011; Oksri-Nelfia et al., 2015; Wu and Luo, 2018), and durability (Evangelista and de Brito, 2010; Pedro et al., 2018), have been overcome by careful cleaning of recycled aggregates (Florea and Brouwers, 2013) or their carbonation (Thiery et al., 2013; Tam et al., 2016). As an alternative solution, the introduction of residual mortar attached to recycled aggregates can be conducted by employing various mixing and proportioning techniques that account for the presence of impurities (Yang and Lee, 2017; Yang, 2018). Unlike the widely accepted use of recycled aggregates, utilization of fine subsieve fractions that constitute about 15–50% of crushed concrete weight (Shui et al., 2008; Ma and Wang, 2013) is highly restricted or even forbidden (Evangelista and de Brito, 2018) due to generally accepted misconceptions about the impact of using fines on concrete performance (Evangelista and de Brito, 2013). However, recent findings (Khatib, 2005; Levy and Helène, 2007; Evangelista and de Brito, 2010; Pereira et al., 2012; Anastasiou et al., 2014; Cartuxo et al., 2015) indicate that incorporation of recycled concrete fines (RCF) can be feasible if a mix is designed carefully and contains suitable admixtures.

It was reported in a recent study (Prošek et al., 2019) that RCF can be incorporated into cementitious composites in large amounts when

* Corresponding author.
E-mail address: vaclav.nezerka@fsv.cvut.cz (V. Nežerka).

https://doi.org/10.1016/j.resconrec.2019.104640
Received 26 July 2019; Received in revised form 29 November 2019; Accepted 9 December 2019
Available online 23 December 2019

blended with fly ash or blast furnace slag without sacrificing mechanical strength. Strength enhancement and shrinkage reduction in such composites were attributed to the following: (i) recycled sand and hydrated particles within RCF can act as microfillers, reducing excessive porosity of interfacial transition zones (Li et al., 1999; Khan, 2003; Bentz et al., 2000; Golewski, 2018), while (ii) stripped cementitious paste contains, in addition to minerals having a beneficial effect on cement hydration (Memon et al., 2002; Khokhar et al., 2010), a portion of anhydrous clinker (Shui et al., 2008; Ma and Wang, 2013; Lidmila et al., 2013). Potential recovery of residual anhydrous clinker (RAC) has been recently investigated by Bordy et al. (2017), who reported up to 24 wt.% of reactive RAC in recycled concrete pastes, but their study was limited to the recycling of cement pastes prepared under laboratory conditions, which cannot be directly translated to practical use.

This study is focused on the detection of RAC in waste concrete from discarded precast elements and demolished structures of different ages, types, and exposures to various weathering conditions. In addition to the chemical composition and morphology of the investigated RCF samples, hydration of cement pastes containing RCF as well as the porosity and development of the mechanical properties of pastes were studied. Commonly available separators and high-speed mills were used in the study so that the materials can be prepared and reproduced on a larger scale, rendering the study potentially useful for the construction industry.

2. Materials

2.1. Input materials

Four types of recycled concrete (Table 1) were prepared using hydraulic crushers and a high-speed Lavaris SKD 600 (2 × 30 kW) electric mill. The first RCF material was produced from a prestressed recycled railway sleeper (RRS). The sleeper had been manufactured from high-quality concrete of class C 45/55-XF1 (Eurocode, 2005) and had been used in a railway track near Prague (Czech Republic), subjected to weathering. Next, powder from a recycled drainage channel (RDC) was prepared from an unreinforced prefabricate containing a lower amount of cementitious matrix. The channel had been manufactured from a Portland cement rich in alite that had ensured rapid strength and stiffness gain (Maruyama et al., 2010; Prošek et al., 2019). Finally, recycled reinforced concrete from monolithic columns was selected as a third material for the production of RCF. The columns had been disposed of during the demolition of the derelict Walter Motors factory built in 1911.

All RCF samples were prepared by concrete crushing to remove fractions larger than 16 mm, separated from rebars (if needed), and then were ground. In the case of demolished columns, the crushed concrete was split into two samples: in the first one (RC1), only a 0–1 mm fraction was separated for grinding so that it contained stripped mortar with a low amount of aggregates, while the other sample (RC2) was ground without removal of aggregates, as for RRS and RDC.

Individual RCF samples were blended with ordinary Portland cement (PC), CEM I/42.5R (EN 197-1:2001, European Committee for Standardization, 2011), to produce cementitious pastes as presented in Section 2.2. The particle size distribution and size characteristics of PC and RCF are provided in Table 2 and Fig. 1, respectively. The size characteristics were analyzed using laser granulometry (Fritsch Analyssete 22 Micro Tec Plus device), while the specific surface was determined using the Blaine method (Matest E009 device). As the value d_{32} indicates, only RC1 contained ultrafine particles below 1 µm, but RDC also contained smaller particles constituting the bulk of the volume when compared to PC, as indicated by d_{43}. The size distribution of RRS and RC2 is by order of magnitude shifted toward larger particles due to the presence of stiff aggregates within the ground material. The fineness of RC1 and RDC was reflected by higher specific surface measurements, which negatively impact the workability of fresh pastes.

While the high pH of all RCF materials could indicate the presence of RAC, the degradation of hydrated clinker minerals to CaO or $Ca(OH)_2$ was more likely the cause.

Table 2
Size characteristics of RCF after grinding, their specific surfaces, and the pH of 1:100 water suspensions after 24 h at 25 °C.

	PC	RRS	RDC	RC1	RC2
Sauter mean diameter, d_{32} [µm]	2.65	7.12	3.71	2.02	7.87
De Brouckere mean diameter, d_{43} [µm]	18.5	106.0	9.98	8.20	104.0
Specific surface [m^2/kg]	380	265	460	860	177
pH	12.5	11.9	11.6	12.9	12.8

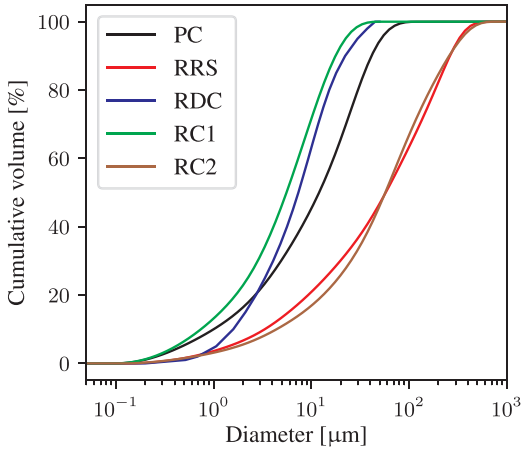

Fig. 1. Particle size distribution curves of input materials.

2.2. Tested materials and samples

The studied cementitious pastes (Table 3) were produced by blending PC with RCF using an electric blender for 5 minutes (dry mixture) and consequently 10 minutes (homogenized mixture with water) at a speed of 235 rpm. Water to PC and RCF (collectively referred to as "binders") ratio (w/b) was kept constant and relatively low, $w/b = 0.35$, to avoid the presence of bubbles and excessive shrinkage cracking (Idiart et al., 2012; Nežerka et al., 2018; Prošek et al., 2019). Results of a flow test (see Table 3), carried out according to EN 12350-2 (European Standard, 2019), indicate poorer workability of pastes containing RCF with smaller particles (RDC and RC1) due to adhesion, the result of a large specific surface (Table 2).

Table 1
Summary of recycled concrete materials.

	Origin	Age	Class (Eurocode, 2005)	Recycling procedure
RRS	Railway sleeper	50 years	C 45/55-XF1	Crushing, grinding
RDC	Drainage channel	4 years	C 20/25	Crushing, grinding
RC1	Monolithic column	107 years	Not available	Crushing, extraction of fines, grinding
RC2	Monolithic column	107 years	Not available	Crushing, grinding

Table 3
Composition of the prepared mixes (amount of individual components expressed in wt.%) and total porosity of the mixes determined by mercury intrusion porosimetry.

Mix	PC	RCF				w/b	Porosity	Flow test [mm]
		RRS	RDC	RC1	RC2			
R	100	–	–	–	–	0.35	22.5	160
RS-10	90	10	–	–	–		22.7	170
RS-20	80	20	–	–	–		22.7	180
RS-30	70	30	–	–	–		23.2	180
RS-40	60	40	–	–	–		25.3	180
RS-50	50	50	–	–	–		27.6	180
DG-10	90	–	10	–	–		23.1	150
DG-20	80	–	20	–	–		24.3	140
DG-30	70	–	30	–	–		24.7	130
DG-40	60	–	40	–	–		25.8	120
DG-50	50	–	50	–	–		26.8	110
C1-10	90	–	–	10	–		23.0	135
C1-20	80	–	–	20	–		23.3	125
C1-30	70	–	–	30	–		24.2	115
C1-40	60	–	–	40	–		26.9	110
C1-50	50	–	–	50	–		28.1	110
C2-10	90	–	–	–	10		22.3	170
C2-20	80	–	–	–	20		22.4	180
C2-30	70	–	–	–	30		22.9	180
C2-40	60	–	–	–	40		26.0	180
C2-50	50	–	–	–	50		27.1	180

The pastes were cast into 40 × 40 × 160 mm prismatic molds, compacted using a shaking table, and removed from molds after 24 h. Hardening took place in air in the laboratory at 22 ± 1 °C and 100% relative humidity for 28 days. Six prismatic specimens represented each mix. Each specimen was subjected to both non-destructive and destructive testing of mechanical properties, and two additional specimens were prepared only for porosimetry, chemical analyses, and microscopic examination. Conducting experiments on pastes instead of concrete mixtures allowed us to more conclusively eliminate effects of aggregate and to identify the role of RAC during hydration and hardening.

3. Experimental methods

3.1. Microscopy and chemical analyses

Chemical composition of all constituents was determined by X-ray fluorescence spectroscopy (XRF) using a SPECTRO XEPOS spectrometer equipped with a 50 W/60 kV X-ray tube. Solid phase composition was investigated using thermogravimetric analysis (TGA). A combination of scanning electron microscopy (SEM-BSE) with X-ray powder diffraction (XRD) analysis enabled a quantitative characterization of microstructural features in the studied pastes.

3.1.1. XRD

XRD data were collected using a PANalytical X'Pert Pro diffractometer operating at 30 mA and 40 kV. XRD provided unique diffraction patterns. All scans were measured over an angular range of 3–60° 2θ with a 0.05° 2θ step size and accumulated time per step of 300 s, resulting in a total measurement time of 31 min per scan. The analysis of XRD data was accomplished using HighScorePlus software. A ICDD PDF-2 database was used for phase identification and matching XRD records were carefully leveraging mineralogy and petrology expertise about locally available materials.

3.1.2. SEM-BSE

SEM-BSE analysis was conducted with an FEG-SEM Merlin ZEISS scanning electron microscope to investigate morphology and distribution of phases. Individual RCF samples were embedded in epoxy resin and sequentially polished in an alcohol-based solution using a Struers Tegramin grinding plate with 1200, 2000, and 4000 grain/cm^2 grit under 5 N compression.

Mapping of microstructure was carried out at a 1000× magnification on 72 images (total area 4.2 mm^2) with a 1024 × 768 px resolution. PyPAIS software (Nežerka and Trejbal, 2019), which allows image segmentation based on the intensity and entropy thresholding, was used for automated identification of phases. The latter technique allowed for distinguishing phases having the same color but different textures such as fragments of aggregates and hydrated cementitious matrix.

Particular attention was paid to the presence of RAC, which had the highest intensity in the BSE images (Zhao and Darwin, 1992). The size and shape characteristics of individual particles, replaced by ellipses for the image analysis, were assessed using ImageJ-Analyze software. These characteristics were circularity, $\rho = 4\pi A/p^2$; roundness, $\phi = 4A/(\pi a^2)$; and a ratio of the length of ellipse semi-axes, $\omega = a/b$, where A is the particle area, p its circumference, and where a and b represent the respective lengths of the major and minor ellipse semi-axes. Unlike circularity, the roundness parameter did not take into account the roughness of the particles.

3.2. Calorimetry

An eight-channel isothermal heat flow calorimeter (TAM Air, manufactured by Thermometric AB Sweden) was used to detect all hydration stages during the first 5 days of hardening. The chambers were tempered to 20° with thermostat accuracy ± 0.02 °C. Ambient temperature was 22 ± 2 °C and relative humidity 55%. Extra samples with w/b increased to 0.45 were prepared, placed into 20 ml polyethylene ampules, and loaded into the calorimeter. The increased w/b allowed placement of mixtures to the ampules and ensured sufficient supply of water needed for hydration. The generated hydration heat was normalized to 1 g of PC in the mix to reveal contributions of individual RCF.

3.3. Porosimetry

Samples of hardened pastes were dried at 105 ± 5 °C for 72 h before porosity assessment, conducted using Pascal 440 and Pascal 140 instruments to detect pores with diameters ranging from 0.003 to 10 μm and above 10 μm, respectively.

3.4. Testing of stiffness and strength

The dynamic Young's modulus of pastes, E_{dyn}, was determined non-destructively on the prismatic specimens using the resonance method (ASTM International, 2006), based on a measurement of longitudinal vibration (Nežerka et al., 2014).

Tensile strength in bending was determined from a three-point bending test as

$$f_t = \frac{3F_{b,max}L_s}{2ab^2}, \quad (1)$$

where $F_{b,max}$ is the maximum force reached during the test, L_s is a span between supports equal to 100 mm, and a and b are respective width and height of the specimens.

A uniaxial compression test was carried out on halves of specimens broken during the bending test. A 10-mm-thick steel plate was used to ensure uniform stress distribution over a 40 × 40 area. Compressive strength was calculated from the maximum force reached during the test, $F_{c,max}$, as

$$f_c = \frac{F_{c,max}}{ab}. \quad (2)$$

The destructive tests were carried out using a LabTest 4.100SP1

Table 4
Most important oxides and loss on ignition (LOI) identified by the XRF in PC and RCF.

Component	PC wt% (±0.5%)	RRS	RDC	RC1	RC2
CaO	65.5	21.1	13.8	23.8	16.4
SiO_2	20.1	40.5	41.5	36.4	44.5
Al_2O_3	4.40	11.8	13.8	7.56	10.7
Fe_2O_3	2.50	4.10	3.97	3.13	3.65
SO_3	3.00	1.22	0.66	1.58	1.20
MgO	1.51	2.30	2.45	1.43	2.03
Na_2O	0.12	1.51	2.69	1.36	1.84
K_2O	0.75	1.83	2.82	1.46	1.65
other	0.21	0.83	0.81	0.58	0.73
LOI	1.91	14.8	17.5	22.7	17.3

Table 5
Amount of C_2S in RCF estimated using the Bogue calculation.

	RRS	RDC	RC1	RC2
C_2S amount [wt%]	9.5	7.9	12.5	7.9

loading frame with displacement-controlled loading at 0.5 mm/min and 0.1 mm/min, set for bending and compression, respectively.

4. Results and discussion

4.1. Chemical composition of input materials

The XRF results (Table 4) were used to estimate the concentration of clinker minerals based on the Bogue calculation (Bogue, 1929; Aldridge, 1982). The calculation revealed that PC contained 72.2% C_3S, 5.8% C_2S, 7.4% C_3A, and 7.6% C_4AF, i.e., 93.0% of clinker in total. After subtracting CaO present in $CaCO_3$ and $CaOH_2$ and SiO_2 present in aggregates, the amount of C_2S could also be calculated for RCF (Table 5). Other clinker minerals, C_3S, C_3A, and C_4AF, were disregarded because they contribute to the initial stage of hydration and their presence could not be expected in RCF.

Unlike cement used in the past (and hence in the studied RCF materials), the modern PC used in this study has relatively low levels of C_2S but is rich in C_3S, responsible for rapid hydration. This fact explains the low amount of C_2S in PC estimated using Bogue calculation, compared to RCF samples (see Table 5).

The XRD results for RCF samples were largely influenced by the presence of crystalline filler phases within the crushed aggregate.

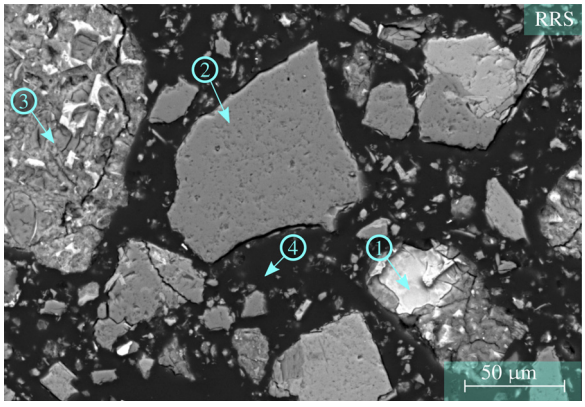

Fig. 3. Microscopy image at 1000× magnification of RRS embedded in epoxy resin with markers denoting phases of interest: (1) white RAC, (2) homogeneous light gray fragments of aggregates, (3) light gray fragments of hydrated cementitious matrix having a rich texture, and (4) dark gray epoxy resin.

Among most distinguishable peaks, the following phases could be reliably identified: quartz, plagioclase and potassium feldspar, muscovite, and chlorite. By employing the semi-quantitative relative intensity ratio (RIR) technique, calcite (2–5 wt.%) and residual portlandite (0.5–2 wt.%) were traced in all RCF samples. Hydrated or anhydrous alumosilicate phases were not detected with sufficient confidence, except for an RC1 sample with approximately 5% of C_2S/C_3S at $2\theta \approx 32.65°$. Such a diffraction angle was also reported for C_2S/C_3S by Idris et al. (2007). Minor contents in other samples resulted in an overlap of diffraction patterns due to the high amount of phases, limiting the applicability of XRD on such materials.

4.2. Microstructure

The total porosity (see Table 3 and Fig. 2) correlates with the particle-size distribution and amount of RCF. The presence of smaller particles within RDC and RC1 resulted in a shift of the pore-size distribution in pastes to smaller values, compared to coarser RRS and RC2. The porosity of pastes was nearly constant for PC replacements with RCF up to 20%, and increased linearly with an almost identical rate for all RCF materials in case of larger replacements.

SEM-BSE images were used for segmentation and assessment of individual phases (Fig. 3). Besides the evaluation of size and shape characteristics, summarized in Table 6, this analysis revealed that coarser RCF contained RAC embedded within the hydrated cementitious matrix. Disintegration of these matrix fragments in RC1 might

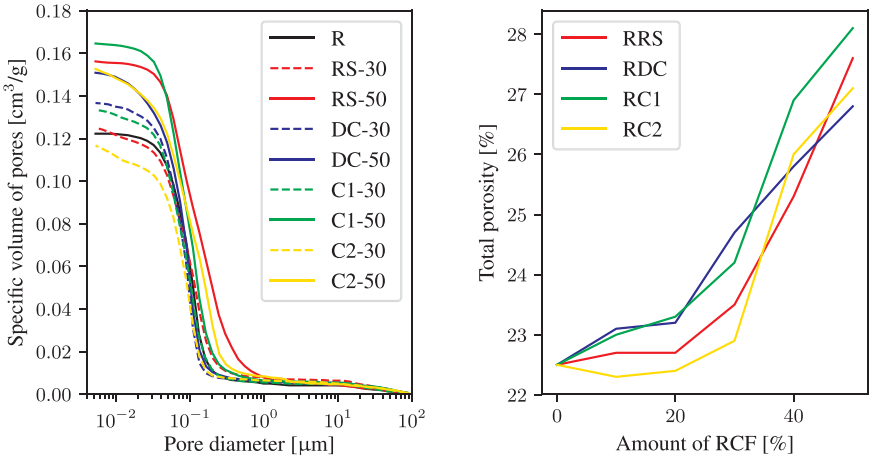

Fig. 2. Pore-size distribution for selected samples (left) and relationship between the amount of RCF and total porosity; both determined by mercury intrusion porosimetry.

Table 6
Results of image analysis of phases from SEM-BSE images.

RCF	Volume fraction [%]			Shape characteristics		
	RAC	Paste	Aggregates	Circularity (ρ)	Roundness (ϕ)	Ellipticality (ω)
RRS	4.91 ± 0.41	12.94 ± 3.52	81.93 ± 7.32	0.73 ± 0.13	0.52 ± 0.11	2.24 ± 0.30
RDC	1.97 ± 0.35	33.32 ± 10.32	63.71 ± 10.52	0.66 ± 0.21	0.53 ± 0.17	2.13 ± 0.44
RC1	8.49 ± 0.55	42.36 ± 8.34	49.15 ± 8.85	0.74 ± 0.17	0.54 ± 0.16	2.06 ± 0.31
RC2	3.19 ± 0.48	34.40 ± 11.33	62.41 ± 10.82	0.69 ± 0.20	0.52 ± 0.17	2.15 ± 0.59

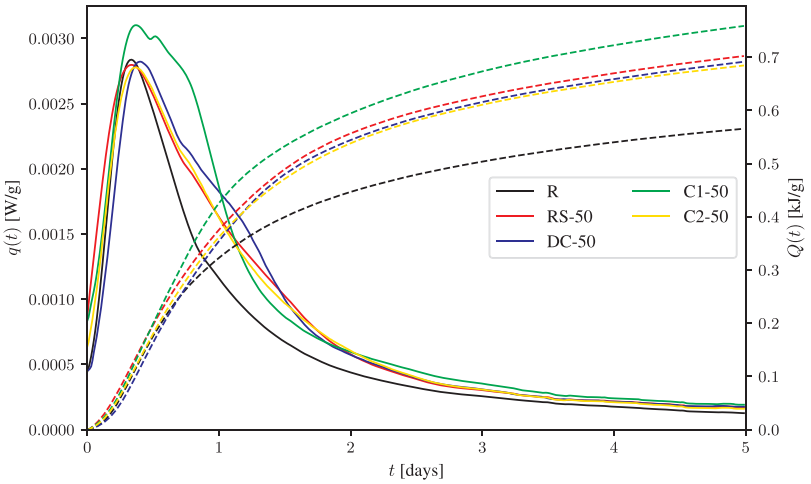

Fig. 4. Specific heat flow $q(t)$ (solid lines) and cumulative hydration heat $Q(t)$ (dashed lines) released during the first 5 days of hydration, normalized to 1 g of PC in the mix.

Table 7
Total amount of heat produced during the first 5 days of hydration, normalized to 1 g of PC in the mix.

	R	RS-50	DC-50	C1-50	C2-50
Q_5 [kJ/g]	0.565	0.702	0.691	0.759	0.684

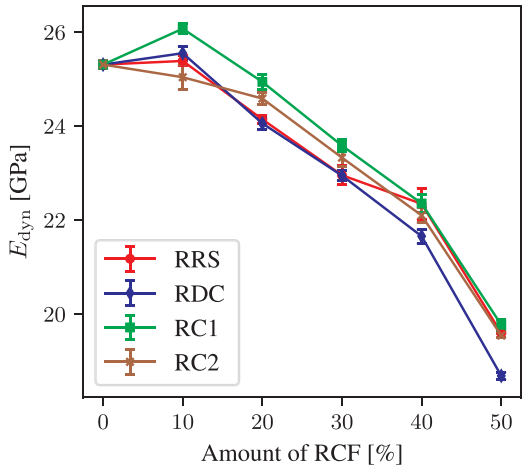

Fig. 5. Impact of individual RCF on stiffness of pastes after 28 days of hardening.

allow better access of water to RAC and promote RAC hydration, as observed during calorimetry measurements (Section 4.3). The lowest amount of RAC was detected in RDC, which is a consequence of finely ground PC rich in C_3S responsible for rapid hydration of modern concretes.

4.3. Hydration heat

Specific heat flow $q(t)$ and cumulative hydration heat $Q(t) = \int q(t)\,\mathrm{d}t$ were measured to identify hydration stages and evaluate the total heat released during the first 5 days of hydration, Q_5, see Fig. 4 and Table 7.

The secondary bump within the deceleration period at around the first day of hydration in the pastes containing RCF can be attributed to a transformation of ettringite to monosulphate (Havlica and Sahu, 1992). On the other hand, the separation of fines during the production of RC1 resulted in an increase in the $q(t)$ peak during hydration of the C1-50 paste. This peak can be attributed to the hydration of C_3S and formation of low-density C-S-H gel (Shi and Day, 1995). C1-50 also generated the highest amount of heat during the first 5 days of hydration, Q_5, when normalized to 1 g of PC in the mix. Therefore, it can be conjectured that the presence of RCF promoted hydration, and some portion of RAC in RCF was reactivated.

4.4. Mechanical properties

The Young's modulus of pastes decreased with an increasing amount of incorporated RCF as demonstrated in Fig. 5, reflecting the increasing porosity of pastes rich in RCF (Fig. 2) (Neville, 1996). Even though the pastes containing RC1 exhibited higher stiffness than those with other RCF materials, the difference was below 10% for all concentrations.

A similar trend was observed for compressive strength (Fig. 6), but the difference between the impact of individual RCF materials was more pronounced. Considering the similar shape of particles in all RCF samples, distribution of pores in pastes, and their total porosity, it can be conjectured the amount of RAC (Tables 5 and 6) is responsible for the different performance of the individual pastes.

The relation between the amount of RCF and the tensile strength of pastes (Fig. 7) is completely different than for compressive strength. Here, RC1 rich in RAC did not outperform other RCF. On the contrary,

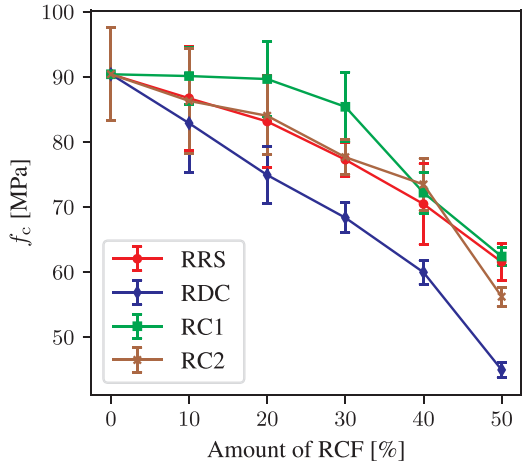

Fig. 6. Impact of individual RCF on compressive strength of pastes after 28 days of hardening.

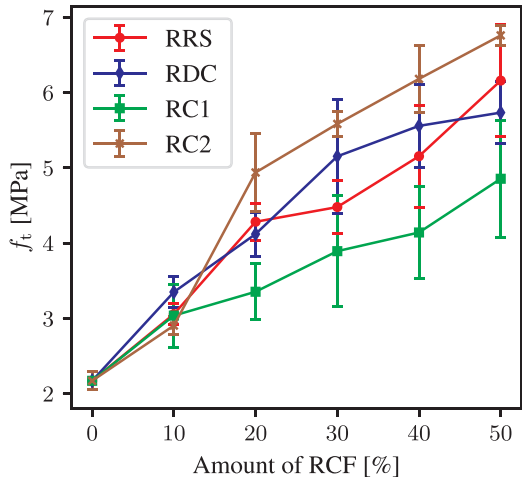

Fig. 7. Impact of individual RCF on tensile strength of pastes after 28 days of hardening.

the replacement of PC with fine-grained RC1 resulted in the lowest strength increase, while the 50% addition of coarse-grained RC2 led to more than 200% tensile strength gain. It can be concluded that the role played by RAC was negligible, but larger particles appeared to take on the role of a fine-grained aggregate, impeding opening and propagation of microcracks due to tensile stresses (Strange and Bryant, 1979; Karihaloo et al., 1993; Rhee et al., 2019).

A qualitative summary of all results, which illustrates what parameters have the highest impact on the mechanical strength of pastes, is provided in Table 8. Even though RAC in RC2 was not present in high amounts and its presence did not contribute significantly to hydration of pastes, the coarse particles contributed to low porosity and had a reinforcing effect when the pastes were subjected to tensile stresses during three-point bending. The highest amount of RAC in RC1 was probably responsible for the matrix strengthening, and replacement of PC with RC1 up to 30% did not result in compressive strength deterioration. The geometry of particles appears to have no effect or very minimal effects on the mechanical properties of pastes as well as on the fluidity of fresh pastes, where size distribution played a major role.

5. Conclusion

This study suggests that residual anhydrous clinker is present in old waste concrete and can be recovered by grinding. This statement is supported by microscopical observation, XRF, and calorimetry measurements. Mixing ground waste concrete with Portland cement had beneficial effects on the mechanical properties of cementitious pastes.

In particular, 50% replacement of Portland cement with fines from recycled 100-year-old concrete resulted in a 200% increase in the tensile strength. This tensile strength enhancement can be attributed to bridging of microcracks by inert inclusions contained in the recycled materials. Compressive strength, on the other hand, was affected negatively by incorporating recycled concrete fines, but replacements up to 30% did not lead to significant deterioration. When combining results of SEM-BSE and uniaxial compression testing, the positive impact of residual anhydrous clinker on compressive strength was revealed.

Based on the results of this study, study, the concept of incorporating recycled concrete fines into Portland cement mixtures appears to hold promise. Given the volume of concrete produced annually worldwide, such incorporation could potentially have a considerable impact on the sustainability of the construction industry. Using recycled concrete fines in Portland cement mixtures appears to make sound economic sense because concrete raw materials and landfilling costs are high and environmental regulations are changing. Furthermore, such methods may be useful in places where raw materials for Portland cement production are scarce or hard to acquire.

Future research focused on the impact of recycled concrete fines on durability and strength of concrete must be carried out to establish the amounts suitable for incorporating these fines into concrete mixes. The suitability of reusing concrete containing such fines in a theoretically endless “reuse life cycle” must also be examined in more detail.

Conflict of interest

The authors declare that there is no conflict of interest.

Funding

This work was supported by the Czech Science Foundation [grant number GA ČR 17-06771S].

Table 8
Qualitative relative evaluation of RCF and their impact on cement pastes.

Method (quantity)	Findings			
	RRS	RDC	RC1	RC2
Granulometry (size of particles)	Coarser than PC	Finer than PC	Very fine	Very coarse
XRD (RAC content)	Not detected	Not detected	Detected	Not detected
SEM-BSE (RAC content)	Moderate	Low	High	Moderate
SEM-BSE (shape of particles)	Smooth, elliptical	Rough	Smooth, circular	Elliptical
Calorimetry (contribution to hydration)	Slight	Slight	Significant	Slight
Porosimetry (porosity of pastes)	Moderate	Moderate	Highest	Lowest
Stiffness testing (deterioration of stiffness)	Moderate	High	Low	Moderate
Compression test (compressive strength)	Moderate	Low	High	Moderate
Bending test (tensile strength)	Moderate	Moderate	Low	High

Acknowledgment

The help of Dr. Stephanie Krueger, who provided editorial assistance, is gratefully acknowledged.

References

Aldridge, L., 1982. Accuracy and precision of phase analysis in Portland cement by Bogue, microscopic and X-ray diffraction methods. Cem. Concr. Res. 12, 381–398. https://doi.org/10.1016/0008-8846(82)90087-4.

Anastasiou, E., Filikas, K.G., Stefanidou, M., 2014. Utilization of fine recycled aggregates in concrete with fly ash and steel slag. Constr. Build. Mater. 50, 154–161. https://doi.org/10.1016/j.conbuildmat.2013.09.037.

ASTM International, 2006. Test Method for Dynamic Youngs Modulus, Shear Modulus, and Poissons Ratio by Impulse Excitation of Vibration. https://doi.org/10.1520/e1876-01r06.

Belin, P., Habert, G., Thiery, M., Roussel, N., 2013. Cement paste content and water absorption of recycled concrete coarse aggregates. Mater. Struct. 47, 1451–1465. https://doi.org/10.1617/s11527-013-0128-z.

Bentz, D., Jensen, O., Coats, A., Glasser, F., 2000. Influence of silica fume on diffusivity in cement-based materials. Cem. Concr. Res. 30, 953–962. https://doi.org/10.1016/s0008-8846(00)00264-7.

Bogue, R.H., 1929. Calculation of the compounds in Portland cement. Ind. Eng. Chem. Anal. Ed. 1, 192–197. https://doi.org/10.1021/ac50068a006.

Bordy, A., Younsi, A., Aggoun, S., Fiorio, B., 2017. Cement substitution by a recycled cement paste fine: role of the residual anhydrous clinker. Constr. Build. Mater. 132, 1–8. https://doi.org/10.1016/j.conbuildmat.2016.11.080.

Cartuxo, F., de Brito, J., Evangelista, L., Jiménez, J., Ledesma, E., 2015. Rheological behaviour of concrete made with fine recycled concrete aggregates – influence of the superplasticizer. Constr. Build. Mater. 89, 36–47. https://doi.org/10.1016/j.conbuildmat.2015.03.119.

Colangelo, F., Forcina, A., Farina, I., Petrillo, A., 2018. Life cycle assessment (LCA) of different kinds of concrete containing waste for sustainable construction. Buildings 8, 70. https://doi.org/10.3390/buildings8050070.

da Silva, S.R., de Oliveira Andrade, J.J., 2017. Investigation of mechanical properties and carbonation of concretes with construction and demolition waste and fly ash. Constr. Build. Mater. 153, 704–715. https://doi.org/10.1016/j.conbuildmat.2017.07.143.

Etxeberria, M., Vázquez, E., Marí, A., Barra, M., 2007. Influence of amount of recycled coarse aggregates and production process on properties of recycled aggregate concrete. Cem. Concr. Res. 37, 735–742. https://doi.org/10.1016/j.cemconres.2007.02.002.

Eurocode 2. Design of Concrete Structures. https://doi.org/10.3403/30096437.

European Committee for Standardization, EN 197-1:2011: Cement. Composition, Specifications and Conformity Criteria for Common Cements. BSI, 2011.

The European Parliament and of the Council on Waste, Directive regarding demolition waste, Official Journal of the European Union 2008/98/EC.

European Standard EN 12350-5, Testing Fresh Concrete; Flow Table Test.

Evangelista, L., de Brito, J., 2010. Durability performance of concrete made with fine recycled concrete aggregates. Cem. Concr. Compos. 32, 9–14. https://doi.org/10.1016/j.cemconcomp.2009.09.005.

Evangelista, L., de Brito, J., 2013. Concrete with fine recycled aggregates: a review. Eur. J. Environ. Civ. Eng. 18, 129–172. https://doi.org/10.1080/19648189.2013.851038.

Evangelista, L., de Brito, J., 2018. Durability of crushed fine recycled aggregate concrete assessed by permeability-related properties. Mag. Concr. Res. 1–9. https://doi.org/10.1680/jmacr.18.00093.

Florea, M., Brouwers, H., 2013. Properties of various size fractions of crushed concrete related to process conditions and re-use. Cem. Concr. Res. 52, 11–21. https://doi.org/10.1016/j.cemconres.2013.05.005.

Gastaldi, D., Canonico, F., Capelli, L., Buzzi, L., Boccaleri, E., Irico, S., 2015. An investigation on the recycling of hydrated cement from concrete demolition waste. Cem. Concr. Compos. 61, 29–35. https://doi.org/10.1016/j.cemconcomp.2015.04.010.

Golewski, G.L., 2018. Evaluation of morphology and size of cracks of the interfacial transition zone (ITZ) in concrete containing fly ash (FA). J. Hazard. Mater. 357, 298–304. https://doi.org/10.1016/j.jhazmat.2018.06.016.

Havlica, J., Sahu, S., 1992. Mechanism of ettringite and monosulphate formation. Cem. Concr. Res. 22, 671–677. https://doi.org/10.1016/0008-8846(92)90019-r.

Idiart, A., Bisschop, J., Caballero, A., Lura, P., 2012. A numerical and experimental study of aggregate-induced shrinkage cracking in cementitious composites. Cem. Concr. Res. 42, 272–281. https://doi.org/10.1016/j.cemconres.2011.09.013.

Idris, M.S., Ismail, K.N., Jamaludin, S.B., Jamaludin, S.B., Ghazali, C.M.R., Hussin, K., 2007. Comparative study of Clinker's transformation at different temperature zone during cement production. Am. J. Appl. Sci. 4, 328–332. https://doi.org/10.3844/ajassp.2007.328.332.

Kapoor, K., Singh, S., Singh, B., 2016. Durability of self-compacting concrete made with recycled concrete aggregates and mineral admixtures. Constr. Build. Mater. 128, 67–76. https://doi.org/10.1016/j.conbuildmat.2016.10.026.

Karihaloo, B., Carpinteri, A., Elices, M., 1993. Fracture mechanics of cement mortar and plain concrete. Adv. Cem. Based Mater. 1, 92–105. https://doi.org/10.1016/1065-7355(93)90014-f.

Katz, A., 2003. Properties of concrete made with recycled aggregate from partially hydrated old concrete. Cem. Concr. Res. 33, 703–711. https://doi.org/10.1016/s0008-8846(02)01033-5.

Khan, M.I., 2003. Permeation of high performance concrete. J. Mater. Civ. Eng. 15, 84–92. https://doi.org/10.1061/(asce)0899-1561(2003)15:1(84.

Khatib, J., 2005. Properties of concrete incorporating fine recycled aggregate. Cem. Concr. Res. 35, 763–769. https://doi.org/10.1016/j.cemconres.2004.06.017.

Khokhar, M., Roziere, E., Turcry, P., Grondin, F., Loukili, A., 2010. Mix design of concrete with high content of mineral additions: optimisation to improve early age strength. Cem. Concr. Compos. 32, 377–385. https://doi.org/10.1016/j.cemconcomp.2010.01.006.

Khoury, E., Ambrós, W., Cazacliu, B., Sampaio, C.H., Remond, S., 2018. Heterogeneity of recycled concrete aggregates, an intrinsic variability. Constr. Build. Mater. 175, 705–713. https://doi.org/10.1016/j.conbuildmat.2018.04.163.

Kwan, W.H., Ramli, M., Kam, K.J., Sulieman, M.Z., 2011. Influence of the amount of recycled coarse aggregate in concrete design and durability properties. Constr. Build. Mater. 26, 565–573. https://doi.org/10.1016/j.conbuildmat.2011.06.059.

Lee, H., Hanif, A., Usman, M., Sim, J., Oh, H., 2018. Performance evaluation of concrete incorporating glass powder and glass sludge wastes as supplementary cementing material. J. Clean. Prod. 170, 683–693. https://doi.org/10.1016/j.jclepro.2017.09.133.

Levy, S., Helène, P., 2007. Durability of concrete mixed with fine recycled aggregates. Exacta 5, 25–34. https://doi.org/10.5585/exacta.v5i1.1027.

Li, Z., Peng, J., Ma, B., 1999. Investigation of chloride diffusion for high-performance concrete containing fly ash, microsilica, and chemical admixtures. ACI Mater. J. 96, 391–396. https://doi.org/10.14359/638.

Lidmila, M., Tesárek, P., Plachy, T., Rácová, Z., Padevět, P., Nežerka, V., Zobal, O., 2013. Utilization of recycled fine-ground concrete from railway sleepers for production of cement-based binder. Appl. Mech. Mater. 486, 323–326. https://doi.org/10.4028/www.scientific.net/amm.486.323.

Ma, X., Wang, Z., 2013. Effect of ground waste concrete powder on cement properties. Adv. Mater. Sci. Eng. 2013, 1–5. https://doi.org/10.1155/2013/918294.

Madi, N., Srour, I., 2019. Managing emergency construction and demolition waste in Syria using GIS. Resour. Conserv. Recycl. 141, 163–175. https://doi.org/10.1016/j.resconrec.2018.10.018.

Maruyama, I., Matsushita, T., Noguchi, T., Hosokawa, Y., Yamada, K., 2010. Rate of hydration of alite and belite in Portland cement. J. Struct. Constr. Eng. (Trans. AIJ) 75, 681–688. https://doi.org/10.3130/aijs.75.681.

Memon, A., Radin, S., Zain, M., Trottier, J.-F., 2002. Effects of mineral and chemical admixtures on high-strength concrete in seawater. Cem. Concr. Res. 32, 373–377. https://doi.org/10.1016/s0008-8846(01)00687-1.

Nežerka, V., Slížková, Z., Tesárek, P., Plachý, T., Frankeová, D., Petráňová, V., 2014. Comprehensive study on microstructure and mechanical properties of lime-pozzolan pastes. Cem. Concr. Res. 64, 17–29. https://doi.org/10.1016/j.cemconres.2014.06.006.

Nežerka, V., Trejbal, J., 2019. Assessment of aggregate-bitumen coverage using entropy-based image segmentation. Road Mater. Pavement Des. 1–12. https://doi.org/10.1080/14680629.2019.1605304.

Nežerka, V., Hrbek, V., Prošek, Z., Somr, M., Tesárek, P., Fládr, J., 2018. Micromechanical characterization and modeling of cement pastes containing waste marble powder. J. Clean. Prod. 195, 1081–1090. https://doi.org/10.1016/j.jclepro.2018.05.284.

Neville, A.M., 1996. Properties of Concrete, fourth edition. Longman.

Oksri-Nelfia, L., Mahieux, P.-Y., Amiri, O., Turcry, P., Lux, J., 2015. Reuse of recycled crushed concrete fines as mineral addition in cementitious materials. Mater. Struct. 49, 3239–3251. https://doi.org/10.1617/s11527-015-0716-1.

Paris, J.M., Roessler, J.G., Ferraro, C.C., DeFord, H.D., Townsend, T.G., 2016. A review of waste products utilized as supplements to Portland cement in concrete. J. Clean. Prod. 121, 1–18. https://doi.org/10.1016/j.jclepro.2016.02.013.

Pedro, D., de Brito, J., Evangelista, L., 2018. Durability performance of high-performance concrete made with recycled aggregates, fly ash and densified silica fume. Cem. Concr. Compos. 93, 63–74. https://doi.org/10.1016/j.cemconcomp.2018.07.002.

Pereira, P., Evangelista, L., de Brito, J., 2012. The effect of superplasticizers on the mechanical performance of concrete made with fine recycled concrete aggregates. Cem. Concr. Compos. 34, 1044–1052. https://doi.org/10.1016/j.cemconcomp.2012.06.009.

Prošek, Z., Nežerka, V., Hlůžek, R., Trejbal, J., Tesárek, P., Karra'a, G., 2019. Role of lime, fly ash, and slag in cement pastes containing recycled concrete fines. Constr. Build. Mater. 201, 702–714. https://doi.org/10.1016/j.conbuildmat.2018.12.227.

Rhee, I., Lee, J.S., Roh, Y.-S., 2019. Fracture parameters of cement mortar with different structural dimensions under the direct tension test. Materials 12, 1850. https://doi.org/10.3390/ma12111850.

Shi, C., Day, R.L., 1995. A calorimetric study of early hydration of alkali-slag cements. Cem. Concr. Res. 25, 1333–1346. https://doi.org/10.1016/0008-8846(95)00126-w.

Shui, Z., Xuan, D., Wan, H., Cao, B., 2008. Rehydration reactivity of recycled mortar from concrete waste experienced to thermal treatment. Constr. Build. Mater. 22, 1723–1729. https://doi.org/10.1016/j.conbuildmat.2007.05.012.

Silva, R., de Brito, J., Dhir, R., 2014. Properties and composition of recycled aggregates from construction and demolition waste suitable for concrete production. Constr. Build. Mater. 65, 201–217. https://doi.org/10.1016/j.conbuildmat.2014.04.117.

Srour, I.M., Chehab, G.R., El-Fadel, M., Tamraz, S., 2013. Pilot-based assessment of the economics of recycling construction demolition waste. Waste Manage. Res. 31, 1170–1179. https://doi.org/10.1177/0734242x13479430.

Strange, P.C., Bryant, A.H., 1979. The role of aggregate in the fracture of concrete. J. Mater. Sci. 14, 1863–1868. https://doi.org/10.1007/bf00551025.

Tabsh, S.W., Abdelfatah, A.S., 2009. Influence of recycled concrete aggregates on strength properties of concrete. Constr. Build. Mater. 23, 1163–1167. https://doi.org/10.1016/j.conbuildmat.2008.06.007.

Tam, V.W., Butera, A., Le, K.N., 2016. Carbon-conditioned recycled aggregate in concrete production. J. Clean. Prod. 133, 672–680. https://doi.org/10.1016/j.jclepro.2016.06.007.

Tam, V.W., Soomro, M., Evangelista, A.C.J., 2018a. A review of recycled aggregate in concrete applications (2000–2017). Constr. Build. Mater. 172, 272–292. https://doi.org/10.1016/j.conbuildmat.2018.03.240.

Tam, V.W.Y., Xiao, J., Liu, S., Chen, Z., 2018b. Behaviors of recycled aggregate concrete-filled steel tubular columns under eccentric loadings. Front. Struct. Civ. Eng. 13, 628–639. https://doi.org/10.1007/s11709-018-0501-7.

Thiery, M., Dangla, P., Belin, P., Habert, G., Roussel, N., 2013. Carbonation kinetics of a bed of recycled concrete aggregates: a laboratory study on model materials. Cem. Concr. Res. 46, 50–65. https://doi.org/10.1016/j.cemconres.2013.01.005.

US Geological Survey & Orienteering S and US Geological Survey, Mineral Commodity Summaries, 2009, Government Printing Office, 2009.

Wu, K., Luo, S., 2018. Influence of replacement level of recycled coarse aggregate on fracture properties of recycled aggregate concrete. IOP Conf. Ser.: Mater. Sci. Eng. 431, 102002. https://doi.org/10.1088/1757-899x/431/10/102002.

Yang, S., Lee, H., 2017. Mechanical properties of recycled aggregate concrete proportioned with modified equivalent mortar volume method for paving applications. Constr. Build. Mater. 136, 9–17. https://doi.org/10.1016/j.conbuildmat.2017.01.029.

Yang, S., 2018. Effect of different types of recycled concrete aggregates on equivalent concrete strength and drying shrinkage properties. Appl. Sci. 8, 2190. https://doi.org/10.3390/app8112190.

Zhao, H., Darwin, D., 1992. Quantitative backscattered electron analysis of cement paste. Cem. Concr. Res. 22, 695–706. https://doi.org/10.1016/0008-8846(92)90022-n.

Appendix D

Prošek, Z.; Nežerka, V.; Hlůžek, R.; Trejbal, J.; Tesárek, P.; Karra'a G.: Role of lime, fly ash, and slag in cement pastes containing recycled concrete fines, *Construction and Building Materials* 201 (2019) 702–714, doi: 10.1016/j.conbuildmat.2018.12.227

Author's contribution: main idea, SEM microscopy, data analysis, design of experiments, preparation of specimens.

Construction and Building Materials 201 (2019) 702–714

Contents lists available at ScienceDirect

Construction and Building Materials

journal homepage: www.elsevier.com/locate/conbuildmat

Role of lime, fly ash, and slag in cement pastes containing recycled concrete fines

Z. Prošek [a], V. Nežerka [a,*], R. Hlůžek [a], J. Trejbal [a], P. Tesárek [a], G. Karra'a [b]

[a] Faculty of Civil Engineering, Czech Technical University in Prague, Thákurova 7, 166 29 Praha 6, Czech Republic
[b] Faculty of Tropical AgriSciences, Czech University of Life Sciences, Kamýcká 961, 165 00 Praha 6, Czech Republic

HIGHLIGHTS

- Cementitious pastes with large amounts of recycled concrete fines were examined.
- Thermal activation of recycled concrete was avoided by using additives.
- Addition of fly ash and slag resulted in higher tensile strength in bending.
- Presence of recycled concrete in cement pastes resulted in shrinkage mitigation.

ARTICLE INFO

Article history:
Received 11 November 2018
Received in revised form 30 December 2018
Accepted 31 December 2018
Available online 8 January 2019

Keywords:
Demolition waste
Concrete recycling
Alkali activation
Fly ash
Slag

ABSTRACT

Construction and demolition waste recycling for production of new concrete is usually limited to the use of coarse aggregates, and efficient utilization of fine subsieve fractions remains an unresolved issue. In the presented research, Portland cement pastes containing 50% finely ground recycled concrete, blended with lime, fly ash, or blast furnace slag, were studied. SEM-BSE microscopy, EDX analysis, and porosimetry were employed for investigating their microstructure, individual stages of hydration were detected using calorimetry, shrinkage was optically monitored in the early stages of hardening, the evolution of Young's modulus was assessed using the resonance method, and strength was determined from destructive tests. The study suggests that recycled concrete fines can be incorporated into cementitious composites in large amounts and even improve their properties, especially when blended with fly ash or blast furnace slag. Substitution of Portland cement in the studied pastes by recycled concrete led to a compressive strength deterioration, but also a reduction of shrinkage, and an increase of the tensile strength in bending by up to 26%.

1. Introduction

Recycling of demolition waste to ensure economic and environmental sustainability in the construction industry has become a worldwide issue. Concrete, being the most abundant construction material, constitutes the biggest portion of that waste [1]. Traditionally, concrete rubble was either disposed in landfills or crushed and used as filling if there was a demand in the vicinity of demolition sites. However, when used as filling or backfilling, its potential is not fully exploited. The newly established environmental laws, or those soon coming into force, have led together with increasing environmental awareness and economic motivation to extensive research into concrete recycling for manufacturing new cement-based products. The primary effort is focused on a maximum possible replacement of primary materials, such as Portland cement and aggregates, in concrete production. Such an effort can contribute to sustainability of construction, because Portland cement is the most widely produced synthetic material [2] and its production contributes to approximately 5–7% of the global anthropogenic CO_2 emissions [3–7].

It has become a common practice to replace a portion of aggregate in concrete with a recycled concrete aggregate [8–11], but little has been accomplished in the utilization of fine subsieve fractions, constituting about 15–50% of crushed concrete weight [12,13]. These fines are mostly the stripped paste/mortar and, besides small aggregate fractions, contain a portion of unhydrated clinker [13]. Their involvement in hydration by providing nucleation centers and activation of unhydrated clinker could result in a reduction of Portland cement (PC) consumption with little or no sacrifice of structural performance.

* Corresponding author.
E-mail address: vaclav.nezerka@fsv.cvut.cz (V. Nežerka).

https://doi.org/10.1016/j.conbuildmat.2018.12.227
0950-0618/

Those few researchers who focused on the activation of liberated concrete fines exploited high temperature dehydration [12,14,15,1], which is energetically demanding and expensive. An alternative way of exploiting grinding and blending with alkali activated binders (ABBs) would render the recycling process significantly more feasible. AABs gain their strength via a chemical reaction between the alkali hydroxides [16–18]. Compared to PC, AABs exhibit higher strength [19–21] and 55%–75% reduction in CO_2 emissions [22–26]. AABs can be categorized into two groups [18]: (i) containing aluminosilicate powder poor on calcium content (such as fly ash), yielding alkali alumino-silicate hydrates [27–29], and (ii) those with high calcium content (such as slags), yielding calcium silicate hydrates containing aluminum [16,30]. Using chemical notation adopted in concrete research the first group (i) of AAB products is abbreviated as N-A-S-H or K-A-S-H, while the latter (ii) as C-(A)-S-H. The final reaction product of AABs is usually a combination (i) and (ii) [31,32]. Both fly ash and slags have pozzolanic properties [33,34] and increase the cement hydraulicity if calcium, magnesium, or aluminum oxides are present [35–37]. On the other hand, those of silicon and manganese may decrease the hydraulicity if present in certain amounts [36,38].

In our study, fly ash and blast furnace slag were blended with recycled concrete fines and Porland cement in an attempt to increase hydraulicity of the pastes. Because recycled concrete can reduce pH of the mixture, small portions of lime were also added in order to increase the alkalinity and promote proper formation of hydration product [39–41]. The impact of individual additives on microstructure and mechanical properties of PC-based pastes containing recycled concrete was investigated.

2. Materials and methods

2.1. Investigated materials and samples

Ordinary PC, CEM I/42.5R (EN 197-1:2001 [42]), was used in this study. Besides a pure reference paste, all tested samples contained 50 wt% finely ground recycled waste concrete (RWC). The waste concrete powder was produced by crushing 20-years old railway sleeper to a 0–32 mm fraction, removal of steel rebars, separation of 0–16 mm fraction, and its grinding to 0–1 mm fraction using a high-speed 2 × 30 kW mill SKD 600, produced by Lavaris company (Czech Republic). The old concrete for recycling was carefully selected for its high quality and use of PC rich in belite. The alkalinity was increased in a set of samples by a common white air-slaked lime (CL90) Čertovy schody produced in the Czech Republic. The hydraulic reactions in another set of samples were supported by fly ash, produced by a Mělník coal-fired power plant, Czech Republic. Fine fractions of blast furnace slag were selected as an alternative alkali activated additive. It was deposited for 45–65 years in a slag heap near the former ironworks Poldi Kladno, Czech Republic.

The chemical composition of all constituents was determined by X-ray fluorescence spectroscopy (XRF) using a SPECTRO XEPOS spectrometer equipped with 50 W/60 kV X-ray tube. A list of measurable oxides is presented in Table 1. The results indicate that PC was rich in CaO and SiO_2 in the ratio 3:2 and therefore the clinker contained mostly C_3S, lower amount of C_2S and less than 5 wt% aluminosilicates. On the other hand, RWC was rich in SiO_2 and Al_2O_3 due to presence of sand and aggregate residues. High amounts of CaO and LOI were expected in the slaked lime composed mostly of $Ca(OH)_2$. The high content of amorphous SiO_2 in fly ash was provided by the soluble glassy components that are chemically activated in alkaline environment [43]. The same applies to slag, which is also rich in Al_2O_3.

The particle size distribution curves, determined using a Fritsch Analyssete 22 Micro Tec Plus laser diffraction particle size analyzer, are provided in Fig. 1. It was found that the particle size distributions of PC, lime, and slag were similar, while the distribution of fly ash was shifted towards smaller diameters, and RWC was on average coarser and contained the largest spectrum of particle sizes. The specific surfaces of PC, RWC, lime, fly ash, and slag were equal to 380, 265, 250, 242, and 452 m^2/kg, respectively.

When preparing the tested pastes, PC was blended with RWC and additives to form binders specified in Table 2 using an electric blender for 5 min at 235 rotations per minute, and for 10 min at the same speed after adding water into the dry homogenized mixture. The ratio between the weight of water and individual binders (w/b) was kept constant and relatively low, $w/b = 0.35$, to avoid the presence of bubbles and excessive shrinkage cracking [44,7]. The pastes were cast into 40 × 40 × 160 mm prismatic molds and removed after 24 h. During casting, the pastes were compacted using a shaking table.

The results of flow test defined in EN 12350-2 [45] are presented in Table 2. These results indicate poorer workability of CR paste due to the sharp-edged shape of the ground particles [46]. A similar effect was observed in the case of pastes containing lime. On the other hand, the components that had not been ground and contained spherical particles, i.e., fly ash and slag, increased the workability of pastes quite significantly. The ability of slag to increase the workability of fresh pastes can also be attributed to its chemical composition [47,22].

After the first day of hardening, the specimens were submerged in water and stored at 22 ± 1 °C. Six prismatic specimens represented each batch. These were subjected to both non-destructive and destructive testing of mechanical properties, along with two specimens prepared only for porosimetry and microscopic examination.

2.2. Microscopy and chemical analyses

The microscopy analyses were carried out on the pure cement paste (C), a sample containing recycled concrete with no activators (CR), and the mixtures containing the highest amount of activators, i.e., CRL_15, CRA_15, and CRS_15. Also, a pure RWC powder was analyzed to assess its morphology and composition. The 10 × 10 × 12 mm sections were extracted from the core of the 90 days old 40 × 40 × 160 mm specimens. The specimens were impregnated with an epoxy resin in vacuum to fill the voids, and sequentially polished under water using a Struers Tegramin grinding plate with 1200, 2000, and 4000 grain/cm^2 grit under 5 N compression. The specimens were cleaned with ethanol after each step using an ultrasound cleaner. Before placing to an electron microscope, the specimens were coated with a 14–18 nm carbon layer to increase the conductivity necessary for EDX analysis and protecting the surface from heat generated by the impact of electrons.

A scanning electron microscope (SEM) FEG-SEM Merlin ZEISS was used for studying the microstructure of pastes. The chemical analysis was carried out using an energy dispersive spectrometer (EDS) produced by Oxford Instruments. The mapping of microstructure was carried out at 300× and 500× magnifications, in order to detect small phases, such as unhydrated clinker, up to larger ones, such as RWC grains. PyPAIS software[1] was used for automated identification of phases. This in-house open-source tool can be used for segmentation of images based on intensity and entropy thresholding. The evaluation of entropy maps was used as a measure of texture roughness. This functionality was needed for

[1] http://mech.fsv.cvut.cz/nezerka/software.html.

Table 1
Chemical composition of PC, RWC, and additives; most important oxides and loss on ignition (LOI) identified by the XRF.

Component	PC	RWC	Lime wt% (±0.5%)	Fly ash	Slag
CaO	66.1	21.1	73.4	1.71	38.0
SiO_2	20.4	40.5	0.50	55.7	24.1
Al_2O_3	3.90	11.8	0.28	30.0	11.3
Fe_2O_3	2.86	4.10	0.23	1.12	4.33
SO_3	2.87	1.22	0.10	1.10	4.46
MgO	1.92	2.30	0.56	0.81	5.09
Na_2O	0.00	1.51	0.03	0.00	2.01
K_2O	0.00	1.83	0.07	0.00	0.95
other	0.10	1.16	0.24	1.09	2.52
LOI	1.85	14.5	24.6	8.53	7.33

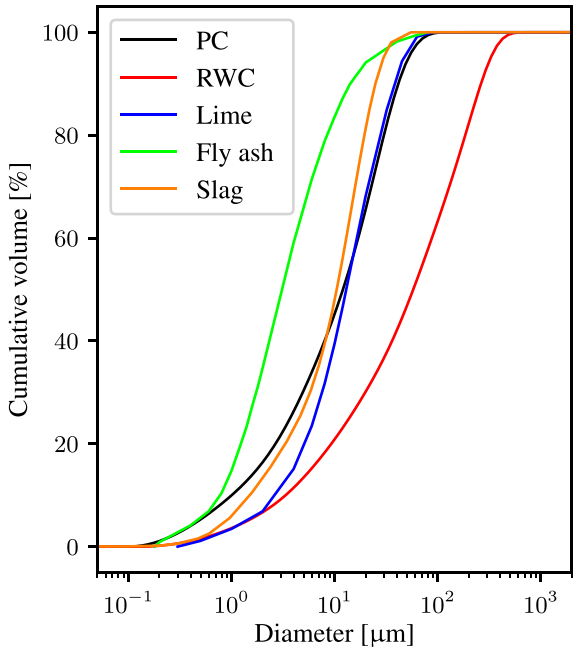

Fig. 1. Particle size distribution curves for all components.

distinguishing several phases having the same grayscale intensity, such as smooth SiO_2 in RWC and rough C-S-H gel.

2.3. Calorimetry

An eight-channel isothermal heat flow calorimeter TAM Air, manufactured by Thermometric AB Sweden, was used to detect and follow all stages of the hydration process during the first 5 days of hardening. The temperature of chambers was tempered to 20 °C with the accuracy of ±1 °C (air thermostat stability equal to ±0.02 °C, measuring precision ±20 μW). Ambient temperature was 22 ± 2 °C and relative humidity 55%. Extra samples, having $w/b = 0.45$ and following the composition from Table 2, were prepared, placed into 20 ml polyethylene ampules after each other and then loaded into the calorimeter at the same time. Their sizes were between ca. 32 and 38 g. The samples lacking RWC (CL_20, CA_20, and CS_20) were prepared only for calorimetry to reveal the impact of RWC on hydration. These samples contained the same ratio of cement and additives (lime, fly ash, and slag) as samples CRL_10, CRA_10, and CRS_10.

2.4. Porosimetry

To determine the pore size distribution, the specimens were dried at 105 ± 5 °C for 72 h, and fragments of approximately 1 g were consequently collected. The analysis was carried out using Pascal 140 and Pascal 440 instruments to detect pores of diameter in ranges 10–500 μm and 0.003–10 μm, respectively.

2.5. Shrinkage measurement

Digital image correlation (DIC) was employed for a continuous evaluation of early-stage shrinkage during the first 14 days in 1 h intervals using RTCorr software developed in Python. This in-house open-source tool, provided at GitHub[2], employs the upsampled matrix-multiplication discrete Fourier transform (DFT), proposed by Guizar-Sicairos et al. [48]. Such an approach allowed for continuous automated monitoring with subpixel accuracy. A monochrome CMOS camera Basler acA2500-60um equipped with Kowa LM50HC C-mount objective lenses ensured sufficient resolution and, combined with a powerful LED illumination, low optical noise. Such a non-contact measurement (Fig. 2) was more accurate than the traditional approach employing calipers. Moreover, the volumetric changes could be evaluated at early stages.

The monitored specimens were stored in a laboratory at 22 ± 1 °C and relative humidity of 50 ± 2%. To avoid their rupture, a thin polypropylene foil was separating the specimens from the 160 × 40 × 40 mm molds. A random pattern formed by grains of crushed limestone scattered over the surface of specimens ensured accurate correlation of images. The displacements were evaluated real-time using virtual extensometers at predefined locations.

2.6. Testing of macroscopic stiffness and strength

The Young's modulus was determined using the resonance method [49] based on measurement of a longitudinal vibration assuming a homogeneous mass distribution as

$$E = \frac{4Lmf_1^2}{ab} \tag{1}$$

where L is the length of a specimen, m is its mass, f_1 is the fundamental longitudinal resonant frequency, and a and b are the specimen width and height, respectively, measured by a caliper for each specimen separately.

The tensile strength in bending was determined from the three-point bending test as

$$f_t = \frac{3F_{b,max}L_s}{2ab^2}, \tag{2}$$

where $F_{b,max}$ is a maximum force reached during the test and L_s is a span between supports, equal to 120 mm.

The uniaxial compression was carried out on portions of beams broken in the bending test. A 10 mm thick steel plate was used to ensure a uniform stress distribution of a 40 × 40 area. The com-

[2] https://github.com/jacobantos/RTCorr.

Table 2
Summary of tested pastes; percentages represent weight ratio of individual constituents; the samples marked with an asterisk (*) were prepared only for calorimetry.

Mixture	PC	RWC	Additives			w/b	Flow test [mm]
			Lime	Fly ash	Slag		
C	100%	0%	0%	0%	0%	0.35/0.45*	218
CR	50%	50%	0%	0%	0%	0.35/0.45*	191
CRL_5	45%	50%	5%	0%	0%	0.35/0.45*	177
CRL_10	40%	50%	10%	0%	0%	0.35/0.45*	168
CRL_15	35%	50%	15%	0%	0%	0.35/0.45*	138
CRA_5	45%	50%	0%	5%	0%	0.35/0.45*	210
CRA_10	40%	50%	0%	10%	0%	0.35/0.45*	210
CRA_15	35%	50%	0%	15%	0%	0.35/0.45*	212
CRS_5	45%	50%	0%	0%	5%	0.35/0.45*	231
CRS_10	40%	50%	0%	0%	10%	0.35/0.45*	239
CRS_15	35%	50%	0%	0%	15%	0.35/0.45*	238
CL_20*	80%	0%	20%	0%	0%	0.45	–
CA_20*	80%	0%	0%	20%	0%	0.45	–
CS_25*	80%	0%	0%	0%	20%	0.45	–

pressive strength was calculated from the maximum force reached during loading, $F_{c,max}$, as

$$f_c = \frac{F_{c,max}}{ab}. \quad (3)$$

Both three-point bending and uniaxial compression tests were carried out using a LabTest 4.100SP1 loading frame. The loading of specimens was displacement-controlled with a rate of 0.5 mm/min and 0.1 mm/min, set for the bending and compression test, respectively.

3. Results and discussion

3.1. Morphology and chemical composition

The atomic weight and percentage for each phase were established from five BSE-EDS measurements on distinct samples under 300× and 500× magnifications. The individual phases were identified using stoichiometry, and their percentage was assessed by employing image analysis. The results are presented in Table 3. The images of microstructure with markers representing individual phases are provided in Fig. 3.

PC contained a high amount of clinker (about 95 vol%), and because C_3S reacts in the early of hydration, pure Portland cement pastes contained about 8.7 vol% unhydrated clinker rich in C_2S. SiO_2 was introduced into the mixture in the form of impurities during the cement production. At the studied scale, the volume fraction of voids (pores and cracks) was low, about 0.7 vol%.

The presence of RWC containing a mineral aggregate resulted in the contamination of pastes by SiO_2. Metallic alloys were also detected in these pastes due to wearing of blades in the mill during RWC grinding. Larger amount of kneading water and its access to clinker grains in PC through RWC embedded in the matrix supported the hydration and resulted in a 70 vol% reduction of unhydrated clinker in the studied specimens. Low amount of $Ca(OH)_2$ corresponded to the 50% lower amount of PC in the mixtures containing RWC. Microscopy investigation revealed a higher concentration of $Ca(OH)_2$ in the vicinity of RWC grains since these are rich in Ca and provide nucleation centers for $Ca(OH)_2$ dissipation. Consequently, the $Ca(OH)_2$ crystals were smaller in these areas. The amount of C-S-H gel did not change in CR pastes because of its presence in RWC.

The amount of $Ca(OH)_2$ was high in CRL_15 pastes due to the presence of lime. The grains of lime were 2–3× larger than portlandite. The hardening of pastes under water prevented the reaction of lime with CO_2. For this reason, the lime acted mostly as a filler and alkaline activator. The developed $Ca(OH)_2$ crystals filled microcracks that formed due to the high w/b. However, the increase in alkalinity did not affect the morphology of phases.

Hydration of glassy components in fly ash in CRA_15 pastes consumed a portion of $Ca(OH)_2$. The CRA_15 pastes had a higher

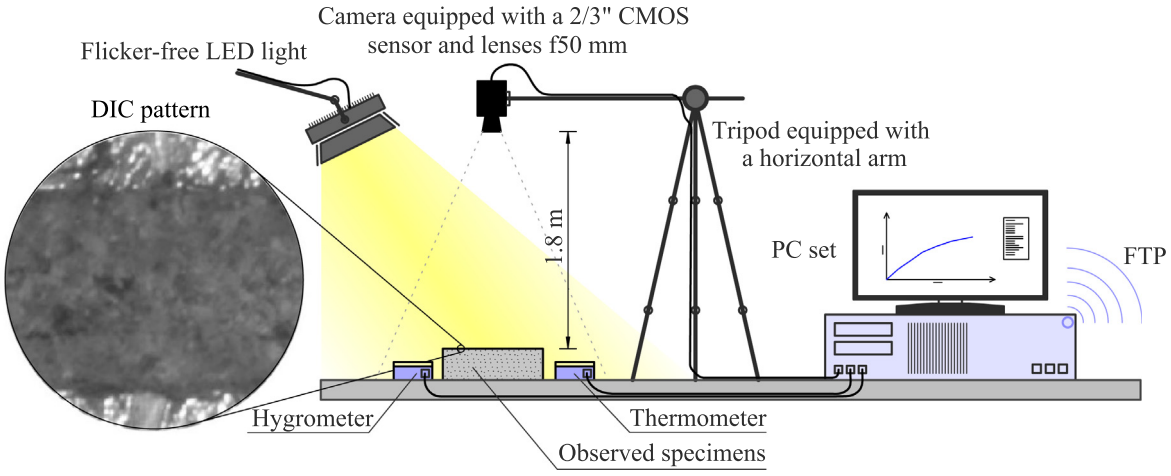

Fig. 2. Experimental setup for the measurement of early-stage shrinkage; control points of virtual extensometers were placed at the ends of the observed prismatic specimens.

Table 3
Volumetric fractions of phases in the studied pastes.

Phase	Paste				
	C	CR	CRL_15	CRA_15	CRS_15
Clinker	8.7 ± 1.4	2.5 ± 0.6	1.8 ± 0.1	1.7 ± 0.9	1.5 ± 0.4
$Ca(OH)_2/CaCO_3$	13.0 ± 2.8	6.3 ± 1.3	13.1 ± 1.5	4.8 ± 1.5	11.2 ± 1.2
C-S-H/C-A-S-H	76.8 ± 3.1	77.1 ± 4.2	70.1 ± 1.7	80.1 ± 2.3	65.3 ± 3.5
Crystalline SiO_2	0.8 ± 0.7	13.0 ± 3.4	12.9 ± 1.8	10.8 ± 1.3	21.6 ± 3.0
Microscopic pores	0.7 ± 0.4	0.7 ± 0.3	0.5 ± 0.3	1.7 ± 0.3	1.8 ± 0.1

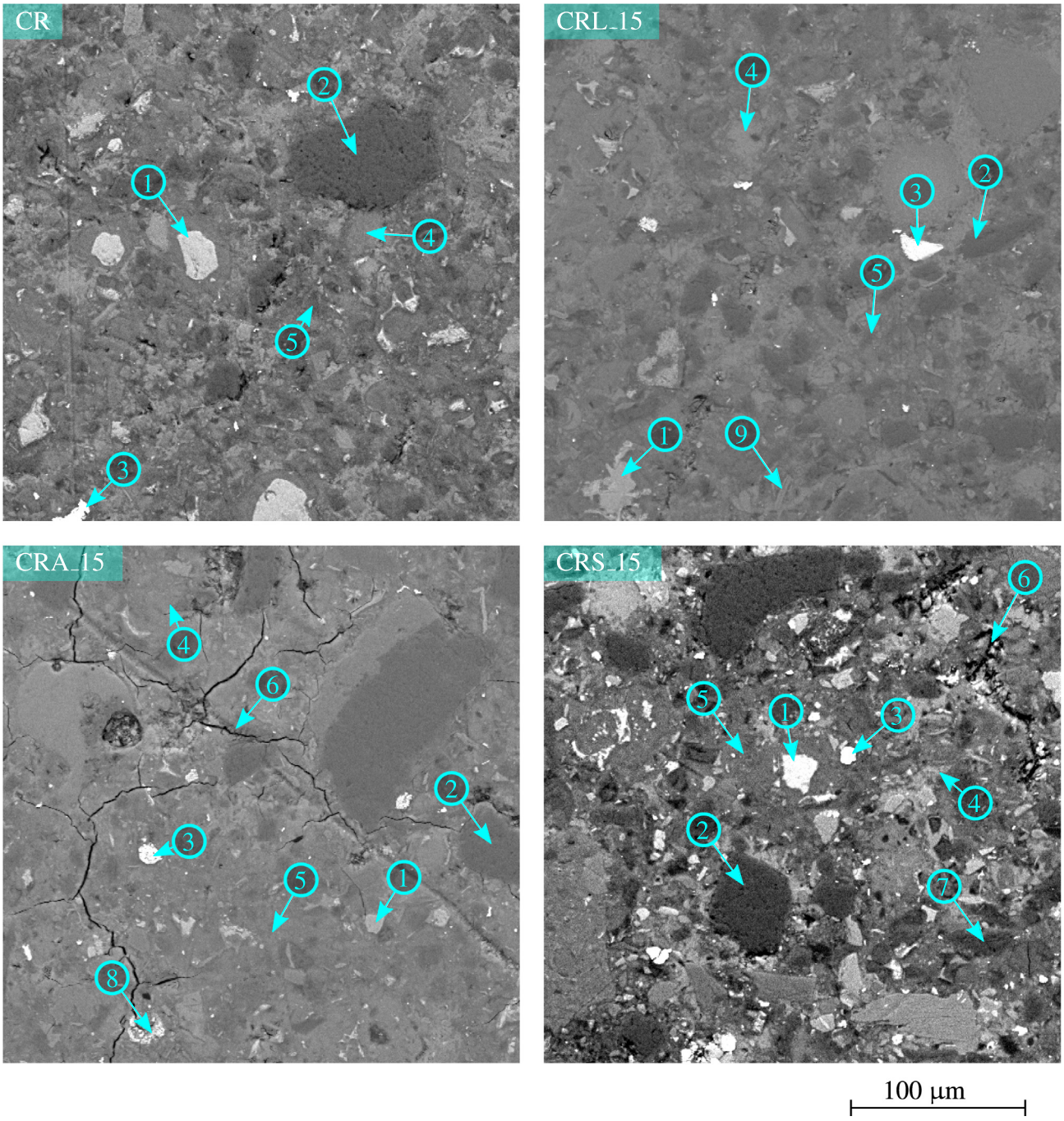

Fig. 3. Microscopy images at 500× magnification of selected pastes with markers denoting phases of interest: 1. unhydrated clinker, 2. SiO_2, 3. metal alloy, 4. $Ca(OH)_2$, 5. C-S-H/C-A-S-H gel, 6. microcracks, 7. $CaCO_3$, 8. glassy components of fly ash, and 9. healed cracks.

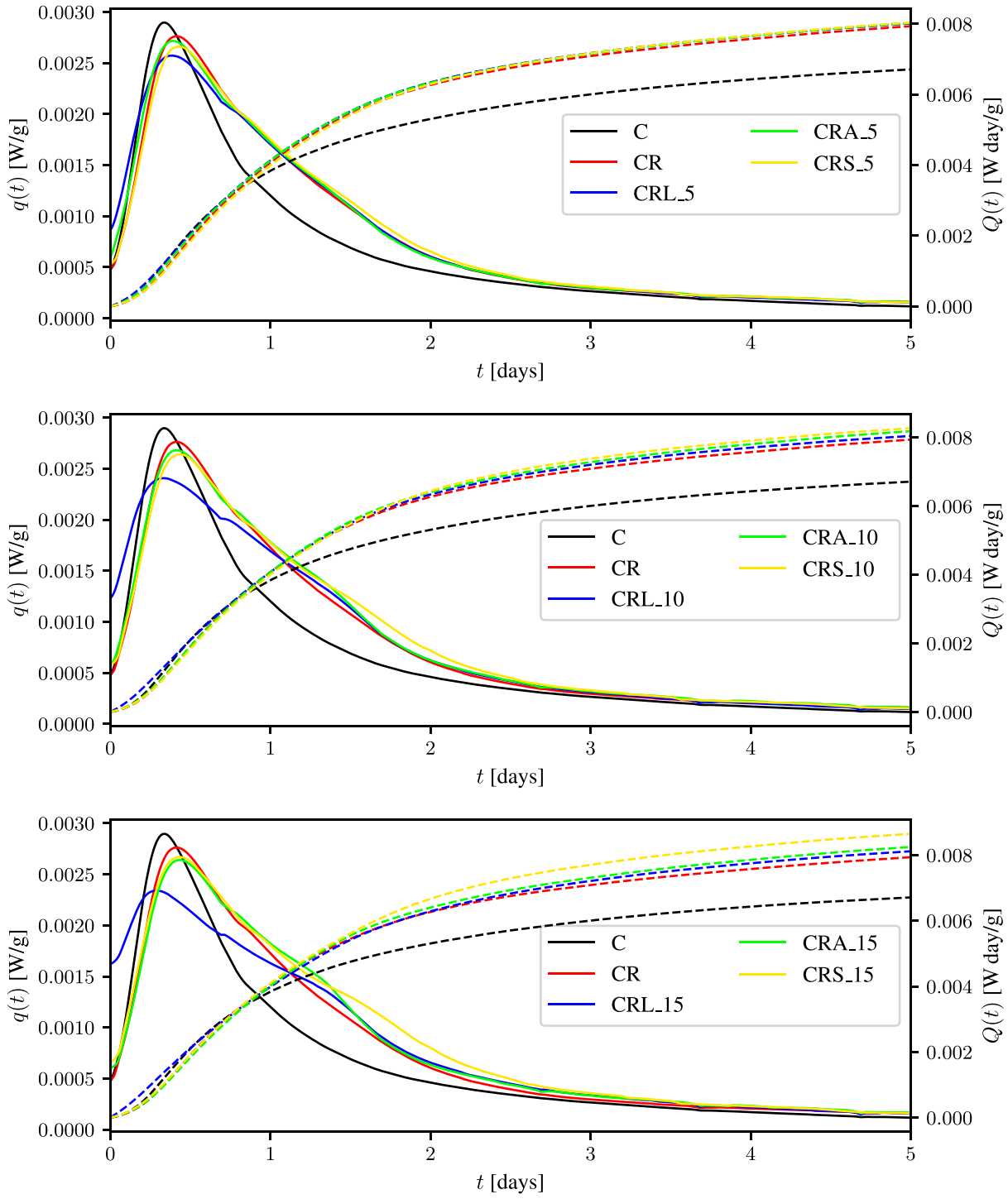

Fig. 4. Specific heat flow $q(t)$ (solid line) and cumulative hydration heat $Q(t)$ (dashed line) released by pastes during the first 5 days of hydration, normalized to 1 g of PC in the mixtures.

concentration of microcracks, attributed to early-stage shrinkage during hardening. Unlike in other pastes, there was a high concentration of more chemically stable C-S-H gel detected in the vicinity of RWC grains, rendering the matrix stronger and potentially more resistant to chemical agents.

CRS_15 pastes also contained a higher amount of microcracks and high content of inert SiO_2 and $CaCO_3$ minerals. Similarly to the pastes with fly ash, the precipitation of $Ca(OH)_2$ around grains of RWC was also detected in CRS_15 pastes.

3.2. Hydration heat

Specific heat flow $q(t)$ and cumulative hydration heat $Q(t) = \int q\,dt$ were measured to identify hydration stages and evaluate the total heat released during the first 5 days of the measurement. The outputs were normalized to 1 g of PC in the mixture to reveal the contribution of individual additives, see Fig. 4.

The presence of additives resulted in lowering the main peak of $q(t)$, related mostly to the hydration of C_3S and formation of low-

Table 4
Summary of measured data; $Q_5, p_{28}, \varepsilon_{0.14}, E, f_c$, and f_b denote the amount of heat produced during first 5 days of hydration, total porosity of 28 days old samples, total shrinkage after 14 days of hardening, Young's modulus, and the compressive and tensile strength in bending, respectively. The age of pastes during the testing of mechanical properties (in days) is indicated by the subscripts 28 or 90.

Sample	Q_5 [$\times 10^{-3}$ W day/g]	p_{28} [%]	$\varepsilon_{0.14}$ [%]	E_{28} [GPa]	E_{90} [GPa]	$f_{c,28}$ [MPa]	$f_{c,90}$ [MPa]	$f_{b,28}$ [MPa]	$f_{b,90}$ [MPa]
C	6.71	20.5	0.34	26.3±0.43	27.0 ± 0.33	116.2 ± 6.72	107.2 ± 5.93	7.2 ± 0.91	6.1 ± 1.36
CR	7.94	22.5	0.30	19.4 ± 0.19	20.0 ± 0.32	50.0 ± 1.44	48.1 ± 1.79	6.2 ± 0.47	7.0 ± 0.27
CRL_5	8.02	25.1	0.22	17.9 ± 0.10	18.3 ± 0.33	45.0 ± 2.58	42.3 ± 1.28	6.0 ± 0.32	6.2 ± 0.41
CRL_10	8.03	–	0.41	15.3 ± 0.15	15.4 ± 0.60	36.0 ± 1.03	31.7 ± 1.14	5.6 ± 0.41	5.4 ± 0.35
CRL_15	8.04	29.2	0.41	13.9 ± 0.01	14.3 ± 0.43	31.0 ± 1.37	28.0 ± 0.65	4.2 ± 1.63	5.1 ± 0.47
CRA_5	8.04	25.6	0.19	17.4 ± 0.05	19.6 ± 0.55	44.4 ± 2.43	50.4 ± 1.59	6.3 ± 0.72	7.6 ± 0.47
CRA_10	8.18	–	0.15	16.8 ± 0.22	18.7 ± 0.31	38.9 ± 3.15	51.0 ± 1.82	6.2 ± 0.34	6.8 ± 0.29
CRA_15	8.27	29.4	0.17	15.6 ± 0.15	18.2 ± 0.25	34.5 ± 1.65	48.1 ± 1.94	5.6 ± 0.48	6.2 ± 0.78
CRS_5	8.12	25.5	0.18	17.9 ± 0.07	19.6 ± 0.34	45.1 ± 1.49	47.4 ± 2.49	7.5 ± 0.27	7.2 ± 0.66
CRS_10	8.25	–	0.24	16.3 ± 0.43	17.5 ± 0.48	37.1 ± 1.38	38.7 ± 0.69	6.4 ± 0.46	7.5 ± 0.46
CRS_15	8.65	29.1	0.30	15.2 ± 0.09	16.4 ± 0.81	32.6 ± 1.50	32.9 ± 1.09	6.3 ± 0.37	5.6 ± 0.51
CL_20	7.26	–	–	–	–	–	–	–	–
CA_20	6.98	–	–	–	–	–	–	–	–
CS_20	7.56	–	–	–	–	–	–	–	–

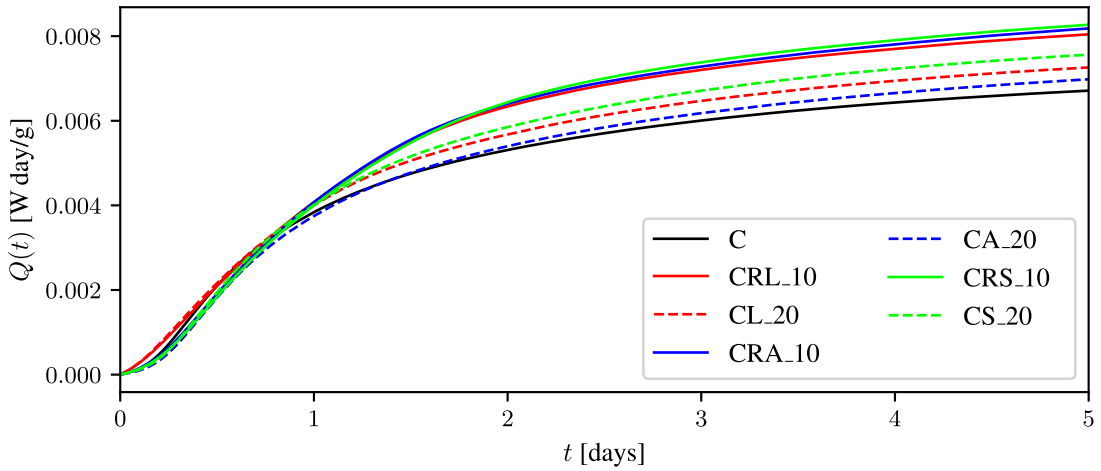

Fig. 5. Specific heat flow $q(t)$ released during the first 5 days of hydration by a pure cement paste (C) and pastes with the same cement-to-activator mass ratio (4:1), containing RWC (solid line) and without RWC (dashed line), all normalized to 1 g of PC in the mixture.

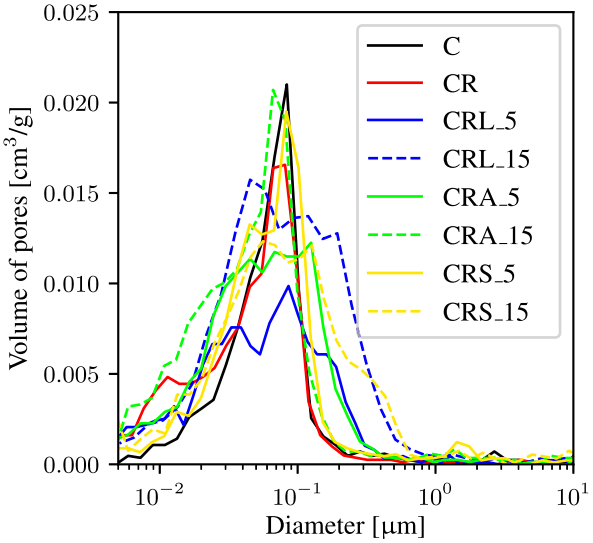

Fig. 6. Pore size distribution in selected pastes.

density C-S-H gel [50]. The secondary bump within the deceleratory period at around first day of hydration in the pastes containing RWC can be attributed to a transformation of ettringite to monosulphate [51] and the reaction of pozzolanic components in RWC and additives [52–54]. The addition of fine-grained slag resulted in the highest amount of heat, normalized to a weight of PC in the pastes. On the other hand, the retardation of hydration due to saturation of the solution by Ca^{2+} could be observed in the pastes containing lime [55].

The total heat normalized to the amount of PC and released during the first 5 days of hydration, Q_5 in Table 4, was higher in the case of all binders containing RWC. This indicates that the presence of RWC promotes hydration and some portion of old clinker or other active components in RWC could be reactivated. This is supported by the measurement of hydration heat presented in Fig. 5, showing that pastes containing the same amount of additives relative to PC (1:4) produced more heat per 1 g of PC in the presence of RWC.

3.3. Porosity

The pore size distribution of selected pastes is presented in Fig. 6. The partial replacement of PC by RWC resulted in a reduction of the average pore size and an increase of the total porosity from 20.5% to 22.5%, see Table 4. A distinct peak of pore-size distribution curve in the C paste can be located at 0.08 μm, similar to the pastes with RWC which had a broader distribution curve Fig. 7.

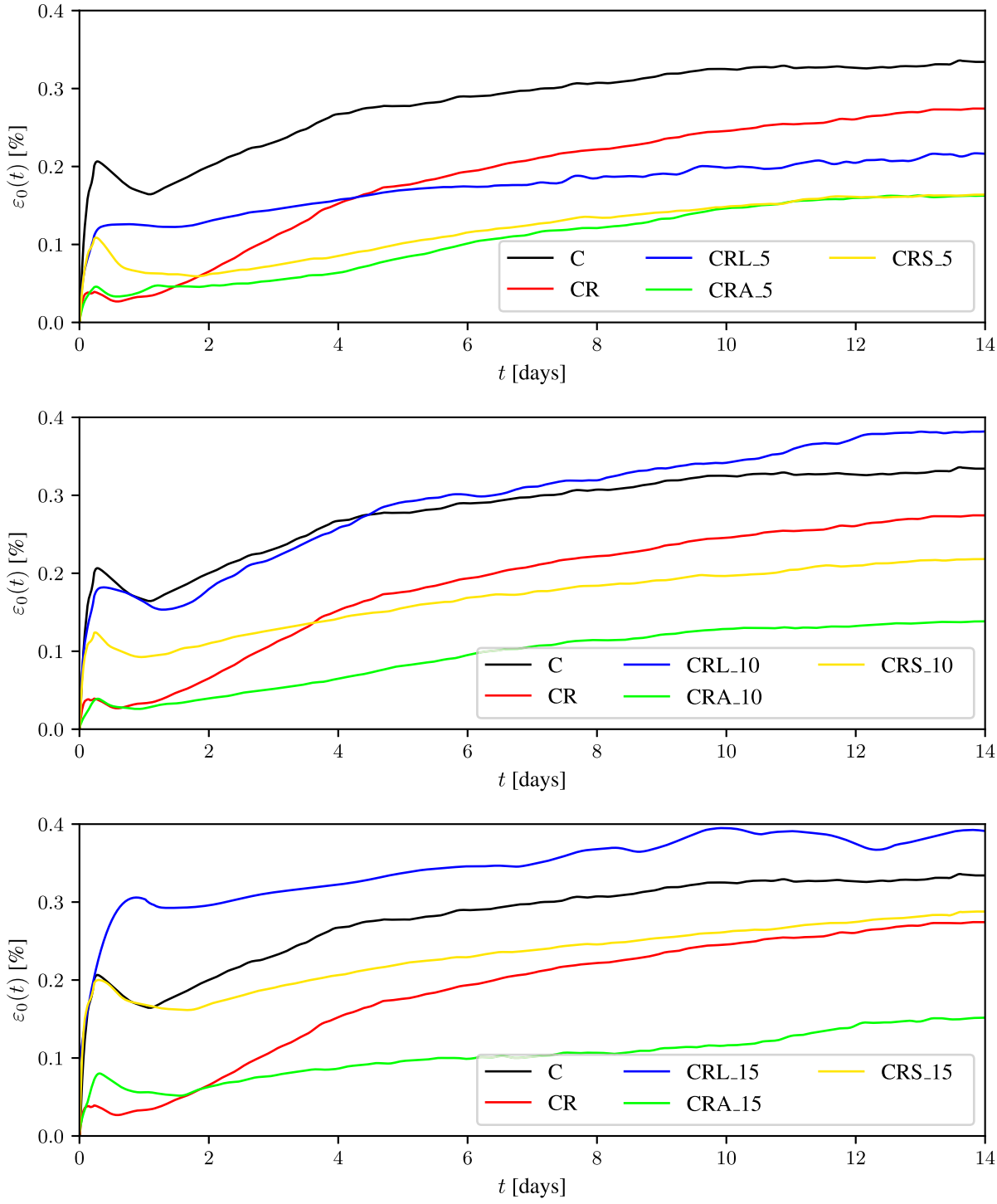

Fig. 7. Shrinkage of pastes $\varepsilon_0(t)$ during the first 14 days of hydration.

An increase of the total porosity compared to CR paste by about 3% could be observed in the pastes containing lime, fly ash, or slag in the 5% concentrations, or by approximately 7% in the case of 15% concentrations. This increase was expected based on studies by other authors dealing with blended cementitious materials [56–58], and is attributed to a high amount of free water resulting in an excessive formation of technological voids.

3.4. Shrinkage

Shrinkage of a cementitious matrix in mortars and concretes can be responsible for the development of microcracks between aggregates [59–61], leading to a reduction of strength and durability of the composites. It is mostly caused by drying of a cementitious matrix, but also autogenous shrinkage is significant in alkali-activated cement pastes [62].

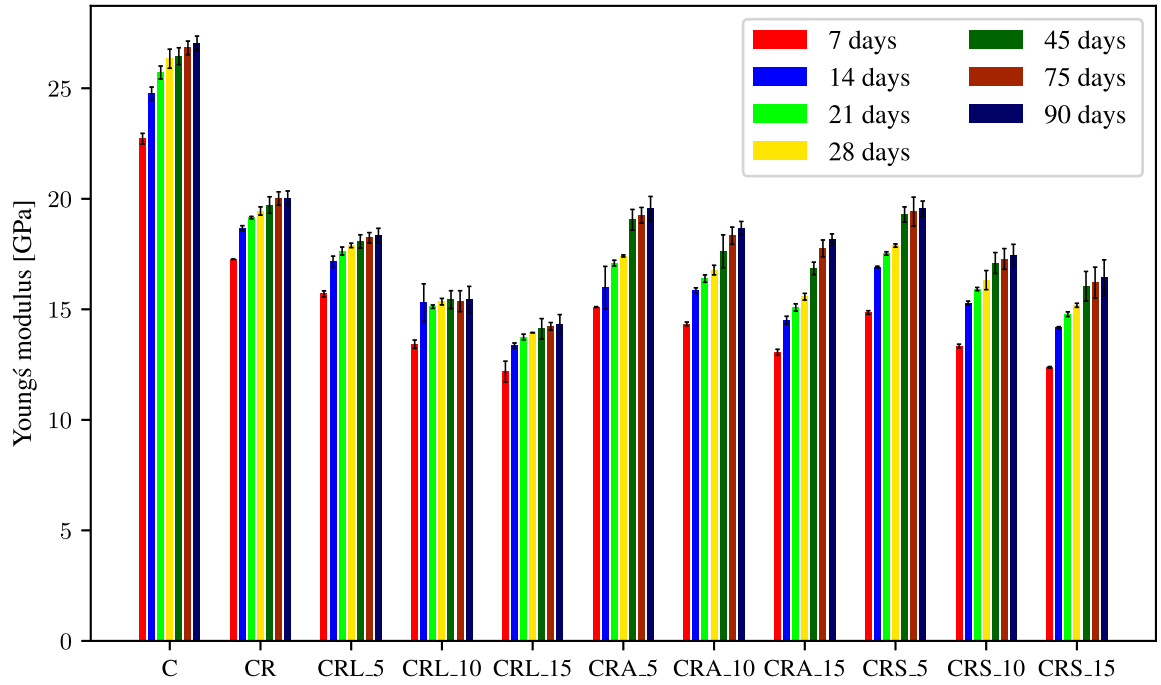

Fig. 8. Development of Young's modulus in pastes during the first 90 days of hardening.

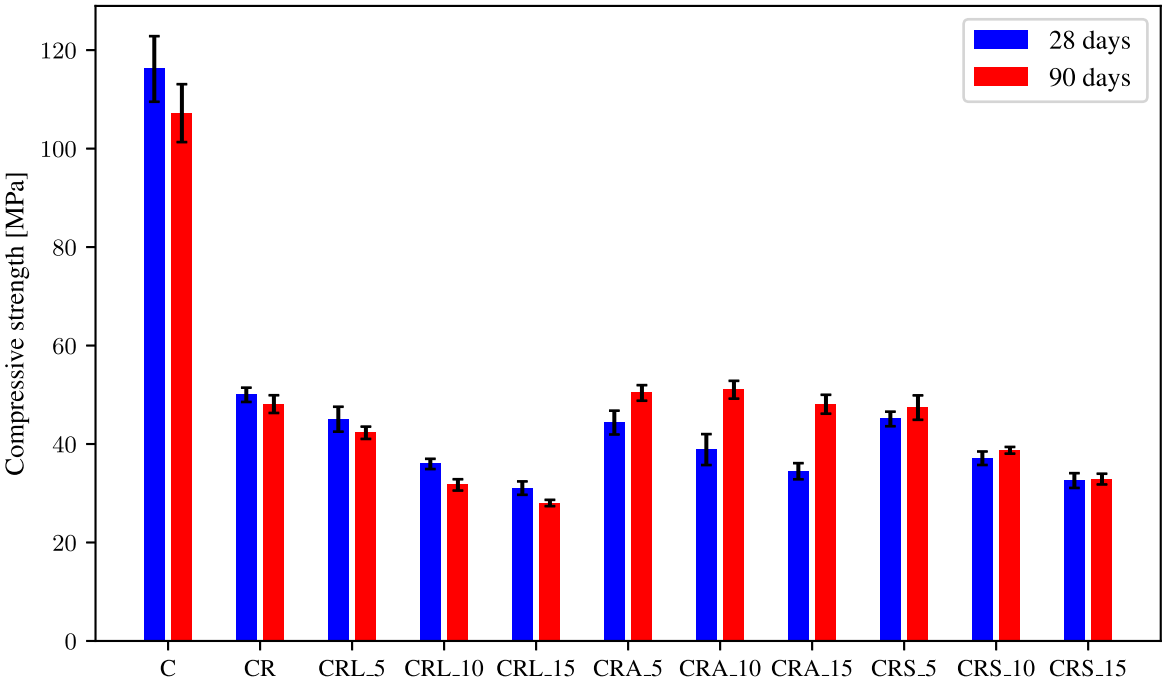

Fig. 9. Compressive strength of pastes after 28 and 90 days of hardening.

The measurement of early stage shrinkage revealed a positive role of RWC, especially when combined with fly ash. Such pastes exhibited about 2–3× smaller shrinkage, compared to the C paste. The impact of slag was not as significant, yet its addition also led to shrinkage mitigation from the second (CRS_5) and fourth day of hardening (CRS_10) compared to the CR paste. For higher concentration (CRS_15), the shrinkage after 14 days of hardening was almost identical as of the CR paste. The addition of lime had a positive impact on the shrinkage mitigation only in the case of its lowest concentration (CRL_5), while higher amounts of lime resulted in shrinkage exceeding that of C paste. The relatively high shrinkage of pastes rich in additives is related to the higher amount of free water. The swelling period encountered in all the pastes after approximately 12 h of hardening can be attributed to the reaction of C_3A in PC and formation of expansive ettringite [63–65].

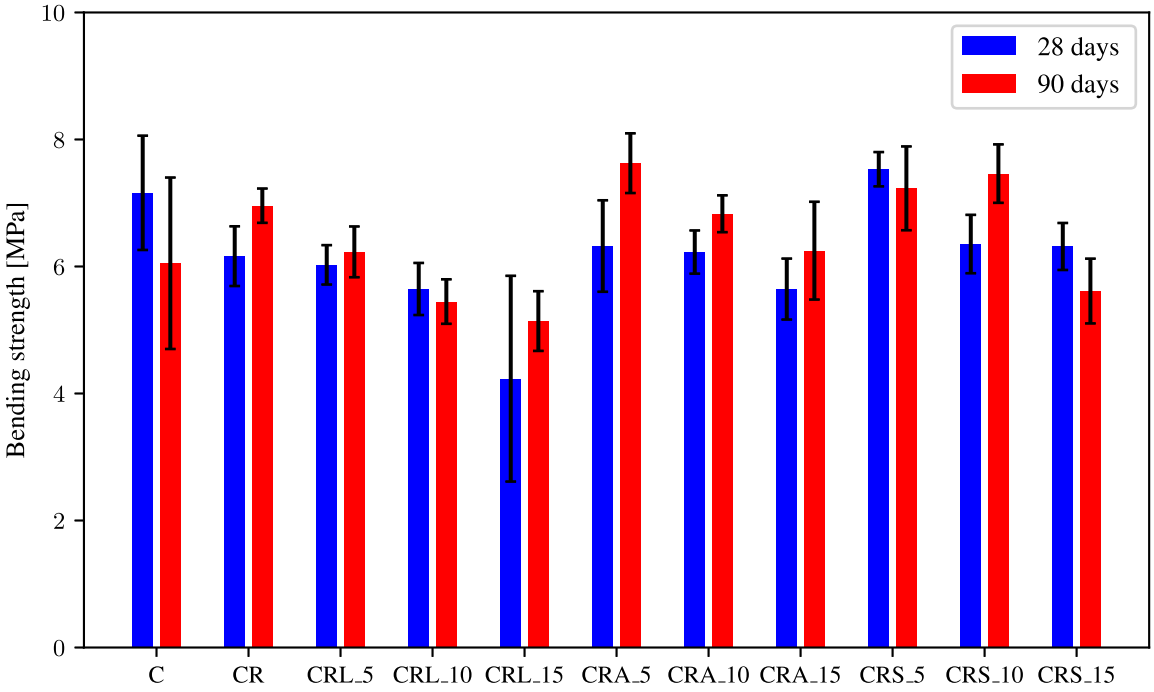

Fig. 10. Tensile strength in bending of pastes after 28 and 90 days of hardening.

3.5. Mechanical properties

It was expected that the introduction of mostly inert fine-grained RWC would result in a less compact and more porous structure of pastes, leading to a deterioration of their strength and stiffness [13,66]. On the other hand, RWC promoted hydration of PC by allowing better access of water to clinker grains and acted as microfiller that reinforced the brittle matrix [67–69].

3.5.1. Young's modulus

The development of Young's modulus can indicate the formation of stiff structures during hardening process or presence of microcracks [70,60,71]. Comparison of the stiffness development between the 7th and 90th day of hardening for all the tested pastes is provided in Fig. 8. The stiffness of pure cement pastes gradually increases with a decreasing rate. The same behavior was observed in all pastes. However, the rate of stiffness development differed and the role of individual additives could be revealed. The pastes containing lime exhibited very small stiffness gains after 28 days of hardening, while the stiffness of pastes containing fly ash and slag was still increasing rather significantly. This increase can be attributed to the filling of voids by newly formed hydration products [72–74]. The low porosity of CR paste (recall Section 3.3) resulted in a superior stiffness in comparison with the pastes containing alkali activated additives or lime.

3.5.2. Strength

The compressive strength is considered the most important characteristic of concrete because its proportionality with tensile strength is generally assumed. However, for pastes, the tensile strength is not directly related to the compressive strength because of microcracks that are not arrested by stones of aggregate. Microfillers, such as RWC, reinforce the brittle cementitious matrix and contribute to enhanced resistance to tensile stresses. A series of compressive and bending tests were carried out to test this hypothesis and reveal the impact of RWC and alkali additives on the strength of pastes.

Hlobil et al. [75] reported that the amount of C-S-H gel, followed by entrapped or entrained air and spatial gradient of C-S-H, have the largest impact on the compressive strength of cement pastes. Even though the pastes with RWC were relatively rich in C-S-H, their compressive strength hardly reached 50% of the C paste strength, independent of the duration of hardening, see Fig. 9 and Table 4. Regarding the hardening duration, all pastes except those containing fly ash and slag exhibited a 3.8–12.8% compressive strength reduction. This phenomenon is quite common in composites containing Portland cements rich in alite at the expense of belite ensuring long-term hydration and strength gain [76,77].

The addition of lime caused a significant reduction in compressive strength. On the other hand, the addition of fly ash in all tested concentrations increased the compressive strength after 90 days of hardening, attributed to the formation of C-S-H gel that was detected in the vicinity of RWC grains. The 5 wt% replacement of PC by slag in CRS_5 paste did not cause any strength reduction, but larger replacements resulted in strength deterioration. This finding is probably related exclusively to the binders containing high percentage of RWC; positive impact of up to 20% slag additions on the strength of pastes without RWC was reported, e.g., by Messina et al. [78]. The compressive strength of pastes blended with fly ash and slag increased from 28th to 90th day of hardening as a consequence of the ongoing pozzolanic reactions and formation of hydration products.

Even though C paste surpassed the blended pastes in resistance to compression, its tensile strength in bending after 90 days of hardening was lower compared to the strength of pastes containing RWC, except those containing lime, see Fig. 10. Microfillers, such as RWC or unhydrated grains of fly ash/slag, can arrest propagating cracks formed in response to tensile stresses [79–81]. Unlike C paste, the majority of blended pastes exhibited an increase in the tensile strength between 28 and 90 days of hardening, indicating ongoing hydration and reduced impact of shrinkage-induced microcracking [82,83].

The relative 90-day strengths presented in Fig. 11 were calculated as

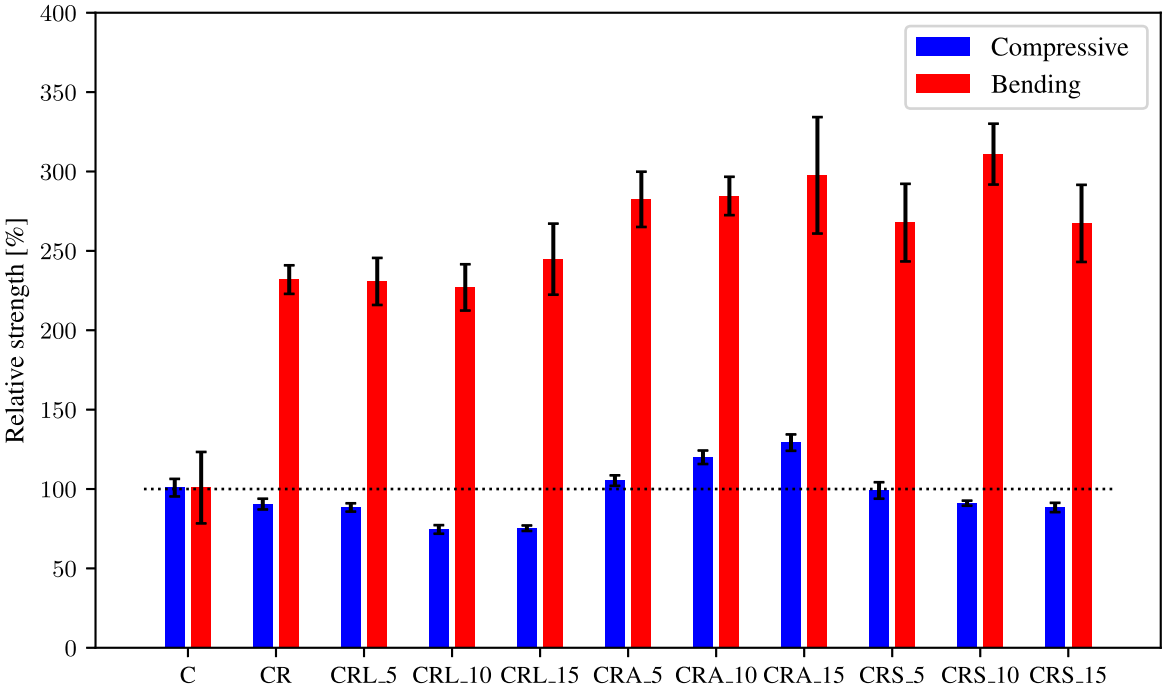

Fig. 11. Relative compressive and tensile strength in bending after 90 days of hydration, normalized by the strength of the reference C paste and the amount of PC in the mixtures according to Eq. (4).

$$f_{rel} = \frac{f}{f_C w_{PC}} \times 100\ [\%], \tag{4}$$

where f_C is the 90-day strength of pure cement paste, equal to 106.3 MPa in compression and 6.0 MPa in bending, and w_{PC} is the weight ratio of PC in the pastes. Such a recalculation of strength makes sense only from an economic/ecological point of view as one can see whether the potential of PC has been exploited efficiently with respect to C pastes. The results indicate that all the pastes containing RWC performed much better in bending. However, only the pastes containing fly ash outperformed C paste also in compression, which can be attributed to the formation of C-(A)-S-H gel in the vicinity of RWC grains in the presence of fly ash minerals, recall Section 3.1.

4. Conclusion

The presented comprehensive study suggests that recycled concrete fines can be used in large amounts for production of concrete, and do not require thermal treatment for their activation by dehydration, especially when using suitable supplementary cementitious materials. The research was focused on a comprehensive study of Portland cement-based pastes containing finely ground recycled concrete and selected additives: lime, fly ash, and blast furnace slag.

The 50 wt% substitution of Portland cement by mostly inert particles of finely ground recycled concrete led to a reduction of strength and stiffness. This deterioration of mechanical properties resulted from a less compact and more porous structure, even though the presence of recycled concrete promoted hydration of Portland cement by allowing better access of water to clinker grains. Recycled concrete acted as microfiller that reinforced the brittle cementitious matrix, thus increasing its tensile strength assessed in bending after 90 days of hardening and reducing its shrinkage.

It was found that increasing alkalinity by replacing a portion of Portland cement by slaked lime neither supported the formation of hydration products nor improved the structural performance of the pastes. On the other hand, the addition of fly ash and slag, both being industrial byproducts, led to an increased formation of C-S-H/C-A-S-H gels in the vicinity of recycled concrete grains. This, in turn, led to an additional shrinkage reduction and strength enhancement. Compared to the reference pure Portland cement paste, the paste containing 50 wt% recycled concrete fines and 5 wt% fly ash exhibited 44% lower shrinkage, 53% lower compressive strength, and 26% higher tensile strength in bending. Similar results were obtained for pastes containing slag in the same mass ratio.

Further research will be focused on behavior of concretes containing recycled concrete fines, fly ash, and slag as these additives appear to be most promising for activation of this waste material. The structural behavior of concrete does not have to be necessarily compromised be the lower strength of the binders, because the tensile stresses dominate concrete failure at the microscale. On the contrary, the shrinkage reduction could eliminate microcracking and reduce the porosity within interfacial transition zone around stiff aggregates.

Conflict of interest

None.

Acknowledgment

The authors wish to thank Dr. Kopecký and Dr. Šmilauer of the Czech Technical University in Prague for valuable suggestions and comments during the paper preparation.

Funding: This work was supported by the Czech Science Foundation [Grant No. GA ČR 17-06771S].

References

[1] D. Gastaldi, F. Canonico, L. Capelli, L. Buzzi, E. Boccaleri, S. Irico, An investigation on the recycling of hydrated cement from concrete demolition waste, Cem. Concr. Compos. 61 (2015) 29–35, https://doi.org/10.1016/j.cemconcomp.2015.04.010.

[2] R.J. Flatt, N. Roussel, C.R. Cheeseman, Concrete: an eco material that needs to be improved, J. Eur. Ceram. Soc. 32 (2012) 2787–2798, https://doi.org/10.1016/j.jeurceramsoc.2011.11.012.

[3] US Geological Survey & Orienteering S and US Geological Survey, Mineral Commodity Summaries, 2009, Government Printing Office, 2009.

[4] J.M. Paris, J.G. Roessler, C.C. Ferraro, H.D. DeFord, T.G. Townsend, A review of waste products utilized as supplements to portland cement in concrete, J. Clean. Prod. 121 (2016) 1–18, https://doi.org/10.1016/j.jclepro.2016.02.013.

[5] S.R. da Silva, J.J. de Oliveira Andrade, Investigation of mechanical properties and carbonation of concretes with construction and demolition waste and fly ash, Constr. Build. Mater. 153 (2017) 704–715, https://doi.org/10.1016/j.conbuildmat.2017.07.143.

[6] H. Lee, A. Hanif, M. Usman, J. Sim, H. Oh, Performance evaluation of concrete incorporating glass powder and glass sludge wastes as supplementary cementing material, J. Clean. Prod. 170 (2018) 683–693, https://doi.org/10.1016/j.jclepro.2017.09.133.

[7] V. Nežerka, V. Hrbek, Z. Prošek, M. Somr, P. Tesárek, J. Fládr, Micromechanical characterization and modeling of cement pastes containing waste marble powder, J. Clean. Prod. 195 (2018) 1081–1090, https://doi.org/10.1016/j.jclepro.2018.05.284.

[8] S.W. Tabsh, A.S. Abdelfatah, Influence of recycled concrete aggregates on strength properties of concrete, Constr. Build. Mater. 23 (2009) 1163–1167, https://doi.org/10.1016/j.conbuildmat.2008.06.007.

[9] K. Kapoor, S. Singh, B. Singh, Durability of self-compacting concrete made with recycled concrete aggregates and mineral admixtures, Constr. Build. Mater. 128 (2016) 67–76, https://doi.org/10.1016/j.conbuildmat.2016.10.026.

[10] F. Colangelo, R. Cioffi, Mechanical properties and durability of mortar containing fine fraction of demolition wastes produced by selective demolition in south Italy, Compos. Part B: Eng. 115 (2017) 43–50, https://doi.org/10.1016/j.compositesb.2016.10.045.

[11] E. Khoury, W. Ambrós, B. Cazacliu, C.H. Sampaio, S. Remond, Heterogeneity of recycled concrete aggregates, an intrinsic variability, Constr. Build. Mater. 175 (2018) 705–713, https://doi.org/10.1016/j.conbuildmat.2018.04.163.

[12] Z. Shui, D. Xuan, H. Wan, B. Cao, Rehydration reactivity of recycled mortar from concrete waste experienced to thermal treatment, Constr. Build. Mater. 22 (2008) 1723–1729, https://doi.org/10.1016/j.conbuildmat.2007.05.012.

[13] X. Ma, Z. Wang, Effect of ground waste concrete powder on cement properties, Adv. Mater. Sci. Eng. 2013 (2013) 1–5, https://doi.org/10.1155/2013/918294.

[14] R. Serpell, M. Lopez, Reactivated cementitious materials from hydrated cement paste wastes, Cem. Concr. Compos. 39 (2013) 104–114, https://doi.org/10.1016/j.cemconcomp.2013.03.020.

[15] M. Florea, Z. Ning, H. Brouwers, Activation of liberated concrete fines and their application in mortars, Constr. Build. Mater. 50 (2014) 1–12, https://doi.org/10.1016/j.conbuildmat.2013.09.012.

[16] P. Duxson, A. Fernández-Jiménez, J.L. Provis, G.C. Lukey, A. Palomo, J.S.J. van Deventer, Geopolymer technology: the current state of the art, J. Mater. Sci. 42 (9) (2006) 2917–2933, https://doi.org/10.1007/s10853-006-0637-z.

[17] K. Komnitsas, D. Zaharaki, Geopolymerisation: a review and prospects for the minerals industry, Miner. Eng. 20 (2007) 1261–1277, https://doi.org/10.1016/j.mineng.2007.07.011.

[18] P. Suraneni, M. Palacios, R.J. Flatt, New insights into the hydration of slag in alkaline media using a micro-reactor approach, Cem. Concr. Res. 79 (2016) 209–216, https://doi.org/10.1016/j.cemconres.2015.09.015.

[19] F. Puertas, B. González-Fonteboa, I. González-Taboada, M. Alonso, M. Torres-Carrasco, G. Rojo, F. Martínez-Abella, Alkali-activated slag concrete: fresh and hardened behaviour, Cem. Concr. Compos. 85 (2018) 22–31, https://doi.org/10.1016/j.cemconcomp.2017.10.003.

[20] C. Shi, Strength, pore structure and permeability of alkali-activated slag mortars, Cem. Concr. Res. 26 (1996) 1789–1799, https://doi.org/10.1016/s0008-8846(96)00174-3.

[21] S. Aydín, B. Baradan, Mechanical and microstructural properties of heat cured alkali-activated slag mortars, Mater. Design 35 (2012) 374–383, https://doi.org/10.1016/j.matdes.2011.10.005.

[22] K.-H. Yang, J.-K. Song, K.-I. Song, Assessment of CO_2 reduction of alkali-activated concrete, J. Clean. Prod. 39 (2013) 265–272, https://doi.org/10.1016/j.jclepro.2012.08.001.

[23] L.K. Turner, F.G. Collins, Carbon dioxide equivalent (CO2-e) emissions: a comparison between geopolymer and OPC cement concrete, Constr. Build. Mater. 43 (2013) 125–130, https://doi.org/10.1016/j.conbuildmat.2013.01.023.

[24] X. Gao, Q. Yu, H. Brouwers, Reaction kinetics, gel character and strength of ambient temperature cured alkali activated slag-fly ash blends, Constr. Build. Mater. 80 (2015) 105–115, https://doi.org/10.1016/j.conbuildmat.2015.01.065.

[25] M. Shojaei, K. Behfarnia, R. Mohebi, Application of alkali-activated slag concrete in railway sleepers, Mater. Design 69 (2015) 89–95, https://doi.org/10.1016/j.matdes.2014.12.051.

[26] A. Gholampour, T. Ozbakkaloglu, Performance of sustainable concretes containing very high volume class-f fly ash and ground granulated blast furnace slag, J. Clean. Prod. 162 (2017) 1407–1417, https://doi.org/10.1016/j.jclepro.2017.06.087.

[27] A. Palomo, M. Grutzeck, M. Blanco, Alkali-activated fly ashes, Cem. Concr. Res. 29 (1999) 1323–1329, https://doi.org/10.1016/s0008-8846(98)00243-9.

[28] Á. Palomo, S. Alonso, A. Fernandez-Jiménez, I. Sobrados, J. Sanz, Alkaline activation of fly ashes: NMR study of the reaction products, J. Am. Ceram. Soc. 87 (2004) 1141–1145, https://doi.org/10.1111/j.1551-2916.2004.01141.x.

[29] S. Alonso, A. Palomo, Calorimetric study of alkaline activation of calcium hydroxide-metakaolin solid mixtures, Cem. Concr. Res. 31 (2001) 25–30, https://doi.org/10.1016/s0008-8846(00)00435-x.

[30] F. Puertas, M. Palacios, H. Manzano, J. Dolado, A. Rico, J. Rodríguez, A model for the c-a-s-h gel formed in alkali-activated slag cements, J. Eur. Ceram. Soc. 31 (2011) 2043–2056, https://doi.org/10.1016/j.jeurceramsoc.2011.04.036.

[31] C. Yip, G. Lukey, J. van Deventer, The coexistence of geopolymeric gel and calcium silicate hydrate at the early stage of alkaline activation, Cem. Concr. Res. 35 (2005) 1688–1697, https://doi.org/10.1016/j.cemconres.2004.10.042.

[32] S. Puligilla, P. Mondal, Role of slag in microstructural development and hardening of fly ash-slag geopolymer, Cem. Concr. Res. 43 (2013) 70–80, https://doi.org/10.1016/j.cemconres.2012.10.004.

[33] C. Shi, J. Qian, High performance cementing materials from industrial slags—a review, Resour. Conserv. Recycl. 29 (2000) 195–207, https://doi.org/10.1016/s0921-3449(99)00060-9.

[34] J.A. Fuente-Alonso, V. Ortega-López, M. Skaf, Á. Aragón, J.T. San-José, Performance of fiber-reinforced EAF slag concrete for use in pavements, Constr. Build. Mater. 149 (2017) 629–638, https://doi.org/10.1016/j.conbuildmat.2017.05.174.

[35] P.Z. Wang, R. Trettin, V. Rudert, T. Spaniol, Influence of al2o3 content on hydraulic reactivity of granulated blast-furnace slag, and the interaction between al2o3 and CaO, Adv. Cem. Res. 16 (2004) 1–7, https://doi.org/10.1680/adcr.16.1.1.36257.

[36] S. Pal, A. Mukherjee, S. Pathak, Investigation of hydraulic activity of ground granulated blast furnace slag in concrete, Cem. Concr. Res. 33 (9) (2003) 1481–1486, https://doi.org/10.1016/s0008-8846(03)00062-0.

[37] M.B. Haha, B. Lothenbach, G.L. Saout, F. Winnefeld, Influence of slag chemistry on the hydration of alkali-activated blast-furnace slag—part i: effect of MgO, Cem. Concr. Res. 41 (2011) 955–963, https://doi.org/10.1016/j.cemconres.2011.05.002.

[38] M. Moranville-Regourd, Cements Made From Blastfurnace Slag, Elsevier (1998), https://doi.org/10.1016/b978-075066256-7/50023-0.

[39] M. Sánchez-Herrero, A. Fernández-Jiménez, A. Palomo, C4a3š hydration in different alkaline media, Cem. Concr. Res. 46 (2013) 41–49, https://doi.org/10.1016/j.cemconres.2013.01.008.

[40] A.R. Ramachandran, M.W. Grutzeck, Effect of pH on the hydration of tricalcium silicate, J. Am. Ceram. Soc. 76 (1993) 72–80, https://doi.org/10.1111/j.1151-2916.1993.tb03691.x.

[41] J.G. Calvo, M.S. Moreno, M.A. Alonso, A.H. López, J.G. Olmo, Study of the microstructure evolution of low-pH cements based on ordinary portland cement (OPC) by mid- and near-infrared spectroscopy, and their influence on corrosion of steel reinforcement, Materials 6 (2013) 2508–2521, https://doi.org/10.3390/ma6062508.

[42] European Committee for Standardization, EN 197-1:2011: Cement. Composition, specifications and conformity criteria for common cements, BSI, 2011.

[43] B.K. Marsh, R.L. Day, Pozzolanic and cementitious reactions of fly ash in blended cement pastes, Cem. Concr. Res. 18 (1988) 301–310, https://doi.org/10.1016/0008-8846(88)90014-2.

[44] A. Idiart, J. Bisschop, A. Caballero, P. Lura, A numerical and experimental study of aggregate-induced shrinkage cracking in cementitious composites, Cem. Concr. Res. 42 (2012) 272–281, https://doi.org/10.1016/j.cemconres.2011.09.013.

[45] European Standard EN 12350-5, Testing fresh concrete; flow table test.

[46] H. He, L. Courard, E. Pirard, F. Michel, Shape analysis of fine aggregates used for concrete, Image Anal. Stereol. 35 (2016) 159, https://doi.org/10.5566/ias.1400.

[47] F. Collins, J. Sanjayan, Workability and mechanical properties of alkali activated slag concrete, Cem. Concr. Res. 29 (1999) 455–458, https://doi.org/10.1016/s0008-8846(98)00236-1.

[48] M. Guizar-Sicairos, S.T. Thurman, J.R. Fienup, Efficient subpixel image registration algorithms, Opt. Lett. 33 (2008) 156–158, https://doi.org/10.1364/ol.33.000156.

[49] ASTM International, Test Method for Dynamic Youngs Modulus, Shear Modulus, and Poissons Ratio by Impulse Excitation of Vibration, 2006. https://doi.org/10.1520/e1876-01r06.

[50] C. Shi, R.L. Day, A calorimetric study of early hydration of alkali-slag cements, Cem. Concr. Res. 25 (1995) 1333–1346, https://doi.org/10.1016/0008-8846(95)00126-w.

[51] J. Havlica, S. Sahu, Mechanism of ettringite and monosulphate formation, Cem. Concr. Res. 22 (1992) 671–677, https://doi.org/10.1016/0008-8846(92)90019-r.

[52] A. Alshamsi, Microsilica and ground granulated blast furnace slag effects on hydration temperature, Cem. Concr. Res. 27 (1997) 1851–1859, https://doi.org/10.1016/s0008-8846(97)00195-6.

[53] G.D. Schutter, Hydration and temperature development of concrete made with blast-furnace slag cement, Cem. Concr. Res. 29 (1999) 143–149, https://doi.org/10.1016/s0008-8846(98)00229-4.

[54] D.E. Angulo-Ramírez, R.M. de Gutiérrez, F. Puertas, Alkali-activated portland blast-furnace slag cement: mechanical properties and hydration, Constr. Build.

Mater. 140 (2017) 119–128, https://doi.org/10.1016/j.conbuildmat.2017.02.092.
[55] Z. Slížková, M. Drdácký, A. Viani, Consolidation of weak lime mortars by means of saturated solution of calcium hydroxide or barium hydroxide, J. Cultural Heritage 16 (2015) 452–460, https://doi.org/10.1016/j.culher.2014.09.003.
[56] L. Bágel, Strength and pore structure of ternary blended cement mortars containing blast furnace slag and silica fume, Cem. Concr. Res. 28 (1998) 1011–1022, https://doi.org/10.1016/s0008-8846(98)00078-7.
[57] C.-S. Poon, L. Lam, S. Kou, Y.-L. Wong, R. Wong, Rate of pozzolanic reaction of metakaolin in high-performance cement pastes, Cem. Concr. Res. 31 (2001) 1301–1306, https://doi.org/10.1016/s0008-8846(01)00581-6.
[58] P. Chindaprasirt, C. Jaturapitakkul, T. Sinsiri, Effect of fly ash fineness on compressive strength and pore size of blended cement paste, Cem. Concr. Compos. 27 (2005) 425–428, https://doi.org/10.1016/j.cemconcomp.2004.07.003.
[59] B.F. Dela, H. Stang, Two-dimensional analysis of crack formation around aggregates in high-shrinkage cement paste, Eng. Fract. Mech. 65 (2000) 149–164, https://doi.org/10.1016/s0013-7944(99)00113-7.
[60] V. Nežerka, J. Zeman, J. Němeček, Micromechanics-based simulations of compressive and tensile testing on lime-based mortars, Mech. Mater. 105 (2017) 49–60, https://doi.org/10.1016/j.mechmat.2016.11.011.
[61] Z.C. Grasley, D.A. Lange, Modeling drying shrinkage stress gradients in concrete, Cem. Concr. Aggregates 26 (2004) 1–8, https://doi.org/10.1520/cca12302.
[62] A.A.M. Neto, M.A. Cincotto, W. Repette, Drying and autogenous shrinkage of pastes and mortars with activated slag cement, Cem. Concr. Res. 38 (2008) 565–574, https://doi.org/10.1016/j.cemconres.2007.11.002.
[63] P. Mehta, Mechanism of expansion associated with ettringite formation, Cem. Concr. Res. 3 (1973) 1–6, https://doi.org/10.1016/0008-8846(73)90056-2.
[64] K. Ogawa, D. Roy, C4a3s hydration ettringite formation, and its expansion mechanism: I. expansion; ettringite stability, Cem. Concr. Res. 11 (1981) 741–750, https://doi.org/10.1016/0008-8846(81)90032-6.
[65] D. Min, T. Mingshu, Formation and expansion of ettringite crystals, Cem. Concr. Res. 24 (1994) 119–126, https://doi.org/10.1016/0008-8846(94)90092-2.
[66] V. Nežerka, Z. Slížková, P. Tesárek, T. Plachý, D. Frankeová, V. Petráňová, Comprehensive study on microstructure and mechanical properties of lime-pozzolan pastes, Cem. Concr. Res. 64 (2014) 17–29, https://doi.org/10.1016/j.cemconres.2014.06.006.
[67] A. Goldman, A. Bentur, The influence of microfillers on enhancement of concrete strength, Cem. Concr. Res. 23 (1993) 962–972, https://doi.org/10.1016/0008-8846(93)90050-j.
[68] V. Penttala, J. Komonen, Effects of aggregates and microfillers on the flexural properties of concrete, Mag. Concr. Res. 49 (1997) 81–97, https://doi.org/10.1680/macr.1997.49.179.81.
[69] F. Curcio, B. DeAngelis, S. Pagliolico, Metakaolin as a pozzolanic microfiller for high-performance mortars, Cem. Concr. Res. 28 (1998) 803–809, https://doi.org/10.1016/s0008-8846(98)00045-3.
[70] V. Nežerka, P. Tesárek, J. Zeman, Fracture-micromechanics based model of mortars susceptible to shrinkage, Key Eng. Mater. 592–593 (2014) 189–192, https://doi.org/10.4028/www.scientific.net/kem.592-593.189.
[71] M. Kachanov, Solids with cracks and non-spherical pores: proper parameters of defect density and effective elastic properties, Int. J. Fract. 97 (2005) 1–32.
[72] A. Bonakdar, B. Mobasher, Multi-parameter study of external sulfate attack in blended cement materials, Constr. Build. Mater. 24 (2010) 61–70, https://doi.org/10.1016/j.conbuildmat.2009.08.009.
[73] X. Kang, L. Ge, G.-C. Kang, C. Mathews, Laboratory investigation of the strength, stiffness, and thermal conductivity of fly ash and lime kiln dust stabilised clay subgrade materials, Road Mater. Pavement Design 16 (2015) 928–945, https://doi.org/10.1080/14680629.2015.1028970.
[74] X. Kang, L. Ge, W.-C. Liao, Cement hydration-based micromechanics modeling of the time-dependent small-strain stiffness of fly ash-stabilized soils, Int. J. Geomech. 16 (2016) 04015071, https://doi.org/10.1061/(asce)gm.1943-5622.0000552.
[75] M. Hlobil, V. Šmilauer, G. Chanvillard, Micromechanical multiscale fracture model for compressive strength of blended cement pastes, Cem. Concr. Res. 83 (2016) 188–202, https://doi.org/10.1016/j.cemconres.2015.12.003.
[76] P. Mehta, D. Pirtz, M. Polivka, Properties of alite cements, Cem. Concr. Res. 9 (1979) 439–450, https://doi.org/10.1016/0008-8846(79)90041-3.
[77] I. Maruyama, T. Matsushita, T. Noguchi, Y. Hosokawa, K. Yamada, Rate of hydration of alite and belite in Portland cement, J. Struct. Constr. Eng. (Trans. AIJ) 75 (2010) 681–688, https://doi.org/10.3130/aijs.75.681.
[78] F. Messina, C. Ferone, F. Colangelo, R. Cioffi, Low temperature alkaline activation of weathered fly ash: influence of mineral admixtures on early age performance, Constr. Build. Mater. 86 (2015) 169–177, https://doi.org/10.1016/j.conbuildmat.2015.02.069.
[79] Å. Grudemo, Microcracks, fracture mechanism, and strength of the cement paste matrix, Cem. Concr. Res. 9 (1979) 19–33, https://doi.org/10.1016/0008-8846(79)90091-7.
[80] K.D. Baldie, P.L. Pratt, Crack growth in hardened cement paste, MRS Proc. 64. doi:10.1557/proc-64-47.
[81] M. Zhang, Canmet, Microstructure, crack propagation, and mechanical properties of cement pastes containing high volumes of fly ashes, Cem. Concr. Res. 25 (1995) 1165–1178, https://doi.org/10.1016/0008-8846(95)00109-p.
[82] J. Bisschop, Effect of aggregates on drying shrinkage microcracking in cement-based composites, Mater. Struct. 35 (2005) 453–461, https://doi.org/10.1617/12627.
[83] L. Liu, X. Wang, H. Chen, C. Wan, Microstructure-based modelling of drying shrinkage and microcracking of cement paste at high relative humidity, Constr. Build. Mater. 126 (2016) 410–425, https://doi.org/10.1016/j.conbuildmat.2016.09.066.

Appendix E

Nežerka, V.; **Prošek, Z.**; Trejbal, J.; Pešta, J.; Ferriz-Papi, J.A.; Tesárek, P.: Recycling of fines from waste concrete: Development of lightweight masonry blocks and assessment of their environmental benefits, *Journal of Cleaner Production* 385 (2023) 135711,
doi: 10.1016/j.jclepro.2022.135711

Author's contribution: main idea, data analysis, design of experiments, preparation of specimens.

Journal of Cleaner Production 385 (2023) 135711

Contents lists available at ScienceDirect

Journal of Cleaner Production

journal homepage: www.elsevier.com/locate/jclepro

Recycling of fines from waste concrete: Development of lightweight masonry blocks and assessment of their environmental benefits

V. Nežerka [a,*], Z. Prošek [b,a], J. Trejbal [a], J. Pešta [b,c], J.A. Ferriz-Papi [d], P. Tesárek [a]

[a] Faculty of Civil Engineering, Czech Technical University in Prague, Thákurova 7, 166 29 Praha 6, Czech Republic
[b] University Center for Energy Efficient Buildings, Czech Technical University in Prague, Třinecká 1024, 273 43 Buštěhrad, Czech Republic
[c] Faculty of Environmental Technology, University of Chemistry and Technology Prague, Technická 5, 166 28 Praha 6, Czech Republic
[d] University of Salford, 43 Crescent, Salford M5 4WT, United Kingdom

ARTICLE INFO

Handling Editor: Jian Zuo

Keywords:
Construction and demolition waste
LCA
Recycling
Masonry blocks
Aerated concrete

ABSTRACT

A significant body of research has been carried out to find suitable waste materials or industrial by-products that could replace portland cement and reduce the environmental footprint of the concrete industry. Many studies focus on technical aspects, lacking an assessment of environmental impacts associated with using these alternative materials, and the contribution to the sustainability of the sector remains unclear. In this paper, we present the development of lightweight blocks containing the finest fractions of waste concrete along with a holistic study of the developed product's structural and environmental performance. The results demonstrate the feasibility of such a recycling strategy and its environmental benefits. However, despite replacing 60 wt.% of portland cement in the developed lightweight blocks, their carbon footprint is not negligible, and to reduce CO_2 emissions in the construction sector significantly will require holistic measures that promote the reuse of whole building elements instead of their disintegration and subsequent recycling.

1. Introduction

Material consumption increased by a factor of 10 in the 20th century (Krausmann et al., 2009) and the projected demand for materials is expected to at least double the levels of consumption from the beginning of the 21st century by 2050 (Allwood et al., 2011). As a response, the European Union attempted to initiate a transformation of linear models into circular economy (Huysman et al., 2017; COM, 2014; Commission et al., 2015) by introducing the initiative on A Resource-Efficient Europe (COM, 2011). This initiative proposes a strategy to involve all key stakeholders to achieve, in addition to other ambitious goals, high material efficiency in the construction sector and most of the construction and demolition waste (CDW) to be recycled by 2030. However, the implementation of the circular economy in this sector is hampered by weak legislation (Mittal and Sangwan, 2014a,b), low management commitment, and also by lack of adequate technologies or customer distrust (Esa et al., 2016; Mangla et al., 2017).

In this regard, concrete has the greatest potential to increase the sustainability of the construction sector. The worldwide use of concrete is more than double the use of other construction materials combined (Van Damme, 2018) and its production is associated with approximately 10% of global anthropogenic CO_2 emissions (Paris et al., 2016; da Silva and de Oliveira Andrade, 2017). Despite the negative impacts on concrete quality (Grabois et al., 2017), higher demands for mixing water (Bravo et al., 2018; Özalp et al., 2016), and technological challenges, supplementing natural quarried aggregates with recycled aggregates (Akhtar and Sarmah, 2018; Colangelo et al., 2018; Martínez et al., 2018; Xiao, 2018) or sand (Ding et al., 2020; Zou et al., 2021) has become a common practice for economic and environmental benefits (Ding et al., 2016; Pacheco-Torgal, 2020). However, this effort to replace quarried aggregates does not contribute to reductions in portland cement (PC) production, which is responsible for the massive carbon footprint (US Geological Survey & Orienteering S and US Geological Survey, 2009; Paris et al., 2016; da Silva and de Oliveira Andrade, 2017; Lee et al., 2018).

PC consumption has increased by almost 3400% over the past 65 years (Scrivener et al., 2018) despite efforts to partially replace PC with various supplementary cementitious materials (SCMs), such as fly ash, different slags, microsilica, or metakaolin (Turner and Collins, 2013; Gao et al., 2015; Shojaei et al., 2015; Gholampour and Ozbakkaloglu, 2017; Nežerka et al., 2019). Many of these SCMs are produced by very pollutant and gradually disappearing industries (e.g., coal power plants, steel factories burning coke, etc.). Although the use of SCMs in the form of industrial by-products increases sustainability, it does not contribute to circularity (Marsh et al., 2022).

* Corresponding author.
E-mail address: vaclav.nezerka@fsv.cvut.cz (V. Nežerka).

https://doi.org/10.1016/j.jclepro.2022.135711
Received 8 October 2022; Received in revised form 15 December 2022; Accepted 19 December 2022
Available online 22 December 2022

Nomenclature

CDW	Construction and demolition waste
PC	Portland cement
SCMs	Supplementary cementitious materials
RCF	Recycled concrete fines
LCA	Life-cycle assessment
AAC	Aerated autoclaved concrete
MFs	Microfibers
SP	Superplasticizer
FA	Foaming agent
XRF	X-ray fluorescence spectroscopy
C_3S	Tricalcium silicate (alite)
C_3A	Tricalcium aluminate
C_2S	Dicalcium silicate (belite)
LOI	Loss on ignition
PP	Polypropylene
w/c	Water-to-cement ratio
ρ_b	Bulk density
FTR	Flow test result
$E_{dyn,r}$	Dynamic Young's modulus (resonance method)
$E_{dyn,u}$	Dynamic Young's modulus (ultrasound method)
f_b	Bending strength
f_c	Compressive strength
λ	Thermal conductivity coefficient

To achieve both, it is desirable to efficiently replace PC with stripped paste generated during the crushing and disintegration of the waste concrete. However, the use of these recycled concrete fines (RCF), which represent approximately 40% of the weight of crushed concrete waste (Villagrán-Zaccardi et al., 2022), is disapproved or even forbidden by building codes due to commonly accepted misconceptions about their impact on concrete performance (Evangelista and de Brito, 2013), although efficient ways to increase reactivity and incorporate RCF into cementitious mixes have been found. The first way, although energetically demanding, is to exploit heat to increase the reactivity of RCF (Shui et al., 2008; Serpell and Lopez, 2013; Florea et al., 2014; Gastaldi et al., 2015; Lotfi and Rem, 2017). Alternatively, RCF can be ground (micronized) to distort the tetrahedral structure of α-SiO_2 and transform it into an amorphous form (Liu et al., 2014) and expose unhydrated cement particles (Prošek et al., 2020b). The reactivity of these disintegrated RCFs can be further enhanced with alkali additives, such as slag or fly ash (Prošek et al., 2019). Eventually, chemical compounds such as tannic acid (Wang et al., 2022), can also improve the binding of RCF to hydration products and improve the strength and durability of the cementitious material produced.

The goal of this study is to propose a technique for producing lightweight masonry blocks containing large amounts of micronized RCF without the need for significant technological changes in standard manufacturing processes or sacrifice in the performance of the end product. A well-documented design procedure based on our previous research (Prošek et al., 2019, 2020b; Nežerka et al., 2020) and the findings of other authors (Khatib, 2005; López-Uceda et al., 2016; González et al., 2021), comprehensive testing, and detailed life cycle assessment (LCA) (Pešta et al., 2020) are expected to contribute to gaining the trust of all involved parties, from investors and producers to environmental protection agencies. Standardized LCA procedures (Finkbeiner et al., 2006) were used not only to evaluate the elementary flows of materials and energies, but also to describe their potential secondary environmental impacts (Knoeri et al., 2013). The standardized LCA procedures involve a thorough inventory of energy and material consumption, as well as emissions associated with the production and use of a specific product or service to provide its overall environmental profile. It has been widely used in construction industry for optimization of a specific material/component, such as PC (Hossain et al., 2017), or composites, such as concrete (Turk et al., 2015; Vieira et al., 2016; Kleijer et al., 2017). It must be kept in mind that technical parameters of compared product have to be also considered, since materials with a smaller ecological footprint may have low strength resulting in the need to use higher amount of this material to provide the required load-bearing capacity (Marinković et al., 2017). In this study, the performance and all environmental impacts associated with the production of the developed lightweight masonry blocks were compared with the environmental product declaration and technical sheet of widely used aerated autoclaved concrete (AAC) blocks having similar technical parameters and use.

2. Materials

The extensive experimental program focused on the testing and design of cement-based foam material used for the production of lightweight masonry blocks. This composite material was produced using the following ingredients: (i) PC of a class CEM I/42.5R (EN 197-1:2011 European Committee for Standardization, 2011), (ii) RCF prepared by crushing and grinding 100-year-old concrete from monolithic columns used in interior using a high-energy electric mill (SBD 800 assembled by the Lavaris company, Czech Republic), (iii) microfibers (MFs) made of 100% recycled polypropylene produced for mortar/concrete reinforcement produced by the Trevos Košťálov company from the Czech Republic (having 32 μm in diameter and length of 4 mm), (iv) polycarboxylate-based/modified polycarboxylate-based superplasticizers (SPs) developed for ready-mix concrete (Table 1), dosed according to the recommendations by the manufacturers, (v) a foaming agent (FA) based on amides and sulfonic acid, and (vi) tap water. PC and RCF used in this study were characterized in detail by Prošek et al. (2020b), who dealt with recovery of anhydrous clinker and used the same input materials for experimental testing.

The amount of mixing water was reduced using SPs to support the FA responsible for the porous structure of the hardened material. FA was used in a 50% concentration to reach foamability of 35 ml/g and foam stability of 465 min. MFs were used to reinforce the brittle structure of the hardened composites. According to the technical sheets of the producer, the MFs had a density of 910 kg/m^3, exhibited the average tensile strength of ≥3.0 cN/dtex (~272 MPa), average elongation at rupture ≥50%, and the elastic stiffness of ~4 GPa. The surface of the MFs was smooth since the filaments were manufactured using the standard technology of melt spinning. The amount of MFs was determined based on our preliminary studies, supported by the findings of Raj et al. (2020).

The chemical composition of PC and RCF used in this study was determined using X-ray fluorescence spectroscopy (XRF) according to the EN 196-2:2013 (European Committee for Standardization, 2013). XRF analysis was performed using a Spectro Xepos spectrometer equipped with 50 W/60 kV X-ray emitters. The list of detected oxides is presented in Table 2; equivalent concentrations of clinker phases were calculated based on these values using the Bogue formula, defined in the ASTM C114 standard (ASTM C114, 2018).

PC used in this study was rich in C_3S (74.6%) and contained smaller proportions of C_3A (8.1%) and C_2S (7.2%). Such an allitic PC was supposed to exhibit an early strength gain. The analyzed RCF powder contained high amounts of SiO_2 due to the presence of ground siliceous sand of 0–1 mm fraction, present in the disintegrated concrete. The high amounts of CaO and loss on ignition (LOI) in RCF can be attributed to the high content of the hydrated cementitious matrix.

The particle size distribution curves for both PC and RCF, determined using a Fritsch Analyssete 22 MicroTec Plus laser diffraction

Table 1
Summary of SPs used in this study.

	Name (brand)	Dosage [wt.%]	pH	Chloride content [%]	Dry extract [%]	Density [kg/dm^3]	Alkali content (Na_2O equiv.) [%]
SP1	Fortesil (Stachema)	0.8	9.75	<0.1	30.0	1.17	8.0
SP2	Premia 196 (Chryso)	0.8	7.50	<0.1	25.3	1.06	1.5
SP3	Premia 330 (Chryso)	1.0	6.50	<0.1	23.6	1.05	2.0
SP4	ViscoCrete-20 Gold (Sika)	2.5	4.50	<0.1	29.0	1.05	1.0

Table 2
Concentration of the most important oxides and LOI [%] identified using XRF for PC and RCF used in this study.

	CaO	SiO_2	Fe_2O_3	Na_2O	MgO	Al_2O_3	SO_3	LOI	Other
PC	64.8	20.1	2.51	0.13	1.92	4.02	3.01	3.05	0.45
RCF	23.8	36.4	3.13	1.36	1.43	7.56	1.58	22.7	2.04

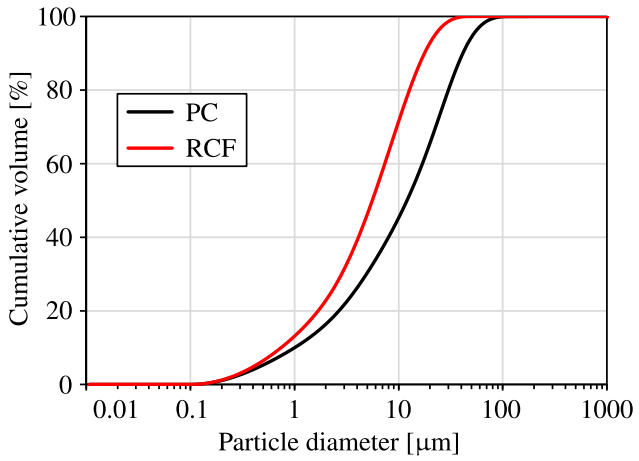

Fig. 1. Particle size distribution curves for PC and RCF.

particle size analyzer, are provided in Fig. 1. RCF contained finer particles than PC; the fineness of PC and FRC corresponds to their specific surface, determined using the Blaine method (Matest E009 device), equal to 380, and 860 m^2/kg, respectively.

2.1. Tested mixtures

The mixture optimization procedure consisted of three stages during which different mixtures were prepared and tested (Tables 3–5). For the first two optimization stages, the water-to-cement ratio (w/c) was adjusted so that the flow test result (FTR) reached 180 ± 5 mm after 15 blows. The optimum w/c, strongly influenced by the presence of fine RCF particles, was then used for the final set tested within Stage 3. The flow test was performed according to EN 12350-2 (European Standard EN 12350-5, 2009). During all stages, fresh pastes were placed in molds, compacted using a shaking table, and removed from molds after 24 h. Hardening took place in a laboratory at 22 ± 1 °C and relative humidity of 50 ± 6% for 28 days. The bulk density (ρ_b) was determined according to the EN 12390-7 standard (EN-, 2009) by employing the gravimetric method.

2.1.1. Mixtures for stage 1

The first set of mixtures (Table 3) consisted of hardened pastes and was used to determine the appropriate PC-to-RCF ratio. The effort was to maximize the RCF content while having the hardened paste compact without disintegration during manipulation with the specimens or low-intensity loading. The FTRs of these mixtures indicate poorer workability of pastes containing RCF as a result of adhesion of this fine-grained component having a large specific surface. This effect is not in accordance with the requirements on sustainable materials and therefore the large water demands had to be reduced using suitable SPs, selected in Stage 2.

Table 3
Composition of mixtures for RCF content optimization, FTR and bulk densities of hardened mortars (Stage 1).

Mix	PC	RCF	w/c	ρ_b	FTR
	[wt.%]			[kg/m^3]	[mm]
10/0	100	0	0.35	2298 ± 16	179
9/1	90	10	0.40	2023 ± 15	180
8/2	80	20	0.46	1970 ± 20	179
7/3	70	30	0.56	1957 ± 7	176
6/4	60	40	0.67	1862 ± 10	177
5/5	50	50	0.84	1837 ± 9	177
4/6	40	60	1.08	1810 ± 11	178
3/7	30	70	1.50	1795 ± 6	180
2/8	20	80	2.35	1790 ± 5	181
1/9	10	90	4.90	1785 ± 8	180

Table 4
Composition of mixtures for testing the effects of different SPs (Stage 2).

Mixture	PC	RCF	SP1	SP2	SP3	SP4	w/c	ρ_b	FTR
	[wt.%]		[wt.% of PC]					[kg/m^3]	[mm]
4/6 SP1	40	60	0.8	–	–	–	0.93	1845 ± 16	175
4/6 SP2	40	60	–	0.8	–	–	0.93	1852 ± 13	175
4/6 SP3	40	60	–	–	1.0	–	0.93	1913 ± 19	180
4/6 SP4	40	60	–	–	–	2.5	0.80	1993 ± 15	178

Table 5
Composition of mixtures for testing the effects of FA and MFs (Stage 3).

Mixture	PC	RCF	SP4	FA	MFs	w/c	ρ_b
	[wt.%]		[wt.% of PC]				[kg/m^3]
4/6 SP4 A	40	60	2.5	3.00	2.5	0.50	810 ± 5
4/6 SP4 B	40	60	2.5	2.25	2.5	0.50	801 ± 4
4/6 SP4 C	40	60	2.5	2.25	–	0.50	980 ± 10
4/6 SP4 D	40	60	2.5	1.50	2.5	0.50	1110 ± 11

2.1.2. Mixtures for stage 2

The second set (Table 4) consisted of mixtures that have the optimal PC-to-RCF ratio (40:60; see Section 4.1) and different SPs. In Stage 2, a suitable SP providing the most compact matrix at the micro-scale, thus exhibiting a superior strength and stiffness, was selected. w/c varied due to the different amounts and efficiency of the SPs used in the study.

2.1.3. Mixtures for stage 3

The third set of samples (Table 5) was lightened with FA and reinforced with MFs. The objective of the Stage 3 testing was to determine whether it is favorable to add MFs and select an appropriate amount of FA to obtain blocks exhibiting sufficient strength while maintaining low heat conductivity. FTR for this set was not measured because the mixtures were liquid before foaming.

3. Methods

Standardized test methods for macroscopic samples, commonly adopted in both industry and research, were used to evaluate the key parameters of the developed composites. All tests were performed on 28 days old specimens at 22 ± 1 °C and relative humidity of 50 ± 5% (CEN, 2021).

3.1. Stiffness assessment

Impact resonant frequency testing according to the ASTM C215 Standard (AST, 2014) was measured for six 40 × 40 × 160 mm specimens representing each mixture using the Brüel & Kjaer 3560-B-120 device. The dynamic Young's modulus was determined from the frequency response function according to the formula presented in the ASTM C215-14 Standard:

$$E_{\mathrm{dyn,r}} = \frac{4Lmf_{\mathrm{I}}^2}{bt}, \tag{1}$$

where L, b, and t are the length, width, and thickness of a specimen, respectively, m is its mass, f_{I} is the measured fundamental longitudinal resonant frequency.

Furthermore, the stiffness of the specimens was evaluated based on the velocity of ultrasound pulse wave propagation, v_{u}, according to the ASTM E1876-01 Standard (AST, 2006), using the Pundit Lab device equipped with 54 kHz probes attached to the surface of the specimens using sonogel. The dynamic Young's modulus was determined on the basis of v_{u} as

$$E_{\mathrm{dyn,u}} = \frac{\rho_{\mathrm{b}} v_{\mathrm{u}}^2 (1+\nu)(1-2\nu)}{1-\nu}, \tag{2}$$

where ν is its Poisson's ratio.

3.2. Determination of strength

Destructive tests were carried out using a Heckert FP100 loading frame with displacement-controlled loading at the rate of 0.1 mm/min. The bending strength was determined based on the load–displacement records from three-point bending tests performed using the 40 × 40 × 1600 mm prismatic specimens as for the stiffness testing according to

$$f_{\mathrm{b}} = \frac{3F_{\mathrm{b,max}}L_{\mathrm{s}}}{2b^2t}, \tag{3}$$

where $F_{\mathrm{b,max}}$ is the maximum force reached during the bending test and L_{s} is the span between the supports, here equal to 100 mm, b is the cross-section height, and t is the cross-section width.

Uniaxial compression tests were carried out on 40 × 40 × 40 mm cubic specimens extracted from the halves of specimens broken during the bending test; each mixture was represented by twelve specimens. The compressive strength was calculated from the maximum force reached during the test, $F_{\mathrm{c,max}}$, as

$$f_{\mathrm{c}} = \frac{F_{\mathrm{c,max}}}{bt}, \tag{4}$$

where $F_{\mathrm{c,max}}$ is the maximum force reached during the compression test.

3.3. Evaluation of heat transfer properties

The thermal conductivity coefficient λ was evaluated for 150 × 150 × 150 mm specimens using an ISOMET 2104 (Applied Precision) heat transfer analyzer, equipped with API210411 and API210403 surface probes capable of measurements in the ranges of 0.04–0.3 W/mK and 0.3–2.0 W/mK, respectively, and with the accuracy of ±5 %. The device employs the dynamic method based on monitoring the response of an examined material to heat flow impulses. Each mixture was represented by six specimens, each measured three times in a different orientation and position of probes.

A scheme of the three-stage optimization process involving all the methods used to evaluate the performance of the developed composites and number of specimens for each test are presented in Fig. 2.

Table 6
Specific distances for the modeled transport of materials, based on real distances between the involved suppliers and facilities near Prague, Czech Republic; pipeline transport of water has been neglected.

Material transported	Distance [km]
PC	70
Recycled concrete	70
RCF	52
Chromium milling parts	100
FA	200
MFs	280
SP	200
CDW collection (used blocks)	100 (assumed)

3.4. LCA

LCA, standardized by ISO 14040 (Finkbeiner et al., 2006) was performed according to procedures for building products provided in the EN 15 804+A2 standard (CEN, 2020). The environmental impacts of one ton of the developed blocks containing RCF were assessed to evaluate its environmental burdens and benefits. The system boundaries included the following lifecycle phases: extraction of raw material, production of materials (including RCF), transport, preparation of the concrete mixture, and the end-of-life product phase. The end-of-life phase involved deconstruction, CDW transport, and landfilling (Fig. 3). The use phase for the developed block was not considered, and the reference service life was assumed to exceed 50 years.

A Gabi Professional software (Gabi Software, 2020) was used to model all the considered system boundaries and describe elementary energies and material flows. Next, the potential impacts caused by these flows were assessed. Generic data was used for models of nonspecific processes such as transport, production of electricity mix (for the Czech Republic), CDW landfilling, and petroleum supply (Kupfer et al., 2020). Generic data from the Gabi database were used for ingredients except for RCF, for which input and output had to be calculated. These calculations were based on data provided by producers of recycled aggregate who prepared RCF from the 0/4 concrete waste fraction using a high-speed mill; the data collected during the processing of RCF were: Electricity consumption equal to 6.25 kWh/t and wearing of the mill at a rate of 268 g/t. Transport was modeled considering a generic process for a truck of the Euro 5 emission category with a specific distance provided in Table 6.

4. Results and discussion

4.1. RCF content optimization

Finding the optimal PC-to-RCF ratio to ensure sufficient matrix strength (set in advance to $f_{\mathrm{c}} \geq 50$ MPa and $f_{\mathrm{b}} \geq 4$ MPa, based on experience (Topič et al., 2017, 2018) to sustain common manipulation without disintegration), while keeping the RCF content as high as possible was a crucial part of the optimization procedure. Stiffness of specimens was not considered crucial for the selecting the most suitable mixture, however, keeping $E_{\mathrm{dyn}} \geq 15$ GPa was expected. The difference between Young's moduli $E_{\mathrm{dyn,r}}$ and $E_{\mathrm{dyn,u}}$ (Fig. 4) for less than 40 wt.% of RCF indicates a low degree of homogeneity due to the presence of cracks or large voids (Brožovský and Dufka, 2015), common for cementitious pastes lacking stiff inclusions (Nežerka et al., 2017). Shrinkage-induced micro-cracks (Nežerka et al., 2020) present in pastes lacking reinforcement provided by the RCF inclusions have large impact on natural frequencies measured to evaluate $E_{\mathrm{dyn,r}}$. The presence of these micro-cracks and the fact that RCF acts as a micro-filler is responsible for non-linearity in the measured E_{dyn} (Niewiadomski et al., 2021).

The addition of RCF resulted in a linear decrease in f_{c}, while f_{b} peaks at the 40:60 PC-to-RCF ratio (60 wt% of RCF), selected for further

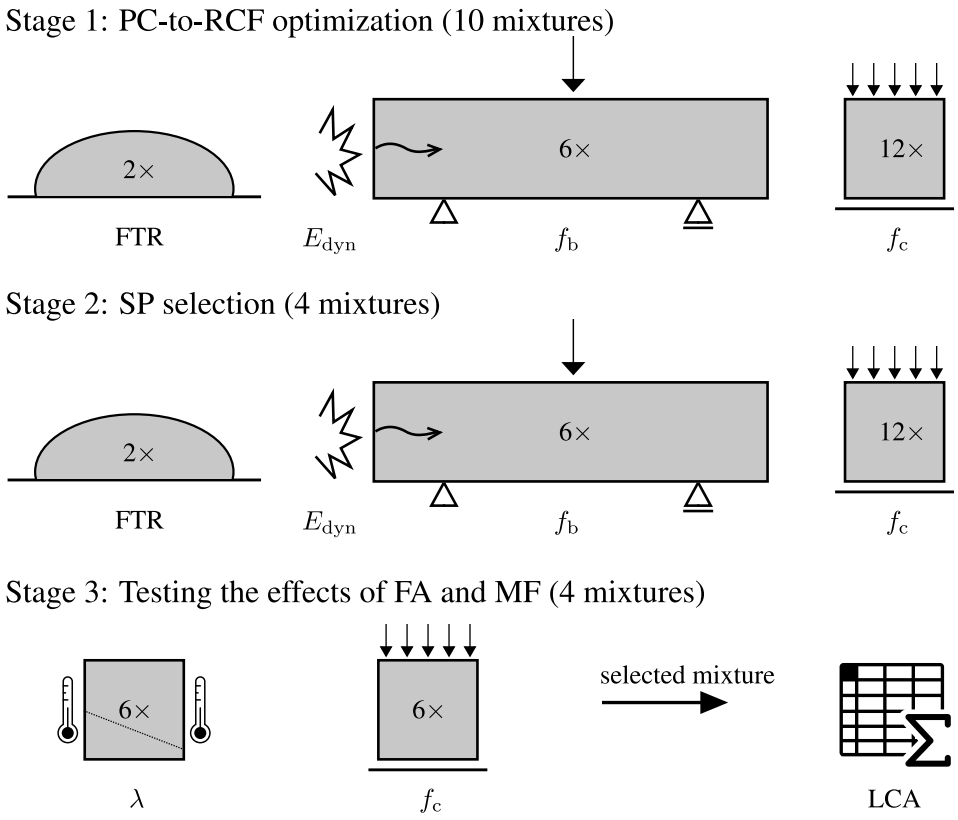

Fig. 2. Three-stage experimentally-based development of a lightweight cementitious composite material containing RCF; number of tested specimens, experimental methods, and output parameters used for performance assessments.

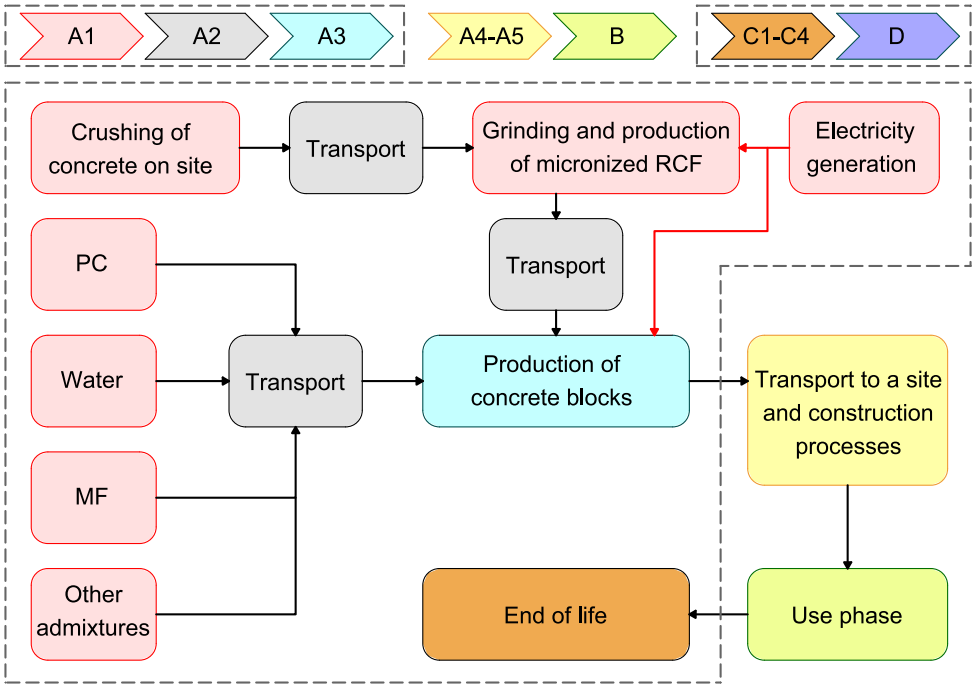

Fig. 3. Processes involved in the modeled system boundaries (separated with the dashed lines) for the developed block production; life-cycle phases according to EN 15 804+A2 (CEN, 2020): A1 = raw material extraction and supply (light red), A2 = transport (gray), A3 = manufacturing (light blue), A4–A5 = construction (yellow), B1–B7 = the use phase (green), C1–C4 = end-of-life phase (orange), D = benefits and loads beyond the system boundary (blue, not considered in our study).

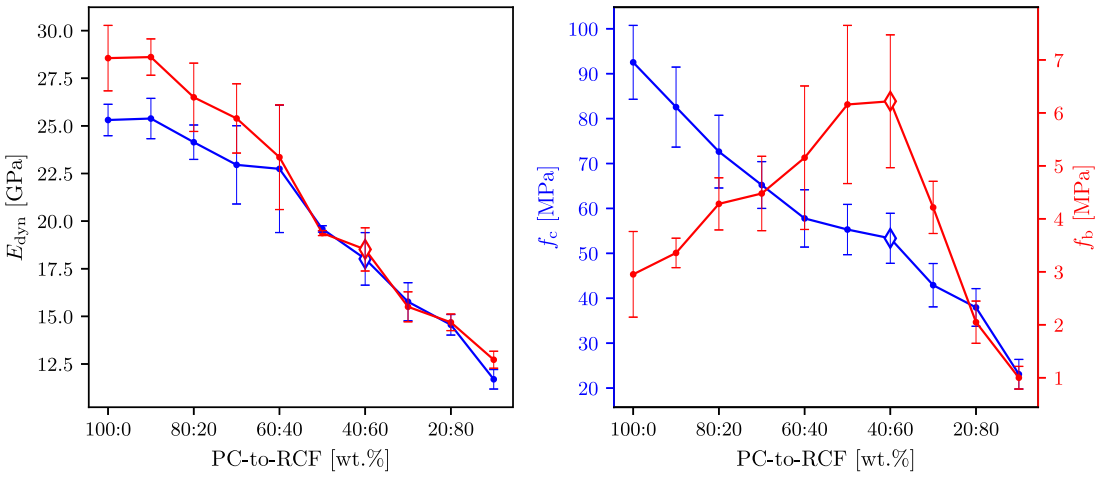

Fig. 4. Relationship between the PC-to-RCF ratio and mechanical properties of hardened cementitious pastes (Stage 1 testing); the mixture selected for further development stages (40:60) is highlighted with diamond markers.

optimization as optimum. The development of f_c roughly correlates with ρ_b (Table 3) and therefore also with porosity, which is consistent with the findings of other authors dealing with the incorporation of RCF into cementitious composites (Ma and Wang, 2013; Bordy et al., 2017; Quan and Kasami, 2018). This conjecture is also supported by the linear decrease in $E_{dyn,u}$ with the replacement of PC with RCF. The peak in f_b can be attributed to the reinforcing effect provided by RCF, which plays the role of fine aggregate that increases fracture toughness (Strange and Bryant, 1979; Nežerka et al., 2014, 2017), prevents shrinkage-induced cracks to develop and propagate (Nežerka et al., 2020), and impedes opening and propagation of micro-cracks due to tensile stresses (Strange and Bryant, 1979; Karihaloo et al., 1993; Rhee et al., 2019). Similar results have been obtained by Prošek et al. (2020a) when studying the effects of limestone powder in cementitous pastes. The drop in f_b beyond the 40:60 threshold is attributed to a lack of binder (PC).

4.2. SP selection

Reducing the amount of water was another crucial step in optimizing the mixture, as large amounts negatively affect the stability of the foam after the addition of FA (Raj et al., 2019). Setting general rules for the selection of SPs is difficult as their performance depends on the type of cement and aggregates used. Here, the selection was based on the impact of individual SPs on the mechanical properties of hardened mortars. These properties are influenced by both the porosity and the uniformity of the dispersion of the cement grains, as suggested by Carazeanu (2002).

The impact of SPs on the porosity of mortars correlates with the values of ρ_b, provided in Table 4. In this regard, the use of SP4 resulted in the most compact matrix, reflected also by the highest values of E_{dyn} and f_c (Fig. 5), which is consistent with the findings by Quan and Kasami (2018) and Barbudo et al. (2013). All mortars tested within Stage 2 exhibited a brittle behavior and large scatter in the measured f_b and therefore high standard deviations. For this reason, MFs were added to the 4/6 SP4 mixture in Stage 3 of the development.

4.3. FA and MFs content optimization

The results of testing at Stage 3 clearly indicate the importance of MFs and the effects of FA on the mixture. The mixtures 4/6 SP4 B and 4/6 SP4 C were identical, except for the content of MFs. The 4/6 SP4 C mixture without MFs exhibited, despite the lower ρ_b (Table 5), 28% lower f_c and 138% higher λ (Fig. 6). This indicates both the reinforcing effect of MFs as well as their positive impacts on the pore size distribution, which has also been suggested in the studies by Namsone et al. (2017) and Steshenko et al. (2017). The measured values of λ correspond to the results of the study by Ganesan et al. (2015) who reported for aerated concrete a linear relationship between λ (range 0.24–0.74 W/mK) and ρ_b (range 700–1400 kg/m^3) .

Taking thermal conductivity as the key parameter, mixture 4/6 SP4 B was selected for large-scale production and assessment of environmental impacts. The blocks made of this mixture exhibited low heat conductivity, $\lambda = 0.21 \pm 0.02$ W/mK, while having sufficient compressive strength, $f_c = 7.1 \pm 0.5$ MPa. This strength exceeds the lower limit set in advance to 5 MPa.

4.4. Large-scale production

To verify applicability of the 4/6 SP4 B, the mixture preparation procedure was translated into semi-production in a concrete plant. The procedure encompassed a whole industrial mixture preparation procedure: mixture preparation, its transport, and placement in molds. The mixture preparation was carried out using a planetary mixer with a whirling drum at the Destro company located in Kladno near Prague, Czech Republic. First, all ingredients were mixed, followed by the addition of water with SP4. FA was aerated using an industrial foam generator and the foam was mixed with fresh mortar and the final mixture was then transported to the molding site using an automatic concrete mixer. Here, the mixture was placed in two molds, each for 44 blocks with dimensions of 500 × 250 × 175 mm (Fig. 7).

Although this was the first semi-production run, the resulting product had properties comparable to those of common commercially produced foam silicates. A 10 m^2 external wall (Fig. 8) was constructed from lightweight hardened blocks in the premises of the University Center for Energy Efficient Buildings of the Czech Technical University in Prague and was exposed to the outdoor environment. The wall is currently subject to long-term monitoring of the moisture content, thermal conductivity, and structural properties during real operating conditions.

4.5. Environmental impacts

From the assessment of environmental impacts (Tables 7 and 8) it is clear that the production of raw materials needed to manufacture the developed lightweight masonry blocks contributes the most to almost every indicator. This is most significant for indicators related to CO_2 production, resource use, eutrophication, energy demands, waste disposal, and toxicity and radioactivity. On the other hand, indicators

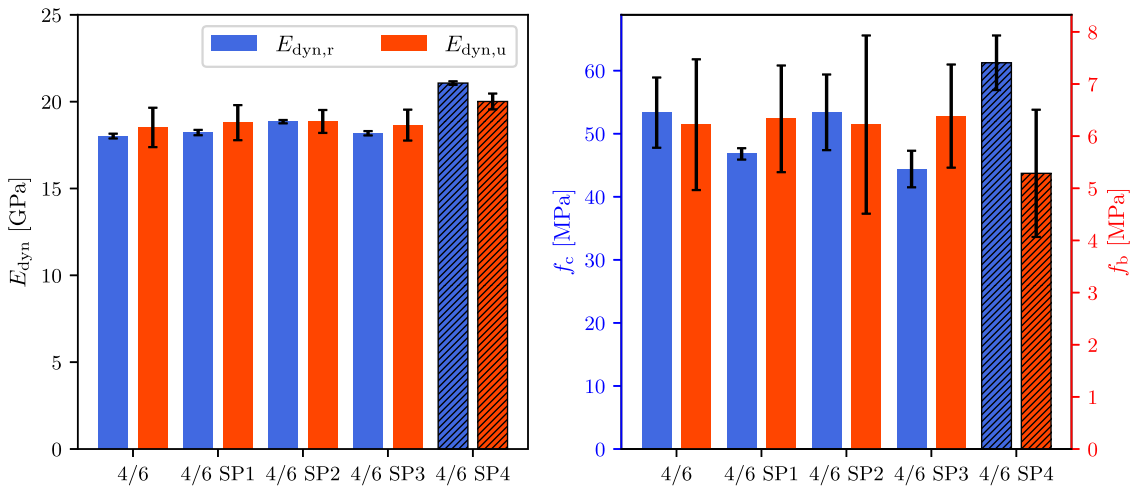

Fig. 5. Effect of different SPs on mechanical properties of hardened cementitious pastes (Stage 2 testing); the mixture selected for further development stage (4/6 SP4) is highlighted with a hatch.

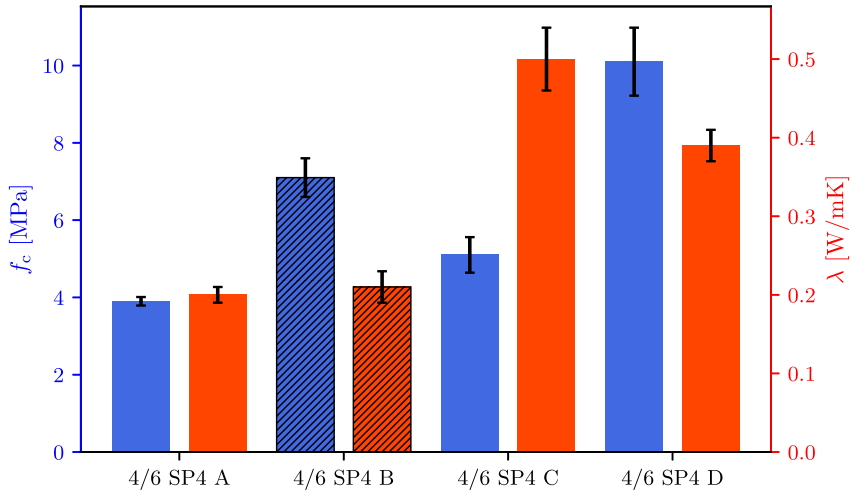

Fig. 6. Effect of FA and MFs on mechanical properties of hardened aerated cementitious composites (Stage 3 testing); the mixture selected for large-scale production and LCA (4/6 SP4 B) is highlighted with a hatch.

related to water use are positively influenced by the exploitation of recycled materials. The revised version of EN 15 804+A2 standard (CEN, 2020) includes calculations for end-of-life benefits in Annex D and these end-of-life benefits reflect circularity and recycling and result in a negative value for the Water use and Use of net fresh water indicators. Indirectly, concrete production contributes almost 20% to the impact in the Ionizing radiation category, being the result of the production of electricity for the processes. The production phase and transport processes are responsible for negligible impacts compared to the production of raw materials.

4.5.1. Contribution analysis

All processes were evaluated to determine their contributions to the potential environmental impact per life cycle of 1 t of the lightweight blocks made of the 4/6 SP4 B mixture. All significant contributions (>10% of the total impact) are listed in Table 9 and graphically represented in Fig. 9.

Concrete recycling contributes beneficially to several impact categories and significantly mitigates the overall use of resources (mineral and metals). Replacement of PC with RCF directly reduces PC production, having the greatest impact on climate change to which it contributes by more than 80%. At the same time, PC production significantly impacts Acidification, Photochemical ozone creation, Resource use (fossil), and Water use categories. These categories are also greatly affected by the contribution of the landfilling process. SP production (used in the amount of 10 kg/1 t of the lightweight blocks) contributes by 96% to ozone depletion and increases the results for other impact indicators, including Eutrophication freshwater, Resource use (mineral and metals), and Water use, as well. In this regard, the use of more user-friendly solutions, such as ultrafine mineral admixtures (Han et al., 2022), should be considered.

These findings clearly justify the effort to incorporate RCF into PC-based composites. The results of a study on the potential environmental impacts of different PC-to-RCF ratios are provided in Table 10, which shows an almost perfectly linear relationship between the critical indicators and the PC-to-RCF ratio. This ratio could be further increased when using recycled cement having binding properties; the technology based on magnetic separation of stripped cement paste and its thermoactivation was proposed and scrutinized by Sousa and Bogas (2021) and Sousa et al. (2022).

Table 7
Environmental indicators calculated for 1 t of the developed lightweight blocks (4/6 SP4 B) according to the EN 15 804+A2 standard (CEN, 2020), part 1.

Indicator	Total	Production of materials	Transport	Concrete production	End of life
Climate change, total [kg CO_2 eq.]	334	298	4.44	9.39	22.8
Climate change, fossil [kg CO_2 eq.]	334	297	4.45	9.33	23,3
Climate change, biogenic [kg CO_2 eq.]	455	58	−0.04	0.06	−0.5
Climate change, land use and land use change [kg CO_2 eq.]	0.312	0.196	0.03	0.001	0.084
Ozone depletion [kg CFC-11 eq.]	1.79×10^{-6}	1.79×10^{-6}	4.38×10^{-13}	7.05×10^{-11}	3.63×10^{-11}
Acidification [Mole of H^+ eq.]	0.70	0.51	0.15	0.22	0.15
Eutrophication, freshwater [kg P eq.]	3.71×10^{-3}	3.61×10^{-3}	1.59×10^{-5}	2.36×10^{-5}	5.55×10^{-5}
Eutrophication, marine [kg N eq.]	0.19	0.13	6.81×10^{-3}	4.26×10^{-3}	0.05
Eutrophication, terrestrial [Mole of N eq.]	2.09	1.42	0.08	0.04	0.55
Photochem. ozone formation, human health [kg NMVOC eq.]	0.57	0.42	0.01	0.01	0.13
Resource use, minerals and metals [kg Sb eq.]	2.31×10^{-4}	2.27×10^{-4}	4.49×10^{-7}	1.05×10^{-6}	2.39×10^{-6}
Resource use, fossils [MJ]	2090	1580	58.5	144	306
Water use [m^3 world equiv.]	−20.3	−22.2	0.05	0.13	1.72

Table 8
Environmental indicators calculated for 1 t of the developed lightweight blocks (4/6 SP4 B) according to the EN 15 804+A2 standard (CEN, 2020), part 2.

Indicator	Total	Production of materials	Transport	Concrete production	End of life
Use of renewable primary energy (PERE) [MJ]	318	244	4.1	32.1	37.1
Total use of renewable primary energy resources (PERT) [MJ]	318	244	4.1	32.1	37.1
Use of non-renewable primary energy (PENRE) [MJ]	2090	1580	58.7	144	307
Total use of non-renewable primary energy resources (PENRT) [MJ]	2090	1580	58.7	144	307
Use of renewable secondary fuels (RSF) [MJ]	1.64×10^{-22}	1.64×10^{-22}	0.00	0.00	0.00
Use of non renewable secondary fuels (NRSF) [MJ]	1.93×10^{-21}	1.93×10^{-21}	0.00	0.00	0.00
Use of net fresh water (FW) [m^3]	-7.09×10^{-2}	-1.80×10^{-1}	4.68×10^{-3}	4.64×10^{-2}	5.85×10^{-2}
Hazardous waste disposed (HWD) [kg]	8.40×10^{-4}	8.40×10^{-4}	3.11×10^{-10}	6.82×10^{-9}	1.07×10^{-8}
Non-hazardous waste disposed (NHWD) [kg]	1000	3.02	0.01	0.06	1000
Radioactive waste disposed (RWD) [kg]	6.63×10^{-2}	4.42×10^{-2}	1.09×10^{-4}	1.96×10^{-2}	2.35×10^{-3}
Particulate matter [Disease incidences]	8.37×10^{-6}	6.61×10^{-6}	8.68×10^{-8}	1.65×10^{-7}	1.51×10^{-6}
Ionizing radiation, human health [kBq U235 eq.]	7.61	6.03	0.02	1.30	0.26
Ecotoxicity, freshwater [CTUe]	1070	785	41.5	53.5	188
Human toxicity, cancer [CTUh]	6.50×10^{-8}	4.47×10^{-8}	8.55×10^{-10}	1.06×10^{-9}	1.83×10^{-8}
Human toxicity, non-cancer [CTUh]	4.95×10^{-6}	2.88×10^{-6}	5.27×10^{-8}	7.35×10^{-8}	1.94×10^{-6}
Land use [Pt]	466	306	24.8	45.9	89.4

Table 9
Relative contributions [%] of processes (listed only those contributing by more than 10% of the total impact in a category).

Indicator	Concrete recycling	Electricity generation	PC production	Landfilling	MFs production	Recycling plant maintenance	SP production
Climate change, total [kg CO_2 eq.]	−2.87	2.81	81.44	4.34	5.06	0.31	3.32
Ozone depletion [kg CFC-11 eq.]	0.00	0.00	0.00	0.00	0.01	3.01	96.04
Acidification [Mole of H^+ eq.]	−1.30	3.10	61.77	15.12	3.14	0.77	5.55
Eutrophication, freshwater [kg P eq.]	0.16	0.64	3.42	0.68	0.85	11.81	80.30
Photochemical ozone formation, human health [kg NMVOC eq.]	−0.42	2.07	60.81	14.45	4.50	0.53	4.89
Resource use, mineral and metals [kg Sb eq.]	−12.73	0.45	7.84	0.67	1.72	10.08	91.23
Resource use, fossils [MJ]	−4.08	6.89	34.31	9.33	27.99	0.67	11.41
Water use [m^3 world equiv.]	−160.59	0.65	13.55	8.03	1.85	2.44	27.88
Particulate matter [Disease incidences]	−3.18	1.97	71.45	15.53	4.16	0.73	3.85
Ionizing radiation, human health [kBq U235 eq.]	3.02	17.08	45.60	3.06	6.81	2.09	13.66
Ecotoxicity, freshwater [CTUe]	1.40	5.00	22.15	10.19	25.98	3.15	16.65
Human toxicity, cancer [CTUh]	−9.28	1.63	28.31	25.69	10.77	19.48	17.66
Human toxicity, non-cancer [CTUh]	−2.33	1.49	49.95	37.40	6.81	0.40	2.14
Land use [Pt]	3.27	9.87	41.78	9.13	6.87	1.75	6.47

Table 10
Selected environmental indicators calculated for 1 t of the developed lightweight blocks (4/6 SP4 B) according to the EN 15 804+A2 standard (CEN, 2020), considering various PC/RCF ratios.

Indicator	55/45	50/50	45/55	40/60	35/65	30/70	25/75
Climate change, total [kg CO_2 eq.]	435	400	366	334	298	264	230
Ozone depletion [kg CFC-11 eq.]	1.78×10^{-6}	1.78×10^{-6}	1.78×10^{-6}	1.79×10^{-6}	1.79×10^{-6}	1.80×10^{-6}	1.80×10^{-6}
Acidification [Mole of H^+ eq.]	0.86	0.80	0.75	0.70	0.64	0.59	0.54
Eutrophication, freshwater [kg P eq.]	3.64×10^{-3}	3.66×10^{-3}	3.69×10^{-3}	3.71×10^{-3}	3.73×10^{-3}	3.75×10^{-3}	3.78×10^{-3}
Eutrophication, marine [kg N eq.]	0.23	0.22	0.20	0.19	0.18	0.17	0.15
Eutrophication, terrestrial [Mole of N eq.]	2.50	2.36	2.22	2.09	1.94	1.80	1.67
Photochemical ozone formation, human health [kg NMVOC eq.]	0.69	0.65	0.61	0.57	0.52	0.48	0.44
Resource use, mineral and metals [kg Sb eq.]	2.39×10^{-4}	2.37×10^{-4}	2.34×10^{-4}	2.31×10^{-4}	2.28×10^{-4}	2.26×10^{-4}	2.23×10^{-4}
Resource use, fossils [MJ]	2360	2270	2170	2090	1990	1900	1810
Water use [m^3 world equiv.]	−11.4	−14.5	−17.5	−20.3	−23.6	−26.6	−29.6

Fig. 7. Pouring of the industrially produced mixture (4/6 SP4 B) into large-scale molds.

Fig. 8. Masonry wall assembled from industrially produced lightweight blocks for long-term monitoring of thermal and hygric properties.

4.5.2. Comparison with AAC blocks

A scenario analysis was carried out to compare the environmental impacts of the developed lightweight blocks (4/6 SP4 B) with impacts of commercially produced AAC blocks (commercial name Sysmic Idro,[1] manufactured by Gasbeton, Italy; ρ_b = 580 kg/m^3), having similar structural and thermal insulation properties (Gasbeton, 2021) and the same intended use. These AAC blocks were also selected because according to the data in the Environdec database (Environdec, 2021), the environmental impacts were assessed according to the same standard.

The results of the scenario analysis are provided in Table 11. In most categories, the developed lightweight block reached better results than the AAC block, except for the Climate change, which is by the biggest share impacted by the production of needed PC. However, the available LCA calculations for both masonry blocks were limited only to the cradle-to-gate scope, including only the A1–A3 phases and omitting the end-of-life phase. Furthermore, the developed blocks were heavier (ρ_b = 580 kg/m^3) and therefore 1 m^3 contained significantly higher amount of material and presumably exhibited higher strength (the manufacturer of AAC blocks declares a compressive strength of 5 MPa). Despite these facts, the difference in the impact on the Climate change category is rather marginal. Moreover, the end-of-life stage of RCF utilized for the production of the developed lightweight blocks presents a large environmental burden, which is mitigated by the utilization of RCF. It can be assumed that the recyclability and service life of both materials are very similar (Zou et al., 2022), but this hypothesis will be scrutinized in future studies.

[1] https://environdec.com/library/epd3048.

5. Conclusion

This study provides compelling evidence on the need to reuse concrete structural elements to increase sustainability and circularity in the construction sector. The disintegration of concrete elements, the transport of materials and the use of the disintegrated material to partially replace portland cement (PC) and aggregates in the production of new products unequivocally contribute to the circularity and protection of natural resources, but the energy demands and carbon footprint associated with these processes are still significant.

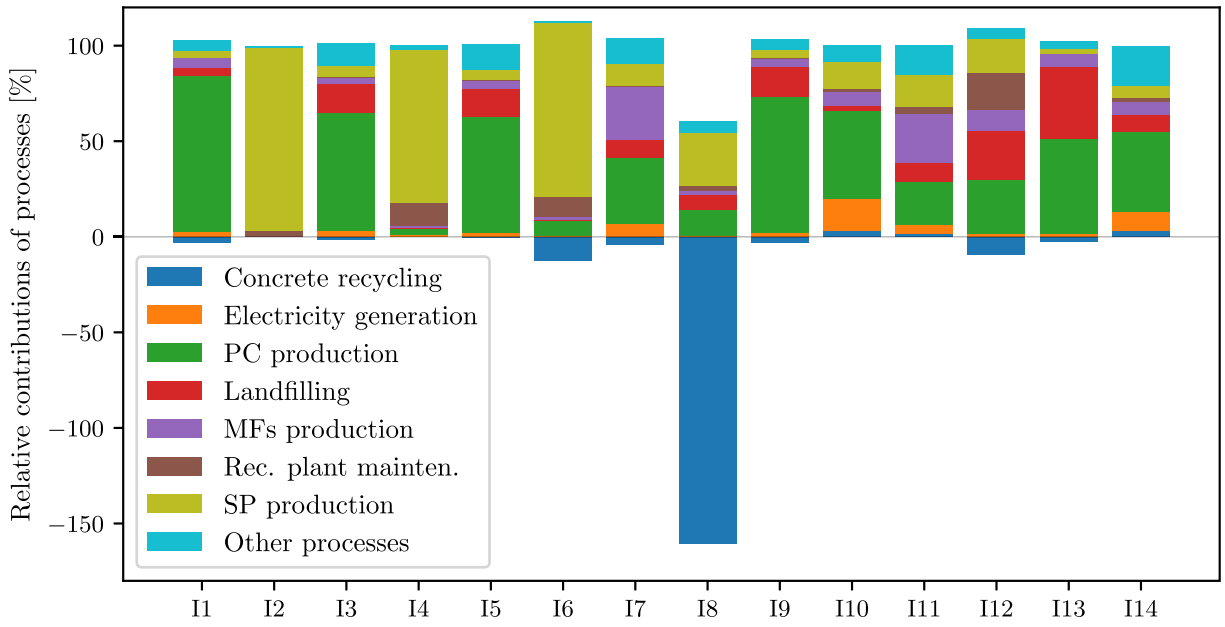

Fig. 9. Graphical representation of results provided in Table 9 to show relative contributions [%] of crucial processes to selected indicators: I1 = Climate change, total; I2 = Ozone depletion; I3 = Acidification; I4 = Eutrophication, freshwater; I5 = Photochem. ozone formation, h. health; I6 = Resource use, mineral and metals; I7 = Resource use, fossils; I8 = Water use; I9 = Particulate matter; I10 = Ionizing radiation, h. health; I11 = Ecotoxicity, freshwater; I12 = Human toxicity, cancer, I13 = Human toxicity, non-cancer, I14 = Land use.

Table 11
Comparison between the environmental performance (environmental impact indicators) of the developed lightweight blocks (4/6 SP4 B) containing RCF and commercially produced AAC blocks (results for critical impact parameters, related to 1 m^3); limited to phases A1–A3.

	4/6 SP4 B	AAC
Climate change, total [kg CO_2 eq.]	249	232
Ozone depletion [kg CFC-11 eq.]	1.43×10^{-6}	1.90×10^{-3}
Acidification [Mole of H^+ eq.]	0.44	0.63
Eutrophication, freshwater [kg P eq.]	2.92×10^{-3}	2.35×10^{-2}
Eutrophication, marine [kg N eq.]	0.11	0.36
Eutrophication, terrestrial [Mole of N eq.]	1.23	2.45
Photochemical ozone formation, human health [kg NMVOC eq.]	0.35	1.03
Resource use, mineral and metals [kg Sb eq.]	1.83×10^{-4}	2.69×10^{-3}
Resource use, fossils [MJ]	1430	1790
Water use [m^3 world equiv.]	−17.6	14.0

In this study, the finest fraction of the discarded concrete was micronized and used as a supplementary material to replace PC in the production of lightweight masonry blocks. This fraction typically contains aggregate fragments and hardened cement paste and represents a huge environmental burden. The experimental agenda was aimed on thorough testing and optimization of mixtures to yield a product that is competitive with commercially produced lightweight blocks made of aerated autoclaved concrete (AAC). The optimized mixture selected for large-scale industrial production was based on the mixture of PC and recycled concrete fines (RCF) in a 2:3 wt% ratio, respectively. Higher ratio of RCF resulted in a paste/matrix that exhibited inferior strength. The workability of the fresh mortar was adjusted using a superplasticizer (SP), and the aerated structure was formed using a foaming agent added to the fresh mortar during the mixing process. The porous structure was reinforced with recycled polypropylene microfibers, needed to ensure sufficient strength. The blocks made of the optimized mixture exhibited low heat conductivity, $\lambda = 0.21 \pm 0.02$ W/mK, and a compressive strength $f_c = 7.1 \pm 0.5$ MPa. Eventually, the industrial large-scale production of the developed blocks was tested in a concrete production plant, which included all the preparation procedures for mixing and placement, proving feasibility of the proposed mixture for practical applications. Hardened blocks were used to build an external masonry wall, which is currently under long-term monitoring of its behavior.

The detailed knowledge of all the processes needed for the production of lightweight blocks containing a large amount of RCF allowed for a precise life-cycle assessment (LCA) and comparison with the environmental performance of common AAC blocks. The LCA results suggest that replacing PC with RCF leads to considerable savings in raw material production, thus significantly reducing CO_2 production, resource use, eutrophication, energy demands, waste disposal, and toxicity and radioactivity. The PC replacement ratio was found to be critical for savings in these categories; however, the amount of RCF in the mixture is limited by structural performance requirements on load-bearing masonry, and replacing more than 60 wt.% of PC with RCF could unacceptably compromise the integrity of the cementitious matrix. Due to this limitation, the use of RCF to produce blocks cannot be considered a 100% environmentally friendly solution, and the reuse of whole structural elements must be promoted to avoid the tolls associated with concrete recycling. In situations where the disposal of structural elements and concrete recycling is inevitable, the production of lightweight blocks according to the procedures outlined in this paper appears to be a feasible solution. However, alternative approaches to

the use of SPs to increase the workability of fresh mortar should be sought to minimize ozone depletion and freshwater eutrophication.

It should be noted that the developed blocks share disadvantages with other cementitious highly-porous materials, e.g., relatively high water intake that negatively impacts the resistance to freeze-thaw degradation or poor resistance to concentrated force loads

CRediT authorship contribution statement

V. Nežerka: Collected the data, Contributed data or analysis tools, Performed the analysis, Wrote the paper. **Z. Prošek:** Conceived and designed the analysis, Collected the data, Contributed data or analysis tools, Performed the analysis. **J. Trejbal:** Collected the data, Contributed data or analysis tools, Performed the analysis. **J. Pešta:** Contributed data or analysis tools, Performed the analysis. **J.A. Ferriz-Papi:** Contributed data or analysis tools. **P. Tesárek:** Conceived and designed the analysis, Contributed data or analysis tools, Performed the analysis.

Declaration of competing interest

The authors declare that they have no known competing financial interests or personal relationships that could have appeared to influence the work reported in this paper.

Data availability

Data will be made available on request.

Funding

This work was supported by the Czech Science Foundation, grant number 22-02702S (V. Nežerka and Z. Prošek) and by the Technology Agency of the Czech Republic, grant number S03010302 (J. Pešta and P. Tesárek).

References

Akhtar, A., Sarmah, A.K., 2018. Construction and demolition waste generation and properties of recycled aggregate concrete: A global perspective. J. Clean. Prod. 186, 262–281. http://dx.doi.org/10.1016/j.jclepro.2018.03.085.

Allwood, J.M., Ashby, M.F., Gutowski, T.G., Worrell, E., 2011. Material efficiency: A white paper. Resour. Conserv. Recy. 55, 362–381. http://dx.doi.org/10.1016/j.resconrec.2010.11.002.

2006. ASTM E1876-01: Test method for dynamic Youngs modulus, shear modulus, and Poissons ratio by impulse excitation of vibration.

2014. ASTM C215-14. Test method for fundamental transverse, longitudinal, and torsional resonant frequencies of concrete specimens.

ASTM C114, 2018. Standard test methods for chemical analysis of hydraulic cement. In: Annual Book of ASTM Standards. ASTM International, West Conshohocken, PA.

Barbudo, A., de Brito, J., Evangelista, L., Bravo, M., Agrela, F., 2013. Influence of water-reducing admixtures on the mechanical performance of recycled concrete. J. Clean. Prod. 59, 93–98. http://dx.doi.org/10.1016/j.jclepro.2013.06.022.

Bordy, A., Younsi, A., Aggoun, S., Fiorio, B., 2017. Cement substitution by a recycled cement paste fine: Role of the residual anhydrous clinker. Constr. Build. Mater. 132, 1–8. http://dx.doi.org/10.1016/j.conbuildmat.2016.11.080.

Bravo, M., de Brito, J., Evangelista, L., Pacheco, J., 2018. Durability and shrinkage of concrete with CDW as recycled aggregates: Benefits from superplasticizer's incorporation and influence of CDW composition. Constr. Build. Mater. 168, 818–830. http://dx.doi.org/10.1016/j.conbuildmat.2018.02.176.

Brožovský, J., Dufka, Á., 2015. Comparison of dynamic Young's modulus of elasticity values measured by ultrasonic pulse and resonance methods. Adv. Mater. Res. 1100, 193–196. http://dx.doi.org/10.4028/www.scientific.net/amr.1100.193.

Carazeanu, I., 2002. Investigation of the hydration process in 3CaO·Al2O3-CaSO4·2H2O-plasticizer-H2O systems by X-ray diffraction. Talanta 57, 617–623. http://dx.doi.org/10.1016/s0039-9140(02)00100-5.

CEN, 2020. EN 15804:2012+A2:2019: Sustainability of Construction Works—Environmental Product Declarations—Core Rules for the Product Category of Construction Products. CEN, Brussels (Belgium), accessed November 27, 2020.

CEN, 2021. EN 772-1:2011+A1:2015 - Methods of Test for Masonry Units - Part 1: Determination of Compressive Strength. CEN, Brussels (Belgium), accessed November 19, 2021.

Colangelo, F., Forcina, A., Farina, I., Petrillo, A., 2018. Life cycle assessment (LCA) of different kinds of concrete containing waste for sustainable construction. Buildings 8, 70. http://dx.doi.org/10.3390/buildings8050070.

COM, E., 2011. Roadmap to a resource efficient Europe. Communication from the Commission to European Parliament, the Council, the European Social and Economic Committee and the Committee of the Regions. European Commission, Brussels.

COM, E., 2014. 398 final "Towards a Circular Economy: A Zero Waste Programme for Europe", Vol. 2. Brussels.

Commission, E., et al., 2015. Closing the loop—An EU action plan for the circular economy. COM/2015/0614 Final.

da Silva, S.R., de Oliveira Andrade, J.J., 2017. Investigation of mechanical properties and carbonation of concretes with construction and demolition waste and fly ash. Constr. Build. Mater. 153, 704–715. http://dx.doi.org/10.1016/j.conbuildmat.2017.07.143.

Ding, T., Xiao, J., Qin, F., Duan, Z., 2020. Mechanical behavior of 3D printed mortar with recycled sand at early ages. Constr. Build. Mater. 248, 118654. http://dx.doi.org/10.1016/j.conbuildmat.2020.118654.

Ding, T., Xiao, J., Tam, V.W., 2016. A closed-loop life cycle assessment of recycled aggregate concrete utilization in China. Waste Manage. 56, 367–375. http://dx.doi.org/10.1016/j.wasman.2016.05.031.

2009. BS EN 12390-3:2009: Testing Hardened Concrete Part 3: Compressive Strength of Test Specimens. British Standards Institution, London, http://dx.doi.org/10.3403/02508604u.

Environdec, 2021. The international EPD system. https://www.environdec.com/home, accessed October 30, 2021.

Esa, M.R., Halog, A., Rigamonti, L., 2016. Developing strategies for managing construction and demolition wastes in Malaysia based on the concept of circular economy. J. Mater. Cycles Waste Manage. 19 (3), 1144–1154. http://dx.doi.org/10.1007/s10163-016-0516-x.

European Committee for Standardization, 2011. EN 197-1:2011: Cement. Composition, Specifications and Conformity Criteria for Common Cements. BSI.

European Committee for Standardization, 2013. EN 196-2:2013: Method of Testing Cement. Chemical Analysis of Cement. BSI.

European Standard EN 12350-5, 2009. Testing fresh concrete; flow table test.

Evangelista, L., de Brito, J., 2013. Concrete with fine recycled aggregates: a review. Eur. J. Environ. Civ. Eng. 18, 129–172. http://dx.doi.org/10.1080/19648189.2013.851038.

Finkbeiner, M., Inaba, A., Tan, R., Christiansen, K., Klüppel, H.-J., 2006. The new international standards for life cycle assessment: ISO 14040 and ISO 14044. Int. J. Life Cycle Assess. 11, 80–85. http://dx.doi.org/10.1065/lca2006.02.002.

Florea, M., Ning, Z., Brouwers, H., 2014. Activation of liberated concrete fines and their application in mortars. Constr. Build. Mater. 50, 1–12. http://dx.doi.org/10.1016/j.conbuildmat.2013.09.012.

Gabi Software, 2020. Life cycle assessment LCA software. http://www.gabisoftware.com/, accessed October 30, 2020.

Ganesan, S., Mydin, M.A.O., Yunos, M.Y.M., Nawi, M.N.M., 2015. Thermal properties of foamed concrete with various densities and additives at ambient temperature. Appl. Mech. Mater. 747, 230–233. http://dx.doi.org/10.4028/www.scientific.net/amm.747.230.

Gao, X., Yu, Q., Brouwers, H., 2015. Reaction kinetics, gel character and strength of ambient temperature cured alkali activated slag–fly ash blends. Constr. Build. Mater. 80, 105–115. http://dx.doi.org/10.1016/j.conbuildmat.2015.01.065.

Gasbeton, 2021. Environmental product declaration. https://portal.environdec.com/api/api/v1/EPDLibrary/Files/d52c0010-ab02-4fd3-02f3-08d8f01e26c9/Data, accessed October 30, 2021.

Gastaldi, D., Canonico, F., Capelli, L., Buzzi, L., Boccaleri, E., Irico, S., 2015. An investigation on the recycling of hydrated cement from concrete demolition waste. Cem. Concr. Compos. 61, 29–35. http://dx.doi.org/10.1016/j.cemconcomp.2015.04.010.

Gholampour, A., Ozbakkaloglu, T., 2017. Performance of sustainable concretes containing very high volume class-f fly ash and ground granulated blast furnace slag. J. Clean. Prod. 162, 1407–1417. http://dx.doi.org/10.1016/j.jclepro.2017.06.087.

González, M.D., Caballero, P.P., Fernández, D.B., Vidal, M.M.J., del Bosque, I.F.S., Martínez, C.M., 2021. The design and development of recycled concretes in a circular economy using mixed construction and demolition waste. Materials 14, 4762. http://dx.doi.org/10.3390/ma14164762.

Grabois, T.M., Cordeiro, G.C., Filho, R.D.T., 2017. The influence of recycled concrete and clay brick particles on the strength and porosity of cement-based pastes. In: RILEM Bookseries. pp. 189–194. http://dx.doi.org/10.1007/978-94-024-1207-9_30.

Han, F., Pu, S., Zhou, Y., Zhang, H., Zhang, Z., 2022. Effect of ultrafine mineral admixtures on the rheological properties of fresh cement paste: A review. J. Build. Eng. 51, 104313. http://dx.doi.org/10.1016/j.jobe.2022.104313.

Hossain, M.U., Poon, C.S., Lo, I.M., Cheng, J.C., 2017. Comparative LCA on using waste materials in the cement industry: A Hong Kong case study. Resour. Conserv. Recy. 120, 199–208. http://dx.doi.org/10.1016/j.resconrec.2016.12.012.

Huysman, S., Schaepmeester, J.D., Ragaert, K., Dewulf, J., Meester, S.D., 2017. Performance indicators for a circular economy: A case study on post-industrial plastic waste. Resour. Conserv. Recy. 120, 46–54. http://dx.doi.org/10.1016/j.resconrec.2017.01.013.

Karihaloo, B., Carpinteri, A., Elices, M., 1993. Fracture mechanics of cement mortar and plain concrete. Adv. Cem. Based Mater. 1, 92–105. http://dx.doi.org/10.1016/1065-7355(93)90014-f.
Khatib, J., 2005. Properties of concrete incorporating fine recycled aggregate. Cem. Concr. Res. 35, 763–769. http://dx.doi.org/10.1016/j.cemconres.2004.06.017.
Kleijer, A., Lasvaux, S., Citherlet, S., Viviani, M., 2017. Product-specific life cycle assessment of ready mix concrete: Comparison between a recycled and an ordinary concrete. Resour. Conserv. Recy. 122, 210–218. http://dx.doi.org/10.1016/j.resconrec.2017.02.004.
Knoeri, C., Sanyé-Mengual, E., Althaus, H.-J., 2013. Comparative LCA of recycled and conventional concrete for structural applications. Int. J. Life Cycle Assess. 18, 909–918. http://dx.doi.org/10.1007/s11367-012-0544-2.
Krausmann, F., Gingrich, S., Eisenmenger, N., Erb, K.-H., Haberl, H., Fischer-Kowalski, M., 2009. Growth in global materials use, GDP and population during the 20th century. Ecol. Econom. 68, 2696–2705. http://dx.doi.org/10.1016/j.ecolecon.2009.05.007.
Kupfer, T., Colodel, C.M., Kokborg, M., Schöll, S., Rudolf, M., Thellier, L., Bos, U., Bosch, F., Gonzalez, M., Schuller, O., Hengstler, J., Stoffregen, A., Thylmann, D., 2020. GaBi Database and Modelling Principles. GaBi.
Lee, H., Hanif, A., Usman, M., Sim, J., Oh, H., 2018. Performance evaluation of concrete incorporating glass powder and glass sludge wastes as supplementary cementing material. J. Clean. Prod. 170, 683–693. http://dx.doi.org/10.1016/j.jclepro.2017.09.133.
Liu, Q., Tong, T., Liu, S., Yang, D., Yu, Q., 2014. Investigation of using hybrid recycled powder from demolished concrete solids and clay bricks as a pozzolanic supplement for cement. Constr. Build. Mater. 73, 754–763. http://dx.doi.org/10.1016/j.conbuildmat.2014.09.066.
López-Uceda, A., Ayuso, J., López, M., Jimenez, J., Agrela, F., Sierra, M., 2016. Properties of non-structural concrete made with mixed recycled aggregates and low cement content. Materials 9, 74. http://dx.doi.org/10.3390/ma9020074.
Lotfi, S., Rem, P., 2017. Recycling of end of life concrete fines (0–4 mm) from waste to valuable resources. In: High Tech Concrete: Where Technology and Engineering Meet. Springer International Publishing, pp. 224–232. http://dx.doi.org/10.1007/978-3-319-59471-2_28.
Ma, X., Wang, Z., 2013. Effect of ground waste concrete powder on cement properties. Adv. Mater. Sci. Eng. 2013, 1–5. http://dx.doi.org/10.1155/2013/918294.
Mangla, S.K., Govindan, K., Luthra, S., 2017. Prioritizing the barriers to achieve sustainable consumption and production trends in supply chains using fuzzy analytical hierarchy process. J. Clean. Prod. 151, 509–525. http://dx.doi.org/10.1016/j.jclepro.2017.02.099.
Marinković, S., Dragaš, J., Ignjatović, I., Tošić, N., 2017. Environmental assessment of green concretes for structural use. J. Clean. Prod. 154, 633–649. http://dx.doi.org/10.1016/j.jclepro.2017.04.015.
Marsh, A.T., Velenturf, A.P., Bernal, S.A., 2022. Circular economy strategies for concrete: implementation and integration. J. Clean. Prod. 362, 132486. http://dx.doi.org/10.1016/j.jclepro.2022.132486.
Martínez, I., Etxeberria, M., Pavón, E., Díaz, N., 2018. Influence of demolition waste fine particles on the properties of recycled aggregate masonry mortar. Int. J. Civ. Eng. 16 (9), 1213–1226. http://dx.doi.org/10.1007/s40999-017-0280-x.
Mittal, V.K., Sangwan, K.S., 2014a. Prioritizing barriers to green manufacturing: Environmental, social and economic perspectives. Proc. CIRP 17, 559–564. http://dx.doi.org/10.1016/j.procir.2014.01.075.
Mittal, V.K., Sangwan, K.S., 2014b. Fuzzy TOPSIS method for ranking barriers to environmentally conscious manufacturing implementation: government, industry and expert perspectives. Int. J. Environ. Technol. Manage. 17, 57. http://dx.doi.org/10.1504/ijetm.2014.059466.
Namsone, E., Šahmenko, G., Korjakins, A., 2017. Durability properties of high performance foamed concrete. Procedia Eng. 172, 760–767. http://dx.doi.org/10.1016/j.proeng.2017.02.120.
Nežerka, V., Bílý, P., Hrbek, V., Fládr, J., 2019. Impact of silica fume, fly ash, and metakaolin on the thickness and strength of the ITZ in concrete. Cem. Concr. Compos. 103, 252–262. http://dx.doi.org/10.1016/j.cemconcomp.2019.05.012.
Nežerka, V., Havlásek, P., Trejbal, J., 2020. Mitigating inclusion-induced shrinkage cracking in cementitious composites by incorporating recycled concrete fines. Constr. Build. Mater. 248, 118673. http://dx.doi.org/10.1016/j.conbuildmat.2020.118673.
Nežerka, V., Slížková, Z., Tesárek, P., Plachý, T., Frankeová, D., Petráňová, V., 2014. Comprehensive study on microstructure and mechanical properties of lime-pozzolan pastes. Cem. Concr. Res. 64, 17–29. http://dx.doi.org/10.1016/j.cemconres.2014.06.006.
Nežerka, V., Zeman, J., Němeček, J., 2017. Micromechanics-based simulations of compressive and tensile testing on lime-based mortars. Mech. Mater. 105, 49–60. http://dx.doi.org/10.1016/j.mechmat.2016.11.011.
Niewiadomski, P., Karolak, A., Stefaniuk, D., Królicka, A., Szymanowski, J., Sadowski, Ł., 2021. Cement paste mixture proportioning with particle packing theory: An ambiguous effect of microsilica. Materials 14, 6970. http://dx.doi.org/10.3390/ma14226970.
Özalp, F., Yılmaz, H.D., Kara, M., Kaya, Ö., Şahin, A., 2016. Effects of recycled aggregates from construction and demolition wastes on mechanical and permeability properties of paving stone, kerb and concrete pipes. Constr. Build. Mater. 110, 17–23. http://dx.doi.org/10.1016/j.conbuildmat.2016.01.030.
Pacheco-Torgal, F., 2020. Introduction to advances in construction and demolition waste. In: Advances in Construction and Demolition Waste Recycling. Elsevier, pp. 1–10. http://dx.doi.org/10.1016/b978-0-12-819055-5.00001-2.
Paris, J.M., Roessler, J.G., Ferraro, C.C., DeFord, H.D., Townsend, T.G., 2016. A review of waste products utilized as supplements to Portland cement in concrete. J. Clean. Prod. 121, 1–18. http://dx.doi.org/10.1016/j.jclepro.2016.02.013.
Pešta, J., Pavlů, T., Fořtová, K., Kočí, V., 2020. Sustainable masonry made from recycled aggregates: LCA case study. Sustainability 12, 1581. http://dx.doi.org/10.3390/su12041581.
Prošek, Z., Nežerka, V., Hlůžek, R., Trejbal, J., Tesárek, P., Karra'a, G., 2019. Role of lime, fly ash, and slag in cement pastes containing recycled concrete fines. Constr. Build. Mater. 201, 702–714. http://dx.doi.org/10.1016/j.conbuildmat.2018.12.227.
Prošek, Z., Nežerka, V., Tesárek, P., 2020a. Enhancing cementitious pastes with waste marble sludge. Constr. Build. Mater. 255, 119372. http://dx.doi.org/10.1016/j.conbuildmat.2020.119372.
Prošek, Z., Trejbal, J., Nežerka, V., Goliáš, V., Faltus, M., Tesárek, P., 2020b. Recovery of residual anhydrous clinker in finely ground recycled concrete. Resour. Conserv. Recy. 155, 104640. http://dx.doi.org/10.1016/j.resconrec.2019.104640.
Quan, H., Kasami, H., 2018. Experimental study on the effects of recycled concrete powder on properties of self-compacting concrete. Open Civ. Eng. J. 12, 430–440. http://dx.doi.org/10.2174/1874149501812010430.
Raj, B., Sathyan, D., Madhavan, M.K., Raj, A., 2020. Mechanical and durability properties of hybrid fiber reinforced foam concrete. Constr. Build. Mater. 245, 118373. http://dx.doi.org/10.1016/j.conbuildmat.2020.118373.
Raj, A., Sathyan, D., Mini, K., 2019. Physical and functional characteristics of foam concrete: A review. Constr. Build. Mater. 221, 787–799. http://dx.doi.org/10.1016/j.conbuildmat.2019.06.052.
Rhee, I., Lee, J.S., Roh, Y.-S., 2019. Fracture parameters of cement mortar with different structural dimensions under the direct tension test. Materials 12, 1850. http://dx.doi.org/10.3390/ma12111850.
Scrivener, K.L., John, V.M., Gartner, E.M., 2018. Eco-efficient cements: Potential economically viable solutions for a low-CO2 cement-based materials industry. Cem. Concr. Res. 114, 2–26. http://dx.doi.org/10.1016/j.cemconres.2018.03.015.
Serpell, R., Lopez, M., 2013. Reactivated cementitious materials from hydrated cement paste wastes. Cem. Concr. Compos. 39, 104–114. http://dx.doi.org/10.1016/j.cemconcomp.2013.03.020.
Shojaei, M., Behfarnia, K., Mohebi, R., 2015. Application of alkali-activated slag concrete in railway sleepers. Mater. Des. 69, 89–95. http://dx.doi.org/10.1016/j.matdes.2014.12.051.
Shui, Z., Xuan, D., Wan, H., Cao, B., 2008. Rehydration reactivity of recycled mortar from concrete waste experienced to thermal treatment. Constr. Build. Mater. 22, 1723–1729. http://dx.doi.org/10.1016/j.conbuildmat.2007.05.012.
Sousa, V., Bogas, J.A., 2021. Comparison of energy consumption and carbon emissions from clinker and recycled cement production. J. Clean. Prod. 306, 127277. http://dx.doi.org/10.1016/j.jclepro.2021.127277.
Sousa, V., Bogas, J.A., Real, S., Meireles, I., 2022. Industrial production of recycled cement: energy consumption and carbon dioxide emission estimation. Environ. Sci. Pollut. Res. 255, 119372. http://dx.doi.org/10.1007/s11356-022-20887-7.
Steshenko, A., Kudyakov, A., Konusheva, V., Syrkin, O., 2017. Structure formation control of foam concrete. AIP Conf. Proc. 1800, 020001. http://dx.doi.org/10.1063/1.4973017.
Strange, P.C., Bryant, A.H., 1979. The role of aggregate in the fracture of concrete. J. Mater. Sci. 14, 1863–1868. http://dx.doi.org/10.1007/bf00551025.
Topič, J., Fládr, J., Prošek, Z., 2017. Flexural and compressive strength of the cement paste with recycled concrete powder. Adv. Mater. Res. 1144, 65–69. http://dx.doi.org/10.4028/www.scientific.net/amr.1144.65.
Topič, J., Prošek, Z., Fládr, J., Tesárek, P., 2018. Vliv jemnosti recyklované betonové moučky na vývin hydratačního tepla a vliv jejího množství na mechanicko-fyzikální vlastnosti cementové pasty. In: Waste Forum, Vol. 2. pp. 268–274.
Turk, J., Cotič, Z., Mladenovič, A., Šajna, A., 2015. Environmental evaluation of green concretes versus conventional concrete by means of LCA. Waste Manage. 45, 194–205. http://dx.doi.org/10.1016/j.wasman.2015.06.035.
Turner, L.K., Collins, F.G., 2013. Carbon dioxide equivalent (CO2-e) emissions: A comparison between geopolymer and OPC cement concrete. Constr. Build. Mater. 43, 125–130. http://dx.doi.org/10.1016/j.conbuildmat.2013.01.023.
US Geological Survey & Orienteering S and US Geological Survey, 2009. Mineral Commodity Summaries, 2009. Government Printing Office.
Van Damme, H., 2018. Concrete material science: Past, present, and future innovations. Cem. Concr. Res. 112, 5–24. http://dx.doi.org/10.1016/j.cemconres.2018.05.002.
Vieira, D.R., Calmon, J.L., Coelho, F.Z., 2016. Life cycle assessment (LCA) applied to the manufacturing of common and ecological concrete: A review. Constr. Build. Mater. 124, 656–666. http://dx.doi.org/10.1016/j.conbuildmat.2016.07.125.
Villagrán-Zaccardi, Y.A., Marsh, A.T., Sosa, M.E., Zega, C.J., De Belie, N., Bernal, S.A., 2022. Complete re-utilization of waste concretes–Valorisation pathways and research needs. Resour. Conserv. Recy. 177, 105955. http://dx.doi.org/10.1016/j.resconrec.2021.105955.
Wang, L., Wang, J., Wang, H., Fang, Y., Shen, W., Chen, P., Xu, Y., 2022. Eco-friendly treatment of recycled concrete fines as supplementary cementitious materials. Constr. Build. Mater. 322, 126491. http://dx.doi.org/10.1016/j.conbuildmat.2022.126491.
Xiao, J., 2018. Recycled Aggregate Concrete Structures. Springer Berlin Heidelberg, http://dx.doi.org/10.1007/978-3-662-53987-3.

Zou, D., Que, Z., Cui, W., Wang, X., Guo, Y., Zhang, S., 2022. Feasibility of recycling autoclaved aerated concrete waste for partial sand replacement in mortar. J. Build. Eng. 52, 104481. http://dx.doi.org/10.1016/j.jobe.2022.104481.

Zou, S., Xiao, J., Ding, T., Duan, Z., Zhang, Q., 2021. Printability and advantages of 3D printing mortar with 100% recycled sand. Constr. Build. Mater. 273, 121699. http://dx.doi.org/10.1016/j.conbuildmat.2020.121699.

Appendix F

Prošek, Z.; Nežerka, V.; Plachý, T.; Bartoš, M.; Tesárek, P.: PVA increases efficiency of bacterially-induced self-healing in cement mortars, *Cement and Concrete Composites* 131 (2022) 104593, doi: 10.1016/j.cemconcomp.2022.104593

Author's contribution: SEM microscopy, data analysis, design of experiments, preparation of specimens.

Cement and Concrete Composites 131 (2022) 104593

Contents lists available at ScienceDirect

Cement and Concrete Composites

journal homepage: www.elsevier.com/locate/cemconcomp

PVA increases efficiency of bacterially-induced self-healing in cement mortars

Z. Prošek [a], V. Nežerka [b,*], T. Plachý [b], M. Bartoš [c,d], P. Tesárek [b]

[a] University Centre for Energy Efficient Buildings, Czech Technical University in Prague, Třinecká 1024, 273 43, Buštěhrad, Czech Republic
[b] Faculty of Civil Engineering, Czech Technical University in Prague, Thákurova 7, 166 29, Praha 6, Czech Republic
[c] Institute of Dental Medicine, First Faculty of Medicine, Charles University and General University Hospital in Prague, Kateřinská 1660/32, 121 08, Praha 2, Czech Republic
[d] Institute of Anatomy, First Faculty of Medicine, Charles University, Kateřinská 1660/32, 121 08, Praha 2, Czech Republic

ARTICLE INFO

Keywords:
Self-healing
Crack
Mortar
Bacteria
PVA

ABSTRACT

Different strains of bacteria capable of calcite precipitation can be incorporated into fresh concrete or cement mortars to efficiently promote self-healing of microcracks after hardening. To date, all bacterial strains investigated have required protection against the highly alkaline environments and high pressures in cementitious matrices. The core objective of this study was to eliminate the inconveniences related to protecting (typically encapsulating) bacteria. Poly(vinyl alcohol) (PVA) doped with spores of *Bacillus pseudofirmus* and nutrients were added to mixing water when cementitious mortars were prepared. The hardened mortar specimens were cracked and studied using microscopy, resonance measurements, X-ray microtomography (μ-CT), and destructive mechanical tests to assess the rate and efficiency of the healing processes. PVA was efficient in promoting remediation in all mortar specimens, both with and without bacteria. Specimens containing PVA plus bacteria showed the most efficient self-repair processes, while autogenous remediation in reference samples lacking PVA or bacteria were least efficient in healing microcracks.

1. Introduction

The formation of microcracks in concrete is inevitable [1], and even though these cracks do not affect structural performance, frequent repairs or application of protective coatings are often required to prevent harmful chemical substances from penetrating cracks. Such substances can cause corrosion of reinforcements and deterioration of cementitious matrices [2], even if these matrices can repair themselves due to activation of unhydrated clinker and precipitation of calcite [3–7]. In most cases, these autogenous remediation processes are not sufficient to fill microcracks, and researchers have long been searching for agents that could enhance autonomous self-healing [8–10]. The use of microorganisms capable of calcium carbonate ($CaCO_3$) precipitation appears to be the most efficient method for promoting self-repair [11–14]. The incorporation of such bacteria into concrete is cheap and does not contribute by any additional environmental burden to already environmentally harmful concrete production processes [15–18].

Bacterially induced calcite precipitation (BICP) was first proposed by Gollapudi et al. [19] and successfully exploited for self-healing of concrete a decade later [20,21], and the topic has attracted widespread interest in the past years. Ersan et al. [22] reported that cracks up to 500 μm wide were almost completely sealed with $CaCO_3$ due to the activity of ureolytic bacteria, while bacteria from the *Bacillus* genus were successfully used by Wang et al. [23] for sealing cracks up to 970 μm wide. Levels of BICP efficiency are not only dependent on the strain of bacteria employed, but are also affected by external factors such as temperature, the concentration of nutrients available to bacteria, the concentration of carbon dioxide and free calcium ions and pH in a matrix, and a density of nucleation sites [12,24].

Despite the large body of research into BICP for healing microcracks in concrete using different strains of bacteria, e.g. Refs. [25–32], fundamental questions regarding the proliferation of bacteria in the hostile environment of fresh concrete mixes remain. Wiktor and Jonkers [33] considered the viability of bacteria and successfully protected spores of *Bacillus alkalinitrilicus* from the highly alkaline environment and high pressures in a cementitious matrix with expanded clay particles. This approach prevented the crushing of the bacterial spores and supported $CaCO_3$ precipitation, but the presence of expanded clay

* Corresponding author.
E-mail address: vaclav.nezerka@fsv.cvut.cz (V. Nežerka).

https://doi.org/10.1016/j.cemconcomp.2022.104593
Received 8 October 2021; Received in revised form 29 April 2022; Accepted 12 May 2022
Available online 18 May 2022

particles resulted in a 50% reduction of compressive strength [34]. Different approaches to encapsulating bacteria were adopted in follow-up studies; e.g., Wang et al. [35] immobilized spores of an ureolytic *Bacillus sphaericus* strain in beads of a hydrogel, Alazhari et al. [36] impregnated coated expanded perlite with spores of *Bacillus pseudofirmus*, and Wang et al. [37] encapsulated *Bacillus sphaericus* in 5 μm melamine-formaldehyde microcapsules using a poly-condensation process.

The core objective of this study was to eliminate encapsulation processes from the preparation of bio-based agents for use in concrete self-healing. Here, *Bacillus pseudofirmus* was selected for its ability to proliferate in a highly alkaline environment (a cementitious matrix) and remain dormant for decades [38]. The bacteria is capable of calcium carbonate precipitation through degradation of organic compounds at the presence of O_2 and Ca^{2+} [32,39,40]. Unlike ureolytic processes, this metabolic pathway does not lead to the production of ammonia and nitric acid [21], and therefore does not impose any additional risk of reinforcement corrosion or concrete matrix degradation. A simple encapsulation was accomplished by adding poly(vinyl alcohol) (PVA) doped with bacteria and nutrients to mixing water while cementitious mortars were prepared. Previous studies have shown that this cheap and non-toxic polymer is suitable for bacteria immobilization [41–43], but it can also be exploited as an agent with positive effects on portland cement hydration [44–46] or as a suitable material for fiber reinforcement to cementitious composites when stabilized [47–51]. The use of PVA for encapsulation/immobilization of bacteria in self-healing concrete is a novel approach and has not yet been reported in any recent study [52–55]. Here, the contribution of PVA on the activity of a self-healing agent (SHA) was placed under scrutiny; the healing processes were monitored using microscopy, μ-CT, resonance measurements, and eventually flexural tensile strength was measured destructively.

2. Materials and methods

2.1. Microbial self-healing agent preparation

The bio-chemical SHA used in this study consisted of *Bacillus pseudofirmus* spores from the Leibniz Institute's DSMZ–German Collection of Microorganisms and Cell Cultures GmbH (DSM No. 2516) and a mixture of nutrients: 1 g/l of a lamb/beef extract, 2 g/l of a yeast extract, 5 g/l of peptone, and 10 g/l of NaCl.

The cultivation inoculum consisted of bacterial spores at a concentration of 10^2 colony forming units (CFU) per ml and the cultivation took place at 30 °C for 48 h. The bacteria were sedimented in a centrifuge (4 min at 8000 rpm) and washed using a sterile saline solution. Using these bacteria, a precipitation medium having a 3×10^6 CFU/ml concentration was prepared.

An alkali carbonate buffer (0.42 g/l of $NaHCO_3$ and 0.53 g/l of Na_2CO_3) was added to the medium in a 1:100 volumetric concentration to adjust pH to 10. A 2% solution of $CaCl_2$ was then added in a 1:50 volumetric concentration to increase Ca ions in order to promote bacterially-induced calcification.

2.2. Preparation of mortar specimens

Four different sets of mortars (Table 1) were produced, each represented by six 40 × 40 × 160 mm specimens. Ordinary portland cement (hereafter PC) CEM I/42.5R (EN 197–1:2001 [56]) and siliceous pit sand (0–4 mm) were mixed for preparation of all mixtures in a 3:7 mass ratio. The chemical composition of PC can be found in the previous studies on concrete recycling [57]. The reference mixture (Ref.) contained neither SHA nor PVA solution. The second mixture (SHA) was enriched with SHA (15 ml of the solution) mixed into 10% of the mixing water. The same approach was adopted for the mixture containing both the SHA and PVA (SHA + PVA), except in this case, a portion of water was mixed with a 16 wt% aqueous PVA solution (commercial name Fichema Sloviol R, molecular weight of PVA 50 mg/mol) before adding the SHA agent. To more closely examine the effects of the SHA and PVA, a control set of specimens (PVA) containing the PVA solution but with no SHA was also produced. It is important to note that the 10% of mixing water containing PVA must be added to fresh mortar already containing the remaining 90% of pure mixing water; reversing this approach would lead to high porosity and excessive coating of clinker grains with PVA [39]. The mortar samples were cast into molds and demolded after 24 h.

Table 1
Composition of the mortar mixtures studied (mass of ingredients [g] per a single batch).

Mixture	PC	Sand 0–4 mm	Water	16% PVA solution (PVA/water)	SHA
Ref.	480	1120	268.8	–	–
SHA	480	1120	268.8	–	15
PVA	480	1120	243.6	30 (4.8/25.2)	–
SHA + PVA	480	1120	243.6	30 (4.8/25.2)	15

Hardening took place for 28 days in a 20 °C water bath, at which point the specimens were carefully broken during three-point bending using displacement-controlled loading at a rate of 0.1 mm/min until reaching a crack opening $\delta = 0.5$ mm, measured approximately 5 mm from the crack mouth (Fig. 1). Releasing elastic deformation during unloading led to a partial closure of cracks on average to 0.23, 0.19, 0.23, and 0.22 mm for the Ref., SHA, PVA, SHA + PVA specimens, respectively. Crack formation and openings were monitored in real-time using subpixel image registration [58,59]. All specimens were reinforced with steel wires (diameter 1.4 mm) to avoid a loss of stability and complete rupture. After fracturing, the specimens were left to heal in a water bath at 18–22 °C for 180 days. The specimens were put on their side (parallel to the crack orientation) to avoid crack closing/opening due to gravity.

2.3. BOD measurements

A reference sample of the self-healing agent (bacteria, nutrition, and PVA) was placed on a Petri dish and the viability of bacteria (or rather their metabolic activity) was studied after the dissolution of PVA using biochemical oxygen demand (BOD) measurements. The BOD values represent milligrams of oxygen consumed per liter of a sample during a 5 day period of incubation at 20 °C. The calibration was accomplished at 25 °C using a reference bacterial strain. The measured samples consisted of 100 ml fresh media and 2 ml of the bacterial inoculates.

2.4. Microscopy

Optical microscopy was used to observe the cracks just after their formation and assess the healing process after 36, 90, and 180 days using a ZEISS Axio Zoom V16 Stereo Zoom microscope. The high-resolution camera provided a resolution of 1 μm at the selected 32 × magnification level with a 16 μm depth of field. Scanning electron microscopy (SEM) was used to perform microstructural and elemental analyses after 180 days of healing using an FEG Merlin ZEISS scanning electron microscope equipped with a Schottky cathode (10 kV accelerating voltage, 1 nA current, 8.5 mm working table distance, 50 μs single point measurement time, and a resolution of 1024 px). Secondary electron (SE) detector allowed to observe the topology of observed surfaces and the detector of back-scattered electrons (BSE) was used to determine distributions of phases in the samples, based on atomic numbers of their elements.

X-ray microanalysis was performed using an X-ray energy-dispersive spectrometer (EDS) from Oxford Instruments to determine the weights and atomic percentages of chemical elements, both pointwise and in 2D fields. Phases were identified from the elemental compositions using

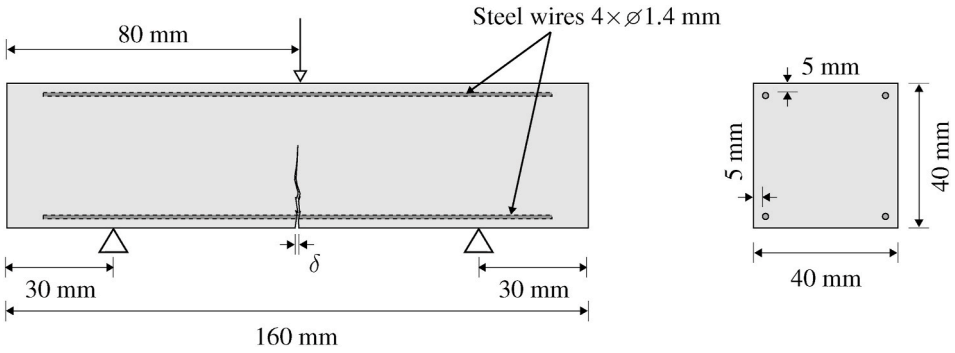

Fig. 1. Scheme for mortar specimens reinforced with steel wires and loading during three-point bending.

stoichiometry. The X-ray spectrum for the EDS analysis was recorded for 120 s.

The samples used for SEM analysis were extracted from 40 × 40 × 160 mm specimens dedicated for microscopy using a Struers Secotom 50 precision cutting machine. In order to avoid disintegration of $CaCO_3$ and its removal during sample preparation, the samples were impregnated with epoxy resin. Each set was represented by a 15 × 15 × 15 mm sample, vacuum impregnated with Struers EpoFix epoxy resin and polished using SiC abrasive foils (500–2000 grain/cm^2 grits) and water-based nanodiamond (3 μm and 1 μm) suspension. The specimens were then coated in argon atmosphere with a 3 nm platinum layer to increase the conductivity necessary for EDS analysis. Such a coating was also applied to samples of spores covered with PVA for investigation using SEM that were placed on sample stubs without any further preparation. SEM images of $CaCO_3$ crystals observed using the detector of secondary electrons were taken after platinum coating from the surface of specimens where the bacteria were also active. These samples were neither cut nor polished.

2.5. Resonance measurements

Impact resonant frequency testing according to the ASTM C215 Standard [60] has been successfully used for evaluation of autogenous remediation in concrete [61,62]. This method is based on the measurement of fundamental resonant frequencies in isotropic homogeneous specimens.

In this study, longitudinal natural frequencies were measured for three 40 × 40 × 160 mm specimens representing each mixture before and after cracking (0, 32, 90, and 180 days) using the Brüel & Kjaer 3560-B-120 device. The dynamic Young's modulus, E_{dyn} [Pa], was determined from frequency response functions according to the formulas presented in the ASTM E1876-01 Standard [63,64]:

$$E_{dyn} = \frac{4Lmf_1^2}{bt}, \tag{1}$$

where L is the length of the specimen [m], m is the mass of the specimen [kg], f_1 is the fundamental longitudinal resonant frequency of the specimen [Hz], b is the width of the specimen [m], and t is the thickness of the specimen [m].

2.6. μ-CT

Previous studies indicated that μ-CT can be used for precise segmentation of phases in mortars or concrete [65,66] based on the degree to which X-rays pass through a sample. The output 3D matrices representing the distribution of density within a volume are displayed as gray-scale voxels, allowing to display internal mesoscopic cracks [67].

In our study, 4 × 4 × 4 mm samples were extracted from SHA + PVA specimens in the vicinity of cracks after 180 days of healing. These cubic samples were scanned using SkyScan 1272 (Bruker micro-CT, Kontich, Belgium), using the following parameters: pixel size 2 μm, voltage 80 kV, current 125 μA, Al filter 1 mm, rotation step 0.1°, and rotation 180°. Scanning took about 6 h. Flat-field correction was updated before each acquisition. Image data were reconstructed, processed and visualized using NRecon, DataViewer, CTVox and CTAn software (Bruker micro-CT).

2.7. Three-point bending tests

Flexural tensile strength calculated from the results of the three-point bending tests was used as an indicator of mechanical strength recovery after 180 days of crack healing. Three specimens for each mixture were loaded by displacement-controlled three-point bending (Fig. 1) at a constant rate of 0.1 mm/s using a LabTest 4.100SP1 device to both create the crack for healing (recall Section 2.2) and to test the strength of crack bridging after 180 days of healing. Bending strength was calculated as the maximum force (F_{max}) reached before a drop in the force-displacement diagram due to cracking as

$$f_b = \frac{3F_{max}L}{2a^3}, \tag{2}$$

where L = 100 mm is the span between supports and a = 40 mm is the width and height of the cross-section.

3. Results and discussion

3.1. Optical microscopy

Fig. 2 presents the healing processes for all the mortar specimens. The dashed lines represent the point 7 mm from the crack mouth, where crack-width development was measured during the healing process (Fig. 3). At this point, the crack width exceeded 50 μm, being critical for autogenous remediation of cementitious materials [61], even after initial reduction due to rheology and shape memory effects [68]. At the crack mouth, the crack widths were influenced by disintegration and spalling of the surface layer. Even though calcite formation was not detected in the measured cross-section after 32 days for any specimen, the crack widths were reduced from the initial 120–200 μm by about 40% for specimens Ref., SHA, and PVA and by 65% for specimen SHA + PVA. Calcite precipitation was detected after 32 days of healing at the crack tip only for specimens SHA, PVA, and SHA + PVA.

Healing near the crack mouth was first detected after 90 days in the SHA + PVA specimens, validating the idea that the combination of SHA and PVA can be efficient in promoting self-healing. However, autogenous remediation was also observed after 90 days, attributed to the activity of clinker rich in C_3S, as indicated by the reduction of crack width in the Ref. and SHA specimens. Wiktor and Jonkers [33] also reported the self-healing capability of mortars lacking SHA, limited to a maximum of 0.18 mm/100 days. After 180 days of healing, the cracks were sealed completely in the SHA + PVA specimens. SHA specimens

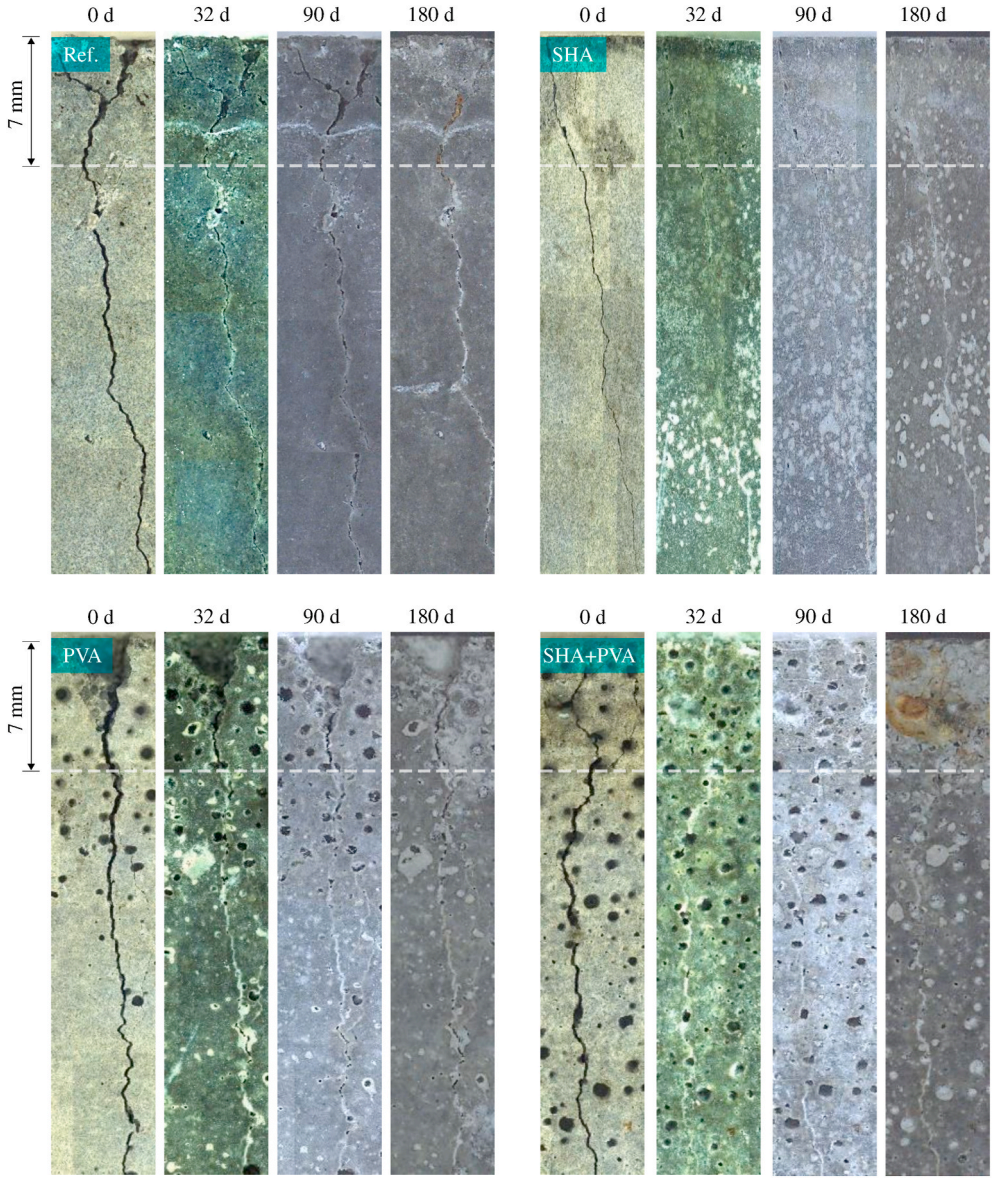

Fig. 2. Optical microscopy images of the cracks in the studied specimens after 0, 32, 90, and 180 days of remediation; the dashed lines indicate a point at which the crack openings were measured.

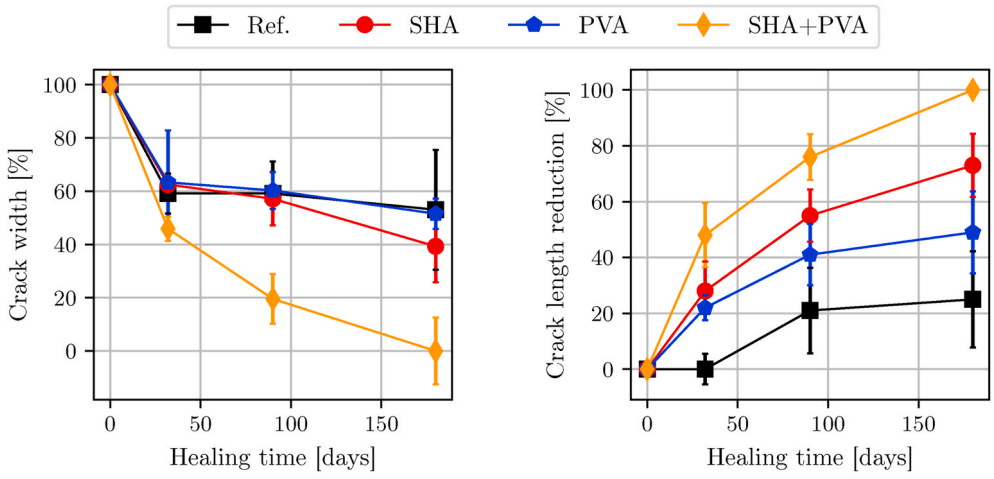

Fig. 3. Rate of crack healing measured using optical microscopy; each mixture was represented by three specimens.

exhibited a lower rate of remediation. However, the presence of PVA without SHA can by itself also contribute to autogenous remediation, as demonstrated by 49% healing of the crack in the PVA specimen, in contrast to 25% healing of the crack in the Ref. specimens.

The impact of adding PVA water solution to fresh mortar on cement hydration was described by Pique and Vazques [69]. They also observed large voids compromising the compressive strength of hardened mortars and reported retarded hydration due to the reduced water accessibility for cement particles. This finding concurs with findings of Knapen and Gemand [70] and could provide an explanation for the remediation capability of control specimens containing PVA but no SHA. The micro-reservoirs of residual clinker can react with CO_2 dissolved in water to form hydration products that fill cracks [57,71,72]. The presence of 0.2–1.4 mm pores, typical for cement pastes containing PVA [64], was confirmed by microscopy images for PVA and SHA + PVA samples, presented in Fig. 2.

The study by Topič et al. [64] also provided the study on the impact of PVA on the setting of cement pastes, measured using a Vicat apparatus, and the rate of hydration, monitored using an isothermal TAM Air calorimeter. Both these tests confirmed the retardation effects of PVA, as conjectured in this study.

3.2. Viability of encapsulated bacteria

The vacuum needed for SEM instantly kills the bacteria, making it impossible to study their viability after encapsulation. However, BOD measurements clearly indicate that the reference bacteria colony after dissolution of PVA started to grow, following an almost identical curve as the uncoated spores (Fig. 4).

3.3. SEM analysis

The *Bacillus pseudofirmus* spores coated with PVA were detected after covering with a 3 nm platinum layer using SEM-SE (Fig. 5). The length of spores, on average, was approximately 1.5 μm. By adhering to the surface of spores, PVA forms microcapsules that protect the spores against the high hydration pressures and alkaline environment of a cementitious matrix. These PVA capsules dissolve in the water that penetrates cracks and the bacteria become active.

Detailed information about the microstructure and crack bridging with precipitated $CaCO_3$ were obtained using SEM-BSE microscopy; Fig. 6 presents images of microstructure with markers indicating individual phases. For each phase, the atomic weights and percentages were calculated based on BSE-EDS measurements. The silicious aggregates consisted mostly of oxygen (65.2%) and silicon (43.6%). The composition of the cementitious matrix was rather complex since it contained unhydrated clinker, hydrosilicates, hydroaluminates, portlandite, and

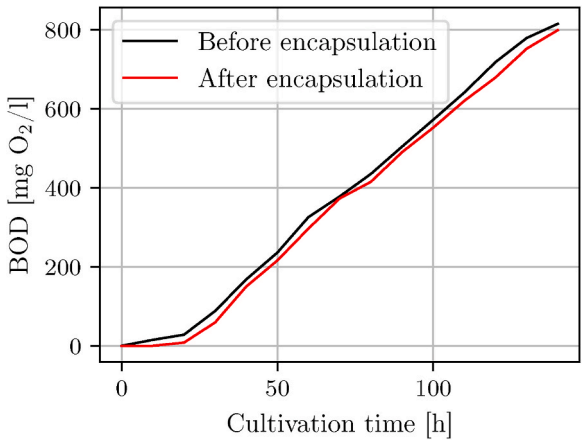

Fig. 4. Oxygen demand of bacteria before and after encapsulation using PVA.

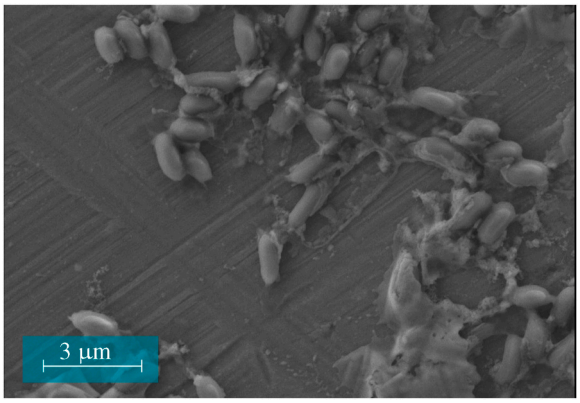

Fig. 5. SEM image of *Bacillus pseudofirmus* spores coated with PVA at 17.2k × magnification, observed using the detector of secondary electrons.

ettringite; therefore, different concentrations of oxygen, silicon, calcium, carbon, and aluminum were identified. The material filling cracks consisted of oxygen (41.1%), calcium (30.2%), and carbon (12.2%), indicating the presence of $CaCO_3$ (Fig. 7).

The structure of precipitated $CaCO_3$ crystals due to the activity of SHA was studied for unpolished samples of A and B after 90 days of self-healing using SEM-SE microscopy at 3k × magnification (Fig. 8). The BSE microscopy images demonstrate the differences in the sizes of $CaCO_3$ crystals when formed spontaneously during autogenous remediation of a cementitious matrix and when *Bacillus pseudofirmus* was present. The autogenous crystalization of Ca, which can be largely attributed to the dissolution of portlandite [73], resulted in larger crystals, while bacterially-induced $CaCO_3$ precipitation yielded closely packed smaller crystals.

3.4. μ-CT

μ-CT scanning revealed almost complete filling of the crack in a sample of SHA + PVA (Fig. 9). The regions corresponding to the precipitated $CaCO_3$ had a lower density than the surrounding matrix. Larger voids such as pores with diameters larger than 1 mm were not filled completely. These findings concur with microscopy analyses. Motivated by the study of Wang et al. [74] we believed that μ-CT could be used for quantification of healing products, but the differentiation using thresholding was not possible, preventing us from quantification of self-healing rate and newly formed products. In this regard, microscopy images served the purpose and enabled much more detailed analysis.

3.5. Recovery of elastic stiffness

Testing of the dynamic Young's modulus was carried out in order to prove that cracks can be sealed by self-healing in a sufficient way to allow the propagation of elastic waves, indicated with stiffness recovery (or increase due to ongoing hydration). The wave propagation has been regarded as a reliable indicator of damage in concrete/mortar specimens [75] and was used for quantification of self-healing e.g. by Xu and Yao [9].

The presence of voids in mortars containing PVA resulted in lower stiffness levels, both before cracking and after 180 days of healing (Fig. 10). The reduction in stiffness for cement pastes containing PVA (2.8 wt%) was also reported by Topič et al. [64], who reported about 50% and 15% lower values for the static and dynamic Young's moduli, respectively. The Young's moduli of mortars consistently exceeded the 28-day stiffness of uncracked specimens after 180 days of healing due to additional hydration of clinker minerals [76] and sealing of cracks. In this regard, the propagation of elastic waves across the healed cracks

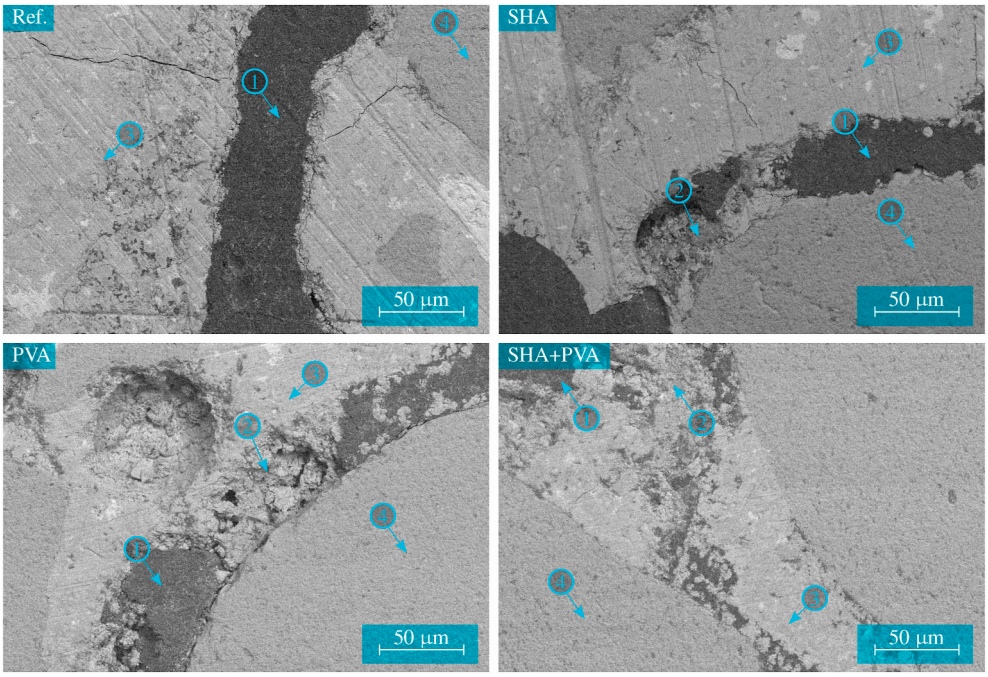

Fig. 6. BSE images of cracks after 180 days of healing at the point 7 mm from the crack mouth; the numbered phases represent (1) the crack, (2) $CaCO_3$, (3) cementitious matrix, and (4) aggregates.

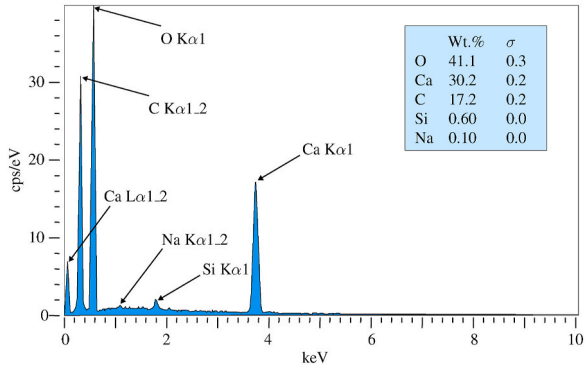

Fig. 7. EDS spectrum of the crack-filling phase identified as $CaCO_3$ (measured for a sample of SHA + PVA).

was not affected by the quality of the $CaCO_3$ bridging. The lowest increase was exhibited by the SHA mortar (16.3%), followed by PVA (29.4%), SHA + PVA (39.8%), and Ref. (44.4%). It is very unlikely that the presence of bacteria in mortars without PVA could negatively impact hydration; a random distribution of non-homogeneities within the mortar more likely played a role in these samples. These findings indicate that strength recovery should be used as a more exact indicator of crack bridging quality.

3.6. Strength recovery

Bending strength recovery (Fig. 11) is indisputably the most direct indicator of the degree of remediation and provides an appropriate complement to microscopy observations. The specimens containing both SHA and PVA reached identical strengths after 180 days of healing compared to their virgin states after 28 days of hardening. SHA specimens exhibited 8% lower strength levels after crack healing, similar to specimens containing only PVA. Autogenous healing in the reference specimens (Ref.) led to the lowest level of crack bridging observed in this

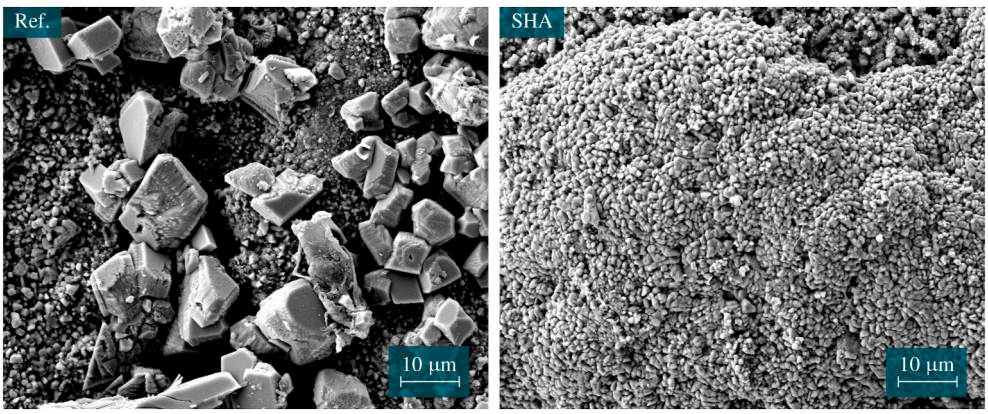

Fig. 8. SEM images of $CaCO_3$ crystals at 3k × magnification, observed using the detector of secondary electrons after 90 days of self-healing; the autogenous remediation of the Ref. sample resulted in the formation of larger $CaCO_3$ crystals when compared to the SHA-promoted calcification.

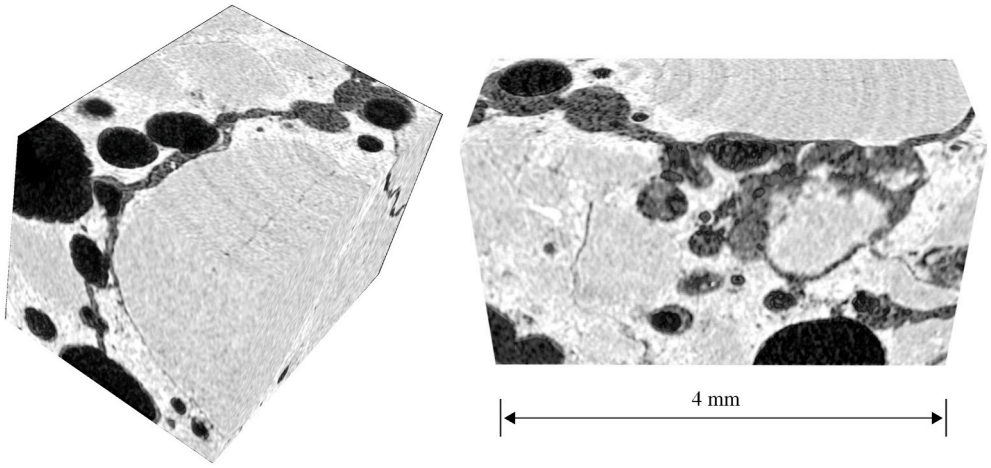

Fig. 9. Sections of the μ-CT scan showing cemented cracks and pores partially filled with $CaCO_3$, SHA + PVA.

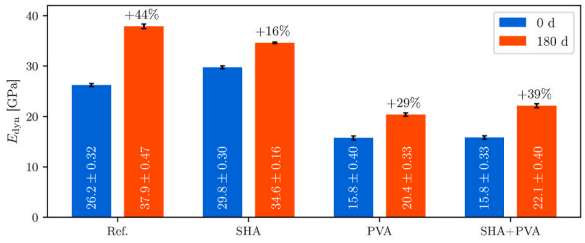

Fig. 10. Dynamic Young's modulus of mortars before cracking and after remediation for 180 days.

study, resulting in a 30% loss of bending strength.

Unlike findings from Knapen and Gemert [70], Morlat et al. [77] and Singh et al. [44], virgin-state bending strengths observed here were not positively affected by the presence of PVA; the difference between bending strengths at day 0 was rather negligible for all specimens. Abd-Emoaty [78] reported that autogenous healing is not negatively impacted by the dispersion of organic polymers in a cementitious matrix. In this study, the presence of PVA contributed to the rehydration and formation of $CaCO_3$ within the cracked volume, which promoted autogenous healing.

The protection of spores by PVA might be crucial not only during mixing and preparation of mortar/concrete, but also in later stages of hardening. Jonkers et al. [21] found that BICP is limited to early-stage hardening and after 28 days the functionality of unprotected bacteria decreases due to change in pore-size distribution and lack of pores capable of accommodating bacterial spores. Unlike protective carriers based on light-weight aggregates (LWA) having high porosity [30,33], bacteria encapsulated using PVA can be more homogeneously distributed in the mortar matrix and occupy also the weak interfacial transition zones in the vicinity of aggregates. The use of fine-grained carriers such as diatomaceous earth (DA) [25] appears more suitable than LWA in these regards, but the cost of DA is high compared to other constituents of common cement-based concretes and mortars. The use of polyurethane (PU) as a protective carrier of bacteria and nutrients in the study by Wang et al. [79] also resulted in high recovery rates of flexural strength, but the healing was rather attributed to PU, since there was no difference between the effects of living and dead bacteria. According to the same study, using bacteria encapsulated silica gel appeared to have negligible effects on healing of cracks and flexural strength recovery.

4. Conclusion

This study investigated how cementitious mortars containing SHA, PVA, and both combined performed in healing microcracks, in terms of rate and efficiency and in comparison to a reference sample. The combination of SHA and PVA was used to investigate if the replacing tedious and technically complicated encapsulation of bacteria capable of $CaCO_3$ production for sealing cracks could be avoided, with PVA providing protection for *Bacillus pseudofirmus* spores and their nutrients. Crack healing took place in a water bed and the process was monitored for 180 days.

During this period, mortars containing both SHA and PVA exhibited complete healing, as observed in microscopy images and strength recovery measurements. Dynamic Young's modulus measurements using the resonance method also indicated a recovery, however, the results of

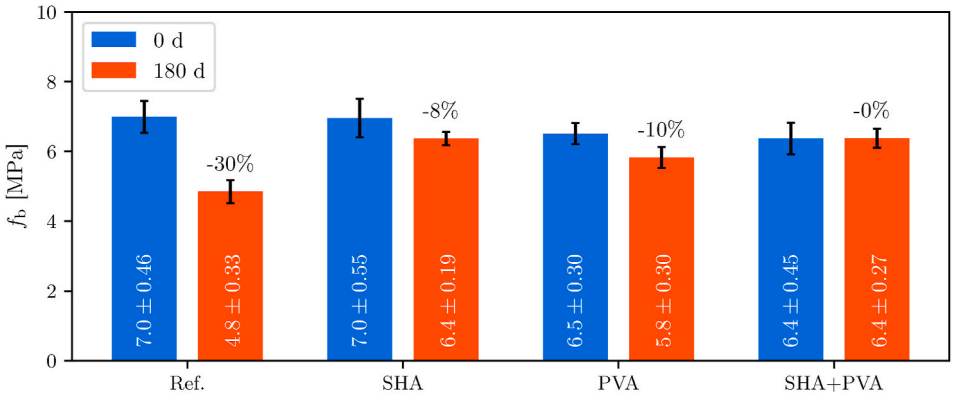

Fig. 11. Bending strength of mortars before cracking and after 180 days of remediation.

these measurements did not correlate with other methods due to the prevailing effects of continuous hydration in the volume of cement pastes.

The healing of mortars containing SHA without PVA was slower than in specimens containing both components (SHA + PVA). Microscopy images indicated that the remediation efficiency in specimens with SHA and with no PVA was about 50% lower and that bending strength recovery reached 8% lower levels, compared to SHA + PVA. It can be assumed that PVA promotes the reliability and repeatability of future self-healing processes, since spores and nutrients are protected with PVA coating, but this hypothesis will be validated in future studies.

Mortars containing PVA without SHA also exhibited a superior self-healing capacity when compared to reference specimens. PVA, besides the protection of bacteria, likely contributes to the retardation of hydration, benefiting the rehydration that takes place during autogenous healing processes. The strength recovery of mortars containing PVA only was almost identical to those containing SHA without PVA, but microscopy images taken in this study revealed that the latter (SHA without PVA) was more efficient in sealing the cracks with $CaCO_3$. The reference mortars without SHA and PVA exhibited 30% lower strength recovery than mortars containing both SHA and PVA and the rate of $CaCO_3$ precipitation was significantly lower compared to other specimens, despite providing optimum conditions for autogenous remediation.

Funding

This work was supported by the Czech Science Foundation [grant GA ČR 18-15697S].

Declaration of competing interest

The authors declare that they have no known competing financial interests or personal relationships that could have appeared to influence the work reported in this paper.

Acknowledgment

The help of Dr. Stephanie Krueger, who provided editorial assistance, is gratefully acknowledged. The authors would also like to thank the Joint Laboratory of Polymer Nanofiber Technologies of the Institute of Physics, Academy of Science of the Czech Republic, and the Faculty of Civil Engineering, CTU in Prague.

References

[1] A.M. Neville, in: Properties of Concrete, fourth ed., Longman, 1996.
[2] F.P. Glasser, J. Marchand, E. Samson, Durability of concrete — degradation phenomena involving detrimental chemical reactions, Cement Concr. Res. 38 (2008) 226–246, https://doi.org/10.1016/j.cemconres.2007.09.015.
[3] C.-M. Aldea, W.-J. Song, J.S. Popovics, S.P. Shah, Extent of healing of cracked normal strength concrete, J. Mater. Civ. Eng. 12 (2000) 92–96, https://doi.org/10.1061/(asce)0899-1561(2000)12:1(92).
[4] H.-W. Reinhardt, M. Jooss, Permeability and self-healing of cracked concrete as a function of temperature and crack width, Cement Concr. Res. 33 (2003) 981–985, https://doi.org/10.1016/s0008-8846(02)01099-2.
[5] T.-H. Ahn, T. Kishi, Crack self-healing behavior of cementitious composites incorporating various mineral admixtures, J. Adv. Concr. Technol. 8 (2010) 171–186, https://doi.org/10.3151/jact.8.171.
[6] L.M. Mauludin, C. Oucif, Computational modeling of fracture in concrete: a review, Front. Struct. Civ. Eng. 14 (2020) 586–598, https://doi.org/10.1007/s11709-020-0573-z.
[7] L.M. Mauludin, C. Oucif, T. Rabczuk, The effects of mismatch fracture properties in encapsulation-based self-healing concrete using cohesive-zone model, Front. Struct. Civ. Eng. 14 (2020) 792–801, https://doi.org/10.1007/s11709-020-0629-0.
[8] S. van der Zwaag, An introduction to material design principles: damage prevention versus damage management, in: Springer Series in Materials Science, Springer Netherlands, 2007, pp. 1–18, https://doi.org/10.1007/978-1-4020-6250-6_1.
[9] J. Xu, W. Yao, Multiscale mechanical quantification of self-healing concrete incorporating non-ureolytic bacteria-based healing agent, Cement Concr. Res. 64 (2014) 1–10, https://doi.org/10.1016/j.cemconres.2014.06.003.
[10] J. Chen, G. Ye, A lattice Boltzmann single component model for simulation of the autogenous self-healing caused by further hydration in cementitious material at mesoscale, Cement Concr. Res. 123 (2019), 105782, https://doi.org/10.1016/j.cemconres.2019.105782.
[11] S. Stocks-Fischer, J.K. Galinat, S.S. Bang, Microbiological precipitation of CaCO3, Soil Biol. Biochem. 31 (1999) 1563–1571, https://doi.org/10.1016/s0038-0717(99)00082-6.
[12] N. K. Dhami, M. S. Reddy, A. Mukherjee, Biomineralization of calcium carbonates and their engineered applications: a review, Front. Microbiol. 4. doi:10.3389/fmicb.2013.00314.
[13] H. Ehrlich, Geomicrobial processes: geomicrobial processes overview, in: Ehrlich's Geomicrobiology, sixth ed., CRC Press, 2015, pp. 129–155, https://doi.org/10.1201/b19121-8.
[14] S. Mondal, A.D. Ghosh, Review on microbial induced calcite precipitation mechanisms leading to bacterial selection for microbial concrete, Construct. Build. Mater. 225 (2019) 67–75, https://doi.org/10.1016/j.conbuildmat.2019.07.122.
[15] J.M. Paris, J.G. Roessler, C.C. Ferraro, H.D. DeFord, T.G. Townsend, A review of waste products utilized as supplements to portland cement in concrete, J. Clean. Prod. 121 (2016) 1–18, https://doi.org/10.1016/j.jclepro.2016.02.013.
[16] S.R. da Silva, J.J. de Oliveira Andrade, Investigation of mechanical properties and carbonation of concretes with construction and demolition waste and fly ash, Construct. Build. Mater. 153 (2017) 704–715, https://doi.org/10.1016/j.conbuildmat.2017.07.143.
[17] H. Lee, A. Hanif, M. Usman, J. Sim, H. Oh, Performance evaluation of concrete incorporating glass powder and glass sludge wastes as supplementary cementing material, J. Clean. Prod. 170 (2018) 683–693, https://doi.org/10.1016/j.jclepro.2017.09.133.
[18] V. Nežerka, V. Hrbek, Z. Prošek, M. Somr, P. Tesárek, J. Fládr, Micromechanical characterization and modeling of cement pastes containing waste marble powder, J. Clean. Prod. 195 (2018) 1081–1090, https://doi.org/10.1016/j.jclepro.2018.05.284.
[19] U. Gollapudi, C. Knutson, S. Bang, M. Islam, A new method for controlling leaching through permeable channels, Chemosphere 30 (1995) 695–705, https://doi.org/10.1016/0045-6535(94)00435-w.
[20] H.M. Jonkers, Self healing concrete: a biological approach, in: Springer Series in Materials Science, Springer Netherlands, 2007, pp. 195–204, https://doi.org/10.1007/978-1-4020-6250-6_9.
[21] H.M. Jonkers, A. Thijssen, G. Muyzer, O. Copuroglu, E. Schlangen, Application of bacteria as self-healing agent for the development of sustainable concrete, Ecol. Eng. 36 (2010) 230–235, https://doi.org/10.1016/j.ecoleng.2008.12.036.
[22] Y. Ersan, J. Wang, N. Boon, N. De Belie, Ureolysis and denitrification based microbial strategies for self-healing concrete, in: Concrete Solutions 2014, CRC Press, 2014, pp. 59–64, https://doi.org/10.1201/b17394-10.
[23] J. Wang, H. Soens, W. Verstraete, N. De Belie, Self-healing concrete by use of microencapsulated bacterial spores, Cement Concr. Res. 56 (2014) 139–152, https://doi.org/10.1016/j.cemconres.2013.11.009.
[24] D.K. Harris, J.M. Civitillo, A. Gheitasi, Performance and behavior of hybrid composite beam bridge in Virginia: live load testing, J. Bridge Eng. 21 (2016), 4016022, https://doi.org/10.1061/(asce)be.1943-5592.0000820.
[25] J.Y. Wang, N. De Belie, W. Verstraete, Diatomaceous earth as a protective vehicle for bacteria applied for self-healing concrete, J. Ind. Microbiol. Biotechnol. 39 (2011) 567–577, https://doi.org/10.1007/s10295-011-1037-1.
[26] R. Siddique, N.K. Chahal, Effect of ureolytic bacteria on concrete properties, Construct. Build. Mater. 25 (2011) 3791–3801, https://doi.org/10.1016/j.conbuildmat.2011.04.010.
[27] Y. Zhang, H. Guo, X. Cheng, Role of calcium sources in the strength and microstructure of microbial mortar, Construct. Build. Mater. 77 (2015) 160–167, https://doi.org/10.1016/j.conbuildmat.2014.12.040.
[28] Y. Ç. Erşan, E. Gruyaert, G. Louis, C. Lors, N. De Belie, N. Boon, Self-protected nitrate reducing culture for intrinsic repair of concrete cracks, Front. Microbiol. 6. doi:10.3389/fmicb.2015.01228.
[29] S. Bhaduri, N. Debnath, S. Mitra, Y. Liu, A. Kumar, Microbiologically induced calcite precipitation mediated by *Sporosarcina pasteurii*, JoVE 110 (2016), e53253, https://doi.org/10.3791/53253.
[30] H. Chen, C. Qian, H. Huang, Self-healing cementitious materials based on bacteria and nutrients immobilized respectively, Construct. Build. Mater. 126 (2016) 297–303, https://doi.org/10.1016/j.conbuildmat.2016.09.023.
[31] M. Luo, C. Qian, Influences of bacteria-based self-healing agents on cementitious materials hydration kinetics and compressive strength, Construct. Build. Mater. 121 (2016) 659–663, https://doi.org/10.1016/j.conbuildmat.2016.06.075.
[32] E. Tziviloglou, V. Wiktor, H. Jonkers, E. Schlangen, Bacteria-based self-healing concrete to increase liquid tightness of cracks, Construct. Build. Mater. 122 (2016) 118–125, https://doi.org/10.1016/j.conbuildmat.2016.06.080.
[33] V. Wiktor, H.M. Jonkers, Quantification of crack-healing in novel bacteria-based self-healing concrete, Cement Concr. Compos. 33 (2011) 763–770, https://doi.org/10.1016/j.cemconcomp.2011.03.012.
[34] K. Van Tittelboom, N. De Belie, Self-healing in cementitious materials—a review, Materials 6 (2013) 2182–2217, https://doi.org/10.3390/ma6062182.
[35] J. Wang, D. Snoeck, S. Van Vlierberghe, W. Verstraete, N. De Belie, Application of hydrogel encapsulated carbonate precipitating bacteria for approaching a realistic self-healing in concrete, Construct. Build. Mater. 68 (2014) 110–119, https://doi.org/10.1016/j.conbuildmat.2014.06.018.
[36] M. Alazhari, T. Sharma, A. Heath, R. Cooper, K. Paine, Application of expanded perlite encapsulated bacteria and growth media for self-healing concrete, Construct. Build. Mater. 160 (2018) 610–619, https://doi.org/10.1016/j.conbuildmat.2017.11.086.

[37] J. Wang, H. Soens, W. Verstraete, N. De Belie, Self-healing concrete by use of microencapsulated bacterial spores, Cement Concr. Res. 56 (2014) 139–152, https://doi.org/10.1016/j.cemconres.2013.11.009.
[38] J. Wang, Y.C. Ersan, N. Boon, N. De Belie, Application of microorganisms in concrete: a promising sustainable strategy to improve concrete durability, Appl. Microbiol. Biotechnol. 100 (2016) 2993–3007, https://doi.org/10.1007/s00253-016-7370-6.
[39] H. Schreiberová, T. Trtík, R. Chylík, Z. Prošek, K. Šeps, J. Fládr, P. Bílý, A. Kohoutková, Self-healing in cementitious composite containing bacteria and protective polymers at various temperatures, Magazine.Civ. Eng. 107 (2021) 10713, https://doi.org/10.34910/MCE.107.13.
[40] V. Nežerka, P. Demo, H. Schreiberová, P. Ryparová, P. Bílý, Self-healing concrete: application of monod's approach for modeling bacillus pseudofirmus growth curves, Eur.J.Environ.Civ.Eng (2022) 1–13, https://doi.org/10.1080/19648189.2021.2021996.
[41] O. Ariga, H. Toyofuku, I. Minegishi, T. Hattori, Y. Sano, M. Nagura, Efficient production of recombinant enzymes using PVA-encapsulated bacteria, J. Ferment. Bioeng. 84 (1997) 553–557, https://doi.org/10.1016/s0922-338x(97)81911-3.
[42] R. Cui, J. Li, K. Zhang, J. Han, Preparation of biomembrane by immobilizing enriched ammonia-oxidizing bacteria (AOB) in polyvinyl alcohol (PVA) for biosensor, in: 2011 International Conference on Remote Sensing, Environment and Transportation Engineering, IEEE, 2011, https://doi.org/10.1109/rsete.2011.5965483.
[43] D. V. Pham, L. T. Bach, Immobilized bacteria by using PVA (polyvinyl alcohol) crosslinked with sodium sulfate, Int. J. Sci. Eng. 7. doi:10.12777/ijse.7.1.41-47.
[44] N. Singh, S. Rai, Effect of polyvinyl alcohol on the hydration of cement with rice husk ash, Cement Concr. Res. 31 (2001) 239–243, https://doi.org/10.1016/s0008-8846(00)00475-0.
[45] A. Mansur, D. Santos, H. Mansur, A microstructural approach to adherence mechanism of poly(vinyl alcohol) modified cement systems to ceramic tiles, Cement Concr. Res. 37 (2007) 270–282, https://doi.org/10.1016/j.cemconres.2006.11.011.
[46] F. Liu, B. Wang, Y. Xing, K. Zhang, W. Jiang, Effect of polyvinyl alcohol on the rheological properties of cement mortar, Molecules 25 (2020) 754, https://doi.org/10.3390/molecules25030754.
[47] J.-P. Won, K.-S. Hwang, C.-G. Park, H.-G. Park, Evaluation of crack control and permeability of hydrophilic PVA fiber reinforced cement composite, J. Kor.Concr. Inst. 16 (2004) 391–396, https://doi.org/10.4334/jkci.2004.16.3.391.
[48] A. Passuello, G. Moriconi, S.P. Shah, Cracking behavior of concrete with shrinkage reducing admixtures and PVA fibers, Cement Concr. Compos. 31 (10) (2009) 699–704, https://doi.org/10.1016/j.cemconcomp.2009.08.004.
[49] S.F.U. Ahmed, H. Mihashi, Strain hardening behavior of lightweight hybrid polyvinyl alcohol (PVA) fiber reinforced cement composites, Mater. Struct. 44 (2010) 1179–1191, https://doi.org/10.1617/s11527-010-9691-8.
[50] A. Noushini, K. Vessalas, B. Samali, Static mechanical properties of polyvinyl alcohol fibre reinforced concrete (PVA-FRC), Mag. Concr. Res. 66 (2014) 465–483, https://doi.org/10.1680/macr.13.00320.
[51] G. Cibilakshmi, J. Jegan, A DOE approach to optimize the strength properties of concrete incorporated with different ratios of PVA fibre and nano-fe2o3, Adv. Compos. Lett. 29 (2020), 2633366X2091388, https://doi.org/10.1177/2633366x20913882.
[52] R. Roy, E. Rossi, J. Silfwerbrand, H. Jonkers, Encapsulation techniques and test methods of evaluating the bacteria-based self-healing efficiency of concrete: a literature review, Nord. Concr. Res. 62 (2020) 63–85, https://doi.org/10.2478/ncr-2020-0006.
[53] M. Rauf, W. Khaliq, R.A. Khushnood, I. Ahmed, Comparative performance of different bacteria immobilized in natural fibers for self-healing in concrete, Construct. Build. Mater. 258 (2020), 119578, https://doi.org/10.1016/j.conbuildmat.2020.119578.
[54] P.K. Jogi, T.V. Lakshmi, Self healing concrete based on different bacteria: a review, Mater. Today Proc. 43 (2021) 1246–1252, https://doi.org/10.1016/j.matpr.2020.08.765.
[55] X. Liu, Q. Li, B. Li, W. Chen, A high-efficiency self-healing cementitious material based on supramolecular hydrogels impregnated with phosphate and ammonium, Cement Concr. Res. 144 (2021), 106427, https://doi.org/10.1016/j.cemconres.2021.106427.
[56] European Committee for Standardization, EN 197-1:2011: Cement. Composition, Specifications and Conformity Criteria for Common Cements, BSI, 2011.
[57] Z. Prošek, J. Trejbal, V. Nežerka, V. Goliáš, M. Faltus, P. Tesárek, Recovery of residual anhydrous clinker in finely ground recycled concrete, Resour. Conserv. Recycl. 155 (2020), 104640, https://doi.org/10.1016/j.resconrec.2019.104640.
[58] J. Antoš, V. Nežerka, M. Somr, Real-time optical measurement of displacements using subpixel image registration, Exp. Tech. 43 (2019) 315–323, https://doi.org/10.1007/s40799-019-00315-1.
[59] R. Hlůžek, J. Trejbal, V. Nežerka, P. Demo, Z. Prošek, P. Tesárek, Improvement of bonding between synthetic fibers and a cementitious matrix using recycled concrete powder and plasma treatment: from a single fiber to FRC, Eur.J.Environ. Civ.Eng (2020) 1–18, https://doi.org/10.1080/19648189.2020.1824821.
[60] ASTM C215-14, Test Method for Fundamental Transverse, Longitudinal, and Torsional Resonant Frequencies of Concrete Specimens, 2014, https://doi.org/10.1520/c0215-02.
[61] V.C. Li, E.-H. Yang, Self healing in concrete materials, in: Springer Series in Materials Science, Springer Netherlands, 2007, pp. 161–193, https://doi.org/10.1007/978-1-4020-6250-6_8.
[62] A. El-Newihy, P. Azarsa, R. Gupta, A. Biparva, Effect of polypropylene fibers on self-healing and dynamic modulus of elasticity recovery of fiber reinforced concrete, Fibers 6 (2018) 9, https://doi.org/10.3390/fib6010009.
[63] ASTM E1876-01, Test Method for Dynamic Youngs Modulus, Shear Modulus, and Poissons Ratio by Impulse Excitation of Vibration, 2006, https://doi.org/10.1520/e1876-00.
[64] J. Topič, Z. Prošek, K. Indrová, T. Plachý, V. Nežerka, L. Kopecký, P. Tesárek, Effect of PVA modification on properties of cement composites, Acta Polytechnica 55 (2015) 64–75, https://doi.org/10.14311/ap.2015.55.0064.
[65] G. Lei, J. Han, F. Dang, Using x-ray CT scanning to study the failure mechanism of concrete under static and dynamic loadings, Adv. Mater. Sci. Eng. 2018 (2018) 1–9. doi:10.1155/2018/3019158.
[66] M. Khormani, V.R.K. Jaari, I. Aghayan, S.H. Ghaderi, A. Ahmadyfard, Compressive strength determination of concrete specimens using x-ray computed tomography and finite element method, Construct. Build. Mater. 256 (2020), 119427, https://doi.org/10.1016/j.conbuildmat.2020.119427.
[67] M. Lanzón, V. Cnudde, T. de Kock, J. Dewanckele, X-ray microtomography (μ-CT) to evaluate microstructure of mortars containing low density additions, Cement Concr. Compos. 34 (2012) 993–1000, https://doi.org/10.1016/j.cemconcomp.2012.06.011.
[68] M.K. Kim, D.J. Kim, Y.-S. Chung, E. Choi, Effects of a short heat treatment period on the pullout resistance of shape memory alloy fibers in mortar, Materials 12 (2019) 2278, https://doi.org/10.3390/ma12142278.
[69] T.M. Pique, A. Vazquez, Control of hydration rate of polymer modified cements by the addition of organically modified montmorillonites, Cement Concr. Compos. 37 (2013) 54–60, https://doi.org/10.1016/j.cemconcomp.2012.12.006.
[70] E. Knapen, D. Van Gemert, Cement hydration and microstructure formation in the presence of water-soluble polymers, Cement Concr. Res. 39 (2009) 6–13, https://doi.org/10.1016/j.cemconres.2008.10.003.
[71] C. Edvardsen, Water permeability and autogenous healing of cracks in concrete, ACI Mater. J. 96 (1999) 448–454, https://doi.org/10.14359/645.
[72] M. Lidmila, P. Tesárek, T. Plachy, Z. Rácová, P. Padevět, V. Nežerka, O. Zobal, Utilization of recycled fine-ground concrete from railway sleepers for production of cement-based binder, Appl. Mech. Mater. 486 (2013) 323–326. https://doi.org/10.4028/www.scientific.net/amm.486.323.
[73] E. Ruiz-Agudo, K. Kudłacz, C.V. Putnis, A. Putnis, C. Rodriguez-Navarro, Dissolution and carbonation of portlandite [ca(OH)2] single crystals, Environ. Sci. Technol. 47 (2013) 11342–11349, https://doi.org/10.1021/es402061c.
[74] J. Wang, J. Dewanckele, V. Cnudde, S. Van Vlierberghe, W. Verstraete, N. De Belie, X-ray computed tomography proof of bacterial-based self-healing in concrete, Cement Concr. Compos. 53 (2014) 289–304, https://doi.org/10.1016/j.cemconcomp.2014.07.014.
[75] W. Zhong, W. Yao, Influence of damage degree on self-healing of concrete, Construct. Build. Mater. 22 (2008) 1137–1142, https://doi.org/10.1016/j.conbuildmat.2007.02.006.
[76] O. Linderoth, L. Wadsö, D. Jansen, Long-term cement hydration studies with isothermal calorimetry, Cement Concr. Res. 141 (2021), 106344, https://doi.org/10.1016/j.cemconres.2020.106344.
[77] R. Morlat, G. Orange, Y. Bomal, P. Godard, Reinforcement of hydrated portland cement with high molecular mass water-soluble polymers, J. Mater. Sci. 42 (2007) 4858–4869, https://doi.org/10.1007/s10853-006-0645-z.
[78] M.A. Elmoaty, Self-healing of polymer modified concrete, Alex. Eng. J. 50 (2011) 171–178, https://doi.org/10.1016/j.aej.2011.03.002.
[79] J. Wang, K. Van Tittelboom, N. De Belie, W. Verstraete, Use of silica gel or polyurethane immobilized bacteria for self-healing concrete, Construct. Build. Mater. 26 (2012) 532–540, https://doi.org/10.1016/j.conbuildmat.2011.06.054.

Appendix G

R. Hlůžek, J. Trejbal, V. Nežerka , P. Demo, **Z. Prošek**, P. Tesárek: Improvement of bonding between synthetic fibers and a cementitious matrix using recycled concrete powder and plasma treatment: from a single fiber to FRC, *European Journal of Environmental and Civil Engineering* (2020) 1–18, doi: 10.1080/19648189.2020.1824821

Author's contribution: SEM microscopy, design and preparation of experiments.

European Journal of Environmental and Civil Engineering

ISSN: (Print) (Online) Journal homepage: https://www.tandfonline.com/loi/tece20

Improvement of bonding between synthetic fibers and a cementitious matrix using recycled concrete powder and plasma treatment: from a single fiber to FRC

R. Hlůžek , J. Trejbal , V. Nežerka , P. Demo , Z. Prošek & P. Tesárek

To cite this article: R. Hlůžek , J. Trejbal , V. Nežerka , P. Demo , Z. Prošek & P. Tesárek (2020): Improvement of bonding between synthetic fibers and a cementitious matrix using recycled concrete powder and plasma treatment: from a single fiber to FRC, European Journal of Environmental and Civil Engineering, DOI: 10.1080/19648189.2020.1824821

To link to this article: https://doi.org/10.1080/19648189.2020.1824821

Published online: 29 Sep 2020.

EUROPEAN JOURNAL OF ENVIRONMENTAL AND CIVIL ENGINEERING
https://doi.org/10.1080/19648189.2020.1824821

Improvement of bonding between synthetic fibers and a cementitious matrix using recycled concrete powder and plasma treatment: from a single fiber to FRC

R. Hlůžek[a], J. Trejbal[a], V. Nežerka[a], P. Demo[a,b], Z. Prošek[a] and P. Tesárek[a]

[a]Faculty of Civil Engineering, Czech Technical University in Prague, Praha 6, Czech Republic; [b]Institute of Physics, Czech Academy of Sciences, Praha 6, Czech Republic

ABSTRACT

Poor adhesion of synthetic macro fibers to a cementitious matrix limits their reinforcing capacity when used in fiber-reinforced cementitious composites (FRCCs). As a remedy to this problem, high concentrations of fibers must be incorporated into such mixtures, which makes their dispersion in fresh mixtures difficult to achieve. Several strategies have been adopted to improve bonding between synthetic fibers and a cementitious matrix, but most of them cause deterioration of fiber properties. In previous studies, plasma treatment of polymer fibers and strengthening of the fiber-matrix interface using recycled concrete powder (RCP) increased pull-out resistance at a scale of a single fiber. Here, it was found that these results cannot be easily scaled, and the tension-softening behavior of FRCCs can be influenced negatively, despite positive pull-out test results, due to random orientation of fibers. Treating fibers with plasma appears reasonable at any scale, but RCP matrix modification must be carefully performed. Nevertheless, RCP may contribute to more sustainable concrete mixtures and considering its use when designing FRCC elements is recommended.

ARTICLE HISTORY
Received 8 April 2020
Accepted 11 September 2020

KEYWORDS
Synthetic macro fibers; polymer fibers; recycled concrete; plasma treatment; bonding; FRC

1. Introduction

In the set of cementitious materials, the use of plain concrete is limited to a very narrow range of engineering applications due to its low tensile strength and brittle nature. This limitation can be overcome by reinforcement, rendering concrete stronger and more ductile (di Prisco et al., 2009; Li, 2003; Maalej et al., 1995; Meddah & Bencheikh, 2009; Zhang & Li, 2002). Steel bars or meshes have been traditionally used for this purpose, but in some applications, it is advantageous to complement or even replace such discrete reinforcement by using fibers (di Prisco et al., 2009; Mazaheripour et al., 2011; Mohammadi et al., 2008; Oh et al., 2007). FRCCs can be produced using steel (Cagatay & Dincer, 2011; Kim & Yoo, 2019; Lee & Kim, 2010; Tiberti et al., 2015), glass (Ali & Qureshi, 2019; Kasagani & Rao, 2018; Schwartzentruber et al., 2004), carbon (Hambach et al., 2016; Lavagna et al., 2018; Xu & Chung, 1999), natural (Krishna et al., 2018; Razak & Ferdiansyah, 2005; Zakaria et al., 2020), and synthetic fibers (Kotecha & Abolmaali, 2019; Li et al., 2018; Ochi et al., 2007; Trejbal et al., 2016).

Synthetic fibers have become a popular alternative to steel fibers because of their high tensile strength, low density, ease of dispersion, relatively low cost, and resistance to chemicals within

CONTACT J. Trejbal jan.trejbal@fsv.cvut.cz Faculty of Civil Engineering, Czech Technical University in Prague, Thákurova 7, Praha 6, 166 29, Czech Republic
Preprint submitted to European Journal of Environmental and Civil Engineering July 24, 2020

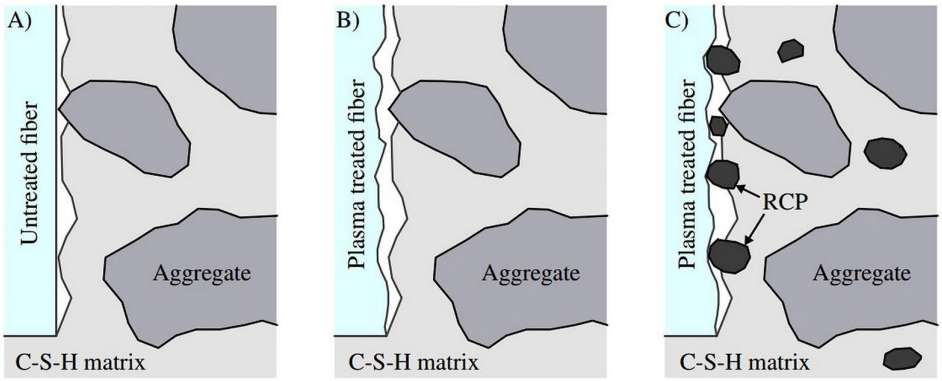

Figure 1. Hypothetical reinforcement of fiber-matrix interfaces with the combination of plasma treatment and the addition of RCP; (A) no reinforcement, (B) roughening of a fiber using plasma treatment, (C) a plasma treated fiber and interlocks provided by RCP.

cementitious materials (Bordelon & Roesler, 2014; Foti, 2016; Kim et al., 2010; Sadrinejad et al., 2018; Silva et al., 2005; Zheng, 1995). Furthermore, the ends of soft synthetic fibers protruding from FRCC elements do not pose a risk of injury and are also less harmful to concreting machines (Luňáček et al., 2012). Even though strong synthetic macro fibers have become broadly accepted by engineers as reliable concrete reinforcements, their limited ability to adhere to a cementitious matrix limits their capacity (Bartos, 1981; Foti, 2019; Lee et al., 1997; Li et al., 1987; Singh et al., 2004). In turn, fibers must be added to a mixture in concentrations high enough to sustain stresses and can become tangled and difficult to homogeneously disperse within mixtures. Various strategies have been developed to make synthetic fibers more hydrophilic and to increase their bonding with a matrix in order to enable use of lower fiber concentrations in mixtures. Wet chemical treatment and flame treatment cause fibers to be weaker and more brittle (Felekoglu et al., 2009), while micro-indentation reduces fiber cross-section and cannot be implemented in the case of fibers with small diameters (Singh et al., 2004). Cold plasma treatment appears to be a suitable, non-damaging alternative with controllable outcomes (Felekoglu et al., 2009; Grundke et al., 2015; Li et al., 1997; Tosun et al., 2012; Wang & He, 2006). Even though plasma can activate polar groups on a surface of polymers and promote chemical bonding (Li et al., 1997; Mittal, 2004; Öktem et al., 2000; Tosun et al., 2012), such activation can be very unstable and temporary (Trejbal et al., 2018); increased bonding can be attributed to fiber surface roughening due to ion beam bombardment.

The properties of the interfacial transition zone (ITZ) in the vicinity of fibers can be also modified to promote fiber bonding and to increase pull-out fiber resistance (Leung et al., 2005; Li & Stang, 1997; Maida et al., 2018; Trejbal, 2018; Trejbal et al., 2015). Adding nano-fillers into a concrete mixture modifies the ITZ by reducing porosity (Bentz et al., 2000; Bentz & Stutzman, 1994; Han et al., 2015; Park & Lee, 2013). In previous studies (Hlůžek & Trejbal, 2019; Trejbal et al., 2018), pull-out resistance at the scale of a single fiber was shown to increase with the addition of finely ground recycled concrete containing sharp fragments into mixtures (Prošek et al., 2020), especially when combined with plasma treatment. A hypothetical mechanism for this process is presented in Figure 1. Meaningful utilization of recycled concrete powder (RCP) would likely be beneficial for environmental reasons, because such subsieve fractions constitute up to 50% of crushed concrete weight (Ma & Wang, 2013; Shui et al., 2008) and there is, to the best of our knowledge, no clear way to reuse this kind of waste (Anastasiou et al., 2014; Cartuxo et al., 2015; Evangelista & de Brito, 2014, 2019). In this study, the focus was on upscaling the results from a single fiber to fiber-reinforced pastes and fiber-reinforced concrete (FRC) to see if plasma treatment and the addition of RCP to mixtures were efficient and led to improved tension-softening behavior in such cementitious composites.

2. Materials and methods

The composition of tested mixtures, design of specimens, and the experimental agenda were proposed in such a way to reveal the role of RCP and plasma treatment on the strength of specimens at multiple

Table 1. Size characteristics, PC and RCP.

	Sauter mean diameter, d32 [μm]	De Brouckere mean diameter, d43 [μm]	Specific surface [m2/kg]
PC	2.65	18.5	380
RCP	3.71	9.98	460

Table 2. Aggregate grading.

				Sand					Gravel	
Sieve size [mm]	0	0.0625	0.125	0.25	0.5	1.0	2.0	4.0	8.0	16.0
Sand passing [%]	0	2.08	3.51	5.40	9.13	16.45	29.74	52.50	78.88	100.00

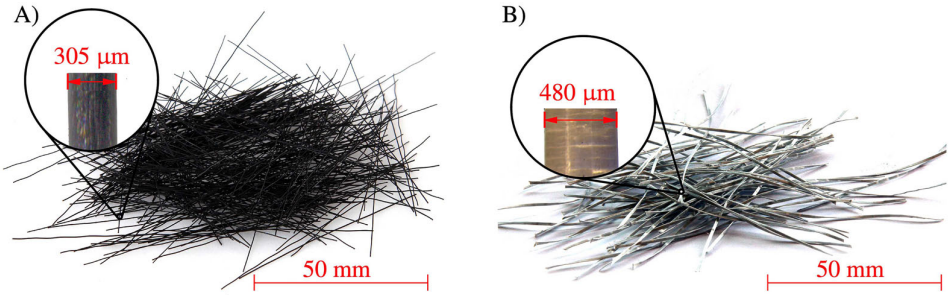

Figure 2. Fibers used in this study: (A) straight PP fibers (round cross-sections), (B) twisted PP + PE fibers (flat cross-sections).

Table 3. Characteristics of fibers.

Cross-section	Material	Shape	Diameter [mm]	Length [mm]	Tensile strength [MPa]	Young's modulus [MPa]
Round	PP	Straight	305	55	440	6100
Flat	PP + PE	Twisted	408	55	610	5170

scales. The study involved two fiber types, but a comparison between the performance of these fibers was out of scope of this study; the emphasis on revealing the role of RCP and plasma treatment is reflected by ordering of specimens in tables and figures throughout this paper.

2.1. Used materials

The input materials for the production of cementitious pastes and concrete were selected based on findings from previous studies (Nežerka et al., 2019; Prošek et al., 2019, 2020). An ordinary PC CEM I/42.5R (EN 197-1:2001, 2001) was selected for production of pastes and concrete. A recycled drainage channel was the source of RCP. The channel, which had been stored in a warehouse for approximately four years, was made of class C 20/25 (EN 1992-1-1:2004, 2004) unreinforced prefabricated concrete. The channel was crushed, and coarse fragments were further processed, yielding a 0-1 mm fraction, using a high-speed Lavaris SKD 600 electric mill (2 × 30 kW). Table 1 provides a comparison of PC and RCP size characteristics analyzed using laser granulometry (a Fritsch Analyssete 22 Micro Tec Plus device). The Blaine method (Matest E009 device) was used to determine the specific surface.

Sieving was used to determine the grading of the pit sand and basalt aggregate used for production of concrete (Table 2).

Two types of polymer macrofibers commonly used in the construction industry were used to study the impact of plasma treatment and the addition of RCP on the cementitious matrix of mixtures studied. These polypropylene (PP)/polypropylene-polyethylene (PE) fibers differed mainly in shape and mechanical properties, see Figure 2 and Table 3. The PP fibers, having a round cross section, were primarily intended for the production of brushes, while the PP + PE fibers having a flat cross-section were originally designed to perform well as concrete reinforcement by their manufacturers.

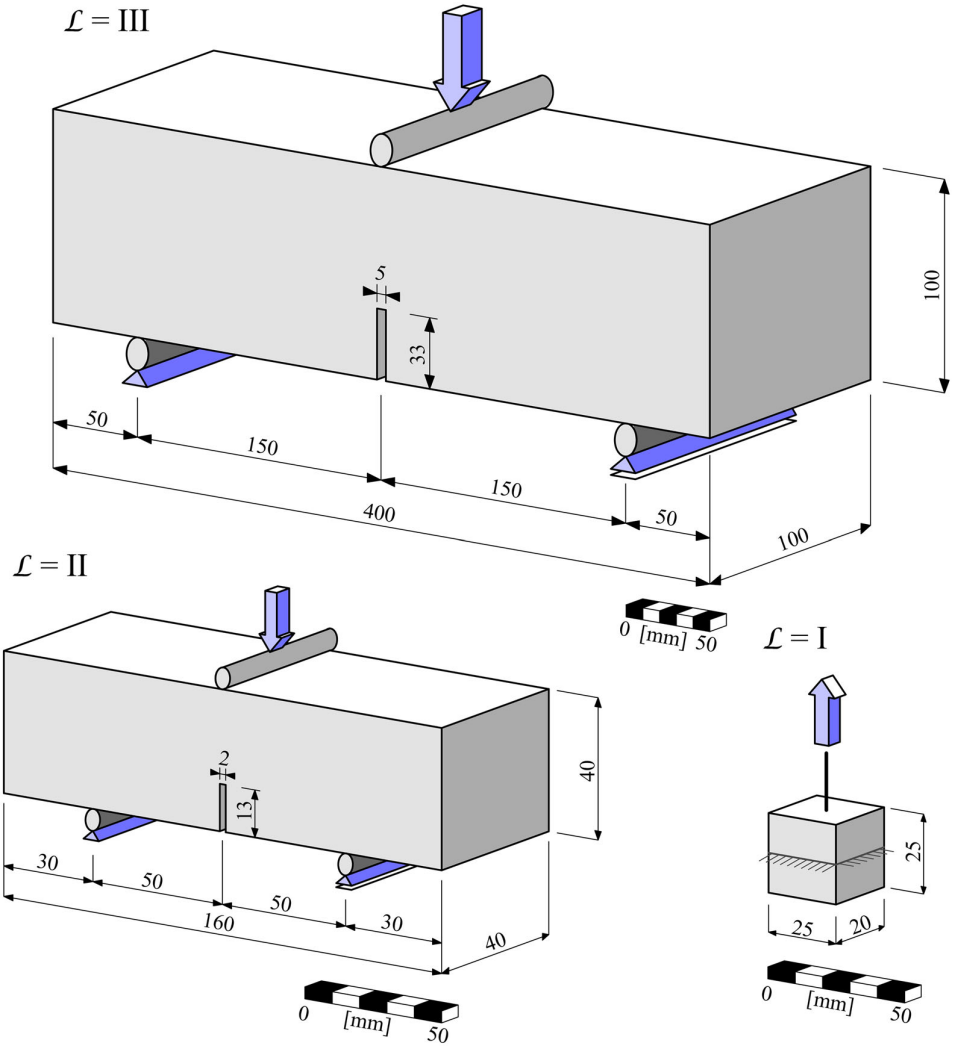

Figure 3. Geometry of specimens tested at the scale of a single fiber (L = I), fiber-reinforced paste (L = II), and FRC (L = III); the arrows indicate the direction of prescribed displacement during testing.

2.2. Mixes and specimens

Three experimental set-ups operating at different length scales were created to reveal the role of fiber-interface modifications at various scales and the scalability of results obtained by wettability and pull-out tests (Figure 3).

First, the ability of fibers to bond to cementious pastes was assessed using pull-out tests (scale L = I). A single fiber per specimen was embedded in $25 \times 20 \times 25$ mm molds filled with fresh pastes. The anchoring length was equal to the height of the specimens, i.e. 25 mm. Eight sets of specimens, each containing different combinations of a paste (pure PC paste and pastes containing different amounts of PC and RCP), fiber type (round and flat), and treatment (untreated or plasma-treated) – see Figure 4 – were prepared and tested. Each set (mixture) at L = I was represented by six specimens. The composition of individual mixtures is provided in Table 4.

The same mixtures were tested at scale L = II using $40 \times 40 \times 100$ mm specimens; only the fibers were incorporated into the mix in a concentration equal to 1.35% of the weight of binder materials (PC/PC

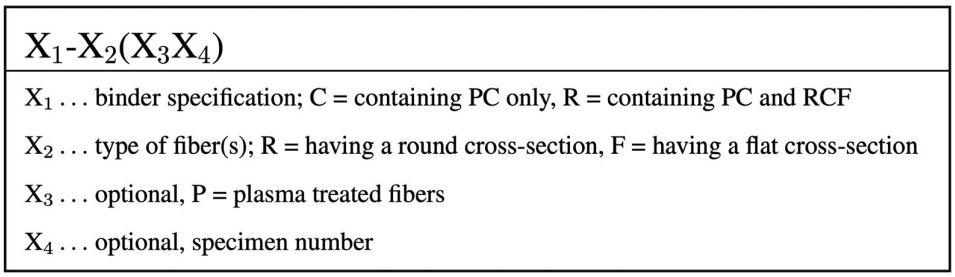

Figure 4. Key for naming mixtures and specimens.

Table 4. Composition of paste mixtures at L = I and II.

	Input materials [wt.%]					
Mixture	PC	RCP	Fibers (only at L = I)	Water	w/b	Fiber type
C-R	70.75	–	0.95	28.3	0.40	round, untreated
C-RP		round, treated				
R-R	42.15	28.10		28.8	0.41	round, untreated
R-RP						round, treated
C-F	70.75	–		28.3	0.40	flat, untreated
C-FP		flat, treated				
R-F	42.15	28.10		28.8	0.41	flat, untreated
R-FP						flat, treated

Table 5. Composition of FRC mixtures at L = III.

			Input materials [kg/m3]						w/c	Fiber type
Mixture	RC	RCP	Sand	Gravel	Gravel	Fibers	Water	Plasticizer		
0–4 mm	4–8 mm	8–16 mm								
C-R	350	–	870	100	860	6.825	192.5	3.0	0.55	round, untreated
C-RP		round, treated								
R-R		174	696							round, untreated
R-RP										round, treated
C-F		–	870							flat, untreated
C-FP		flat, treated								
R-F		174	696							flat, untreated
R-FP										flat, treated

and RCP combined). This concentration was selected based on findings by other authors (Khaloo et al., 2014; Machovič et al., 2013; Ochi et al., 2007) and findings from previous studies (Trejbal et al., 2016; 2018). The high water-to-binder ratio ($w/b \approx 0.4$) facilitated dispersion of fibers. Each mixture at L = II was represented by six specimens.

$100 \times 100 \times 400$ mm FRC specimens at scale L = III were prepared according to EN 14845-1 (BS EN 14845-1:2007, 2007) and EN 14651 (BS EN 14651:2005, 2005) standards, requiring: maximum aggregate size equal to 16 mm, maximum PC amount 350 kg/m3, and water-to-cement ratio $w/c = 0.55$. The concentration of fibers, 0.75% of mixture volume, was selected to facilitate dispersion and sufficient workability. This concentration also ensured a plateau in the load-deflection diagrams and hardening following a drop after the matrix failure during three-point bending tests. FRC mixture workability was enhanced by using a Stachement 2180 FM plasticizer, produced by Stachema CZ. Here, RCP replaced sand and the amount of PC was kept constant to rule out the impact of a poor cementitious matrix on the tensile parameters due to an insufficient amount of PC in the mix. Table 5 provides a summary of the concrete mixtures. Each mixture at L = III was represented by six specimens. Similar FRC mixtures have also been tested by other authors (Buratti et al., 2011; Maida et al., 2018; Nobili et al., 2013; Paegle et al., 2016).

All specimens were compacted and kept completely sealed at $22 \pm 1\,^{\circ}C$ for 24 h prior to unmolding. They were then submerged in tap water for 27 days. After this period, the specimens at L = II and III were

partially cut at midspan with a water-cooled diamond circular saw to produce 2 and 5 mm thick notches, respectively, reaching 1/3 of the height of specimens.

2.3. Plasma treatment

Low pressure, inductively coupled oxygen plasma was used to treat the smooth and chemically inert fibers. This treatment makes surfaces more hydrophilic by reducing surface energy (Mittal, 2004; Mutlu et al., 2008; Öktem et al., 2000) and creating microscopic dents (Trejbal et al., 2016). A Tesla VT 214 device (50 sccm oxygen flow, 56 Pa gas 100 pressure) was used to induce cold plasma. Based on previous research (Trejbal et al., 2018), an optimal treatment for macroscopic polymer fibers was employed: a power supply of 100 W for 30 s.

2.4. Microscopy

A FEG SEM Merlin ZEISS scanning electron microscope (SEM) equipped with Schottky emission cathodes and a detector for secondary electrons was used to investigate the surface topology of fibers before and after plasma treatment. Fiber surfaces were coated with platinum dust (3 nm thick) in an argon atmosphere in order to provide the required electric conductivity. The accelerating voltage was set to 5 kV and the current to 120 pA.

2.5. Contact angle measurement

Static contact angles were evaluated using images of fibers submerged in demineralized water. An in-house software, CAMTIA (Nežerka et al., 2018), was used to quantify changes in wettability due to plasma treatment. A single-lens reflex Canon EOS 600 D digital camera was used for taking images of fibers half-submerged in distilled water. The camera was equipped with a Tamron 70–300 mm objective lens and a grey neutral-density filter. Backlight illumination was provided by an LED lamp together with a dispersing screen. The images were taken one day after plasma treatment. Ten fibers represented each set.

2.6. Destructive testing

The pull-out tests at L = I were displacement controlled at a rate of 2 mm/min, using Veb Tiw Rauenstein FP 100 loading frame. The specimens were fixed with self-tightening clamps, while fiber free-ends were anchored using special clamping jaws to prevent notch formation. The response of fibers during pull-out testing was evaluated in the form of force versus free-end displacement diagrams; displacements were recorded using an in-built linear position sensor.

The same frame was used for testing of notched specimens in three-point bending at L = II and L = III, but the displacements were evaluated using RTCorr in-house digital image correlation (DIC) software (Antoš et al., 2019). These results were verified using the Ncorr DIC package (Blaber et al., 2015; Nežerka, n.d.) on selected specimens. The three-point bending tests were displacement-controlled at a rate of 1 mm/min to provide sharp images for DIC analysis.

3. Results and discussions

3.1. Treatment impacts on morphology and wettability of fibers

Changes in the surface morphologies of the investigated fibers were observed using SEM under a 12k× magnification. The microscopy images presented in Figure 5 show that the longitudinal grooves formed during the extrusion of round PP fibers were more pronounced after plasma treatment. Moreover, surface roughening due to plasma treatment was more significant for flat PP + PE fibers, making their effective area larger. The longitudinal grooves and loose polymer droplets on their surfaces were eliminated, but newly formed transversal fissures emerged.

To measure fiber surface wettability, the mean of contact angles measured between the menisci of the water level in the vicinity of a fiber and the fiber itself was used. The measurements revealed that

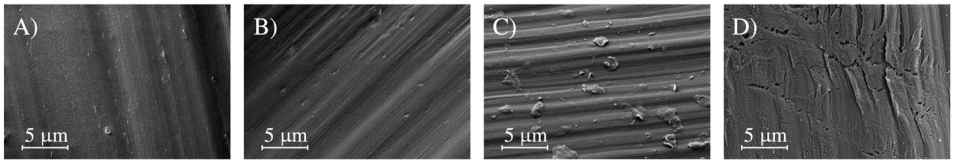

Figure 5. Surface of fibers under 12k× magnification: (A) an untreated round fiber, (B) a treated round fiber, (C) an untreated flat fiber, and (D) a treated flat fiber.

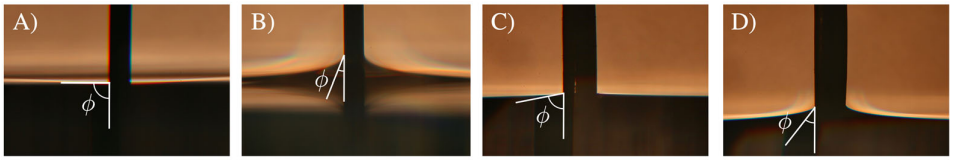

Figure 6. Silhouettes of water level and partially submerged fibers showing the impact of plasma treatment contact angles φ: (A) an untreated round fiber, (B) a treated round fiber, (C) an untreated flat fiber, and (D) a treated flat fiber.

Table 6. Contact angles for untreated fibers and fibers subjected to 30 s plasma treatment.

Fiber	Round	Round treated	Flat	Flat treated
Contact angle [°]	88.3 ± 0.6	29.1 ± 5.2	82.6 ± 4.6	36.9 ± 3.0

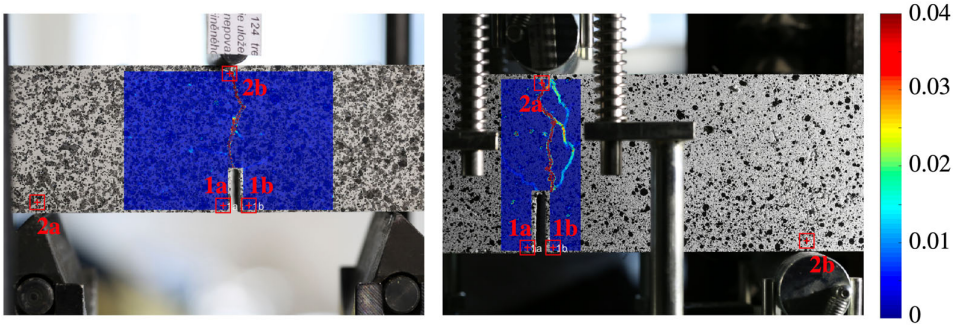

Figure 7. Maps of principal strain on C-RP specimens at L = II (left) and III (right) evaluated using Ncorr software (Blaber et al., 2015; Nežerka et al., 2016) and position of virtual extensometers 1a–1b and 2a–2b for evaluation of CMODs and deflections using RTCorr software (Antoš et al., 2019).

plasma treatment rendered fibers more hydrophilic and resulted in a decrease of contact angles, as shown in Figure 6. The results summarized in Table 6 indicate that hydrophilization resulting from plasma treatment was more efficient for round fibers.

3.2. Performance of fiber reinforcement at different scales

To compare the performance of individual fiber/matrix configurations, pull-out/bending forces $F_{0.5}$, $F_{1.5}$, $F_{2.5}$, and $F_{3.5}$, respectively, were evaluated at CMOD levels 0.5, 1.5, 2.5, and 3.5, following the methodology proposed in the EN 14651 (BS EN 14651:2005, 2005) standard. Locations of virtual extensometers for evaluation of deflections and CMOD using DIC are plotted in Figure 7. According to Li et al. (1991) and Li and Leung (1992), the maximum interfacial shear stress, $\tau_{max} = F_{max}/C_f\, l_e$, is related mainly to chemical bonding, while after reaching a maximum force during fiber pull-out, the magnitude of interfacial shear stress is exclusively related to mechanical bonding. C_f and l_e refer to a fiber circumference and effective fiber length, respectively. By capturing post-peak behavior during mechanical loading, the impact of plasma treatment and the presence of RCP could be assessed from the displacement-controlled

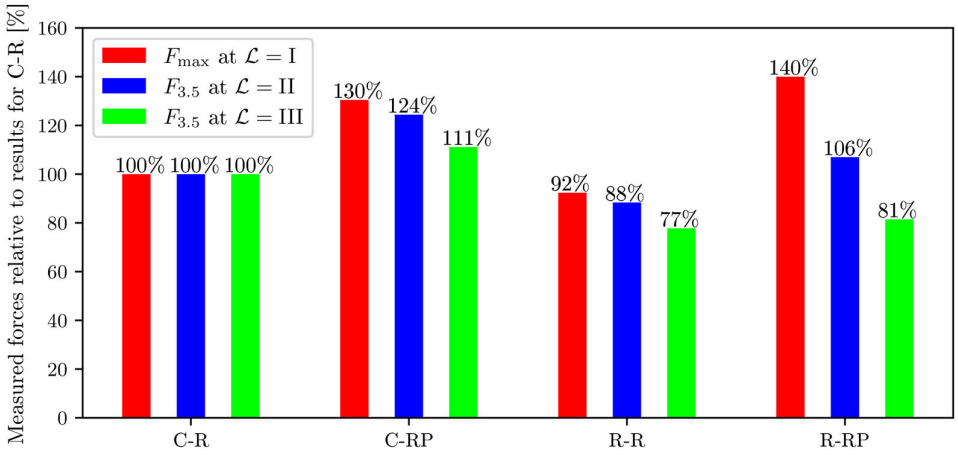

Figure 8. Effect of RCP in a cementitious matrix and plasma treatment of round fibers on performance of specimens at L = I, II, and III; the results for modified specimens are related to the results for reference configuration C-R.

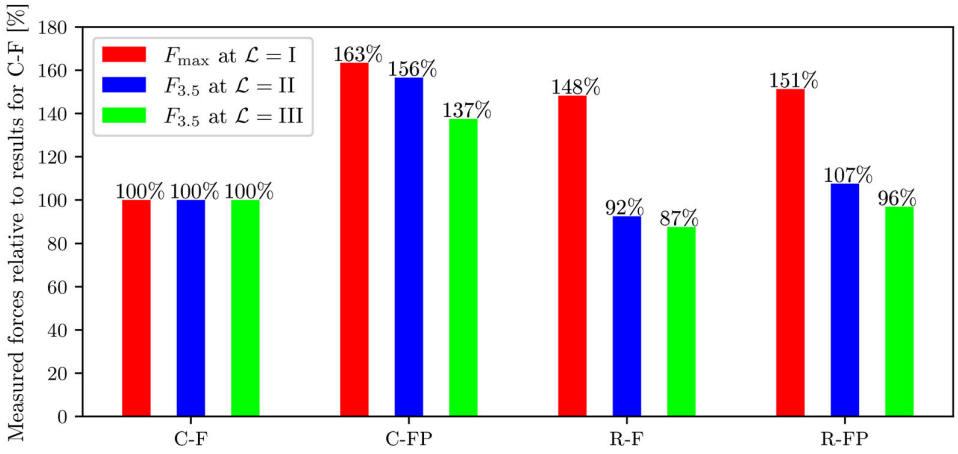

Figure 9. Effect of RCP in a cementitious matrix and plasma treatment of flat fibers on performance of specimens at L = I, II, and III; the results for modified specimens are related to the results for reference configuration C-F.

loading of notched specimens. All measured force-displacement curves are provided in Appendix A, Figures A1–A10, along with the summary of these results in Tables A1–A3.

Force-displacement diagrams at the scale of a single fiber pull-out, L = I, exhibited an almost bilinear relationship without significant drops after fiber debonding for both types of fibers. The stiffer response and higher pull-out strength for flat fibers, compared to round ones, can be attributed to their larger effective surface areas. To assess the impact of plasma treatment and the presence of different amounts of RCP in specimens, a summary of average values F_{max} for individual mixtures normalized by F_{max} for a reference configuration (cement paste and untreated fibers) is provided for round and flat fibers in Figures 8 and 9, respectively. In these plots, plasma treatment increased F_{max} at L = I, regardless of fiber type and matrix composition. The addition of RCP led to greater pull-out resistance except for untreated round fibers, which had the smoothest surface. In other cases, the impact of plasma treatment and RCP additions was significant, increasing F_{max} by 30–63%.

For three-point bending test results at levels L = II and III, $F_{3.5}$ averages were compared. $F_{3.5}$ was selected as the most appropriate indicator of residual post-peak strength because the course of force-displacement curves stabilized before reaching a CMOD level of 3.5 mm, the point at which their tangents were nearly parallel.

The positive impacts of plasma treatment for L = I were also reflected in the performance of fiber-reinforced pastes at L = II. Pastes containing plasma-treated fibers were 15–56% stronger than their counterparts containing untreated fibers. On the other hand, the addition of RCP to pastes at L = II reduced their residual strength. Only in combination with plasma-treated fibers did the addition of RCP to reference mixtures not cause residual strength to deteriorate.

At L = III, the matrices containing RCP performed even worse. The bond strengthening resulting from plasma treatment increased residual strength less than for L = I and L = II, but the increase by 11–37% in mixtures without RCP cannot be considered negligible. Adding RCP to mixtures at L = III resulted in reducing residual strength by up to 23% for untreated round fibers.

The 'unscability' of pull-out test results can most likely be attributed to substantial differences in the micromechanical behavior of matrices at the distinct scales. Matrices containing RCP are weaker (Prošek et al., 2020), which can amplify the impact of snubbing if fibers are not perpendicular to a fracture plane (Li, 1992; Morton & Groves, 1976). Pull-out of these inclined fibers may result in a failure of the matrix weakened by the presence of RCP as in the research by Hong et al. (Hong et al., 2020). The effect of bond strength might be counteracted by the impact of fibers on porosity, homogeneity (Khaloo et al., 2014), and microstructure development during hardening (Leung et al., 2005; Shen et al., 2008) at the scale of FRC, but an examination of these impacts was beyond the scope of this study.

4. Conclusion

This study assessed the impacts of plasma treatment and RCP added to specimens on their tension-softening behavior. Pull-out forces at scales of a single fiber, reinforced cementitious paste, and FRC were examined. Among the most important findings:

1. Plasma treatment affected the morphology of fibers, making them rougher and less hydrophobic,
2. Plasma treatment and additions of RCP to paste/concrete mixes led to most significant effects at the scale of a single fiber pull-out and least significant at the FRC scale,
3. Plasma treatment led to enhanced bonding of fibers to a cementitious matrix and increased pull-out/residual strength for all specimens examined in this study,
4. The addition of RCP to specimens was advantageous only for the single fiber pull-out and for flat PP + PE fibers, but it appears that plasma treatment may diminish or reverse any negative effects of adding RCP to a mixture.

Based on these findings, plasma treating of synthetic macro fibers before producing any fiber-reinforced cementitious composite appears to be beneficial. Despite relatively low cost of low-pressure plasma treatment (about €0,5/h), the procedure is slow and therefore not feasible for real-world applications. This limitation can be overcome by employing plasma treatment induced at atmospheric pressure.

For increasing the residual strength of such composites, RCP additions appear to weaken a cementious matrix and thus cannot be recommended because a weakened matrix is susceptible to failure when fiber pull-out is not perpendicular to a crack plane. However, replacing large amounts of PC/sand with RCP in cement mixtures and further improving the performance of such mixtures using plasma treatment may still hold promise. This concept is worth investigating in future studies due to the potential environmental benefits of using RCP in a sustainable manner.

Acknowledgment

The authors wish to thank Dr. Šeps (Faculty of Civil Engineering, CTU in Prague) for his assistance during experimental testing. The help of Dr. Stephanie Krueger, who as an English native speaker provided editorial assistance, is gratefully acknowledged. Thanks also go to the Joint Laboratory of Polymer Nanofiber Technologies of Institute of Physics AS CR and Faculty of Civil Engineering, CTU in Prague.

Disclosure statement

No potential conflict of interest was reported by the authors.

Funding

This work was supported by the Czech Science Foundation [grant number GA ČR 17-06771S] and the Faculty of Civil Engineering at CTU in Prague [grant number SGS20/037/OHK1/1T/11].

References

Ali, B., & Qureshi, L. A. (2019). Influence of glass fibers on mechanical and durability performance of concrete with recycled aggregates. *Construction and Building Materials*, *228*, 116783. https://doi.org/10.1016/j.conbuildmat.2019.116783

Anastasiou, E., Filikas, K. G., & Stefanidou, M. (2014). Utilization of fine recycled aggregates in concrete with fly ash and steel slag. *Construction and Building Materials*, *50*, 154–161. https://doi.org/10.1016/j.conbuildmat.2013.09.037

Antoš, J., Nežerka, V., & Somr, M. (2019). Real-time optical measurement of displacements using sub-pixel image registration. *Experimental Techniques*, *43*(3), 315–323. https://doi.org/10.1007/s40799-019-00315-1

Bartos, P. (1981). Review paper: Bond in fibre reinforced cements and concretes. *International Journal of Cement Composites and Lightweight Concrete*, *3*(3), 159–177. https://doi.org/10.1016/0262-5075(81)90049-X

Bentz, D., Jensen, O., Coats, A., & Glasser, F. (2000). Influence of silica fume on diffusivity in cement-based materials. *Cement and Concrete Research*, *30*(6), 953–962. https://doi.org/10.1016/S0008-8846(00)00264-7

Bentz, D. P., & Stutzman, P. E. (1994). Evolution of porosity and calcium hydroxide in laboratory concretes containing silica fume. *Cement and Concrete Research*, *24*(6), 1044–1050. https://doi.org/10.1016/0008-8846(94)90027-2

Blaber, J., Adair, B., & Antoniou, A. (2015). Ncorr: Open-source 2d digital image correlation matlab software. *Experimental Mechanics*, *55*(6), 1105–1122. https://doi.org/10.1007/s11340-015-0009-1

Bordelon, A. C., & Roesler, J. R. (2014). Spatial distribution of synthetic fibers in concrete with x-ray computed tomography. *Cement and Concrete Composites*, *53*, 35–43. https://doi.org/10.1016/j.cemconcomp.2014.04.007

BS EN 14651:2005. (2005). *Test method for metallic fibre concrete. Measuring the flexural tensile strength (limit of proportionality (*LOP), *R*esidual). BSI British Standards. https://doi.org/10.3403/30092475

BS EN 14845-1:2007. (2007). *Test methods for fibres in concrete. Reference concretes.* BSI British Standards. https://doi.org/10.3403/30095427u.

Buratti, N., Mazzotti, C., & Savoia, M. (2011). Post-cracking behaviour of steel and macro-synthetic fibre-reinforced concretes. *Construction and Building Materials*, *25*(5), 2713–2722. https://doi.org/10.1016/j.conbuildmat.2010.12.022

Cagatay, L. H., & Dincer, R. (2011). Modeling of concrete containing steel fibers: Toughness and mechanical properties. *Computers & Concrete*, *8*(3), 357–369. https://doi.org/10.12989/cac.2011.8.3.357

Cartuxo, F., de Brito, J., Evangelista, L., Jimenez, J., & Ledesma, E. (2015). Rheological behaviour of concrete made with fine recycled concrete aggregates – Influence of the superplasticizer. *Construction and Building Materials*, *89*, 36–47. https://doi.org/10.1016/j.conbuildmat.2015.03.119

di Prisco, M., Plizzari, G., & Vandewalle, L. (2009). Fibre reinforced concrete: New design perspectives. *Materials and Structures*, *42*(9), 1261–1281. https://doi.org/10.1617/s11527-009-9529-4

EN 197-1:2011. (2011). *Cement. Composition, specifications and conformity criteria for very low heat special cements*. BSI British Standards. https://doi.org/10.3403/03054726.

EN 1992-1-1:2004. (2004). *Design of concrete structures, Part 1-1: General rules and rules for buildings*. BSI British Standards. https://doi.org/10.12691/ajcea-4-1-6.

Evangelista, L., & de Brito, J. (2014). Concrete with fine recycled aggregates: A review. *European Journal of Environmental and Civil Engineering*, *18*(2), 129–172. https://doi.org/10.1080/19648189.2013.851038

Evangelista, L., & de Brito, J. (2019). Durability of crushed fine recycled aggregate concrete assessed by permeability-related properties. *Magazine of Concrete Research*, *71*(21), 1142–1149. https://doi.org/10.1680/jmacr.18.00093

Felekoglu, B., Tosun, K., & Baradan, B. (2009). A comparative study on the flexural performance of plasma treated polypropylene fiber reinforced cementitious composites. *Journal of Materials Processing Technology*, *209*(11), 5133–5144. https://doi.org/10.1016/j.jmatprotec.2009.02.015

Foti, D. (2016). Innovative techniques for concrete reinforcement with polymers. *Construction and Building Materials*, *112*, 202–209. https://doi.org/10.1016/j.conbuildmat.2016.02.111

Foti, D. (2019). *Recycled waste PET for sustainable fiber reinforced concrete*. Woodhead Publishing.

Grundke, K., Pöschel, K., Synytska, A., Frenzel, R., Drechsler, A., Nitschke, M., Cordeiro, A., Uhlmann, L. P., & Welzel, P. B. (2015). Experimental studies of contact angle hysteresis phenomena on polymer surfaces – Toward the understanding and control of wettability for different applications. *Advances in Colloid and Interface Science*, *222*, 350–376. https://doi.org/10.1016/j.cis.2014.10.012.

Hambach, M., Möller, H., Neumann, T., & Volkmer, D. (2016). Portland cement paste with aligned carbon fibers exhibiting exceptionally high flexural strength (>100 MPa). *Cement and Concrete Research*, *89*, 80–86. https://doi.org/10.1016/j.cemconres.2016.08.011

Han, J.-W., Jeon, J.-H., & Park, C.-G. (2015). Bond characteristics of macro polypropylene fiber in cementitious composites containing nanosilica and styrene butadiene latex polymer. *International Journal of Polymer Science*, *2015*, 1–9. https://doi.org/10.1155/2015/207456

Hlůžek, R., & Trejbal, J. (2019). Use of finely ground recycled concrete for improvement of interfacial adhesion in fiber-reinforced cementitious composites. *Acta Polytechnica CTU Proceedings*, *21*, 5–9. https://doi.org/10.14311/app.2019.21.0005.

Hong, L., Chen, Y., Li, T., Gao, P., & Sun, L. (2020). Microstructure and bonding behavior of fiber-mortar interface in fiber-reinforced concrete. *Construction and Building Materials*, *232*, 117235. https://doi.org/10.1016/j.conbuildmat.2019.117235

Kasagani, H., & Rao, C. (2018). Effect of graded fibers on stress strain behaviour of glass fiber reinforced concrete in tension. *Construction and Building Materials*, *183*, 592–604. https://doi.org/10.1016/j.conbuildmat.2018.06.193

Khaloo, A., Raisi, E. M., Hosseini, P., & Tahsiri, H. (2014). Mechanical performance of self-compacting concrete reinforced with steel fibers. *Construction and Building Materials*, *51*, 179–186. https://doi.org/10.1016/j.conbuildmat.2013.10.054

Kim, J.-J., & Yoo, D.-Y. (2019). Effects of fiber shape and distance on the pullout behavior of steel fibers embedded in ultra-high-performance concrete. *Cement and Concrete Composites*, *103*, 213–223. https://doi.org/10.1016/j.cemconcomp.2019.05.006

Kim, S. B., Yi, N. H., Kim, H. Y., Kim, J.-H J., & Song, Y.-C. (2010). Material and structural performance evaluation of recycled PET fiber reinforced concrete. *Cement and Concrete Composites*, *32*(3), 232–240. https://doi.org/10.1016/j.cemconcomp.2009.11.002

Kotecha, P., & Abolmaali, A. (2019). Macro synthetic fibers as reinforcement for deep beams with discontinuity regions: Experimental investigation. *Engineering Structures*, *200*, 109672. https://doi.org/10.1016/j.engstruct.2019.109672

Krishna, N. K., Prasanth, M., Gowtham, R., Karthic, S., & Mini, K. (2018). Enhancement of properties of concrete using natural fibers. *Materials Today: Proceedings*, *5*(11), 23816–23823. https://doi.org/10.1016/j.matpr.2018.10.173

Lavagna, L., Musso, S., Ferro, G., & Pavese, M. (2018). Cement-based composites containing functionalized carbon fibers. *Cement and Concrete Composites*, *88*, 165–171. https://doi.org/10.1016/j.cemconcomp.2018.02.007

Lee, C., & Kim, H. (2010). Orientation factor and number of fibers at failure plane in ring-type steel fiber reinforced concrete. *Cement and Concrete Research*, *40*(5), 810–819. https://doi.org/10.1016/j.cemconres.2009.11.009

Lee, S. D., Sarmadi, M., Denes, E., & Shohet, J. L. (1997). Surface modification of polypropylene under argon and oxygen-RF-plasma conditions. *Plasmas and Polymers*, *2*(3), 177–197. https://doi.org/10.1007/BF02766153

Leung, C. K., Lai, R., & Lee, A. Y. (2005). Properties of wet-mixed fiber reinforced shotcrete and fiber reinforced concrete with similar composition. *Cement and Concrete Research*, *35*(4), 788–795. https://doi.org/10.1016/j.cemconres.2004.05.033

Li, R., Ye, L., & Mai, Y.-W. (1997). Application of plasma technologies in fibre-reinforced polymer composites: A review of recent developments. *Composites Part A: Applied Science and Manufacturing*, *28*(1), 73–86. https://doi.org/10.1016/S1359-835X(96)00097-8

Li, V. C. (1992). Postcrack scaling relations for fiber reinforced cementitious composites. *Journal of Materials in Civil Engineering*, *4*(1), 41–57. https://doi.org/10.1061/(asce)

Li, V. C. (2003). On engineered cementitious composites (ECC). *Journal of Advanced Concrete Technology*, *1*(3), 215–230. https://doi.org/10.3151/jact.1.215

Li, V. C., & Leung, C. K. Y. (1992). Steady-state and multiple cracking of short random fiber composites. *Journal of Engineering Mechanics*, *118*(11), 2246–2264. https://doi.org/10.1061/(ASCE)0733-9399(1992)118:11(2246)

Li, V. C., & Stang, H. (1997). Interface property characterization and strengthening mechanisms in fiber reinforced cement based composites. *Advanced Cement Based Materials*, *6*(1), 1–20. https://doi.org/10.1016/S1065-7355(97)90001-8

Li, V. C., Wang, Y., & Backer, S. (1987). Effect of fiber-matrix bond strength on the crack resistance of synthetic fiber reinforced cementitious composites. *MRS Proceedings*, *114*, 167–173. https://doi.org/10.1557/PROC-114-167

Li, V. C., Wang, Y., & Backer, S. (1991). A micromechanical model of tension-softening and bridging toughening of short random fiber reinforced brittle matrix composites. *Journal of the Mechanics and Physics of Solids*, *39*(5), 607–625. https://doi.org/10.1016/0022-5096(91)90043-N

Li, Y., Li, W., Deng, D., Wang, K., & Duan, W. H. (2018). Reinforcement effects of polyvinyl alcohol and polypropylene fibers on flexural behaviors of sulfoaluminate cement matrices. *Cement and Concrete Composites*, *88*, 139–149. https://doi.org/10.1016/j.cemconcomp.2018.02.004

Luňáček, M., Suchánek, P., & Bader, R. (2012). Application of bicomponent synthetic macro fibres Concrix in tunneling. *Tunnel*, *8*, 54–56.

Ma, X., & Wang, Z. (2013). Effect of ground waste concrete powder on cement properties. *Advances in Materials Science and Engineering*, *2013*, 1–5. https://doi.org/10.1155/2013/918294

Maalej, M., Li, V. C., & Hashida, T. (1995). Effect of fiber rupture on tensile properties of short fiber composites. *Journal of Engineering Mechanics*, *121*(8), 903–913. https://doi.org/10.1061/(ASCE)0733-9399(1995)121:8(903)

Machovič, V., Lapčák, L., Borecká, L., Lhotka, M., Andertová, J., Kopecký, L., & Mišková, L. (2013). Microstructure of interfacial transition zone between PET fibers and cement paste. *Acta Geodynamica et Geomaterialia*, *10*, 121–127. https://doi.org/10.13168/agg.2013.0012.

Maida, P. D., Sciancalepore, C., Radi, E., & Bondioli, F. (2018). Effects of nano-silica treatment on the flexural post cracking behaviour of polypropylene macro-synthetic fibre reinforced concrete. *Mechanics Research Communications*, *88*, 12–18. https://doi.org/10.1016/j.mechrescom.2018.01.004

Mazaheripour, H., Ghanbarpour, S., Mirmoradi, S. H., & Hosseinpour, I. (2011). The effect of polypropy-lene fibers on the properties of fresh and hardened lightweight self-compacting concrete. *Construction and Building Materials*, *25*(1), 351–358. https://doi.org/10.1016/j.conbuildmat.2010.06.018

Meddah, M. S., & Bencheikh, M. (2009). Properties of concrete reinforced with different kinds of industrial waste fibre materials. *Construction and Building Materials*, *23*(10), 3196–3205. https://doi.org/10.1016/j.conbuildmat.2009.06.017

Mittal, K. L. (2004). *Polymer surface modification: Relevance to adhesion*. Taylor & Francis Group.

Mohammadi, Y., Singh, S. P., & Kaushik, S. K. (2008). Properties of steel fibrous concrete containing mixed fibres in fresh and hardened state. *Construction and Building Materials*, *22*(5), 956–965. https://doi.org/10.1016/j.conbuildmat.2006.12.004

Morton, J., & Groves, G. W. (1976). The effect of metal wires on the fracture of a brittle-matrix composite. *Journal of Materials Science*, *11*(4), 617–622. https://doi.org/10.1007/BF01209446

Mutlu, S., Çökeliler, D., ¸ Shard, A., Goktas, H., Ozansoy, B., & Mutlu, M. (2008). Preparation and characterization of ethylenediamine and cysteamine plasma polymerized films on piezo-electric quartz crystal surfaces for a biosensor. *Thin Solid Films*, *516*(6), 1249–1255. https://doi.org/10.1016/j.tsf.2007.06.074

Nežerka, V. (2014). *Ncorr post: DIC post-processing tool*. http://mech.fsv.cvut.cz/nezerka/dic/index.htm

Nežerka, V., Antoš, J., Litoš, J., Tesárek, P., & Zeman, J. (2016). An integrated experimental-numerical study of the performance of lime-based mortars in masonry piers under eccentric loading. *Construction and Building Materials*, *114*, 913–926. https://doi.org/10.1016/j

Nežerka, V., Bílý, P., Hrbek, V., & Fládr, J. (2019). Impact of silica fume, fly ash, and metakaolin on the thickness and strength of the ITZ in concrete. *Cement and Concrete Composites*, *103*, 252–262. https://doi.org/10.1016/j.cemconcomp.2019.05.012

Nežerka, V., Somr, M., & Trejbal, J. (2018). Contact angle measurement tool based on image analysis. *Experimental Techniques*, *42*(3), 271–278. https://doi.org/10.1007/s40799-017-0231-0

Nobili, A., Lanzoni, L., & Tarantino, A. (2013). Experimental investigation and monitoring of a polypropylene-based fiber reinforced concrete road pavement. *Construction and Building Materials*, *47*, 888–895. https://doi.org/10.1016/j.conbuildmat.2013.05.077

Ochi, T., Okubo, S., & Fukui, K. (2007). Development of recycled PET fiber and its application as concrete-reinforcing fiber. *Cement and Concrete Composites*, *29*(6), 448–455. https://doi.org/10.1016/j.cemconcomp.2007.02.002

Oh, B. H., Kim, J. C., & Choi, Y. C. (2007). Fracture behavior of concrete members reinforced with structural synthetic fibers. *Engineering Fracture Mechanics*, *74*(1-2), 243–257. https://doi.org/10.1016/j.engfracmech.2006.01.032

Öktem, T., Seventekin, N., Ayhan, H., & PİŞKİN, E. (2000). Modification of polyester and polyamide fabrics by different in situ plasma polymerization methods. *Turkish Journal of Chemistry*, *24*, 269–274.

Paegle, I., Minelli, F., & Fischer, G. (2016). Cracking and load-deformation behavior of fiber reinforced concrete: Influence of testing method. *Cement and Concrete Composites*, *73*, 147–163. https://doi.org/10.1016/j.cemconcomp.2016.06.012

Park, C.-G., & Lee, J.-W. (2013). Effect of nanosilica and silica fume content on the bond properties of macro-synthetic fibre in cement-based composites. *Magazine of Concrete Research*, *65*(3), 148–157. https://doi.org/10.1680/macr.12.00036

Prošek, Z., Nežerka, V., Hlůžek, R., Trejbal, J., Tesárek, P., & Karra'a, G. (2019). Role of lime, fly ash, and slag in cement pastes containing recycled concrete fines. *Construction and Building Materials*, *201*, 702–714. https://doi.org/10.1016/j.conbuildmat.2018.12.227

Prošek, Z., Trejbal, J., Nežerka, V., Goliáš, V., Faltus, M., & Tesárek, P. (2020). Recovery of residual anhydrous clinker in finely ground recycled concrete. *Resources, Conservation and Recycling*, *155*, 104640–104648. 104640. https://doi.org/10.1016/j.resconrec.2019

Razak, H. A., & Ferdiansyah, T. (2005). Toughness characteristics of arenga pinnata fibre concrete. *Journal of Natural Fibers*, *2*(2), 89–103. https://doi.org/10.1300/J395v02n02_06

Sadrinejad, I., Madandoust, R., & Ranjbar, M. M. (2018). The mechanical and durability properties of concrete containing hybrid synthetic fibers. *Construction and Building Materials*, *178*, 72–82. https://doi.org/10.1016/j.conbuildmat.2018.05.145

Schwartzentruber, A., Philippe, M., & Marchese, G. (2004). Effect of PVA, glass and metallic fibers, and of an expansive admixture on the cracking tendency of ultrahigh strength mortar. *Cement and Concrete Composites*, *26*(5), 573–580. https://doi.org/10.1016/S0958-9465(03)00076-3

Shen, B., Hubler, M., Paulino, G. H., & Struble, L. J. (2008). Functionally-graded fiber-reinforced cement composite: Processing, microstructure, and properties. *Cement and Concrete Composites*, *30*(8), 663–673. https://doi.org/10.1016/j.cemconcomp.2008.02.002

Shui, Z., Xuan, D., Wan, H., & Cao, B. (2008). Rehydration reactivity of recycled mortar from concrete waste experienced to thermal treatment. *Construction and Building Materials*, *22*(8), 1723–1729. https://doi.org/10.1016/j.conbuildmat.2007.05.012

Silva, D. A., Betioli, A. M., Gleize, P. J. P., Roman, H. R., Gómez, L. A., & Ribeiro, J. L. D. (2005). Degradation of recycled PET fibers in portland cement-based materials. *Cement and Concrete Research*, *35*(9), 1741–1746. https://doi.org/10.1016/j.cemconres.2004.10.040

Singh, S., Shukla, A., & Brown, R. (2004). Pullout behavior of polypropylene fibers from cementitious matrix. *Cement and Concrete Research*, *34*(10), 1919–1925. https://doi.org/10.1016/j.cemconres.2004.02.014

Tiberti, G., Minelli, F., & Plizzari, G. (2015). Cracking behavior in reinforced concrete members with steel fibers: A comprehensive experimental study. *Cement and Concrete Research*, *68*, 24–34. https://doi.org/10.1016/j.cemconres.2014.10.011

Tosun, K., Felekoğlu, B., & Baradan, B. (2012). Multiple cracking response of plasma treated polyethy-lene fiber reinforced cementitious composites under flexural loading. *Cement and Concrete Composites*, *34*(4), 508–520. https://doi.org/10.1016/j.cemconcomp.2011.12.001

Trejbal, J. (2018). Mechanical properties of lime-based mortars reinforced with plasma treated glass fibers. *Construction and Building Materials*, *190*, 929–938. https://doi.org/10.1016/j.conbuildmat.2018.09.175

Trejbal, J., Ďureje, J., Hlůžek, R., & Prošek, Z. (2018). Interaction assessment between fiber reinforcement and cement matrix containing finely ground recycled concrete. *IOP Conference Series: Materials Science and Engineering*, *379*, 012016. https://doi.org/10.1088/1757-899X/379/1/012016

Trejbal, J., Kopecký, L., Tesárek, P., Fládr, J., Antoš, J., Somr, M., & Nežerka, V. (2016). Impact of surface plasma treatment on the performance of PET fiber reinforcement in cementitious composites. *Cement and Concrete Research*, *89*, 276–287. https://doi.org/10.1016/j.cemconres.2016.08.018

Trejbal, J., Nežerka, V., Somr, M., Fládr, J., Potocký, Š., Artemenko, A., & Tesárek, P. (2018). Deterioration of bonding capacity of plasma-treated polymer fiber reinforcement. *Cement and Concrete Composites*, *89*, 205–215. https://doi.org/10.1016/j.cemconcomp.2018.03.010

Trejbal, J., Šmilauer, V., Kromka, A., Potocký, S., Kopecky, L. (2015). *Wettability enhancement of polymeric and glass micro fiber reinforcement by plasma treatment*. Proceedings of the 7-th International Conference on Research & Application, Brno, pp. 315-–320.

Wang, C., & He, X. (2006). Polypropylene surface modification model in atmospheric pressure dielectric barrier discharge. *Surface and Coatings Technology*, *201*(6), 3377–3384. https://doi.org/10.1016/j.surfcoat.2006.07.205

Xu, Y., & Chung, D. (1999). Carbon fiber reinforced cement improved by using silane-treated carbon fibers. *Cement and Concrete Research*, *29*(5), 773–776. https://doi.org/10.1016/S0008-8846(99)00015-0

Zakaria, M., Ahmed, M., Hoque, M., & Shaid, A. (2020). A comparative study of the mechanical properties of jute fiber and yarn reinforced concrete composites. *Journal of Natural Fibers*, *17*(5), 676–612. https://doi.org/10.1080/15440478.2018.1525465

Zhang, J., & Li, V. C. (2002). Monotonic and fatigue performance in bending of fiber-reinforced engineered cementitious composite in overlay system. *Cement and Concrete Research*, *32*(3), 415–423. https://doi.org/10.1016/S0008-8846(01)00695-0

Zheng, Z. (1995). Synthetic fibre-reinforced concrete. *Progress in Polymer Science*, *20*(2), 185–210. https://doi.org/10.1016/0079-6700(94)00030-6

Appendix A. Load-displacement diagrams

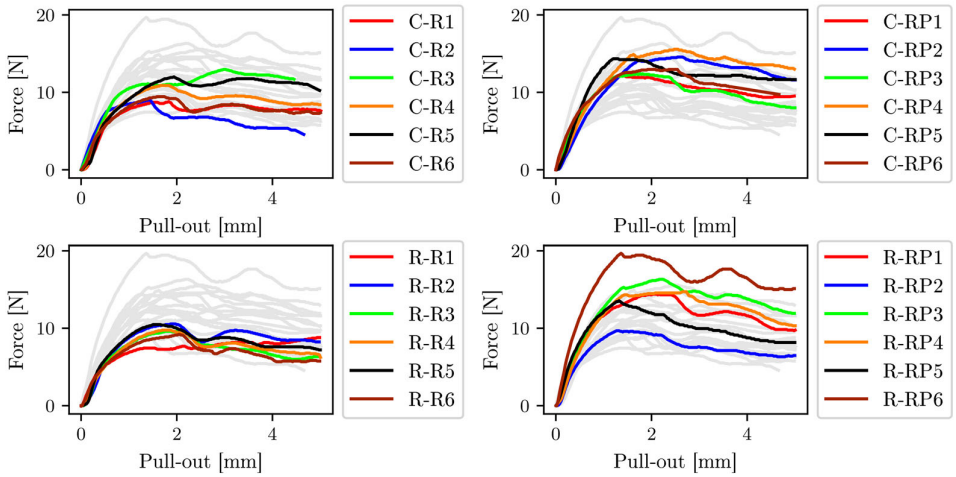

Figure A1. Load-displacement diagrams recorded during pull-out tests on round fiber specimens at L = l.

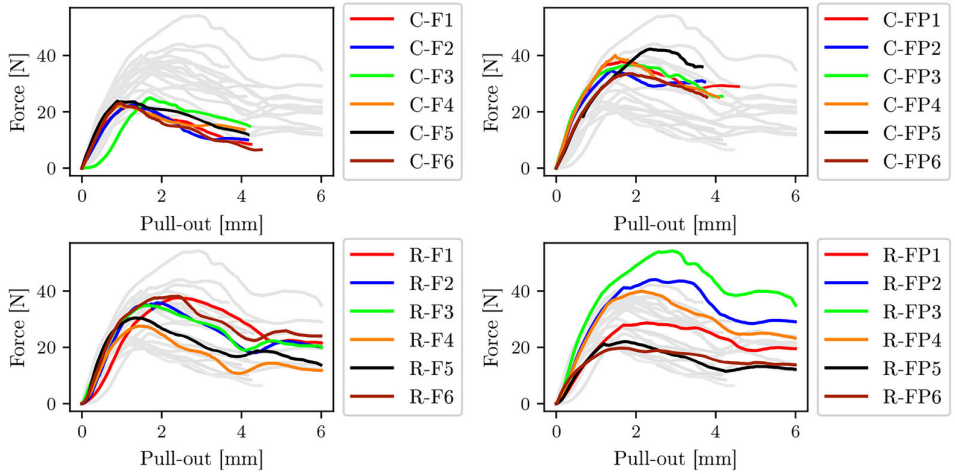

Figure A2. Load-displacement diagrams recorded during pull-out tests on flat fiber specimens at L = I.

Table A1. Averages and standard deviations for maximum force F_{max} and forces at displacements 0.5, 1.5, 2.5, and 3.5 ($F_{0,5}$, $F_{1,5}$, $F_{2,5}$, and $F_{3,5}$, respectively), measured during pull-out tests at L = I for individual fiber/matrix configurations.

Set of specimens	Fmax [N]	F0.5 [N]	F1.5 [N]	F2.5 [N]	F3.5 [N]
C-R	10.5 ± 1.56	6.3 ± 0.54	9.9 ± 1.07	9.0 ± 1.85	9.2 ± 2.32
C-RP	13.7 ± 1.22	7.0 ± 0.78	13.1 ± 0.92	13.0 ± 1.61	11.9 ± 1.66
R-R	9.7 ± 0.63	5.4 ± 0.26	9.3 ± 1.01	7.9 ± 0.44	8.0 ± 0.84
R-RP	14.7 ± 3.00	8.1 ± 1.74	14.1 ± 2.86	13.3 ± 3.10	12.3 ± 3.34
C-F	23.0 ± 1.07	13.1 ± 4.80	21.4 ± 0.90	18.0 ± 2.35	17.7 ± 2.50
C-FP	37.6 ± 2.93	19.1 ± 2.56	35.3 ± 2.49	34.6 ± 3.99	32.8 ± 3.24
R-F	34.1 ± 3.83	14.0 ± 3.76	32.2 ± 2.84	30.4 ± 6.50	24.3 ± 6.47
R-FP	34.8 ± 12.36	13.8 ± 3.87	31.1 ± 9.17	33.8 ± 12.81	30.4 ± 12.36

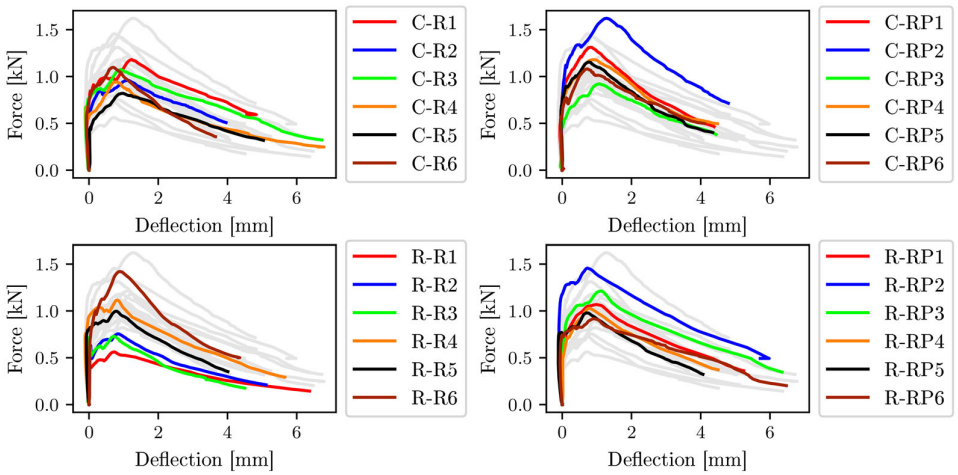

Figure A3. Deflection of specimens reinforced with round fibers tested at L = II.

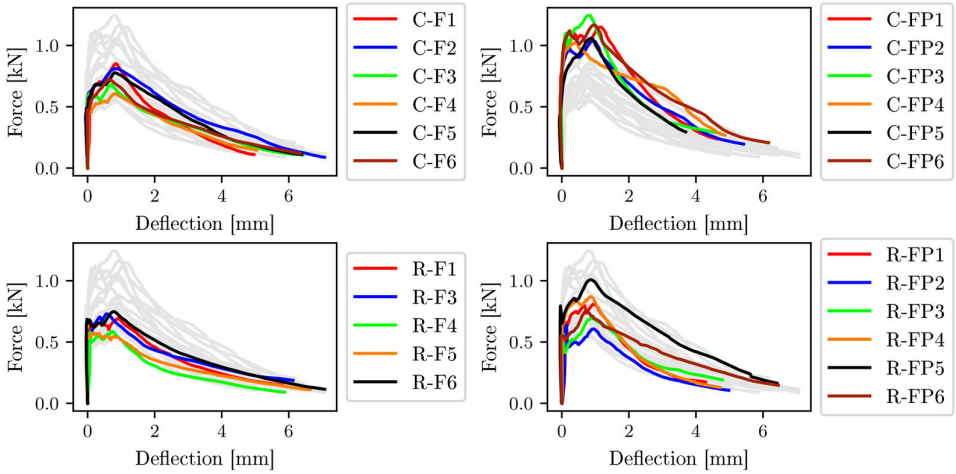

Figure A4. Deflection of specimens reinforced with flat fibers tested at L = II.

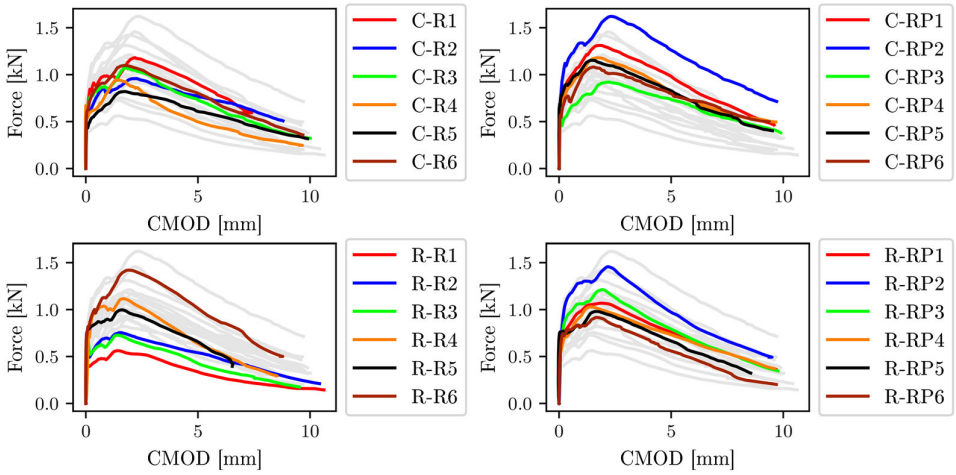

Figure A5. CMOD measured on specimens reinforced with round fibers tested at L = II.

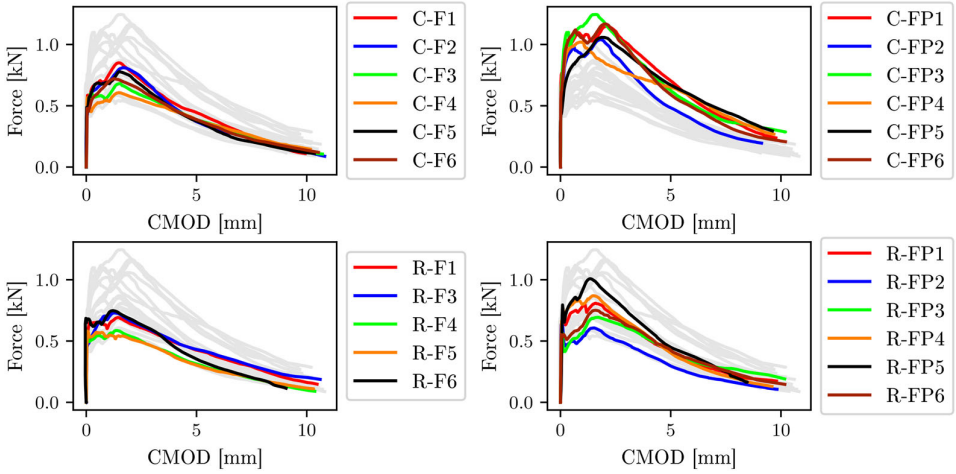

Figure A6. CMOD measured on specimens reinforced with flat fibers tested at L = II.

Table A2. Averages and standard deviations for maximum force F_{max} and forces at CMODs equal to 0.5, 1.5, 2.5, and 3.5 mm ($F_{0.5}$, $F_{1.5}$, $F_{2.5}$, and $F_{3.5}$, respectively), measured during three-point bending tests at L = II for individual fiber/matrix configurations.

Set of specimens	F_{max} [N]	$F_{0.5}$ [N]	$F_{1.5}$ [N]	$F_{2.5}$ [N]	$F_{3.5}$ [N]
C-R	1.01 ± 0.118	0.77 ± 0.111	0.95 ± 0.090	0.96 ± 0.133	0.86 ± 0.135
C-RP	1.21 ± 0.218	0.89 ± 0.182	1.15 ± 0.185	1.17 ± 0.226	1.07 ± 0.215
R-R	0.93 ± 0.285	0.76 ± 0.207	0.91 ± 0.265	0.86 ± 0.287	0.76 ± 0.260
R-RP	1.11 ± 0.180	0.88 ± 0.147	1.06 ± 0.126	1.05 ± 0.189	0.92 ± 0.158
C-F	0.74 ± 0.082	0.62 ± 0.060	0.74 ± 0.081	0.65 ± 0.065	0.53 ± 0.028
C-FP	1.11 ± 0.079	0.97 ± 0.079	1.04 ± 0.099	0.99 ± 0.109	0.83 ± 0.081
R-F	0.67 ± 0.071	0.61 ± 0.047	0.65 ± 0.076	0.57 ± 0.062	0.49 ± 0.055
R-FP	0.79 ± 0.122	0.65 ± 0.136	0.79 ± 0.126	0.68 ± 0.097	0.57 ± 0.070

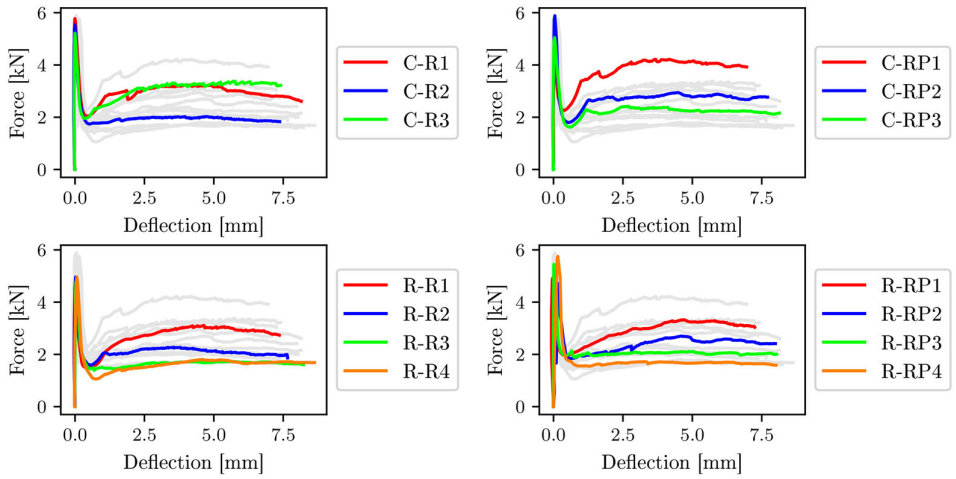

Figure A7. Deflection of specimens reinforced with round fibers tested at L = III.

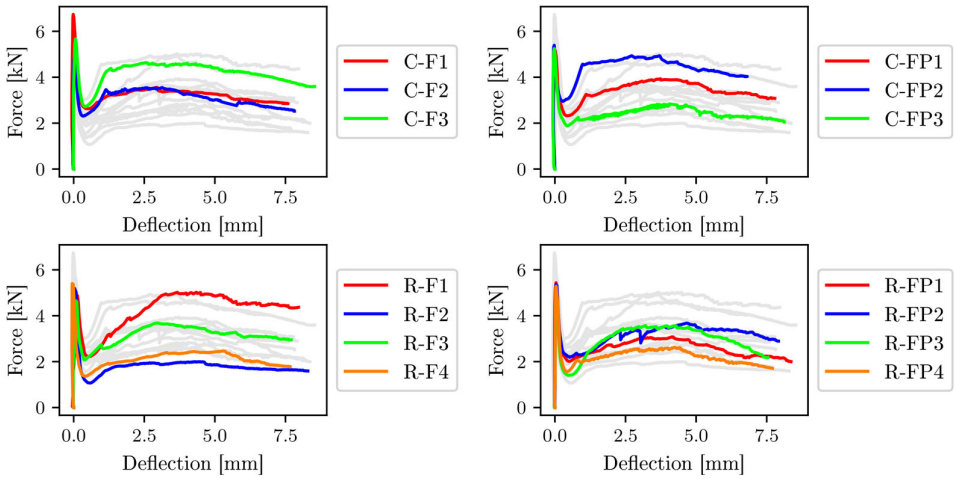

Figure A8. Deflection of specimens reinforced with flat fibers tested at L = III.

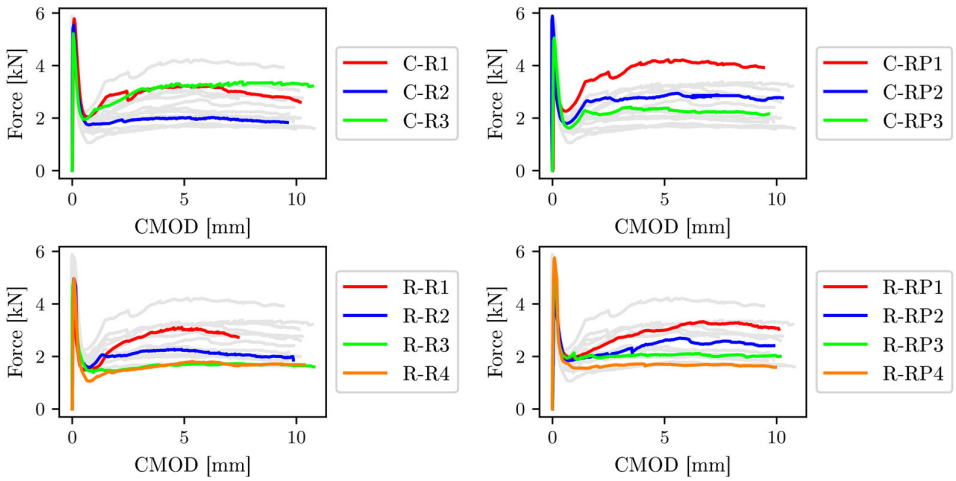

Figure A9. CMOD measured on specimens reinforced with round fibers tested at L = III.

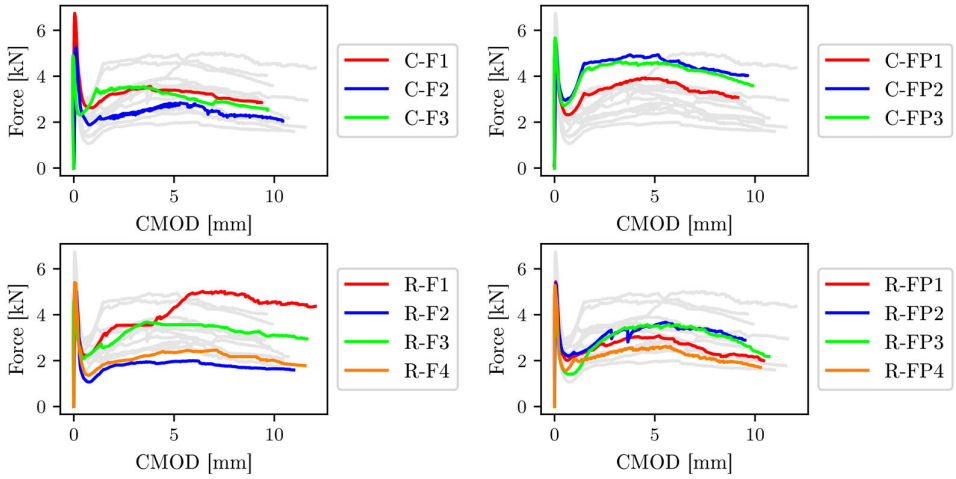

Figure A10. CMOD measured on specimens reinforced with flat fibers tested at L = III.

Table A3. Averages and standard deviations for maximum force F_{max} and forces at CMODs equal to 0.5, 1.5, 2.5, and 3.5 mm ($F_{0.5}$, $F_{1.5}$, $F_{2.5}$, and $F_{3.5}$, respectively), measured during three-point bending tests at L = III for individual fiber/matrix configurations.

Set of specimens	F_{max} [N]	$F_{0.5}$ [N]	$F_{1.5}$ [N]	$F_{2.5}$ [N]	$F_{3.5}$ [N]
C-R	5.5 ± 0.23	2.0 ± 0.12	2.3 ± 0.41	2.5 ± 0.42	2.7 ± 0.52
C-RP	5.1 ± 0.68	2.0 ± 0.22	2.8 ± 0.47	2.9 ± 0.63	3.0 ± 0.66
R-R	4.9 ± 0.12	1.6 ± 0.16	1.7 ± 0.31	1.9 ± 0.45	2.1 ± 0.53
R-RP	5.2 ± 0.41	2.0 ± 0.11	1.9 ± 0.22	2.0 ± 0.32	2.2 ± 0.40
C-F	5.6 ± 0.80	2.5 ± 0.25	2.8 ± 0.51	3.0 ± 0.51	3.2 ± 0.47
C-FP	5.4 ± 0.21	2.7 ± 0.23	4.0 ± 0.56	4.2 ± 0.53	4.4 ± 0.47
R-F	5.1 ± 0.28	1.8 ± 0.41	2.3 ± 0.61	2.6 ± 0.73	2.8 ± 0.77
R-FP	5.3 ± 0.17	1.9 ± 0.34	2.2 ± 0.18	2.7 ± 0.33	3.1 ± 0.37